MODELING THE CIRCULATION AND WATER QUALITY IN CHARLOTTE HARBOR ESTUARINE SYSTEM, FLORIDA

By

KIJIN PARK

A DISSERTATION PRESENTED TO THE GRADUATE SCHOOL
OF THE UNIVERSITY OF FLORIDA IN PARTIAL FULFILLMENT
OF THE REQUIREMENTS FOR THE DEGREE OF
DOCTOR OF PHILOSOPHY

UNIVERSITY OF FLORIDA

2004

ACKNOWLEDGMENTS

I would like to thank my advisor, Dr. Y. Peter Sheng, for his guidance, support and financial assistance throughout my study. In addition, much appreciation is owned to my other committee members, Dr. Robert G. Dean, Dr. Robert J. Thieke, Dr. Louis H. Motz and Dr. K. Ramesh Reddy, for their review of my dissertation.

I would like to thank the South Florida Water Management District and Southwest florida Water Management District for sponsoring research project and providing data for Charlotte Harbor estuarine system. I would like to express my thanks to Justin, Jeffery, Yangfeng, Taeyoon, Jun, Vadim, and Vladimir whose help with class, research and writing this dissertation. Many thanks go to Becky, Lucy, Sonna, Sidney, Kim and Halen for making life easier.

I would like to dedicate this dissertation to my parents whose love and support made this degree possible. Last, but not least, I would like to thank my wife, Kyung-Mi, who have been praying for me to be faithful, kind, and honest all the time.

TABLE OF CONTENTS

Page

ACKNOWLEDGMENTS ii

LIST OF TABLES vi

LIST OF FIGURES ix

ABSTRACT xvii

CHAPTER
1 INTRODUCTION 1

2 CHARLOTTE HARBOR CHARACTERIZATION 9

2.1 Climate 11
2.2 Hydrodynamics 11
2.2.1 Tidal Stage, Discharge at Inlet, and Tidal Circulation 13
2.2.2 Freshwater Flow 14
2.2.3 Salinity 14
2.3 Water Quality 15
2.3.1 Nutrients 16
2.3.2 Dissolved Oxygen 18
2.3.3 Phytoplankton 19
2.4 Sediment 20
2.5 Light Environment 21

3 HYDRODYNAMIC AND SEDIMENT TRANSPORT MODEL 23

3.1 Governing Equation 24
3.1.1 Hydrodynamic Model 24
3.1.2 Sediment Transport Model 26
3.2 Boundary and Initial Conditions 27
3.2.1 Boundary Conditions 27
3.2.2 Initial Conditions 30
3.3 Heat-Flux at Air-Sea Interface 30
3.3.1 Short-Wave Solar Radiation 31
3.3.2 Long-Wave Solar Radiation 32

3.3.3 Sensible and Latent Heat Fluxes 33

4 WATER QUALITY MODEL 36

4.1 Mathematical Formulae 38
4.2 Phytoplankton Dynamics 40
4.2.1 Modeling Approach 40
4.2.2 Relationship between Phytoplankton and Nutrients 42
4.3 Nutrient Dynamics 43
4.4 Oxygen Balance 45
4.5 Effects of Temperature and Light Intensity on Water Quality Model 59
4.5.1 Temperature 59
4.5.2 Light intensity 61
4.6 Light Attenuation Model 61
4.7 Model Parameters and Calibration Procedures 69

5 APPLICATION OF CIRCULATION AND TRANSPORT MODEL 81

5.1 A High-Resolution Curvilinear Grid for Charlotte Harbor Estuarine System 82
5.2 Forcing Mechanism and Boundary Condition 86
5.3 Simulations for 1986 Hydrodynamics 94
5.3.1 Sensitivity and Calibration Simulations 99
5.3.2 Results of the 1986 simulation 101
5.4 Simulations for 2000 Hydrodynamic 118
5.4.1 Sensitivity and Calibration Simulations 118
5.4.2 Results of the 2000 Simulation 130
5.4.3 Application of the 2000 hydrodynamic Simulations 146

6 APPLICATION OF WATER QUALITY MODEL 167

6.1 Forcing Mechanism and Boundary Condition for Circulation 167
6.2 Initial and Boundary Condition for the Water Quality Model 172
6.3 Simulations of Water Quality in 1996 180
6.3.1 Calibration 180
6.3.2 Results for 1996 Water Quality Simulations 191
6.4 Simulations of Water Quality in 2000 212
6.4.1 Verification 212
6.4.2 Results of 2000 Water Quality Simulations 215
6.4.3 Application of 2000 Water Quality Simulations 235

7 CONCLUSION AND DISCUSSION 258

APPENDIX
A FLOW CHARTS FOR CH3D_IMS 263

B DIMENSIONLESS EQUATIONS IN CURVILINEAR BOUNDARY-FITTED AND SIGMA GRID 278

C COMPARISON OF WATER QUALITY MODELS 284

D NUMERICAL SOLUTION TECHNIQUES FOR WATER QUALITY MODEL .. 289

E NUTRIENT DYNAMICS 294

F SEDIMENT FLUX MODEL 306

G MODEL PERFORMANCE TEST WITH PARALLEL CH3D_IMS 309

H TIDAL BENCH MARKS FOR CHARLOTTE HARBOR 313

REFERENCES 314

BIOGRAPHICAL SKETCH 325

LIST OF TABLES

Table page

1.1 Component models of the CH3D-IMS 6

2.1 Ratios of nitrogen and phosphorous constituents. 18

3.1 Mean latitudinal values of the coefficient λ. 33

4.1 Average values of oxygen uptake rates of bottom. 54

4.2 The spectrum of incident sunlight data. 64

4.3 Coefficient ranges to use in stand along light model 67

4.4 The best fit light model coefficients for Charlotte Harbor estuarine system 67

4.5 Dixon and Gray's model coefficients for the Charlotte Harbor estuarine system.. . 67

4.6 Temperature adjustment functions for water quality parameters. 70

4.7 Water quality parameters related to conversion rate 71

4.8 Water quality parameters related to phytoplankton and zooplankton. 71

4.9 Water quality parameters in the nitrogen dynamics. 72

4.10 Water quality parameters in the phosphorous dynamics. 73

4.11 Water quality parameters in the oxygen balance. 74

4.12 The relationship between water quality parameters and model constituents. 79

5.1 Descriptions of 1986 and 2000 river boundary conditions for Charlotte Harbor estuarine system.. 87

5.2 Locations of tidal stage and velocity-salinity measured stations by USGS.. 96

5.3 The effect of removing selected boundary conditions on the accuracy of simulated water level, velocity and salinity in July 1986. Value shown are average RMS differences vs. baseline simulation at all data stations. 99

5.4 The effect of varying bottom roughness, z_0, on the accuracy of simulated water level, velocity and salinity in July 1986. Value shown are average RMS errors at all data stations.. 100

5.5 The effect of varying horizontal diffusion, A_H, on the accuracy of simulated water level, velocity and salinity in July 1986. Value shown average RMS errors at all data stations.. 101

5.6 A summary of boundary conditions and model parameters used in the 1986 simulation. 102

5.7 Calculated RMS errors between simulated and measured water level for 1986 simulation. 102

5.8 Calculated RMS errors between simulated and measured current velocity for 1986 simulation.. 104

5.9 Calculated RMS errors between simulated and measured salinity for 1986 simulation. 105

5.10 The effect of horizontal grid resolution, on the accuracy of simulated water level and salinity. Values shown are average RMS errors for 2000 calibration at all available stations. Values shown in parenthesis are % RMS error normalized by maximum values.. 121

5.11 The effect of vertical grid resolution, on the accuracy of simulated water level and salinity. Values shown are average RMS errors for 2000 calibration at all available stations. Values shown in parenthesis are % RMS error normalized by maximum values.. 122

5.12 The effect of varying bottom roughness, z_0, on the accuracy of simulated water level and salinity in 2000. Values shown are average RMS errors all data stations. . 123

5.13 The effect of varying salinity advection scheme on the accuracy of simulated water level and salinity in 2000. Values shown are average RMS errors at all data stations. 128

5.14 The effect of modifying bathymetry on the accuracy of simulated water level and salinity in 2000. Values shown are average RMS errors for all data stations. . 129

5.15 A summary of boundary conditions and model parameters used in the 2000 simulation. 130

5.16 Calculated RMS errors between simulated and measured water level for 2000 simulation 131

5.17 Calculated RMS errors between simulated and measured salinity for 2000 simulation. 133

5.18 The effect of hydrologic alternations on 2000 water level. Value shown are average RMS differences with baseline simulation for all selected stations. . . 154

5.19 The effect of hydrologic alternations on 2000 salinity. Value shown are average RMS differences with baseline simulation for all selected stations.. 155

6.1 Locations of water quality measured stations. 173

6.2 Sediment types for Charlotte Harbor water quality simulations. 174

6.3 Water quality parameters, baseline values, and ranges used in the sensitivity analysis. 183

6.4 Sensitivity analysis results in RMS difference w.r.t. baseline for 1996 water quality calibration simulation. 184

6.5 The water quality model coefficients used for the Charlotte Harbor simulation. . . 185

6.6 The temporally averaged water quality species concentrations for baseline 2000 simulation. 240

6.7 Normalized RMS differences of water quality species concentrations at 11 stations during April to June 2000, showing the effect of no causeway islands. 240

6.8 Normalized RMS differences of water quality species concentrations at 11 stations during April to June 2000, showing the effect of no ICW. 241

6.9 Normalized RMS differences of water quality species concentrations at 11 stations during April to June 2000, showing the effect of no causeway islands and ICW241

C.1 Comparison of water quality models 287

G.1 CPU time for the parallel, shared memory, CH3D procedures on SGI origin platform. 311

H.1 Tidal datum referred to Mean Low Low Water (MLLW), in meter. 313

LIST OF FIGURES

Figure Page

1.1 Charlotte Harbor estuarine system and its subarea boundaries. 2

2.1 Drainage basins of Charlotte Harbor estuarine system 10

2.2 Seasonal wind pattern in Florida. 12

2.3 Average monthly concentration of dissolved oxygen in upper Charlotte Harbor, site CH-006, 1976-84. 19

4.1 The connection between nitrogen, phosphorous and carbon cycle 44

4.2 CBOD cycle and DO cycle 46

4.3 Comparison of wind-dependent re-aeration formula 49

4.4 The relationship between POM flux and SOD flux related in the oxidation and reduction of organic matter in sediment column 53

4.5 Effect of dissolved oxygen on sediment consumption and SOD release 57

4.6 The scatter plots for k_d(PAR) during calibration period with best fit coefficients . . 68

4.7 Systematic calibration procedure 80

5.1 Boundary-fitted grid (92 x 129) used for numerical simulation for Charlotte Harbor estuarine system 84

5.2 Bathymetry in the boundary-fitted grid for Charlotte Harbor estuarine system (92 x 129) 85

5.3 Tidal forcing and river discharges for 1986 simulations of Charlotte Harbor circulation. 89

5.4 Wind velocity for 1986 simulations for Charlotte Harbor circulation 90

5.5 Tidal forcing and river discharges for 2000 simulations of Charlotte Harbor circulation. 91

5.6 Wind velocity for 2000 simulation of Charlotte Harbor circulation 92

5.7 Air temperature for 2000 simulation of Charlotte Harbor circulation 93

5.8 Locations of the available 1986 water level and discharge measurement stations of USGS 97

5.9 Locations of available 1986 velocity and salinity measurement stations of USGS . 98

5.10 Comparison between simulated and measured water level in July 1986 108

5.11 Comparison between simulated and measure spectra of water level in July 1986 110

5.12 Comparison between simulated and measured current velocity in July 1986 . . . 111

5.13 Comparison between simulated and measured salinity in July 1986 115

5.14 Typical flow pattern of Charlotte Harbor estuarine system during one tidal cycle for August 6, 1986.. 116

5.15 The 29-day residual flow and salinity for Charlotte Harbor estuarine system during July 2 to July 30, 1986. 117

5.16 Locations of the available 2000 water level and salinity measured stations at Caloosahatchee River operated by SFWMD. 119

5.17 The comparison of the coarse grid (71x92) and the fine grid (92x129) for Charlotte Harbor estuarine system. 120

5.18 A comparison between simulated and measured salinity at Shell Point using ultimate QUICKEST, QUICKEST, and upwind advection schemes.. 124

5.19 A comparison between simulated and measured salinity at Fort Myers using ultimate QUICKEST, QUICKEST, and upwind advection schemes.. 125

5.20 A comparison between simulated and measured salinity at BR31 using ultimate QUICKEST, QUICKEST, and upwind advection schemes.. 126

5.21 Simulated longitudinal-vertical salinity along the Caloosahatchee River at slack-water before flood tide on September 7, 2000.. 127

5.22 Comparison between simulated and measured water level in 2000. 136

5.23 Comparison between simulated and measured salinity at S79 in 2000. 137

5.24 Comparison between simulated and measured salinity at BR31 in 2000. 138

5.25 Comparison between simulated and measured salinity at Fort Myers in 2000. . . 139

5.26 Comparison between simulated and measured salinity at Shell Point in 2000. . . 140

5.27 Comparison between simulated and measured salinity near Sanibel Causeway in 2000. 141

5.28 Comparison between simulated and measured temperature at Fort Myers in 2000. 142

5.29 Typical flow pattern of San Carlos Bay during ebb and flood tide for August, 7 on 2000.. 143

5.30 One-year residual flow in San Carlos Bay in 2000.. 144

5.31 One-year residual salinity distribution in San Carlos Bay in 2000.. 145

5.32 The locations of Sanibel Causeway and IntraCoastal Waterway and stations for comparing the effect of hydrologic alterations 148

5.33 The comparison of bathymetry and shoreline for each hydrologic alteration case scenarios which are Baseline, the absence of IntraCoastal Waterway, and the absence of causeway. 149

5.34 The comparisons of water level for three cases at three selected stations: ST05 (Pine Island Sound), ST08 (San Carlos Bay), and ST10 (Caloosahatchee River mouth). 150

5.35 The comparisons of surface and bottom salinity for three cases at three selected stations: ST05 (Pine Island Sound), ST08 (San Carlos Bay), and ST10 (Caloosahatchee River mouth) 151

5.36 The comparisons of surface residual flow and salinity fields for three cases. . . . 152

5.37 The comparisons of bottom residual flow and salinity fields for three cases. . . . 153

5.38 The vertical-longitudinal salinity profiles along the axis of the Caloosahatchee River during wet season in 2000. 159

5.39 The vertical-longitudinal salinity profiles along the axis of the Caloosahatchee River during dry season in 2000. 160

5.40 Time histories of river discharge at S-79 and the locations of 1, 10, and 20 ppt surface salinity along the Caloosahatchee River during 2000 simulation period.161

5.41 Time histories of river discharge at S-79 and the 1 ppt salinity location along Caloosahatchee River.. 162

5.42 The 1-day averaged 20 ppt surface salinity location and 30-day averaged 10 ppt surface salinity location during 2000 simulation period. 163

5.43 The locations of 10 ppt surface salinity due to river discharge rate at S-79 during 2000 baseline simulation. 164

5.44 The relationship between location of specific salinity value vs. river discharge at S-79. 165

5.45 The relationship between salinity at Fort Myers station vs. river discharge at S-79. 166

6.1 Tidal forcing and river discharges for 1996 simulations of Charlotte Harbor.. . . . 169

6.2 Wind velocity for 1996 simulations of Charlotte Harbor. 170

6.3 Air temperature for 1996 simulations of Charlotte Harbor 171

6.4 Locations of 1996 water quality measurement stations operated by EPA 176

6.5 Locations of 2000 water quality measurement stations operated by SFWMD and SWFWMD 177

6.6 Light intensity at water surface for 1996 and 2000 simulations 178

6.7 Segments for Charlotte Harbor estuarine system 179

6.8 The scatter plots for water quality constituents during calibration period 189

6.9 Temporal water quality variations at CH002 station in 1996. 194

6.10 Temporal water quality variations at CH004 station in 1996. 195

6.11 Temporal water quality variations at CH005 station in 1996. 196

6.12 Temporal water quality variations at CH006 station in 1996. 197

6.13 Temporal water quality variations at CH007 station in 1996. 198

6.14 Temporal water quality variations at CH09B station in 1996. 199

6.15 Temporal water quality variations at CH009 station in 1996. 200

6.16 Temporal water quality variations at CH010 station in 1996. 201

6.17 Temporal water quality variations at HB002 station in 1996. 202

6.18 Temporal water quality variations at HB006 station in 1996. 203

6.19 Temporal water quality variations at HB007 station in 1996. 204

6.20 Temporal water quality variations at CH013 station in 1996. 205

6.21 Simulated dissolved oxygen concentration in Charlotte Harbor estuarine system for August 21, 1996. 206

6.22 Simulated chlorophyll a concentration in Charlotte Harbor estuarine system for August 21, 1996. 207

6.23 Simulated dissolved ammonium nitrogen concentration in Charlotte Harbor estuarine system for August 21, 1996. 208

6.24 Simulated soluble organic nitrogen concentration in Charlotte Harbor estuarine system for August 21, 1996. 209

6.25 Simulated soluble reactive phosphorous concentration in Charlotte Harbor estuarine system for August 21, 1996. 210

6.26 Simulated soluble organic phosphorous concentration in Charlotte Harbor estuarine system for August 21, 1996. 211

6.27 The scatter plots for water quality constituents in 2000. 213

6.28 Temporal water quality variations at CH002 station in 2000. 218

6.29 Temporal water quality variations at CH004 station in 2000. 219

6.30 Temporal water quality variations at CH005 station in 2000. 220

6.31 Temporal water quality variations at CH006 station in 2000. 221

6.32 Temporal water quality variations at CH007 station in 2000. 222

6.33 Temporal water quality variations at CH09B station in 2000. 223

6.34 Temporal water quality variations at CH009 station in 2000. 224

6.35 Temporal water quality variations at CH010 station in 2000. 225

6.36 Temporal water quality variations at CES02 station in 2000. 226

6.37 Temporal water quality variations at CES03 station in 2000. 227

6.38 Temporal water quality variations at CES08 station in 2000. 228

6.39 Temporal water quality variations at CH013 station in 2000. 229

6.40 The comparison between simulated dissolved oxygen concentration and the possible causes hypoxia: river discharge, salinity, temperature, and re-aeration and SOD fluxes at CH006 water quality measured station. 230

6.41 Simulated longitudinal-vertical salinity and dissolved oxygen concentration along the Peace River at 1 pm on June 18 (Julian Day 170), 2000.. 231

6.42 Simulated longitudinal-vertical salinity and dissolved oxygen concentration along the Peace River at 1 pm on October 6 (Julian Day 280), 2000.. 232

6.43 Simulated near-surface chlorophyll a concentration in Charlotte Harbor estuarine system for February 9, May 9, August 7, November 5, 2000. 233

6.44 Simulated near-bottom dissolved oxygen concentration in Charlotte Harbor estuarine system for February 9, May 9, August 7, November 5, 2000. 234

6.45 Comparisons of simulated surface chlorophyll a concentration for three cases at three selected stations: ST05 (Pine Island Sound), ST08 (San Carlos Bay), and ST10 (Caloosahatchee River mouth) 237

6.46 Comparisons of simulated surface chlorophyll a concentration fields in San Carlos Bay after 90 days of simulation for three cases. 238

6.47 Comparisons of simulated surface dissolved ammonium nitrogen (NH4) concentration fields in San Carlos Bay after 90 days of simulation for three cases. 239

6.48 The water quality species at CH004 water quality measured station before and after 100 % nitrogen load reduction from Peace River. 247

6.49 The water quality species at CH006 water quality measured station before and after 100 % nitrogen load reduction from Peace River. 248

6.50 The water quality species at CH004 water quality measured station before and after 100 % phosphorous load reduction from Peace River. 249

6.51 The water quality species at CH006 water quality measured station before and after 100 % phosphorous load reduction from Peace River. 250

6.52 The water quality species at CES02 water quality measured station before and after 100 % nitrogen load reduction from Caloosahatchee River. 251

6.53 The water quality species at CES08 water quality measured station before and after 100 % nitrogen load reduction from Caloosahatchee River. 252

6.54 The water quality species at CES02 water quality measured station before and after 100 % phosphorous load reduction from Caloosahatchee River. 253

6.55 The water quality species at CES08 water quality measured station before and after 100 % phosphorous load reduction from Caloosahatchee River. 254

6.56 Dissolved oxygen and Chlorophyll a concentrations at CH006 water quality measured station before and after 100 % organic matter load reduction from Peace River using DiToro's sediment flux model. 255

6.57 Dissolved oxygen concentrations at CH004 and CH006 water quality measured stations before and after 50 % SOD reduction and 75% SOD reduction. 256

6.58 The comparison of hypoxia area at Upper Charlotte Harbor according to varying SOD constant rate at 20°C. 257

A.1 Flow chart for main CH3D program. 264

A.2 Flow chart for driving subroutine for the time stepping of the solution. 266

A.3 Flow chart for initializing sediment transport model. 271

A.4 Flow chart for main sediment transport model. 272

A.5 Flow chart for initializing water quality model 277

A.6 Flow chart for main water quality model. 275

A.7 Flow chart for computing temperature and light attenuation functions for water quality model. 277

D.1 The vertical one-dimensional z-grid 292

E.1 Nitrogen cycle. 296

E.2 Phosphorous cycle. 302

G.1 Parallel speedup gained in performing the simulation on the SGI Origin platform.312

Abstract of Dissertation Presented to the Graduate School
of the University of Florida in Partial Fulfillment of the
Requirements for the Degree of Doctor of Philosophy

MODELING THE CIRCULATION AND WATER QUALITY
IN CHARLOTTE HARBOR ESTUARINE SYSTEM, FLORIDA

By

Kijin Park

August 2004

Chair: Y. Peter Sheng
Department: Civil and Coastal Engineering

This study aims to develop an enhanced version of a three-dimensional curvilinear-grid modeling system, CH3D-IMS, which include a 3-D hydrodynamics model, a 3-D sediment transport model, and a 3-D water quality model, to simulate circulation and water quality of the Charlotte Harbor Estuarine System and to provide quantitative assessment of various management practices.

In the past decade, the upper Charlotte Harbor system has been suffering summer hypoxia in bottom water. Field study indicated that hypoxia in the upper Charlotte Harbor is related to a strong stratification caused by high freshwater flows and dissolved oxygen fluxes at the air-sea and sediment-water interfaces. To simulate the hypoxia event, models of oxygen balance and oxygen fluxes at the air-sea and sediment-water interfaces in previous versions of CH3D-IMS are enhanced. The three dimensional temperature model and physics-based light model in CH3D-IMS are also enhanced to enable better understanding

of the temporal and spatial variations of temperature and light and their effect on water quality processes.

The hydrodynamics component of the integrated model CH3D-IMS for Charlotte Harbor has been successfully calibrated, using hydrodynamic data gathered by the National Oceanic and Atmospheric Administration (NOAA) and the United States Geological Survey (USGS) in 1986 and 2000. This calibrated model was applied to assess the impact of the removal of the Sanibel Causeway and the IntraCoastal Waterway on the circulation in the San Carlos Bay area and to provide a quantitative evaluation of the minimum flow and level (MFL) for Caloosahatchee River. The results show that the hydrologic alterations would not noticeably affect the circulation, salinity, and water quality in San Carlos Bay except near the mouth of Caloosahatchee River. The minimum flow required to produce a salinity of no more than 10 ppt at Fort Myers is about 18 m^3/s.

The water quality model of the CH3D-IMS was calibrated with the systematic calibration procedure and validated using hydrodynamic, sediment, and water quality data provided by the USGS and the United States Environmental Protection Agency (USEPA) in 1996, and by the USGS, the South Florida Water Management District (SFWMD) and the Southwest Florida Water Management District (SWFWMD) in 2000. This validated model was used to examine the temporal and spatial dynamics of factors which can affect hypoxia in upper Charlotte Harbor, such as freshwater inflow, tidal variation, sediment oxygen demand (SOD), water column oxygen consumption, and dissolved oxygen (DO) re-aeration. The model results suggest that hypoxia in the upper Charlotte Harbor System is primarily caused by a combination of vertical salinity stratification and SOD, while water quality also affected by the oxygen re-aeration and water column oxygen consumption. This model was

applied to assess the effects of hydrologic alterations and to provide a preliminary evaluation of pollutant load reduction goal (PLRG). Due to lack of detailed data and insufficient understanding on the causes of SOD and how SOD is related to the loading, the present model cannot simulate the complete effect of nutrient load reduction on the DO concentration in the estuary. Further research and more complete data are needed

A systematic calibration procedure has been developed for a more efficient and more objective calibration of the water quality model. A consistent framework for systematic calibration is formulated, which include in the following steps: model parameterization, selection of calibration parameters, and formulation of calibration criteria.

CHAPTER 1
INTRODUCTION

Charlotte Harbor (Figure 1.1) is a shallow estuarine system in southwest Florida. The estuary receives freshwater from the Caloosahatchee, Peace, and Myakka Rivers; is connected to the Gulf of Mexico through the Boca Grande Pass, Gasparilla Pass, Captiva Pass, Blind Pass, and San Carlos Bay; and provides water resources for several counties in Southwest Florida. Charlotte Harbor is dominated by rivers that flow into the coastal area. While most estuaries in Southwest Florida are influenced by the Gulf of Mexico, the characteristics of the Charlotte Harbor system are strongly influenced by large rivers such as the Caloosahatchee and Peace Rivers. Large fluctuations of river flow between wet and dry seasons strongly affect the salinity and water characteristics in Charlotte Harbor (Estevez, 1998).

Population growth and development in the surrounding areas during the past few decades have led to concerns over human impacts on the quality of the estuarine system. Industrial and agriculture development also increase environment pollution. Growth and development will cause an increased demand for fresh water and a corresponding increase in urban, agricultural, and industrial waste. The inflow of freshwater is essential to the integrity and health of the estuarine system. Increased freshwater withdrawal or diversion, or increased wastewater discharges to the rivers and streams that flow into the estuary will create environmental stress in the estuary (McPherson et al., 1996).

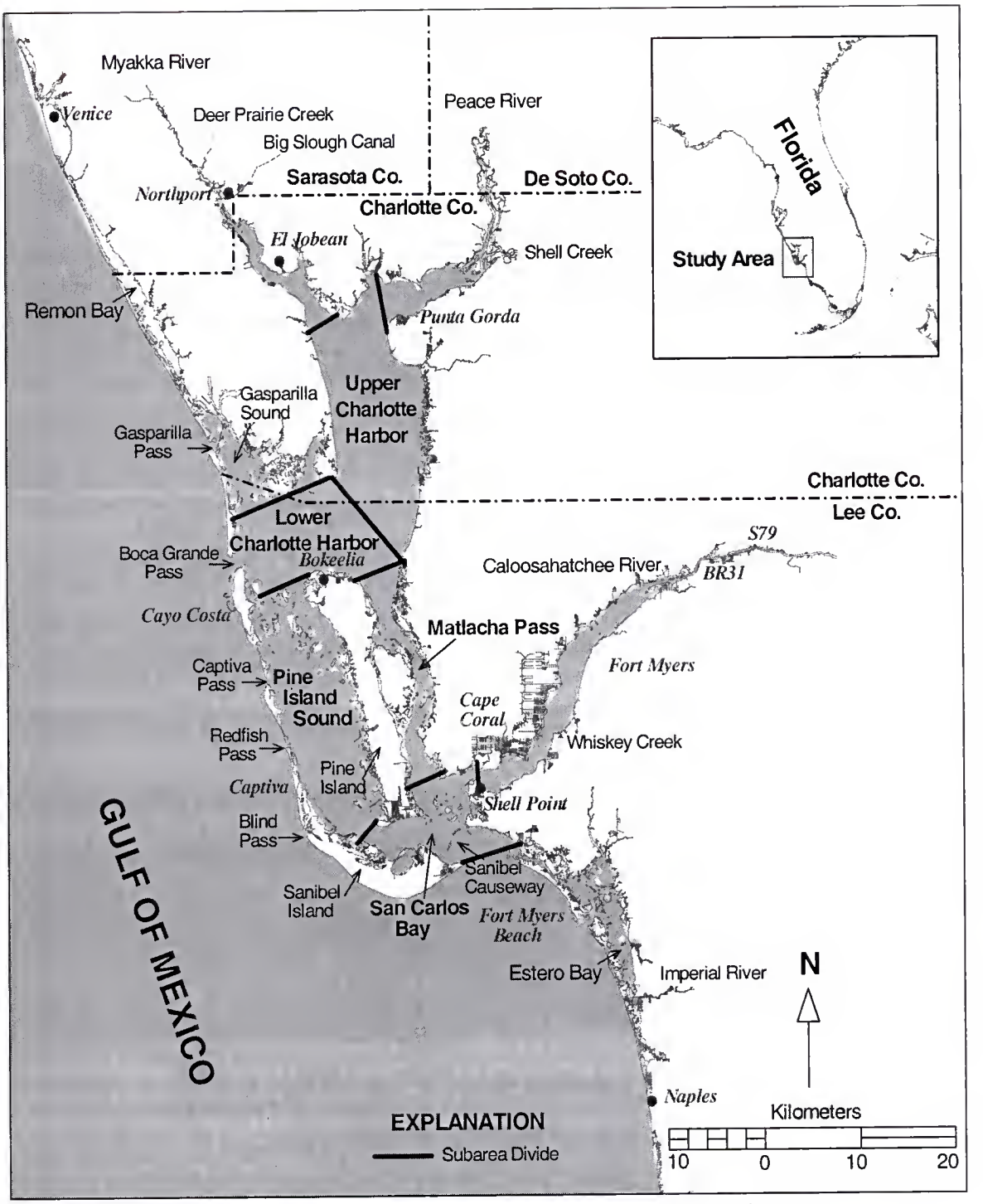

Figure 1.1 Charlotte Harbor estuarine system and its subarea boundaries

Water quality in the southern Charlotte Harbor estuarine system (the Caloosahatchee Estuary, San Carlos Bay, and Pine Island Sound) appear to be influenced by freshwater discharge from the Franklin Lock and Dam, also known as United States Army Corps of Engineers Structure Number 79 (S-79). Waste load allocation studies conducted by the Florida Department of Environmental Regulation (Degrove, 1981; Degrove, and Nearhoof, 1987; Baker, 1990) concluded that the Caloosahatchee Estuary had reached its nutrient loading limits as indicated by elevated chlorophyll-a and depressed dissolved oxygen (DO) levels. Similarly, McPherson and Miller (1990) concluded that increased nitrogen loading would result in undesirable increases in phytoplankton and benthic algae. In order to effectively manage the loading of pollutants such as nutrients in a shallow estuary such as Charlotte Harbor, and control eutrophication, it is necessary to have a quantitative understanding of the transport and transformation processes of nutrients in system.

Increased nutrient loading from tributaries, the atmosphere, and bottom sediments have been known to cause eutrophication in estuaries. Eutrophication varies both spatially and temporally. Eutrophication does not necessarily occur in regions with high nutrient loading because the circulation and sediment dynamics affect nutrient fate and transport. In the Upper Charlotte Harbor where a pycnocline develops frequently during high river flow conditions, hypoxia usually develops within two days of the formation of the pycnocline, when coupled with significant sediment oxygen demand (SOD) (CDM, 1998). In fact, hypoxia can occasionally extend all the way to the Boca Grande area. This strong linkage between hydrodynamics and water quality dynamics suggests the importance of having a comprehensive understanding of hydrodynamics.

Nutrient dynamics in estuaries are not only determined by biological and chemical

processes, but is also strongly affected by weather and climate (wind, air temperature, etc.), hydrodynamics (wave, tide, current, turbulence mixing, etc.), and sediment transport processes (resuspension, deposition, flocculation, etc.). In this study, integrated modeling of the system is conducted to understand the complex water quality processes, which are strongly linked to hydrodynamics and sediment processes. The primary objective of this study is to use models and field data to produce a detailed characterization of hydrodynamics, sediment, and water quality dynamics within the Charlotte Harbor estuarine system.

The Chesapeake Bay model (Cerco and Cole, 1994) and Moreton Bay model (McEwan and Garbric, 1998) are coupled hydrodynamics-water quality models. These coupled models are more suitable for managing nutrient loads and predicting eutrophication-related problems than uncoupled models. Because these models were not coupled with a dynamic model for sediment transport, however, they could not accurately consider sediment-process effects such as resuspension, deposition, flocculation, and settling on nutrient dynamics in estuaries. Therefore, these loosely coupled models cannot account for nutrient release by sediments in episodic events (Chen and Sheng, 1994)

Chen and Sheng (1994) developed a coupled hydrodynamic-sediment-water quality model and applied it to Lake Okeechobee. Their 3-D model includes a hydrodynamic model, a sediment transport model, and a water quality model with a nitrogen and a phosphorous cycle on a rectangular grid. Measured nitrogen and phosphorous dynamics during episodic events in 1993 and monthly sampling events in 1989 were accurately simulated with absorption-desorption reactions and the exchange of nutrients between the sediment and water column.

While Chen and Sheng (1994) developed a rectangular grid model, Yassuda and Sheng (1996) developed an integrated model in curvilinear grids and applied it to Tampa Bay. Their water quality model, based on the Chen and Sheng (1994) model, includes a nitrogen cycle and an oxygen cycle, but not a phosphorous cycle. Zooplankton distribution is allowed to influence the phytoplankton dynamics. Their integrated model also includes a wave model, a light model, and a seagrass model. Although Yassuda and Sheng (1996) simulated the observed hypoxia in Tampa Bay during 1991, their model did not include dynamic fluxes of oxygen at the air-sea interface (re-aeration) and the sediment-water interface (sediment oxygen demand). Their model could not simulate the daily fluctuation and vertical stratification of DO. Although the phytoplankton growth rate in their model is controlled by temperature and light, it is difficult to reproduce the vertical distribution of phytoplankton because the temperature is not simulated. The light model in Yassuda and Sheng (1996) has not been sufficiently validated with Tampa Bay data, thus limiting the predictability of their model for vertical distribution of phytoplankton and dissolved oxygen. Their model could not produce the low dissolved oxygen phenomena in upper Charlotte Harbor because there are no dissolved oxygen fluxes at the air-water and sediment-water interfaces, such as reaeration and sediment oxygen demand (SOD).

Sheng (2000) developed the framework for an integrated modeling system: CH3D-IMS (http://ch3d.coastal.ufl.edu). The integrated modeling system (Table 1.1) is based on the curvilinear-grid hydrodynamic model CH3D (Sheng, 1987, 1989; Sheng et al., 2002) and also includes a wave model, a sediment transport model (Sheng et al., 2002a), a water quality model, (Sheng et al., 2001b), a light attenuation model (Sheng et al., 2002c, Christian and Sheng, 2003), and a seagrass model (Sheng et al., 2002d). Sheng et al. (2002) applied the

CH3D-IMS to the Indian River Lagoon (IRL), Florida. The water quality model (Sheng et al., 2001b) includes a nitrogen cycle, a phosphorous cycle, a phytoplankton cycle, and a DO cycle. The CH3D-IMS was validated with comprehensive data collected from the IRL.

Table 1.1 Component Models of the CH3D-IMS

Component Model	*Model Name*
Hydrodynamic Model Flow Model Salinity Transport Model	CH3D
Wave Model	SMB
Sediment Transport Model	CH3D-SED3D
Water Quality Model Dissolved Oxygen Model Phytoplankton and zooplankton Model Nitrogen Model Phosphorous Model	CH3D-WQ3D
Light Attenuation Model	CH3D-LA
Seagrass Model	CH3D-SAV

The CH3D-IMS was able to successfully simulate the observed circulation, wave, sediment transport, water quality, light attenuation, and seagrass biomass in IRL during 1998. However, several aspects of the model were identified for further improvement. For example, although a temperature model was developed during the later phase of the IRL study, it was not sufficiently validated with data. The water quality model, while capable of simulating the annual variation in DO, could not simulate the diurnal DO variation.

In this study, the CH3D-IMS is enhanced and used to study the circulation and water quality dynamics in the Charlotte Harbor estuarine system. The validated model will be used to determine minimum flow and level and pollutant load reduction goal by management agencies. Specially, the CH3D-IMS used for this study includes the simulation of

temperature in addition to the flow and salinity simulations. An air-sea heat flux model is implemented along with the temperature equation. The water quality model is enhanced to include a re-aeration model and a sediment oxygen demand (SOD) model, such that hypoxia and daily fluctuation and vertical stratification of DO can be simulated. Moreover, the same basic light attenuation model developed for the IRL is used for this study.

Although the factors that cause hypoxia have not been positively identified, it is generally accepted that hypoxia is related to strong stratification caused by high freshwater inflow. The modified CH3D-IMS is used in this study to examine the major factors of the observed hypoxia in 2000, including freshwater inflow, tidal variation, SOD, water column oxygen consumption, and DO reaeration.

This study includes the following objectives:

- To validate the CH3D-IMS with extensive hydrodynamic and water quality data from Charlotte Harbor,
- To improve the simulation of dissolved oxygen processes, including the observed daily dissolved oxygen fluctuation, and hypoxia in bottom water during high flow event with vertical stratification,
- To validate the ability of temperature model and heat flux model to simulate seasonal and spatial temperature distribution in Charlotte Harbor,
- To apply the physics-based light attenuation model to improve Charlotte Harbor simulations, and
- To demonstrate the feasibility of the validated modeling system for simulating the effects of various anthropogenic impacts on the Charlotte Harbor estuarine system.

More specifically, the objectives of my research are to:

- Reproduce observed circulation and transport dynamics in 1986 and 2000,
- Reproduce observed water quality dynamics in 1996 and 2000,
- Investigate the effect of the Sanibel causeway islands and IntraCoastal Waterway on the flow, salinity, and water quality distribution in San Carlos Bay and Pine Island

Sound,

- Reproduce the main factors for bottom water hypoxia and habitat loss in Charlotte Harbor estuarine system,
- Provide a preliminary determination of pollutant load reduction goal (PLRG) and minimum flow and levels (MFL),
- Perform sensitivity tests to quantify the influence of each model parameter and to determine the most sensitive parameters and most plausible parameter set, and
- Establish a systematic calibration procedure.

To achieve these goals, the characteristics of Charlotte Harbor estuarine system are presented in Chapter 2. Chapter 3 discusses the general hydrodynamic circulation and transport of temperature, salinity, and sediment in the estuarine system. This chapter will include initial and boundary conditions for the hydrodynamic and transport models. As an air/sea interface boundary condition, a heat flux model is also presented in this chapter. Chapter 4 describes the water quality processes and models of phytoplankton, zooplankton, nitrogen, phosphorous, dissolved oxygen, and light attenuation processes in estuarine system. The effects of temperature and light intensity, numerical solution technique, and model parameters and calibration procedure are also discussed in this chapter. Chapter 5 presents hydrodynamic field data and model simulations of hydrodynamics in Charlotte Harbor estuarine system. These model simulations include model calibration and verification of 1986 and 2000 data, simulation of the effect of causeway islands and navigation channel, and determination of minimum flow and levels (MFL). Chapter 6 presents water quality and sediment field data and model simulations of circulation, sediment transport and water quality processes in the study area. These model simulations include calibration and verification of 1996 and 2000 data and determination of pollutant load reduction goal (PLRG). Discussions and conclusions are presented in Chapter 7.

CHAPTER 2
CHARLOTTE HARBOR CHARACTERIZATION

Charlotte Harbor, a coastal-plain estuarine system is one of the largest estuarine systems on the southwest florida coast and is an important part of the Gulf of Mexico watershed. It is located on the southwest corner of the Florida peninsula, between 26° 20' and 27° 10'N and 81° 40' and 82° 30' W. As shown in Figure 1.1, the Charlotte Harbor estuarine system is sub-divided into Upper Charlotte Harbor, Lower Charlotte Harbor, Pine Island Sound, Matlacha Pass, San Carlos Bay, Gasparilla Bay, Peace River, Myakka River and Caloosahatchee River. The drainage area (Figure 2.1) consists of the Peace, Myakka, and Caloosahatchee River Watersheds and the coastal area and islands that drain directly into the harbor. The estuary has a surface area of 648 km^2, a drainage area of a more than 10000 km^2, and a average depth of 2.1 m. The upper harbor has an average depth of 2.6 m, and the lower harbor has an average depth of 1.6 m (Stoker, 1986). The estuary is separated from the Gulf of Mexico by barrier islands and is connected to the Gulf through two major inlets: Boca Grande and San Carlos; and through several smaller passes: Gasparilla, Captiva, Redfish (McPherson et al., 1996).

In 1995, the Charlotte Harbor National Estuary Program (CHNEP) was established by U.S. Environmental Protection Agency (USEPA) and the State of Florida. In its planning documents, CHNEP identified three draft major problems: (1) hydrologic alterations, (2) nutrient enrichment, and (3) habitat loss. In order to address these problems, it is useful to

have a comprehensive understanding of the climate, hydrodynamics, sediment properties, and biological and chemical characteristics of the system.

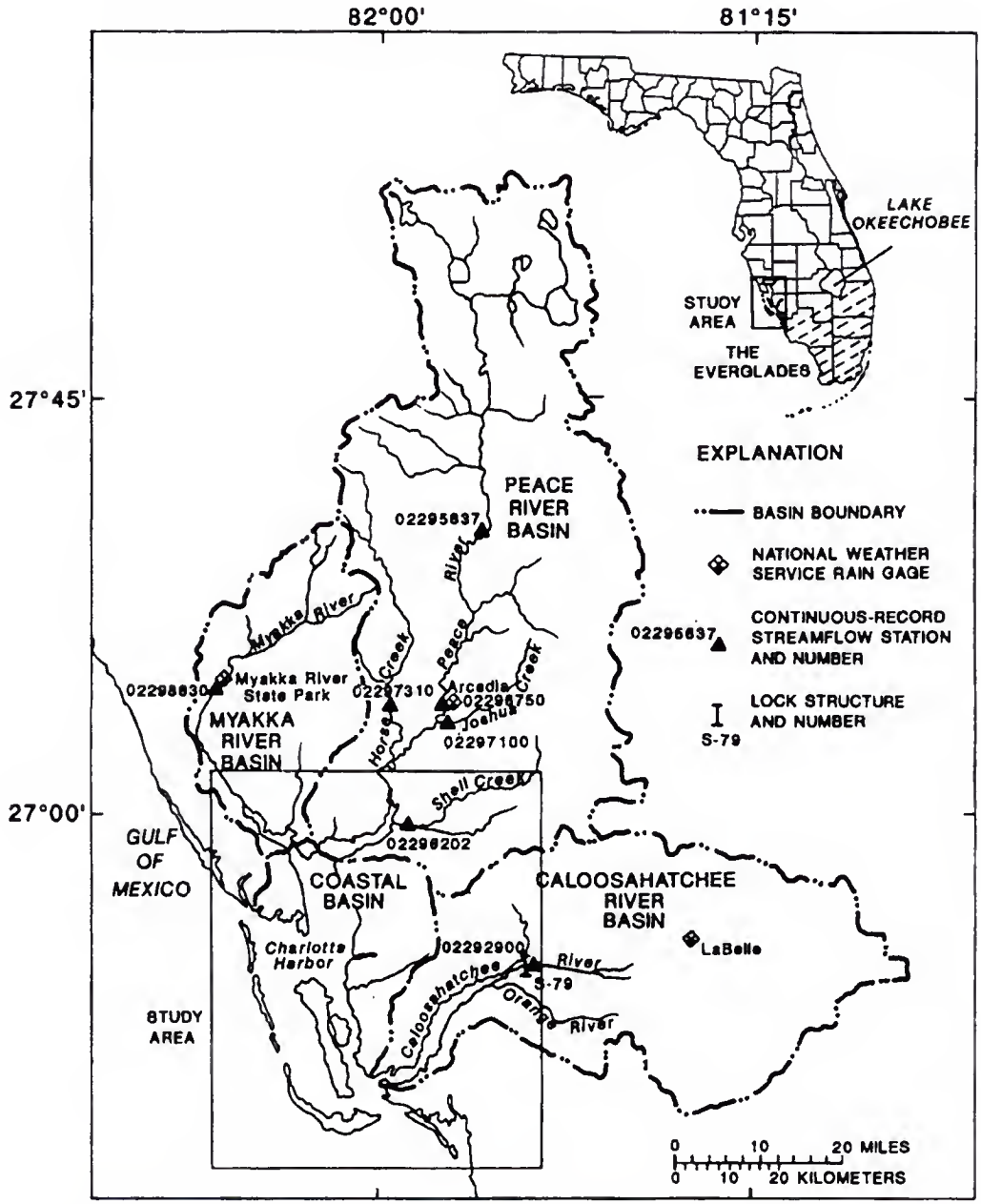

Figure 2.1 Drainage basins of Charlotte Harbor estuarine system (Stoker, 1992)

2.1 Climate

The climate of the Charlotte Harbor estuarine system is subtropical and humid. The mean annually average temperature is 72 °F, with low mean of 60°F in December and January and a high mean of 80 °F during the summer (McPherson et al., 1996).

Annual rainfall averages 132 cm, of which more than half occurs from June through September, during local thundershowers and squalls. Rain during the fall, winter, and spring seasons is usually the result of large frontal systems and tends to be more broadly distributed than rain associated with local thunderstorms and squalls. The period from October through February is characteristically dry, with November usually being the driest month. The months of April and May also are characteristically dry. Low rainfall in April and May coincides with high evaporation and generally results in the lowest streamflow, lake stage, and ground-water levels of the year (Hammett, 1990).

The annual average wind speed is 3.9 m/s from the east. Four typical seasonal wind-field patterns are shown in Figure 2.2. In the Winter months, the easterly trade winds dominate the region south of latitude 27° N, while the westerlies dominate the area north of latitude 29°N. Spring and Summer generally exhibit more southerly winds, and Fall is characterized by easterly or northeasterly winds. Wind speed can exceed 10 m/s during the passage of Winter storms or during Summer squalls, hurricanes and tornadoes (Wolfe and Drew, 1990).

2.2 Hydrodynamics

The hydrodynamic behavior of the Charlotte Harbor estuarine system is affected by physical characteristics (bathymetry and geometry) as well as weather, climate, and oceanographic and hydrologic characteristics, such as wind, atmosphere heating and cooling,

evaporation and precipitation, tidal-stage oscillations, discharge through tidal inlets, tidal velocity, and freshwater inflow.

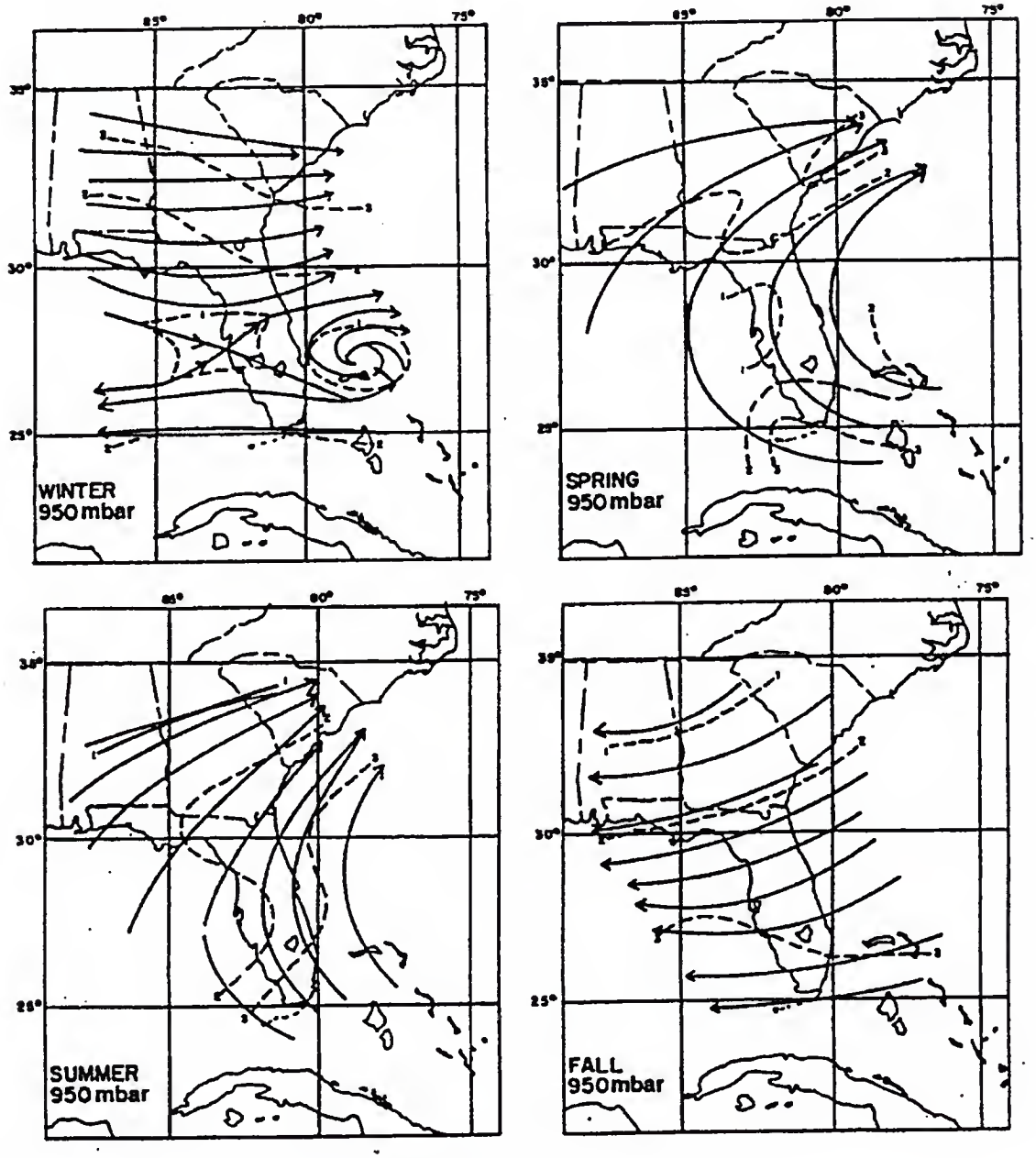

Figure 2.2 Seasonal wind pattern in Florida (Echternacht, 1975)

2.2.1 Tidal Stage, Discharge at Inlet, and Tidal Circulation

Tides along the Gulf coast of West-Central Florida in the vicinity of Charlotte Harbor have a range of 30 to 140 cm and are of the mixed type with both diurnal and semidiurnal characteristics (Goodwin and Michaelis, 1976). Spring tides, which have the largest range, sometimes have only a diurnal fluctuation, whereas neap tides, which have the smallest range, approach semidiurnal conditions of two nearly equal high and low water levels per day.

The boundary between the Charlotte Harbor estuarine system and the Gulf of Mexico extends about 40 mi from Gasparilla Pass on the north to San Carlos Pass on the south. Tidal characteristics in the Gulf of Mexico are nearly uniform from Gasparilla Island to the western face of Sanibel Island, but are of a larger range off the southern shore of Sanibel Island (Goodwin, 1996).

Circulation in the system is primarily driven by Gulf tides, entering the system through San Carlos Pass, Boca Grande Pass, Captita Pass, Redfish Pass, Gasparilla Pass and Blind Pass. San Carlos Pass has a maximum depth of 5.3 m and a width of 3.3 km; Boca Grande Pass has a maximum depth of a 18.3 m and a width of 1.28 km. The discharge through Boca Grande Pass is about twice the discharge through San Carlos Bay and three to four times the discharge through Captiva and Redfish Passes (Goodwin, 1996). The geometric narrowing that occurs at passes focuses tidal energy, resulting in high velocities associated with the large volume of water moving through the pass. This tidal energy is dispersed inside the harbor and influences the harbor and tidal rivers as much as 40 to 44 km upstream from the Peace River mouth. There is about a 2-hour lag between tide phases at Boca Grande and tide phase in the upper harbor near the mouth of the Peace River (Stoker,

1992). Tide and wind keep the water column well mixed in the southern part of the estuary. In the northern part of the estuary, vertical stratification can develop during moderate to high fresh water inflows and can persist for weeks after a high freshwater inflow event (Sheng, 1998).

2.2.2 Freshwater Inflow

The majority of the freshwater that enters Charlotte Harbor come from the Myakka River, Peace River and Caloosahatchee River. Average flows are 17.8 m^3/s, 56.9m^3/s and 56.7 m^3/s, respectively. Flows in the Myakka and Peace Rivers are largely unregulated, while flow in the Caloosahatchee is controlled by operation of the Franklin Lock about 43 km upstream from the mouth. Discharge in the Peace and Myakka Rivers tend to peak in August and September when rainfall totals are generally the greatest. Discharges are usually lowest in April and May (Stoker, 1992). The Caloosahatchee River discharge does not always correspond to rainfall patterns in the basin, since it is controlled by S-79.

Analyses of long-term streamflow trends in the Charlotte Harbor area have indicated statistically significant decreases in streamflow at several gages in the Peace River basin from 1931 to 1984 (Hammett, 1990). The long-term decrease in streamflow of the Peace River is probably related to the increased use of ground water and subsequent decline of the potentiometric surface of the upper Florida aquafer (Hammett, 1990). A sustained significant reduction in streamflow could result in an increase of salinity in Upper Charlotte Harbor, possibly approaching the Gulf of Mexico salinity (Sheng, 1998). The impact of freshwater reduction is of major ecological and economic significance.

2.2.3 Salinity

As in any other typical estuarine system, Charlotte Harbor generally exhibits

significant horizontal gradients in salinity. The higher salinity values in the adjacent Gulf of Mexico fluctuate around 36 ppt, whereas the lower salinity levels nearly zero in wet season occur near the mouth of creeks and rivers. Seasonal changes in salinity occur primarily in response to changes in freshwater inflow from the Peace, Myakka, and Caloosahatchee River basins. Other sources of freshwater, including direct rainfall, runoff form coastal areas, ground-water seepage, and domestic influence, have smaller and usually more local effects on salinity in the estuary (McPherson et al., 1996).

Stoker (1992) described salinity characteristics in the system based on data collected from June 1982 to May 1987. Salinity generally is the lowest during the wet season between July and September, and is the highest during the dry season from January through March. Salinity also varies daily in response to tidal fluctuation. Peak salinity is near the flood-tide stage, and lowest salinity is near the ebb-tide stage.

Due to the shallow depth and because of significant vertical mixing, salinity is generally not stratifed in the southern part of the estuary. Vertical salinity stratification in the Upper Charlotte Harbor is a common seasonal occurrence (Environmental Quality Laboratory, Inc., 1979). In high river inflow events, a stable vertical salinity gradient is created which suppresses vertical mixing unless there are sufficient mixing by wind or tide.

2.3 Water Quality

Water quality refers to the condition of water (e.g., dissolved oxygen concentration, chlorophyll concentration, light attenuation, etc.) relative to legal standard, social expectations or ecological health. Overall, water quality in the Charlotte Harbor estuarine system is fair or good, but some areas have poor water quality or declining trends (Estevez, 1998). The water quality of an estuary is strongly influenced by hydrodynamic processes

(e.g., circulation and flushing), and chemical and biological processes (e.g., ammonification, mineralization, decomposition, algae uptake, excretion, and mortality, etc.) in the estuary and basin.

Color levels and concentrations of nitrogen, phosphorous and chlorophyll-a in Charlotte Harbor exhibit pronounced salinity-related gradients which extend from the head of the estuary to its mouth (Morrison, 1997). The water quality in the Caloosahatchee system is more degraded than the water quality in the Myakka or Peace systems. Oxygen depletion is common upstream of Franklin Lock. Nutrient and chlorophyll levels are high, and algal blooms occur regularly in the tidal river (Estevez, 1998).

2.3.1 Nutrients

Nutrient availability is a key factor in the regulation of primary productivity in estuarine and coastal water (Ketchum, 1967). Increased nutrient loads related to the urban development of coastal basins have been implicated in estuarine nutrient enrichment, increased phytoplankton productivity, and incresed phytoplankton biomass (Jaworski, 1981), and in declines of seagrass communities (Orth and Moore, 1983).

The distribution of nutrients in the system is mainly the result of nutrient input from rivers, freshwater and tidal flushing, and recycling processes in the estuary (McPherson and Miller, 1990). The major factor that influences estuarine nutrient distribution is freshwater inflow from rivers, which contributes substantial nutrient loads and flushes nutrients seaward. NOAA estimates that Charlotte Harbor receives about 2,500 tons of nitrogen as total Kjeldahl nitrogen, or TKN, and 1,000 tons of phosphorous per year. Relative to its dimensions and flushing characteristics, phosphorous loads are high, signifying a nitrogen limited system (Estevez, 1986).

Molar ratios of dissolved inorganic nitrogen to dissolved inorganic phosphorous were below the Redfield ratio of 16, averaging 5.7 at Caloosahatchee River during two sampling periods, which are from 1985 to 1989 and from 1994 to 1995 (Doering and Chamberlain, 1997). By contrast, total nitrogen to total phosphorous ratios were above 16, averaging 35 in Caloosahatchee River. With these results, dissolved inorganic N:P ratios (<16) suggest that nitrogen could limit phytoplankton productivity in agreement with McPherson and Miller (1990), while total N:P ration (>16) indicated that phosphorous could limit productivity (Doering, 1996). In fact, nutrient addition studies conducted by FDER found N and P to be co-limiting (Degrove, 1981)

The distributions of phosphorous in the system were nearly conservative and a function of river phosphorous concentration, flow, and physical mixing (McPherson and Millor, 1990). A large amount of phosphorous from the watershed is carried by freshwater discharge into the tidal reaches of the Peace River, with subsequent dilution by the lower-nutrient seawater entering the estuary from the Gulf of Mexico. Concentrations of total phosphorous averaged about 0.08 mg/L in Pine Island Sound, 0.15 mg/L in the tidal Caloosahatchee River, and 0.62 mg/L in the tidal Peace River according to USGS nutrient data from 1982 to 1989 (McPherson and Miller, 1990).

Most of the nitrogen in the rivers and estuary is organic nitrogen (McPherson and Miller, 1990). Organic nitrogen concentrations decreased over the salinity gradient, indicating river input as a source. The relatively low concentrations of inorganic nitrogen could limit plant growth in the estuary (McPherson and Miller, 1990). Ratios of nitrogen and phosphorous constituents at the Peace River, Myakka River, and Upper Charlotte Harbor determined by USGS nutrient data during 1975 through 1990 are shown in Table 2.1 (Pribble

et al., 1998)

Table 2.1 Ratios of nitrogen and phosphorous constituents (Pribble et al., 1998)

RATIO	Peace River	Myakka River	Upper Harbor
NH3 : TN	0.0327	0.0349	0.0338
NO3 : TN	0.4378	0.0505	0.2442
ON : TN	0.5614	0.9096	0.7355
PO4 : TP	0.9384	0.9371	0.9361
OP : TP	0.0616	0.0683	0.0650

Concentrations of ammonia were highly variable along the salinity gradient and were in about the same range as concentrations in the rivers (McPherson and Miller, 1990). Ammonia concentrations increased in the deeper water of Charlotte Harbor during summer (Fraser, 1986). Ammonia enrichment probably was related to density stratification and to low concentrations of dissolved oxygen in bottom waters (McPherson et al, 1996). Concentrations of nitrate and nitrite nitrogen were nonconservative and decreased sharply along the salinity gradient (McPherson and Miller, 1990). The sharp decline of the nitrate and nitrite nitrogen in the low salinity regions indicates a substantial removal of nitrogen from the water column due to biological uptake.

2.3.2 Dissolved Oxygen

Dissolved oxygen is critical for survival of plants and animals in fresh and salt water, and a major constituent of interest in water quality study. Dissolved oxygen concentrations in the near surface water of the system ranged from about to 6 to 8 mg/L during daylight sampling in 1982 - 84 (Stoker, 1986). Dissolved oxygen concentrations of near bottom water of the estuary generally are lower than near surface concentrations.

Bottom water hypoxia (dissolved oxygen $\leq$2 mg/L) in Charlotte Harbor has been reported periodically by the Environmental Quality Laboratory (EQL) since 1975 (Heyl,

1996). Dissolved oxygen concentrations were measured monthly from 1976 to 1984 in the river mouth of Peace River near Punta Gorda (CH-006) (Fraser, 1986). The average monthly near-surface concentrations declined from 8.5 to 6.7 mg/L from January to July and then began to rise (Figure 2.3). Near-bottom average monthly concentrations at this area were highest in February, declined slowly through May, and then declined more rapidly until July (Fraser, 1986). The hypoxia conditions during summer are attributed to strong stratification, which cause restricted reaeration, and to SOD. After breakup of the stratification, the concentration increased from October to December.

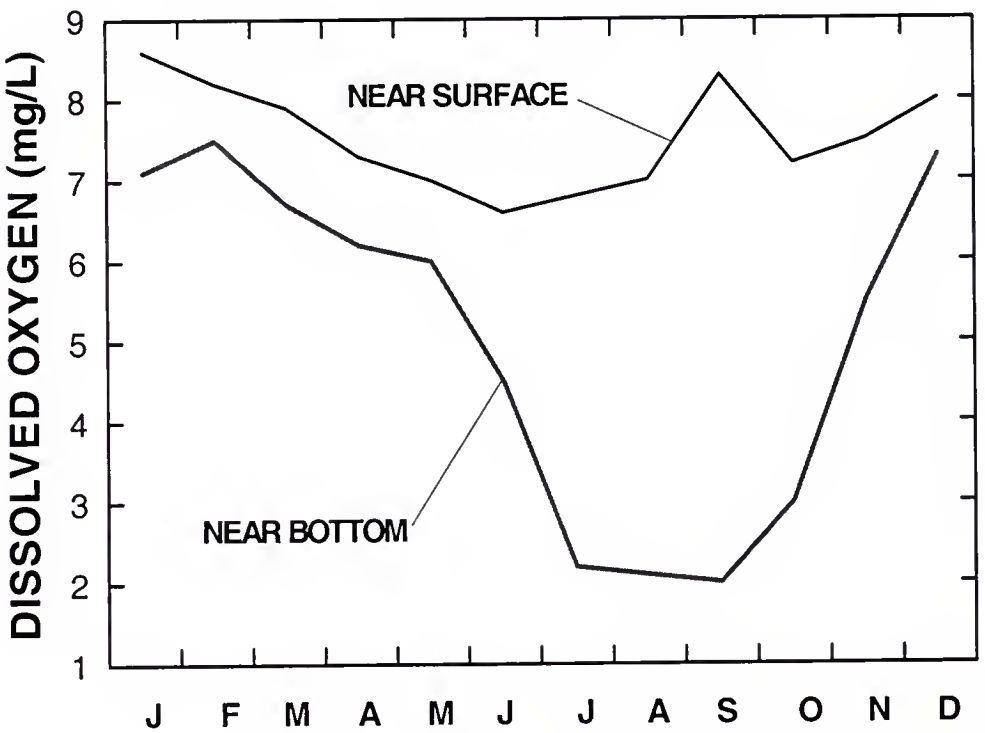

Figure 2.3 Average monthly concentration of dissolved oxygen in upper Charlotte Harbor, site CH-006, 1976-84 (Fraser, 1986)

2.3.3 Phytoplankton

Phytoplankton is an important component of water quality processes and a major primary producer in coastal and estuarine waters. The temporal and spatial variability of

phytoplankton productivity and biomass in Charlotte Harbor have been investigated by Environmental Quality Laboratory, Inc (EQL) (1987). Phytoplankton productivity and biomass (as *chlorophyll_a*) in the system are relatively low most of time. Productivity ranged from 5 to 343 (mgC/m^3)/h and averaged 59 (mgC/m^3)/h from 1985 to 1986 (McPherson et al., 1990). *Chlorophyll_a* concentrations ranged from 1 to 46 mg/m^3 and averaged 8.5 mg/m^3. Both productivity and biomass were greater during summer near the mouth of tidal rivers which has middle range salinity of 6 to 12 ppt (McPherson et al., 1990).

Phytoplankton productivity and biomass in the system are affected by freshwater inflow that lowers salinity, increases nutrient availability, and reduces light penetration in the water column. The nutrient rich colored water is diluted by seawater at middle range salinity of 10 to 20 ppt, so that availability of light increases and sufficient nutrient concentrations remain available from runoff, to stimulate productivity and growth of phytoplankton in these areas (McPherson et al., 1990). Of the major nutrients for phytoplankton productivity, inorganic nitrogen is in lowest supply and most critical in limiting phytoplankton productivity and growth in the system (Fraser and Wilcox, 1981).

The composition of the phytoplankton in the system varied with location and season (McPherson et al., 1990). Diatoms were dominant in 55 % of 289 phytoplankton samples collected in the system between 1983 and 1984, cryptophytes in 35 %, cyanophytes (blue-green algae) in about 6 %, dinoflagellates in about 4 %, and other classes in 1 % (McPherson et al., 1996).

2.4 Sediment

Sediment quality data from Charlotte Harbor are scarce. Organic carbon, nitrogen and phosphorous data exist in only two studies. Hwang (1966) obtained data in 1965 from

119 stations throughout the study area. The FDEP Coastal Sediment Contaminant Survey obtained carbon, nitrogen phosphorous, and metal data in the sediment column from 33 stations during 1985 through 1989, in all areas except the Gulf of Mexico (Sloane, 1994). Mean carbon/nitrogen ratios in the six different areas of Charlotte Harbor ranged from 8.9 at Lower Charlotte Harbor to 16.4 at Gasparilla Sound (Schropp, 1998). Despite data limitation, the available data indicate that Charlotte Harbor is relatively free of sediment contamination in comparison with Tampa Bay and Biscayne Bay, where sediment contaminations are widespread and are present in higher concentrations (Schropp, 1998).

2.5 Light Environment

The amount of photosynthetically active radiation (PAR) in natural water is fundamentally important in determining the growth and vigor of aquatic plants (McPherson et al., 1996). Light is reflected, absorbed, and refracted by dissolved and suspended substances in the water column, and by water itself. The controlling factors are chlorophyll-a, dissolved substances, and non-algal particulate matter (Christian and Sheng, 2003).

Dissolved and suspended matter are the major causes of light attenuation in the system: phytoplankton and chlorophyll-a are generally minor causes of attenuation (McPherson and Miller, 1990). On average, non-chlorophyll suspended matter accounted for 72% of light attenuation, dissolved organic matter (color) accounted for 21%, phytoplankton chlorophyll for 4%, and water for the remaining 3% (McPherson et al., 1996). Water color can cause light attenuation at tidal rivers because the source of the water color is terrestrial dissolved organic matters. Dissolved organic matter has little effect on light attenuation in much of the southern part of the estuary, where suspended matter is the major cause of light attenuation (McPherson and Miller, 1996). The source of suspended matter

includes the bottom of the estuary, which consisted of very fine to fine sand (Hwang, 1966) and organic detrital-material (McPherson and Miller, 1990), and the major rivers.

CHAPTER 3
HYDRODYNAMICS AND SEDIMENT TRANSPORT MODEL

Biological processes in an estuarine system are strongly affected by hydrodynamics and sediment transport processes. Therefore, as the first step to study nutrient cycling in an estuary, hydrodynamics and sediment transport processes must be investigated and understood.

The three-dimensional hydrodynamics model CH3D (Sheng et al., 2001) and the associated sediment transport model CH3D-SED3D (Sheng et al., 2000a) are used for numerical simulations in this study. The model framework has been improved and modified from earlier versions in order to develop an integrated model that couples hydrodynamics, sediment and water quality dynamics. The code of the enhanced integrated model is optimized to achieve more efficient coupling and more systematic structure. The detail structure of enhanced model is explained in Appendix A as flow chart. The application of the circulation and transport model to produce a detailed characterization of hydrodynamics within system is the first step in the development of the integrated model of the system.

The CH3D model for Tampa Bay and Indian River Lagoon did not include the simulation of temperature distribution. In this study, the temperature field is simulated by solving the temperature equation with an air-sea interface boundary condition. Temperature is an important factor for baroclinic circulation and water quality processes, in which almost all reaction parameters in the nutrient cycle are a functions of temperature. Therefore,

improved simulation of temperature is expected to produce more accurate baroclinc and water quality simulations.

3.1 Governing Equation

Hydrodynamics and sediment transport processes in estuaries are complicated, three-dimensional and time-dependent. Mathematical descriptions of these processes generally require simplifying assumptions.

3.1.1 Hydrodynamic Model

The governing equations that describe the velocity and surface elevation fields in shallow water are derived from the Navier-Stokes equations. In general, four simplifying approximations are applied: 1) the flow is incompressible, which results in a simplified continuity equation, 2) the horizontal scale is much larger than the vertical scale such that the hydrostatic pressure distribution is valid, 3) the Boussinesq approximation can be used to simplify the treatment of the baroclinic terms, 4) the eddy-viscosity concept, which assumes that the turbulent Reynolds stresses are the product of mean velocity gradients and "eddy viscosity", can be employed. With the above assumptions, the continuity equation and x- and y- momentum equations have the following form (Sheng, 1983):

$$\frac{\partial u}{\partial x}+\frac{\partial v}{\partial y}+\frac{\partial w}{\partial z}=0 \tag{3.1}$$

$$\frac{\partial u}{\partial t}+\frac{\partial uu}{\partial x}+\frac{\partial uv}{\partial y}+\frac{\partial uw}{\partial z}=-g\frac{\partial \zeta}{\partial x}+fv+A_H\left(\frac{\partial^2 u}{\partial x^2}+\frac{\partial^2 u}{\partial y^2}\right)+\frac{\partial}{\partial z}\left(A_V\frac{\partial u}{\partial z}\right) \tag{3.2}$$

$$\frac{\partial v}{\partial t}+\frac{\partial vu}{\partial x}+\frac{\partial vv}{\partial y}+\frac{\partial vw}{\partial z}=-g\frac{\partial \zeta}{\partial y}-fu+A_H\left(\frac{\partial^2 v}{\partial x^2}+\frac{\partial^2 v}{\partial y^2}\right)+\frac{\partial}{\partial z}\left(A_V\frac{\partial v}{\partial z}\right) \tag{3.3}$$

where $u(x,y,z,t)$, $v(x,y,z,t)$, $w(x,y,z,t)$ are the velocity components in the horizontal x- and y-directions, and vertical z-direction; t is time; $\zeta(x,y,t)$ is the free surface

elevation; g is the gravitational acceleration; and A_H and A_V are the horizontal and vertical turbulent eddy coefficients, respectively.

In Cartesian coordinates, the conservation of salt and temperature can be written as

$$\frac{\partial S}{\partial t}+\frac{\partial uS}{\partial x}+\frac{\partial vS}{\partial y}+\frac{\partial wS}{\partial z}=\frac{\partial}{\partial x}\left(D_H\frac{\partial S}{\partial x}\right)+\frac{\partial}{\partial y}\left(D_H\frac{\partial S}{\partial y}\right)+\frac{\partial}{\partial z}\left(D_V\frac{\partial S}{\partial z}\right) \qquad (3.4)$$

$$\frac{\partial T}{\partial t}+\frac{\partial uT}{\partial x}+\frac{\partial vT}{\partial y}+\frac{\partial wT}{\partial z}=\frac{\partial}{\partial x}\left(K_H\frac{\partial T}{\partial x}\right)+\frac{\partial}{\partial y}\left(K_H\frac{\partial T}{\partial y}\right)+\frac{\partial}{\partial z}\left(K_V\frac{\partial T}{\partial z}\right) \qquad (3.5)$$

where S is salinity; T is temperature; D_H and K_H are the horizontal turbulent eddy diffusivity coefficients for salinity and temperature, respectively; and D_V and K_V are the vertical turbulent eddy diffusivity coefficients for salinity and temperature, respectively.

Since the length scales of horizontal motion in estuarine systems are much greater than those of vertical motion, it is common to treat vertical turbulence and horizontal turbulence separately. In shallow estuaries, the effect of the horizontal eddy viscosities on circulation are much smaller than the effect of the vertical eddy viscosity, although the horizontal eddy viscosity is typically 2-3 orders of magnitude larger than the vertical eddy viscosity.

Vertical turbulent mixing is an important process, which can significantly affect circulation and transport in an estuary. Since turbulence is a property of the flow instead of the fluid, it is essential to use a robust turbulence model to parameterize the vertical turbulent mixing. In this study, the vertical eddy coefficients (A_V , D_V and K_V) are computed from a simplified second-order closure model developed by Sheng and Chiu (1986), and Sheng and Villaret (1989).

Various form forms of the equation of state can be used. The present model uses the equation given by (Eckart, 1958)

$$\rho = \frac{P}{(\alpha + 0.698P)}$$
$$P = 5890 + 38T - 0.357T^2 + 3S \tag{3.6}$$
$$\alpha = 1779.5 + 11.25T - 0.0475T^2 - (3.8 + 0.01T)S$$

where T is in $^{\circ}C$, S is in ppt and ρ is in g/cm^3.

The complete details of model equations in the curvilinear boundary-fitted and sigma coordinates have been derived (Sheng, 1989), and are presented in Appendix B.

3.1.2 Sediment Transport Model

The suspended sediment model includes the advection-diffusion processes, which are computed by the hydrodynamics model, as well as such processes as erosion, deposition, flocculation, settling, consolidation, and entrainment (Sheng, 1986; Metha, 1986).

The governing equation that represents the transport of suspended sediments is given by:

$$\frac{\partial c}{\partial t} + \frac{\partial uc}{\partial x} + \frac{\partial vc}{\partial y} + \frac{\partial (w + w_s)c}{\partial z} = \frac{\partial}{\partial x}\left(B_H \frac{\partial c}{\partial x}\right) + \frac{\partial}{\partial y}\left(B_H \frac{\partial c}{\partial y}\right) + \frac{\partial}{\partial z}\left(B_V \frac{\partial c}{\partial z}\right) \tag{3.7}$$

where c is the suspended sediment concentration, w_s is the settling velocity of suspended sediment particles (negative downward), B_H is the horizontal turbulent eddy diffusivity, and B_V is the vertical turbulent eddy diffusivity.

Four simplifying approximations are implied in the above equation: 1) the concept of eddy diffusivity is valid for the turbulent mixing of suspended sediments, 2) the suspended sediment dynamics are represented by the concentrations of two particle size groups (Sheng et al., 2002a), 3) the suspended sediment concentrations are sufficiently small that all

particles follow turbulent eddy motions, 4) the SSC is sufficiently low that non-Newtonian behavior can be neglected.

In this study, the determination of settling, flocculation, deposition, erosion, flocculation, and consolidation processes are based on the previous work of Sheng and Lick (1979), Sheng(1986), Metha (1989), Sheng et al. (1990), Chen and Sheng (1994) and Sun and Sheng (2001).

3.2 Boundary and Initial Conditions

Obtaining solutions for Equations (3.1) Through (3.7) requires the specification of appropriate boundary and initial conditions.

3.2.1 Boundary Conditions

The boundary conditions at the free surface (σ=0) in a non-dimensional, vertically stretched, boundary-fitted coordinate system are:

For Hydrodynamics:
$$A_V \frac{\partial u}{\partial \sigma} = \frac{H}{E_V} \tau_{s\xi}^w$$
$$A_V \frac{\partial v}{\partial \sigma} = \frac{H}{E_V} \tau_{s\eta}^w$$

For Salinity:
$$\frac{\partial S}{\partial \sigma} = 0 \qquad (3.8)$$

For Temperature:
$$\frac{\partial T}{\partial \sigma} = \frac{H \, \mathrm{Pr}_V}{E_V} q_T$$

For Sediment:
$$w_{si} c_i + \frac{D_V}{H} \frac{\partial c_i}{\partial \sigma} = 0$$

where E_V is a vertical Ekman number and Pr_V is a vertical Prandtl number; The Cartesian wind stress, τ^w, is calculated using

$$\tau_x^w = \rho_a C_{ds} u_w \sqrt{u_w^2 + v_w^2}$$
$$\tau_y^w = \rho_a C_{ds} v_w \sqrt{u_w^2 + v_w^2} \qquad (3.9)$$

where ρ_a is the air density (0.0012 g/cm^3), u_w and v_w are the components of wind speed measured at some height above the sea level. C_{ds}, the drag coefficient, is given as a function of the wind speed measured at 10 meters above the water surface by (Garrat, 1977).

$$C_{ds} = 0.001(0.75 + 0.067W_s) \tag{3.10}$$

Boundary conditions, if specified in a Cartesian coordinate system, such as wind stress, must be transformed before being used in the boundary-fitted equations. For example, the surface stress in the transformed system is given by

$$\tau_{s\xi} = \frac{\partial \xi}{\partial x}\tau_{sx} + \frac{\partial \xi}{\partial y}\tau_{sy}$$
$$\tau_{s\eta} = \frac{\partial \eta}{\partial x}\tau_{sx} + \frac{\partial \eta}{\partial y}\tau_{sy} \tag{3.11}$$

The second surface boundary condition is the kinematic free surface boundary condition which states

$$w = \frac{\partial \zeta}{\partial t} + u\frac{\partial \zeta}{\partial x} + v\frac{\partial \zeta}{\partial y} \tag{3.12}$$

The boundary conditions at the bottom in a non-dimensional, vertically stretched (σ = -1), boundary-fitted coordinate system are

For Hydrodynamics:

$$A_V \frac{\partial u}{\partial \sigma} = \frac{H}{E_V}\tau_{b\xi}^w = \frac{U_r}{A_{vr}} H_r Z_r C_d \left[g_{11}u_b^2 + 2g_{12}u_b v_b + g_{22}v_b^2 \right] u_b$$
$$A_V \frac{\partial v}{\partial \sigma} = \frac{H}{E_V}\tau_{b\eta}^w = \frac{U_r}{A_{vr}} H_r Z_r C_d \left[g_{11}u_b^2 + 2g_{12}u_b v_b + g_{22}v_b^2 \right] v_b$$

For Salinity: $$\frac{\partial S}{\partial \sigma} = 0 \tag{3.13}$$

For Temperature: $$\frac{\partial T}{\partial \sigma} = 0$$

For Sediment: $$w_{si}c_i + \frac{D_V}{H}\frac{\partial c_i}{\partial \sigma} = D_i - E_i$$

where u_b and v_b are the contravarient velocity components at the first grid point above the bottom. E_i is the erosion rate and D_i is the deposition rate for sediment group i. C_d is drag coefficient which is a function of the size of bottom roughness elements, z_0, and the height at which u_b is measured, so long as z_1 is within the constant flux layer above the bottom. The drag coefficient is given by (Sheng, 1983)

$$C_d = \left(\frac{\kappa}{\ln(z_1/z_0)} \right)^2 \tag{3.14}$$

where κ=0.4 is the von Karman constant, $z_0=k_s/30$ and k_s is the bottom roughness.

Along the shoreline where river inflow may occur, the conditions are generally

$$\begin{aligned} u &= u(x, y, \sigma, t) \\ v &= v(x, y, \sigma, t) \\ w &= 0 \\ S &= S(x, y, \sigma, t) \\ T &= T(x, y, \sigma, t) \\ c_i &= c_i(x, y, \sigma, t) \end{aligned} \tag{3.15}$$

Contravarient velocity components provide lateral boundary conditions similar to those in Cartesian systems (x,y). Along solid boundaries, the normal velocity component must be zero to satisfy the no-slip condition. In addition, normal derivatives of salinity, temperature and suspended sediment concentration are assumed to be zero. When flow is specified at a boundary, the normal velocity component is prescribed. Tidal boundary conditions are specified using water level, ζ, directly When tidal boundary conditions are given in terms of ζ, the normal velocity component is assumed to be of zero slope, while tangential velocity component may be either zero, of zero slope, or computed from the momentum equations. During an ebb tide, the concentrations of salinity, temperature, and suspended sediment flowing out are calculated using a 1-D advection equation while during

a flood tide the offshore concentrations are generally prescribed as either fixed or time varying.

3.2.2 Initial Conditions

To initiate a simulation, the initial spatial distribution of ζ, u, v, w, S, T, and c_i must be specified. When these values are unknown, "zero" initial fields can be used. When these values are known at a limited number of locations, an initial field can be generated by spatial interpolation. In the principle, the interpolated field should satisfy the conservation equation for a particular variable. For practical simulations, a "spin-up" period is required to damp out transients caused by the initial condition, which does not satisfied conservation. The length of a spin up period is variable and depends on such factors as basin size, flushing time, and current velocity.

3.3 Heat Flux at the Air-Sea Interface

The ocean receives energy through the air-sea interface by exchange of momentum and heat. The temperature of ocean waters varies from place to place and from time to time. Such variations are indications of heat transfer by currents, absorption of solar energy, and loss by evaporation. The size and character of the temperature variations depends on the net rate of heat flow into or out of water body (Pickard and Emery, 1990). The transfer of heat across the air-sea interface determines the distribution of temperature in the ocean as a surface boundary condition for the temperature equation, as follow:

$$\rho_0 K_v \frac{\partial T}{\partial z} = q_T \tag{3.16}$$

where q_T is the net heat flux across the surface water.

To estimate the net heat flux at the air-sea interface, it is necessary to consider the following processes: net heat flux across the surface, q_T; heating by incoming solar radiation

(insolation), q_s ; warming by conductive heat exchange across the surface (sensible heat flux), q_h ; cooling by net outgoing long wave radiation, q_b ; heat loss as water evaporated (latent heat flux), q_l ; heat flux from precipitation. Other source of heat flow, such as that from the earth's interior, change of kinetic energy of waves into heat at the surf; heat from chemical or nuclear reactions, are small and can be neglected. The net heat exchange at the surface can be divided into four terms:

$$q_T = q_s - q_b - q_h - q_l \tag{3.17}$$

Direct measurement of these fluxes is the best way to provide the net heat flux at the air-sea interface. However, directly measured air-sea fluxes are only available at very few stations to allow calculation of air-sea interface over a large area. Instead, directly measured air-sea fluxes are used for developing, calibrating, and verifying the parametric formulae for estimating the fluxes from the primary variables including wind speed, air temperature, water temperature, and cloud cover (Taylor et al., 2000). These required parametric formulae are then used to compute heat fluxes over a large area.

3.3.1 Short-Wave Solar Radiation

The main source of heat flux through the air-sea interface is short-wave solar radiation, q_s (incoming solar radiation), received either directly or by reflection and scattering from clouds and the atmosphere. The incoming solar radiation is based on the empirical formula of Reed (1977):

$$q_s = S \sin\gamma \left(A + B \sin\gamma\right)\left(1 - 0.62n - 0.0019\gamma\right)\left(1 - \alpha\right) \tag{3.18}$$

where S is solar constant =1353 w/m^2

γ is solar elevation angle

n is cloud cover = 0 ~ 1

α is the albedo = 0.06

A and B are empirically determined coefficients for each category of reported total cloud amount and the solar elevation

The solar elevation angle was computed to the nearest 0.1° from date and time for the latitude and longitude of the study area, using the following equations (Miller and McPherson, 1995):

$$\varphi = (d-1)\frac{360}{365.242}$$
$$\delta = 12 + 0.1236\sin\varphi - 0.0043\cos\varphi + 0.1538\sin 2\varphi + 0.0608\cos 2\varphi$$
$$\sigma = 279.9348 + \varphi + 1.9148\sin\varphi - 0.0795\cos\varphi + 0.00199\sin 2\varphi + 0.0016\cos 2\varphi$$
$$\Upsilon = 15(\tau - \delta) - \lambda \qquad (3.19)$$
$$\kappa = \arcsin(0.39785077 \times \sin\sigma)$$
$$\sin\beta = \sin\gamma\sin\kappa + \cos\gamma\cos\kappa\cos\Upsilon$$

where φ is the angular fraction of the year, in degree; d is Julian date; δ is true solar noon, in hours; Υ is the solar hour angle, in degrees; τ is the Greenwich Mean Time, in hours; λ is the longitude, in degrees; σ is an estimate of the true longitude of the sun, in degrees; κ is the solar declination, in degrees; γ is the latitude, in degrees; and β is the solar elevation angle, in degrees.

3.3.2 Long-Wave Solar Radiation

The back radiation term, q_b, is the net amount of energy lost by the sea as long-wave radiation. The amount of long wave flux is dependent on surface water temperature, atmospheric temperature, humidity and cloud cover (Clark et al, 1974)

$$q_b = \varepsilon\sigma T_s^4\left(0.39 - 0.05e^{0.5}\right)\left(1 - \lambda n^2\right) + 4\varepsilon\sigma T_s^3\left(T_s - T_a\right) \qquad (3.20)$$

where ε is the emittance of the sea surface = 0.98

σ is Stefan-Boltzman constant = 5.673×10^{-8} W/m^2

e is the water vapor pressure

T_a and T_s are the air and sea temperatures in K.

λ is a cloud cover coefficient which varies with latitude

The Antoine constants (http://www.owlnet.rice.edu/~ceng301/31.html) give the vapor pressure as a function of temperature so that the approximate value for water vapor pressure is:

$$e = \exp\left(16.5362 - \frac{3985.44}{T_s - 38.997}\right) \tag{3.21}$$

where T_s is the surface water temperature (°K).

A theoretical calculation of the mean values of the coefficient λ for different latitudes has been made by M. E. Berliand (1952). In this calculation, the mean frequency of clouds of different layers at each latitude is taken into account. The values obtained for the coefficient λ are given in Table 3.1 (Budyko, 1974). The reduction of values of this coefficient in low latitudes is explained mainly by a higher mean altitude of clouds in these regions.

Table 3.1 Mean latitudinal values of the coefficient λ

ϕ	75°	70°	65°	60°	55°	50°	45°	40°
λ	0.82	0.80	0.78	0.76	0.74	0.72	0.70	0.68
ϕ	35°	30°	25°	20°	15°	10°	5°	0°
λ	0.65	0.63	0.61	0.59	0.57	0.55	0.52	0.50

3.3.3 Sensible and Latent Heat Fluxes

The most significant part in terms of heat transfer from the sea to the atmosphere is latent heat flux. The rate of heat loss is equal to the rate of vaporization times the latent heat of evaporation. Sensible heat flux is due to temperature gradient in the air above the sea. The rate of loss or gain of heat is proportional to the temperature gradient, heat conductivity

and the specific heat of air at constant pressure. Sensible and latent heat fluxes are estimated by using the bulk aerodynamic equations (Mellor, 1996):

$$q_h = \rho c_p C_H U_{10} \left(T_s - T_a\right) \tag{3.22}$$

$$q_l = \rho C_E L U_{10} \left(h_s - h_a\right) \tag{3.23}$$

where ρ is the density of air

C_H and C_E are transfer coefficients for sensible and latent heat respectively

U_{10} is the wind speed at 10 m height above surface

T_s and T_a are the sea surface and air temperatures

c_p is the specific heat of air, 1.0048 x 10^3 J/kg°K

L is the latent heat of evaporation, 2.4 x 10^6 J/kg

h_s and h_a are specific humidities at the surface and at a 10 m height above the surface

The air density is determined from the ideal gas equation in the form, $\rho = P_a / \left(RT_a\right)$, where P_a is air pressure and R is universal gas constant, 287.04 J/kg °K.

The traditional estimates of C_H and C_E over the ocean tend to support a fairly constant value over a wide range of wind speed. Smith (1989) recommended a constant "consensus" value $C_E = (1.2 \pm 0.1) \times 10^{-3}$ for winds between 4 and 14 m/s. DeCosmo et al. (1996) also suggested a near constant value with $C_E = (1.12 \pm 0.24) \times 10^{-3}$ for winds up to 18 m/s. For the Stanton number, C_H, Friehe and Schmitt (1976) obtained slightly different values for unstable and stable conditions, 0.97 x10^{-3} and 0.86 x10^{-3} respectively. Smith (1989) suggested C_H = 1.0 x 10^{-3}. C_E = 1.2 x10^{-3} and C_H = 1.0 x 10^{-3} were used for this study.

The formulae used for air specific heat, c_p, and latent heat for evaporation, L, have been taken from Stull (1988),

$$c_P = 1004.67 + 0.84 q_a \tag{3.24}$$

$$L = 10^6 \left[2.501 - 0.00237 \left(T_s - 273.16 \right) \right] \tag{3.25}$$

An empirical relation (based on the Clausius-Clapeyron theory) provides the saturation, water vapor partial pressure, $e_s = 10^{(0.7859+0.03477T)/(1+0.00412T)}$ mb. A general relation between specific humidity and partial pressure is $q = \left(0.622e/P\right)/\left(1-0.378e/P\right)$, where P is the atmospheric pressure (Mellor, 1996). Specific humidities at surface and at a 10 m height above the surface, h_s and h_a, can be calculated using these empirical formulae with T_s and T_a respectively.

CHAPTER 4
WATER QUALITY MODEL

In this chapter, a water quality model for simulating water quality processes occurring in the Charlotte Harbor estuarine system in both the water and sediment columns is presented. This is an extension of an earlier model developed to simulate water quality for Lake Okeechobee (Sheng et al., 1993; Chen and Sheng, 1994), Tampa Bay (Yassuda and Sheng, 1996) and the Indian River Lagoon (Sheng et al., 2001 and 2002). These models include the effect of sediment transport on nutrient dynamics through the explicit use of a sediment transport model and the incorporation of a nutrient resuspension flux.

The water quality model incorporates on the interactions between oxygen balance, nutrient dynamics, light attenuation, temperature, salinity, phytoplankton and zooplankton dynamics. To develop the water quality model, the mass conservation principle can be applied to each water quality parameter, as it relates to phytoplankton and zooplankton dynamics, nitrogen and phosphorous cycles, and oxygen balance.

The nitrogen and phosphorous cycles in an estuarine system, are modeled through a series of first order kinetics. Nutrient concentrations in the estuarine system are constantly changing in time and space due to loading from rivers, exchanges with the ocean, seasonal climatic changes, biogeochemical transformations, hydrodynamics, and sediment dynamics. Nitrogen species include ammonia nitrogen (NH3), soluble ammonium nitrogen (NH4), nitrate and nitrite nitrogen (NO3), particulate ammonium nitrogen (PIN), soluble organic

nitrogen (SON), particulate organic nitrogen (PON), phytoplankton nitrogen (PhyN), and zooplankton nitrogen (ZooN). Similar to the nitrogen species, phosphorous species include soluble reactive phosphorous (SRP), particulate inorganic phosphorous (PIP), soluble organic phosphorous (SOP), particulate organic phosphorous (POP), phytoplankton phosphorous (PhyP), and zooplankton phosphorous (ZooP).

Phytoplankton kinetics are the central part of this water quality model, since the primary water quality issue in the estuarine system is eutrophication (Boler et al., 1991). Phytoplankton population is a complex variable to measure in the field. However, the lack of data on each specific species prevented a more detail characterization, the entire phytoplankton community is represented in this study by a single state variable and quantified as carbonaceous biomass. *Chlorophyll_a* concentrations, for comparison with observations, are obtained through division of computed carbonaceous biomass by the carbon-to-*chlorophyll_a* ratio.

The oxygen balance couples dissolved oxygen to other state variables. Reaeration through the air-sea interface, and phytoplankton production during photosynthesis are the main source for oxygen. Oxidation, nitrification, respiration, mortality and SOD reduce oxygen in the system. Oxidation of organic matter and carbonaceous material, respiration by zooplankton and phytoplankton, and oxygen consumption during the nitrification process are collectively grouped into the CBOD (Carbonaceous-Biogeochamical Oxygen Demand) variable, which is a sink for dissolved oxygen (Ambrose et al., 1994).

The methods of coupling with hydrodynamic and sediment transport models, the simulated parameters, the assumptions, the chemical/biological processes of the CH3D water quality model (CH3D-WQ3D) was compared with those for existing water quality models,

specially Water Quality Analysis ans Simulation Program (WASP), the integrated Compartment water quality model developed by the US Army Corps (CE-QUAL-ICM) in Appendix C.

Temperature, salinity, and light are important parameters that effect the rate of biogeochemical reactions. Most of the transformation processes in the nutrient cycle are affected by temperature. Salinity also influences DO saturation concentration and is used in the determination of kinetics constants that differ in saline and fresh water. Light intensity affects the photosynthesis process and thus algae growth rate.

The water quality model is enhanced to include a reaeration model and a sediment oxygen demand (SOD) model and newly coupled with temperature model and physics-based light attenuation model. Applying enhanced water quality model and a more accurate light model and temperature model could improve the vertical distribution and daily fluctuation of both phytoplankton and dissolved oxygen. Furthermore, the bottom water hypoxia at upper Charlotte Harbor which is caused by SOD and vertical stratification can be reproduced and analyzed in this study.

4.1 Mathematical Formulae

The water quality equations are derived from a Eulerian approach, using a control volume formation. In this method, the time rate of the concentration of any substance within this control volume is the net result of (i) concentration fluxes through the sides of the control volume, and (ii) production and sink terms inside the control volume. The conservation equation for each of the water quality parameters is given by:

$$\underset{(i)}{\frac{\partial \varphi_i}{\partial t}} + \underset{(ii)}{\nabla \cdot \left(\varphi_i \vec{u}\right)} = \underset{(iii)}{\nabla \cdot \left[D \nabla \left(\varphi_i \vec{u}\right)\right]} + \underset{(iv)}{Q_i} \qquad (4.1)$$

where (I) is the evolution term (rate of change of concentration in the control volume), (ii) is the advection term (fluxes into/out of the control volume due to the advection of the flow field), (iii) is the diffusion term (fluxes into/out of the control volume due to turbulent diffusion of the flow field), and (iv) is the sink and source term, representing the kinetics and transformations due to sorption/desorption, oxidation, excretion, decay, growth, and bio-degradation. In the finite difference solution of the water quality model, the advection and horizontal diffusion terms are treated explicitly, whereas the vertical diffusion and biogeochemical transformations are treated implicitly. The detail descriptions of numerical solution technique are described in Appendix D. The water quality equations in the curvilinear non-orthogonal boundary fitted system (ξ, η, σ) are given by:

$$\begin{aligned}\frac{\partial H\varphi_i}{\partial t} = {} & \frac{E_V}{H\cdot S_{CV}}\frac{\partial}{\partial\sigma}\left(D_V\frac{\partial\varphi_i}{\partial\sigma}\right) \quad -R_0\frac{\partial(H\omega)\varphi_i}{\partial\sigma} \\ & -\frac{R_0}{\sqrt{g_0}}\left[\frac{\partial}{\partial\xi}\left(\sqrt{g_0}Hu\varphi_i\right)+\frac{\partial}{\partial\eta}\left(\sqrt{g_0}Hv\varphi_i\right)\right] \\ & +\frac{E_V}{S_{CH}\sqrt{g_0}}\left[\frac{\partial}{\partial\xi}\left(\sqrt{g_0}Hg^{11}\frac{\partial\varphi_i}{\partial\xi}+\sqrt{g_0}Hg^{12}\frac{\partial\varphi_i}{\partial\eta}\right)\right] \\ & +\frac{E_V}{S_{CH}\sqrt{g_0}}\left[\frac{\partial}{\partial\eta}\left(\sqrt{g_0}Hg^{21}\frac{\partial\varphi_i}{\partial\xi}+\sqrt{g_0}Hg^{22}\frac{\partial\varphi_i}{\partial\eta}\right)\right] \quad +Q_i\end{aligned} \tag{4.2}$$

where φ_i represents any water quality parameter, $\sqrt{g_0}$ is the Jacobian of horizontal transformation, (g^{11}, g^{12}, g^{22}) are the metric coefficients of coordinate transformation, and Q_i represent biogeochemical processes. Equation (4.2) is in dimensionless form and the dimensionless constants are defined in Appendix B.

In the following sections, the biogeochemical processes controlling the sink/source term of Equation (4.2) will be discussed in detail for nutrient dynamics, zooplankton and

phytoplankton dynamics, and oxygen balance in system.

4.2 Phytoplankton Dynamics

The overall water quality in the system is markedly influenced by the dynamics of zooplankton and phytoplankton communities (Boler et al., 1991). Phytoplankton dynamics and nutrient dynamics are closely linked, since nutrient uptake during phytoplankton growth is the main process to remove dissolved nutrients from the water, and phytoplankton and zooplankton respiration and mortality are major components of nutrient recycling. The diurnal variation of dissolved oxygen is related with photosynthetic oxygen production during the day and oxygen consumption due to phytoplankton respiration during the night.

4.2.1 Modeling Approach

Phytoplankton kinetics are represented by growth, respiration, non-predator-mortality, grazing by zooplankton, and a settling term. The phytoplankton sources and sinks in the conservation equation can be written as:

$$\frac{\partial PhyC}{\partial t} = \left(\mu_a - K_{ax} - K_{as} + \frac{\partial}{\partial z} WS_{algae} \right) \cdot PhyC - \mu_z \cdot ZooC \qquad (4.3)$$

Where $PhyC$ is phytoplankton biomass, expressed as carbon (gCm^{-3}); μ_a is phytoplankton growth rate (1/d); K_{as} is respiration rate (1/d); K_{ax} is non-predator mortality (1/d); WS_{algae} is the phytoplankton settling velocity(m/d); $ZooC$ is zooplankton biomass (gCm^{-3}); and μ_z is zooplankton growth rate (1/d).

Phytoplankton growth is determined by the intensity of light, by the availability of nutrients, and by the ambient temperature. Light limitation is formulated according to the photo inhibition relationship (Steel, 1965). The quantity of the growth limitation factor for nutrients is related with a half-saturation constant. The half-saturation constant refers to the concentration of the nutrient at which the growth rate is one half its maximum value. This

results in a hyperbolic growth curve. An exponential increasing function is applied for temperature limitation..

The minimum formation approach has been used to combine the limiting factor of light and each limiting nutrient. The minimum formation is based on "Liebig's law of the minimum" which states that the factor in shortest supply will control the growth of algae (Bowie et al., 1980)

$$\begin{aligned}\mu_a &= (\mu_a)_{\max} \cdot f(T) \cdot f(l) \cdot f(N,P) \\ &= (\mu_a)_{\max} \cdot \theta_a^{T-20} \cdot \min\left[\frac{I}{I_S}\exp\left(1-\frac{I}{I_S}\right), \frac{NH_4+NO_3}{H_n+NH_4+NO_3}, \frac{SRP}{H_p+SRP}\right]\end{aligned} \tag{4.4}$$

where $(\mu_a)_{\max}$ is the phytoplankton maximum growth rate (1/day); θ is temperature adjustment coefficient; T is temperature (°C); I is the light intensity, calculated by the light attenuation model; I_S is the optimum light intensity for algae growth; H_n is half saturation concentration for nitrogen uptake (gN $^{-3}$); H_p is half saturation concentration for phosphorous uptake (gP $^{-3}$); *NH4* is ammonium concentration (gN $^{-3}$); NO_3 is nitrate concentration (gN $^{-3}$); and *SRP* is soluble reactive phosphorous concentration (gP $^{-3}$).

Respiration and mortality are considered to be an exponentially increasing functions of temperature:

$$\begin{aligned}K_{as} &= (K_{as})_{T_r} \cdot \theta_{ks}^{T-T_r} \\ K_{ax} &= (K_{ax})_{T_r} \cdot \theta_{kx}^{T-T_r}\end{aligned} \tag{4.5}$$

where $(K_{as})_{Tr}$ and $(K_{ax})_{Tr}$ are respiration and mortality rate at Tr (1/day); and Tr is reference temperature of respiration and mortality.

For phytoplankton, literature values of algae settling velocity, which account for the limited vertical motion of these organisms will be used.

Zooplankton are included in water quality models primarily because of their effects

on algae and nutrients. Phytoplankton and zooplankton dynamics are closely tied through predator-prey interaction. Phytoplankton dynamics are of major concern in this study while no attempt is made to investigate zooplankton dynamics due to lack of zooplankton data. Zooplankton is only considered as the predators of phytoplankton, utilizing their available biomass as food supply. Zooplankton kinetics, influenced by growth, respiration and mortality, are represented in a source and sink term as (Bowie, 1985):

$$\frac{\partial ZooC}{\partial t} = \left(\mu_z - K_{zx} - K_{zs}\right) \cdot ZooC \tag{4.6}$$

where μ_z is zooplankton growth rate (1/day); K_{as} is respiration rate (1/day); and K_{ax} is mortality (1/d)

Zooplankton growth is represented by a temperature-dependent maximum growth rate, which is limited by phytoplankton availability:

$$\mu_z = \left(\mu_z\right)_{\max} \cdot \theta_z^{T-20} \cdot \frac{PhyC - Trs_{phy}}{H_{phy} + PhyC - Trs_{phy}} \tag{4.7}$$

where $(\mu_z)_{\max}$ is the zooplankton maximum growth rate (1/day); θ is temperature adjustment coefficient; H_{phy} is half saturation concentration for phytoplankton uptake (gC^{-3}); and Trs_{phy} is threshold phytoplankton concentration for zooplankton uptake (μg/l).

4.2.2 Relationship between Phytoplankton and Nutrients

Phytoplankton biomass is quantified in units of carbon. In order to express the effects of phytoplankton on nitrogen and phosphorous, the ratio of nitrogen-to-carbon and phosphorous-to-carbon in phytoplankton biomass must be specified. Global mean values of these ratios are well known (Redfield et al., 1966). The amounts of nitrogen and phosphorous incorporated in algae biomass is quantified through a stoichiometric ratio. Thus, total nitrogen and total phosphorous in the model are expressed as:

$$TotN = NH_4 + NH_3 + NO_3 + SON + PON + PIN + Anc \cdot PhyC + Anc \cdot ZooC$$
$$TotP = SRP + SOP + POP + PIP + Apc \cdot PhyC + Apc \cdot ZooC \quad (4.8)$$

where TotN is total nitrogen (gN^{-3}); NH4 is dissolved ammonium nitrogen (gN^{-3}); NH3 is ammonia nitrogen (gN^{-3}); NO3 is nitrate and nitrite nitrogen (gN^{-3}); SON is soluble organic nitrogen (gNm^{-3}); PON is particulate organic nitrogen (gN^{-3}); PIN is particulate inorganic nitrogen (gN^{-3}); Anc is Algae nitrogen-to-carbon ratio (gN/gC) ; TotP is total phosphorous (gP^{-3}); SRP is soluble reactive phosphorous (dissolved phosphate) (gPm^{-3}); SOP is soluble organic phosphorous (gP^{-3}); POP is particulate organic phosphorous (gP^{-3}); PIP is particulate inorganic phosphorous (gP^{-3}); and Apc is algae phosphorous-to carbon ratio (gP/gC).

The connection between the carbon, nitrogen and phosphorous cycle is shown in Figure 4.1. Phytoplankton uptakes dissolved ammonium nitrogen, nitrate and nitrite nitrogen, and soluble reactive phosphorous during production and releases dissolved ammonium nitrogen, soluble reactive phosphorous and organic nitrogen, organic phosphorous during respiration and mortality processes. Zooplankton has similar kinetic processes as phytoplankton. The measured phytoplankton as algae mass per volume, was converted to phytoplankton carbon with a algae to carbon ratio. The amounts of nitrogen and phosphorous from phytoplankton can be converted with a nitrogen to carbon ratio and a phosphorous carbon ratio, respectively.

4.3 Nutrient Dynamics

Nutrients are essential elements for life processes of aquatic organisms. Nutrients of concern include carbon, nitrogen, phosphorous, silica and sulfur. Among these nutrients, the first three elements are utilized most heavily by zooplankton and phytoplankton. Since carbon is usually available in excess, nitrogen and phosphorous are the major nutrients

regulating the ecological balance in an estuarine system. Nutrients are important in water quality modeling for several reasons. For example, nutrient dynamics are critical components of eutrophication models since nutrient availability is usually the main factor controlling algae bloom. Algae growth is typically limited by either phosphorous or nitrogen (Bowie et al., 1980). Details on the nutrient dynamics including all the equations used by the water quality model to calculate the nitrogen and phosphorous, can be found in Appendix-E.

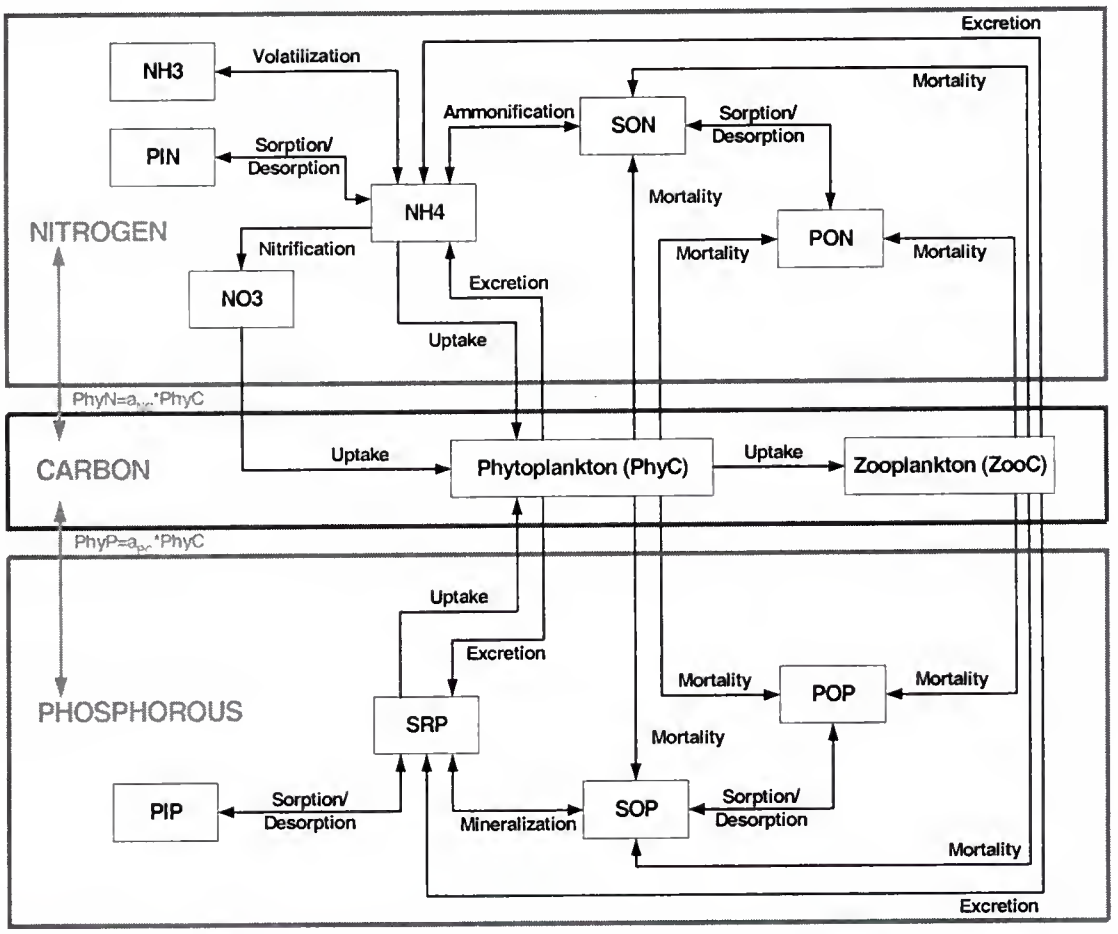

Figure 4.1 The connection between nitrogen, phosphorous and carbon cycle

4.4 Oxygen Balance

Dissolved oxygen (DO) refers to the volume of oxygen contained in water. Five state variables participate in the dissolved oxygen balance: phytoplankton carbon (PhyC), ammonia (NH4), nitrate (NO3), carbonaceous biochemical oxygen demand (CBOD), and dissolved oxygen (DO). A summary is illustrated in Figure 4.2. The methodology for the analysis of dissolved oxygen dynamics in natural water, particularly in streams, rivers, and estuaries is reasonably well-developed (O'Connor and Thomann, 1972). Dissolved oxygen evolution depends on the balance between production from photosynthesis, consuming from respiration and mortality, and exchanges with the atmosphere and sediment.

The main physical mechanisms influencing DO concentration are horizontal and vertical dispersion and diffusion. Vertical diffusion occurs across the air-sea interface as a function of wind, waves, currents, and DO saturation rate. Laboratory experiments show that the bottom shear stress controls the dissolved oxygen diffusive layer thickness and the flux at the sediment-water interface (Steinberger and Hondzo, 1999). Slow oxygen diffusion rates and high oxygen demand by sediment results in a thin aerobic layer. Two distinct sediment zones are created in the sediment column: an aerobic layer and an anaerobic layer. The thickness of the aerobic soil zone is influenced by oxygen concentration in the overlying water column, and concentration of the reduced compounds in the anaerobic soil zone. The model dissolved oxygen cycle includes the following processes

1) Reaeration

2) Carbonaceous oxygen demand (CBOD)

3) Nitrification

4) Sediment oxygen demand (SOD)

5) Photosynthesis and respiration

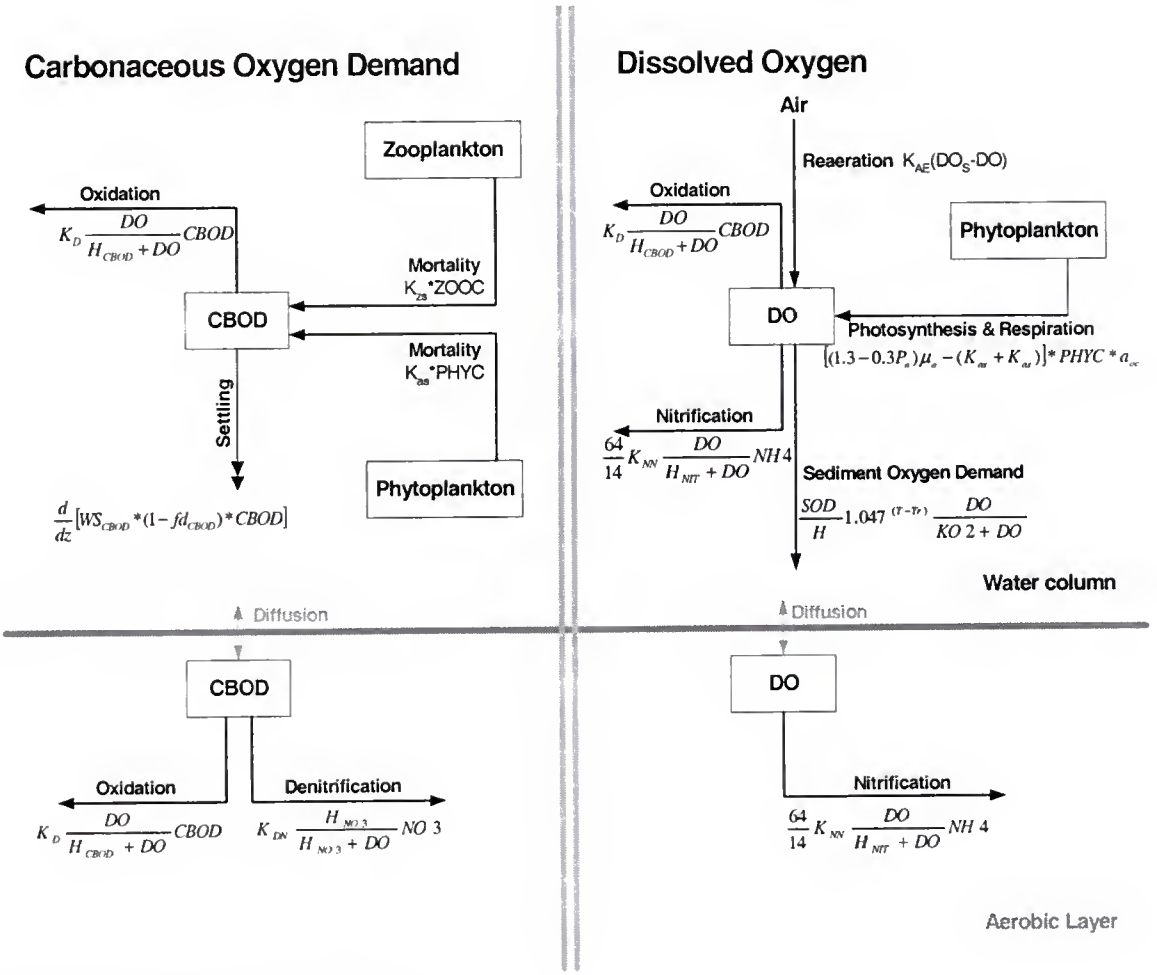

Figure 4.2 DO and CBOD cycles

Reaeration

Reaeration is the process of oxygen change between the atmosphere and sea surface. Typically, dissolved oxygen diffuses into surface waters because dissolved oxygen levels in most natural waters are below saturation. However, when water is super-saturated as a result of photosynthesis, dissolved oxygen returns the atmosphere. Dissolved oxygen saturation in seawater is determined as function of temperature and salinity (APHA, 1985)

$$\ln DO_s = -139.34411 + \frac{1.575701\times10^5}{T} - \frac{6.642308\times10^7}{T^2} + \frac{1.2438\times10^{10}}{T^3} - \frac{8.621949\times10^{11}}{T^4} - \frac{Sa}{1.80655}\left(3.1929\times10^{-2} - \frac{1.9428\times10}{T} + \frac{3.8673\times10^3}{T^2}\right) \quad (4.9)$$

where DO_s is equilibrium oxygen concentration, mg/l, at standard pressure

T is temperature, °K, °K = °C + 273.150

Sa is salinity, ppt

The reaeration process is modeled as the flux of dissolved oxygen across the water surface:

$$V\frac{dDO}{dt} = K_{AE}A_s\left(DO_s - DO\right) \quad (4.10)$$

where V and As are volume and surface area of the water body

In case where the air-sea interface is not constricted, the volume is $V = A_s \cdot \Delta z$. The equation for reaeration can be expressed as

$$\frac{dDO}{dt} = \frac{K_{AE}}{\Delta z}\left(DO_s - DO\right) \quad (4.11)$$

where DO is dissolved oxygen concentration (mg/l); K_{AE} is reaeration coefficient (m/day).

Many empirical formulas have been suggested for estimating reaeration rate coefficient specially in the river. Bowie et al. (1985) have reviewed thirty-one reaeration formulas, and have tried to evaluate the performance of the each formulas. Most formulae have been developed based on hydraulic parameters, most often depth and velocity. This review of stream reaeration has shown that no one formula is best under all conditions, and depending on the data set used, the range of the reaeration coefficients in the data set, and error measurement selected, the best formula may change. Among these formulas, the most

common method of simulating reaeration in rivers is the O'Connor-Dobbins formula. This method has the widest applicability being appropriate for moderate to deep streams with moderate low velocities. With approximately 2.09×10^{-5} cm^2/s diffusivity of oxygen in natural waters, the O'Connor-Dobbins formula can be expressed as

$$K_a = 3.93 \frac{U^{0.5}}{H^{0.5}} \tag{4.12}$$

For standing water, such as lake, impoundments, and wide estuaries, wind becomes the predominant factor in causing reaeration. The oxygen-transfer coefficient itself can be estimated as a function of wind speed by a number of formulas. Chapra (1997) compared four common wind-dependent reaeration formulas: Broecker et al. (1978), Banks and Herrera (1977), O'Connor (1983), and Wanninkhof et al. (1991). The comparison shown in Figure 4.3 show all these methods except Broecker et al.'s have similar reaeration coefficients when wind speed is less than 5 m/s. When wind speed is greater than 5 m/s, Bank and Herrera's formula produce the middle range of reaeration coefficient among these three formulas. This formula uses various wind dependencies to attempt to characterize the difference regimes that result at air-water interface as wind velocity increase (Banks 1975; Banks and Herrera, 1977).

$$K_l = 0.728 U_w^{0.5} - 0.317 U_w + 0.0372 U_w^2 \tag{4.13}$$

Since estuary gas transfer can be affected by both water and wind velocity, effort to determine reaeration in estuaries combines elements of current and wind-driven approaches. Thomann and Fitzpatrick (1982) combined the two approaches for estuaries affected by both tidal velocity and wind,

$$K_{AE} = 3.93 \sqrt{\frac{U_0}{H}} + 0.728 U_w^{0.5} - 0.317 U_w - 0.0372 U_w^2 \tag{4.14}$$

where U_0 is depth averaged velocity (m/s); H is a depth (m); U_w is wind speed (m/s).

For the Charlotte Harbor estuarine system, The aeration coefficient is assumed to be proportional to the water velocity, depth, and wind speed following Thomman and Fitzpatrick (1982).

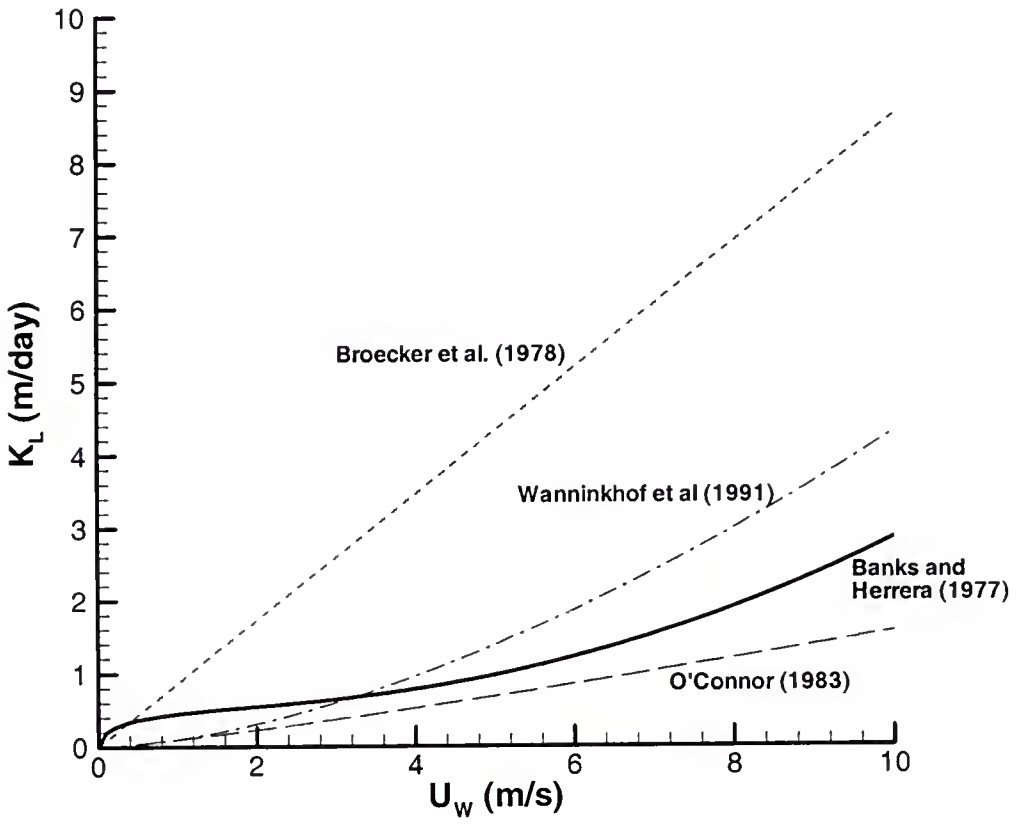

Figure 4.3 Comparison of wind-dependent reaeration formulas.

Carbonaceous Oxygen Demand

The use of carbonaceous oxygen demand (CBOD) as a measure of the oxygen-demanding processes simplified modeling efforts by aggregating their potential efforts (Ambrose et al., 1994). Oxidation organic matter, nitrification, non-predatory mortality and respiration by zooplankton and phytoplankton are nitrogenous-carbonaceous-oxygen-demand, collectively combined into the state variable CBOD.

The kinetic pathway of CBOD is represented in the source term of the equation as (Ambrose et al., 1994):

For water column:

$$\frac{\partial}{\partial t}CBOD = -\frac{\partial}{\partial z}\left[ws_{CBOD}\cdot\left(1-fd_{CBOD}\right)\cdot CBOD\right] - K_D\cdot\frac{DO}{H_{CBOD}+DO}\cdot CBOD$$
$$-\frac{5}{4}\cdot\frac{32}{14}\cdot K_{DN}\cdot\frac{H_{no3}}{H_{no3}+DO}\cdot NO_3 + A_{OC}\left(K_{as}\cdot PhyC + K_{zx}\cdot ZooC\right) \quad (4.15)$$

For sediment column:

$$\frac{\partial}{\partial t}CBOD = +\frac{\partial}{\partial z}\left[ws_{CBOD}\cdot\left(1-fd_{CBOD}\right)\cdot CBOD\right] - K_D\cdot\frac{DO}{H_{CBOD}+DO}\cdot CBOD$$
$$-\frac{5}{4}\cdot\frac{32}{14}\cdot K_{DN}\cdot\frac{H_{no3}}{H_{no3}+DO}\cdot NO_3 \quad (4.16)$$

where fd_{CBOD} corresponds to the fraction of the dissolved CBOD; ws_{CBOD} is the settling velocity for the particulate fraction of CBOD ; K_D is oxidation coefficient which is a temperature function; H_{CBOD} is a half saturation constant for denitrification; K_{DN} is denitrification constant; H_{NO3} is a half saturation rate for denitrification; and A_{OC} is oxygen-carbon ratio (gO_2/gC).

The consumption of oxygen, as a function of water column CBOD decay, can be expressed as CBOD oxidation;

$$\frac{\partial}{\partial t}DO = K_D\frac{DO}{H_{CBOD}+DO}CBOD \quad (4.17)$$

Note that non-oxidative processes such as settling, denitrification, and mortality do not contribute to dissolved oxygen depletion, and are not included in the expression.

Nitrification

The transformation of reduced forms of nitrogen to more oxidized forms (nitrification) consumes oxygen. Although nitrification is also a nutrient transformation, this section addresses oxygen consumption. First order kinetics is the most popular approach for

simulating nitrification in natural system:

$$\frac{\partial}{\partial t} DO = -\frac{64}{14} K_{NN} \cdot \frac{DO}{H_{nit} + DO} \cdot NH_4 \tag{4.18}$$

where K_{NN} is nitrification rate which is a function of temperature; and H_{nit} is the half-saturation constant for the bacteria growth.

Sediment Oxygen Demand

Sediment oxygen demand is a dissolved oxygen flux at water/sediment interface due to the oxidation of organic matter in bottom sediments. The particulate organic matters are from a source outside the system such as wastewater particulate or leaf litter materials, and generated inside system as occurs with plant growth in highly productive environments. According to accumulate these particulate organic matter in the bottom sediment, the sediment oxygen demand will increase due to oxidation of the accumulated organic matter at aerobic sediment layer. Figure 4.4 shows the mechanism of SOD flux with particulate organic matters in the sediment column. Particulate organic matter (POM) is delivered to the sediments by settling. Within the anaerobic sediment layer, the organic carbon, sulfate, nitrate undergo reduction reactions to yield dissolved methane, sulfide, dissolved ammonium nitrogen. These reduced species (CH4, H2S, NH4) diffuses upward to the aerobic layer where these are oxidized. During these oxidation reactions, SOD is generated. Any residual reduced species that are not oxidized in the aerobic layer is diffused back into the water column where additional oxygen is consumed by oxidation. Developing an SOD model is quite complicated task since many aerobic and anaerobic reactions in the sediments are involved and many chemical species are included in mass balance equation. Therefore, these redox chemistry with POM are usually treated as a composite characteristics of the particular system. Recently, techniques have been developed for investigating these factors.

DiToro et al. (1990) developed a model of the SOD process in a mechanistic fashion using the square-root relationship of SOD to sediment oxygen carbon content. Using similar analysis as applied to carbon, they also evaluate the effect of nitrification on SOD. In this model, carbon and nitrogen diagenesis are assumed to occur at uniform rates in a homogeneous layer of the sediment of constant depth (active layer). The sediment oxygen demand and sediment fluxes are calculated by the concentrations of particulate organic carbonaceous material and of particulate organic nitrogenous material in this active layer. The more detail description of sediment flux model developed by DiToro and Fitzpatrick (1993) is presented in Appendix F. Their framework has been applied to the Chesapeake Bay (Cerco and Cole, 1994; DiToro and Fitzpatrick, 1993) with sediment flux model which include ammonia and nitrate flux and the sulfide, oxygen, phosphorous and silica flux.

A calculation of the detailed redox chemistry of the sediment interstitial water is required for a detail understanding of the situation for each reduced species and chemical parameters for redox reaction such as pH, Eh in the system. In the absence of data for CH4, H2S, Iron, Methane, and CO2, and detail understanding of redox chemistry of the system, applying this model could create more uncertainty than the simple empirical formula based on the measurement technique.

The process of oxygen demand in the sediment/water interface is usually referred to as sediment oxygen demand (SOD) because of the typical mode of measurement: enclosing the sediments in the chamber and measuring the change in the dissolved oxygen concentration at several time increments. The major factors affecting SOD are: temperature, oxygen concentration at the sediment water interface, organic and physical characteristics of the sediment, and current velocity over the sediments (Bowie, 1985).

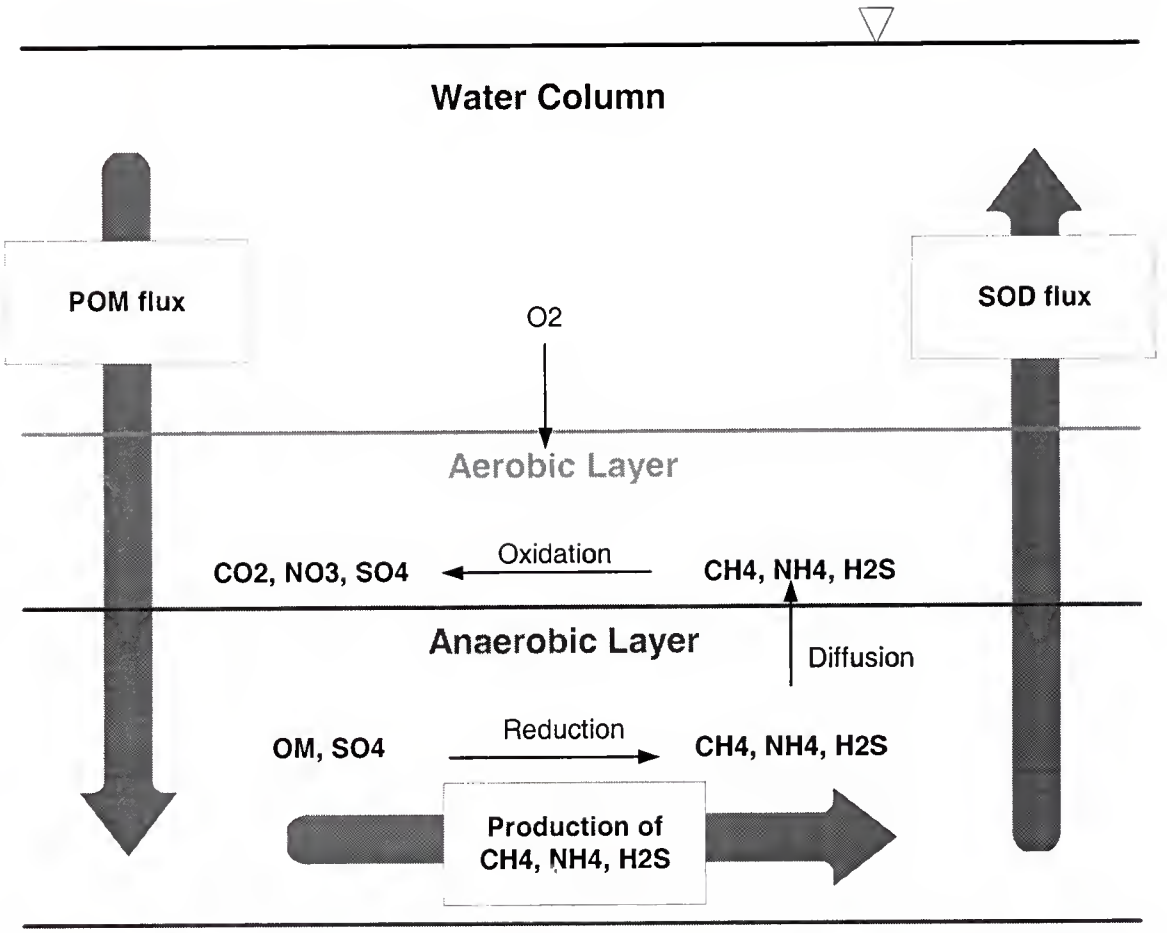

Figure 4.4 The relationship between POM flux and SOD flux related in the oxidation and reduction of organic matter in sediment column.

Typical values of SOD are listed in Table 4.1 (Chapra, 1997). In general, values from about 1 to 10 gO_2/m^2-day are considered indicative of enriched sediments. According to this table, SOD at a mud bottom is higher than SOD at a sandy bottom. In Charlotte Harbor estuarine system, the sediment type near upper Charlotte Harbor is finer and includes more clay and mud than those for the other study area. The finer sediment which has clay, silt, and mud would have higher SOD as more organically rich sediments. From this assumption, SOD can be applied as a function of sediment bottom type (sediment size).

Table 4.1 Average Values of Oxygen Uptake Rates of Bottom (Chapra, 1997)

Bottom type and Location	SOD rate at 20°C (gO_2/m^2-day)	
	Average Value	Range
Sphaerolitus (10 g-dry wt $^{-2}$)	7	
Municipal sewage sludge:		
Outfall vicinity	4	2-10
Downstream of outfall	1.5	1-2
Estuarine mud	1.5	1-2
sandy bottom	0.5	0.2-1
Mineral soil	0.07	0.05-1

The effect of temperature and sediment type on SOD can be represented by

$$S_B(T) = S_{B,20} \cdot ST \cdot \theta^{T-20} \tag{4.19}$$

where $S_{B,20}$ is an areal SOD rate at 20 °C (gO_2/m^2-day) which is user defined value; ST is a fractional coefficient for sediment type. (When sediment type ≤ 2, ST=1, when sediment type >3, ST=0.5) ; θ is temperature coefficient. Zison et al. (1978) have reported a range of 1.04 to 1.13 for θ. A value 1.065 is commonly employed and is used in this study.

Oxygen is another factor that affects sediment oxygen demand. Sediment oxygen consumption is reduced as oxygen concentration in the overlying water decrease. Lam et al. (1984) use a Michealis-Menten relationship to represent the dependence, by a saturation relationship,

$$S_B(DO) = \frac{DO}{K_{SOD} + DO} S_B(T) \tag{4.20}$$

where K_{SOD} is half saturation rate for SOD. Lam et al. (1984) have suggested a value for K_{SOD} of 1.4 mg/l.

The decay of substrate is assumed to balance continued settling resulting in a steady-state sediment concentration of oxygen demand substrate. According to this assumption, the kinetic equation for sediment oxygen demand is (Ambrose et al., 1994):

$$\frac{\partial DO}{\partial t} = -\frac{SOD}{H} \tag{4.21}$$

where H is water depth (m); and SOD is sediment oxygen demand (as measured), gO_2/m^2-day. SOD can be calculated as a function of temperature, dissolved oxygen at the water-sediment interface, and sediment bottom type based on characteristics of SOD measurement.

Exchange of material between the water column and benthic sediment is an important component of the eutrophication process. Sediment oxygen demand may comprise a substantial fraction of total system oxygen consumption (Cerco and Cole, 1995).

Oxygen consumption in the sediments depends upon water-column temperature and oxygen availability, and sediment type. As temperature increases, respiration in the sediment increases. Sediment oxygen consumption is reduced as oxygen concentration in the overlying water decreases. Therefore, the kinetic equation for sediment oxygen consumption (SOC) in sediment column can be represented as (Cerco and Cole, 1995):

$$\frac{\partial DO_{sed}}{\partial t} = -\frac{SOC}{H} = -\frac{1}{H} \cdot S_{B,20} \cdot \theta^{T-20} \cdot \frac{DO_{water}}{K_{SOD} + DO_{water}} \tag{4.22}$$

where $S_{B,20}$ is a function of sediment bottom type (from table 4.1).

The processes that create sediment oxygen demand are little affected by the

concentration of oxygen in the overlying water. When oxygen is unavailable to fulfill sediment oxygen demand, the demand is exported to the water column. The exported demand may be in the form of reduced iron, manganese, methane, or sulfide, which are represented in the model as sediment oxygen demand and provides a function which computes additional release as oxygen consumption in the sediment is restrained (Cerco and Cole, 1995).

$$\frac{\partial DO}{\partial t} = -\frac{SOD}{H} = -\frac{1}{H} \cdot S_{B,20} \cdot \theta^{T-20} \cdot \frac{K_{SOD}}{K_{SOD} + DO} \tag{4.23}$$

The relationship between sediment oxygen consumption and sediment oxygen demand is represented in Figure 4.5. The SOD is negligible when DO much higher than K_{SOD}. When dissolved oxygen is absent from the water column, the maximum oxygen demand is released to the water as sediment oxygen demand.

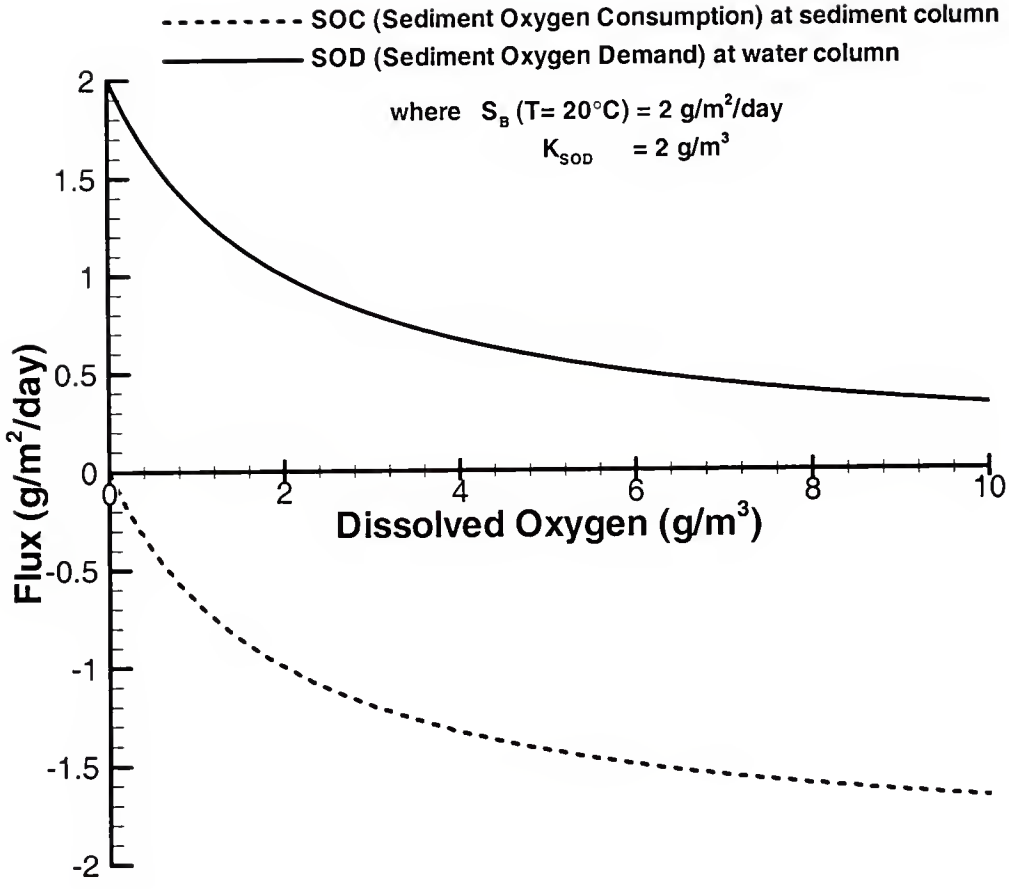

Figure 4.5 Effect of dissolved oxygen on sediment oxygen consumption and SOD release

Photosynthesis and Respiration

The photosynthesis and respiration of phytoplankton can add and deplete significant quantities of oxygen from natural systems. The produced oxygen concentration by photosynthesis depends on the form of the nitrogen species accessed for phytoplankton growth. One mole carbon dioxide can produce one mole oxygen when ammonium is the nitrogen source, while one mole carbon dioxide produces 1.3 moles oxygen when nitrate is the nitrogen source, according to Morel's equation (1983)

$$\begin{aligned} 106CO_2 + 16NH_4^+ + H_2PO_4^- + 106H_2O &\rightarrow protoplasm + 106O_2 + 15H^+ \\ 106CO_2 + 16NO_3^- + H_2PO_4^- + 122H_2O + 17H^+ &\rightarrow protoplasm + 138O_2 \end{aligned} \tag{4.24}$$

The simple representation of the respiration process can be used to determine how much oxygen would be consumed in the decomposition of a unit mass of organic carbon,

$$6CO_2 + 6H_2O \rightleftarrows C_6H_{12}O_6 + 6O_2 \tag{4.25}$$

The dissolved oxygen-to-carbon ratio in respiration can be calculate from this equation.

$$A_{OC} = \frac{6(32)}{6(12)} = 2.67\ gO/gC \tag{4.26}$$

The equation that describes photosynthesis and respiration on dissolved oxygen is:

$$\frac{\partial DO}{\partial t} = \left[\left(1.3 - 0.3 \cdot P_n\right)\mu_a - K_{as} - K_{ax}\right] \cdot A_{OC} \cdot PhyC \tag{4.27}$$

where P_n is nitrogen preference coefficient; μ_a is phytoplankton growth rate, which is a function of the intensity of light, the availability of nutrients, and the ambient temperature; and K_{as} and K_{ax} are respiration and mortality, which are functions of temperature.

The mass balance equation for dissolved oxygen is written by combining all oxygen transformation processes.

For water column:

$$\frac{\partial DO}{\partial t} = +\frac{K_{AE}}{\Delta z}(DO_s - DO) - K_D \cdot \frac{DO}{H_{CBOD} + DO} \cdot CBOD - \frac{64}{14} K_{NN} \cdot \frac{DO}{H_{NIT} + DO} \cdot NH_4 - \frac{SOD}{\Delta z} + \left[(1.3 - 0.3 \cdot P_n)\mu_a - K_{as} - K_{ax}\right] \cdot A_{OC} \cdot PhyC \quad (4.28)$$

which include reaeration, oxidation by CBOD, nitrification, sediment oxygen demand, and photosynthesis and respiration terms.

Fore sediment column:

$$\frac{\partial DO}{\partial t} = -K_D \cdot \frac{DO}{H_{CBOD} + DO} \cdot CBOD - \frac{64}{14} K_{NN} \cdot \frac{DO}{H_{NIT} + DO} \cdot NH_4 - \frac{SOC}{\Delta z} \quad (4.29)$$

which include oxidation by CBOD, nitrification, and sediment oxygen consumption.

4.5 Effects of Temperature and Light Intensity on Water Quality Processes

Temperature and light intensity are the most important parameters for transformation processes. To achieve a better understanding of water quality processes, it is necessary to improve the spatial and temporal variation of these parameters.

4.5.1 Temperature

In the nutrient cycle, almost all the reaction parameters are affected by temperature, such as zooplankton and phytoplankton growth, respiration and mortality, nitrification, denitrification, NH3 stability, mineralization, oxidation, sediment oxygen demand, and sorption/desorption reactions. The effect of temperature on reaction rates can be explained by the Van't Hoff-Arrhenius equation, as follows:

$$\frac{d(\ln K)}{dt} = \frac{\Delta H}{RT^2} \quad (4.30)$$

where K is reaction rate at temperature T, ΔH is the amount of heat required to bring the molecules of the reactant to the energy state required for the reaction, and R is universal gas

constant.

Integrating Equation (4.44) from temperature T_1 to T_2 gives:

$$\frac{K_2}{K_1} = \exp\left[\frac{\Delta H}{RT_1T_2}(T_2 - T_1)\right] \tag{4.31}$$

where K_1 and K_2 are reaction rate at temperature T_1 and T_2, respectively. The temperature adjustment function ($\theta = \exp\left[\frac{\Delta H}{RT_1T_2}\right]$) is almost constant at the temperature range of interest (0° ~ 30°C), ranging from 1.01 to 1.2. This equation can be rearranged into a more useful form as:

$$K(T) = K(T_{ref}) \cdot \theta^{(T-T_{ref})} \tag{4.32}$$

where *K(T)* is the reaction coefficient at temperature *T*, such as μ_a (phytoplankton growth rate), K_{ax} (phytoplankton respiration rate), K_{as} (phytoplankton mortality rate), μ_z (zooplankton growth rate), K_{zx} (zooplankton respiration rate), K_{zx} (zooplankton mortality rate), K_{AI} (ammonia instability), K_{ONM} (ammonification rate), K_{NN} (nitrification rate), d_{on} (sorption/desorption rate for organic nitrogen), d_{an} (sorption/desorption rate for inorganic nitrogen), K_{OPM} (mineralization rate), d_{op} (sorption/desorption rate for organic phosphorous), d_{ap} (sorption/desorption rate for inorganic phosphorous), K_D (oxidation rate),or *SOD* (sediment oxygen demand). Each rate term has a unique temperature adjustment function.

Most models, which use exponential temperature functions, assume a reference temperature of 20 °C (Chen and Orlob, 1975; Thomann and Frizpatrick, 1982). Eppley (1972) showed that an exponential relationship describes the envelope curve of growth rate versus temperature data. The determination was made with a large number of studies, with

many different species.

4.5.1 Light intensity

Light intensity affects the photosynthesis process and thus the phytoplankton growth rate. The effects of light intensity on nutrient cycling is often modeled by a light intensity limiting function as follow (Steele, 1974)

$$f(I) = \frac{I}{I_s} \exp\left[1 - \frac{I}{I_s}\right] \tag{4.33}$$

where I is the light intensity, and I_s is the optimum light intensity for phytoplankton growth . According to the Lambert-Beer equation, the light intensity over the water depth is:

$$I(z) = I_0 \cdot \exp\left[-K_d(PAR) \cdot z\right] \tag{4.34}$$

where $I(z)$ is the light intensity at depth z, and I_0 is the light intensity at the water surface. $K_d(PAR)$ is a function of suspended sediment concentration, algae concentration, and color. This value was calculated by the light attenuation model, which will be discussed in the next section.

4.6 Light Attenuation Model

One of the most important variables controlling phytoplankton photosynthesis is "photosynthetically active radiation" (PAR), or light, in the range of wavelengths from 400-700nm, which provides the predominant source of energy for autotrophic organisms (Day et al., 1989). Absorption and scattering of light by water and dissolved and suspended matter determine the quantity and spectral quality of light at a given depth (Jerlov, 1976; Prieur and Sathyendranath, 1981), which in tern affect the photosynthesis of aquatic plants.

One way to develop a light attenuation model is to find a simple regression relationship between K_d (PAR), calculated from light measurements, and water quality

measurements collected at the same instant as the K_d (PAR) vales. This type of empirical model is a simple way to relate light attenuation to water quality, at a certain time. This method was used by Mcpherson and Miller (1994) in Tampa Bay and Charlotte Harbor. A physics-based light attenuation model was developed as part of the CH3D-IMS (Sheng et al. 2001c, Christian and Sheng, 2003) and successfully applied to the Indian River Lagoon. This light model is adopted for the Charlotte Harbor study.

In the light model, the vertical light attenuation coefficient (K_d) is a function of solar zenith angle (μ_0), scattering (b) and total absorption (a_t) (Kirk, 1984)

$$K_d = \frac{1}{\mu_0}\left[a_t^2 + G(\mu_0)\cdot a_t \cdot b\right]^{1/2} \qquad (4.35)$$
$$and \quad G(\mu_0) = g_1 \cdot \mu_0 - g_2$$

with g_1 =0.473 and g_2=0.218 determined for the mid point of euphotic zone (Kirk, 1984).

The scattering coefficient, b, is determined only using particles since scattering due to particles is much greater than scattering due to water (Gallegos, 1994). Scattering can be described as a function of turbidity (Morel and Gentili, 1991) as follow:

$$b(\lambda) = (550/\lambda)\cdot[Turbidity] \qquad (4.36)$$

Total absorption (a_t) is partitioned into attributes of water (a_w), phytoplankton (a_{ph}), dissolved color (a_{dc}), and detritus (a_d).

$$a_t = a_w + a_{ph} + a_{dc} + a_d \qquad (4.37)$$

The absorption of water (a_w) can be determined from literature values (Smith and Baker, 1981) with 1 nm linearly interpolated from 5 nm found in the literature. Chlorophyll-specific absorption (a_{ph}) is calculated for the model from the linear relationship between the maximum absorption and analytical *chlorophyll_a* concentration (Dixon and Gary, 1999):

$$a_{ph}(\lambda) = \left(a_{ph}\right)_{MAX} \cdot Normalized\_Spectra(\lambda)$$
$$\left(a_{ph}\right)_{MAX} = 0.0209 \cdot (Chlorophyll\ a,\ \ corrected) \tag{4.38}$$

where $(a_{ph})_{MAX}$ is the maximum absorption of chlorophyll-a. To calculate *normalized_spectra* (λ), individual spectra are normalized to the maximum absorption (437 - 440 nm), and averaged for all samples for an overall normalized spectra.

The absorption by dissolved color, a_{dc}, for each wavelength in the visible spectrum can be found using a negative exponential function (Bricaud et al., 1981)

$$a_{dc}(\lambda) = g_{440} \cdot \exp\left[-s_{dc} \cdot (\lambda - 440)\right] \tag{4.39}$$

where g440 is the absorption by dissolved color at 440 nm and s_{dc} is spectral slope. Dixon and Gary (1999) calculated empirical absorption at 440 nm and spectral slope as a function of color (in PCU) at Charlotte Harbor in the form:

$$g_{440} = 0.0667 \cdot [color], \qquad n = 129, r^2 = 0.9329$$
$$s_{dc} = 0.00003 \cdot [color] - 0.0178, \qquad n = 129, r^2 = 0.5111 \tag{4.40}$$

Absorption due to organic and mineral detritus is represented as a function of turbidity (Gallegos, 1994):

$$a_d = \sigma_d(\lambda) \cdot [Turbidity] \tag{4.41}$$

where turbidity is in NTUs and $\sigma_d(\lambda)$ is the wavelength specific absorption cross section of turbidity as calculated in:

$$\sigma_d(\lambda) = \sigma_{bl} + \sigma_{400} \cdot \exp\left[-s_d(\lambda - 400)\right] \tag{4.42}$$

in which σ_{bl} is the longwave absorption cross section, σ_{400} is the maximum detritus absorption at 400 nm, and s_d is exponential slope.

The total absorption and scattering are used in Equation (4.49) to calculate the

vertical attenuation coefficient, $K_d(\lambda)$, for each wavelength depending on color, chlorophyll_*a* , and turbidity. This $K_d(\lambda)$ value and incident irradiation $E_0(\lambda)$ can be used in the equation for calculating irradiance $E_z(\lambda)$ at the reference depth, z_r:

$$E_z(\lambda) = E_0(\lambda) \cdot \exp\left[-K_d(\lambda) \cdot z_r\right] \tag{4.43}$$

The spectrum of incident sunlight data from table F-200 in Weast (1977) is used for incident spectral information, $E_0(\lambda)$, as in Gallegos's work (1994) . These data are shown in Table 4.2.

Table 4.2 The spectrum of incident sunlight data (Gallegos, 1994)

λ (nm)	E_0	λ (nm)	E_0	λ (nm)	E_0
400	4.780				
405	5.568	505	8.108	505	8.332
410	6.003	510	8.026	510	8.340
415	6.052	515	7.894	515	8.323
420	6.135	520	7.970	520	8.305
425	6.017	525	8.130	525	8.289
430	5.893	530	8.163	530	8.271
435	5.940	535	8.133	535	8.267
440	6.659	540	8.051	540	8.263
445	7.152	545	7.993	545	8.239
450	7.548	550	7.993	550	8.213
455	7.826	555	7.982	555	8.207
460	7.947	560	7.937	560	8.201
465	7.963	565	8.055	565	8.180
470	7.990	570	8.160	570	8.157
475	8.119	575	8.265	575	8.136
480	8.324	580	8.318	580	8.114
485	8.014	585	8.375	585	8.106
490	7.990	590	8.387	590	8.089
495	8.113	595	8.369	595	8.052
500	8.119	600	8.359	600	8.013

$E_0(\lambda)$ and $E_z(\lambda)$ are integrated over the visible spectrum to get PAR_0 for the incident PAR and $\widehat{PAR}_Z$ for the calculated PAR at the reference depth. The spectrally sensitive

attenuation coefficient $K_d(P\hat{A}R)$ is calculated from these integrated values by using the rearranged form of the Lambert-Beer equation:

$$K_d(P\hat{A}R) = \frac{1}{z_r}\ln\left(\frac{P\hat{A}R_Z}{PAR_0}\right) \tag{4.44}$$

This $K_d(P\hat{A}R)$ will be used in the model to calculate light levels throughout the water column as a function of measured incident light intensity. Dixon and Gray (1999) calibrated the light attenuation model with measured data and applied the model to determine the light requirements for seagrasses of the Charlotte Harbor estuarine system. The results of the optical model are very good, with mean percentage agreement between modeled and observed K_d of 110%. Using water quality data from all stations as inputs, Dixon and Gray (1999) determined that chlorophyll, color, and turbidity account for 4%, 66%, and 31% of water column light attenuation, respectively. The maximum annual average chlorophyll contribution is 6%, with an individual maximum of 18% during a phytoplankton bloom. Color dominated water column attenuation, ranging from 40% to 78%. Stations in the lower Harbor and southern sites showed increased attenuation due to turbidity, compared to the upper Harbor site (Dixon and Gary, 1999). For the southern sites, a much larger portion of light attenuation is produced by turbidity, up to 55% for the station near Captiva pass.

To provide a light attenuation component which can be coupled with water quality, hydrodynamic, and sediment model components in the Charlotte Harbor estuarine system. A stand alone light model needs to be developed and calibrated with measured data. The stand alone light model has been calibrated by finding best fit between simulated and measured light attenuation with various coefficient sets.

For calibration of the light model, σ_{bl}, σ_{400}, s_d, *and* s_y are allowed to vary within

certain ranges. The predicted $k_d(PAR)$ values for the stand alone light model are compared to the corresponding $k_d(PAR)$ values from data provided by the SFWMD. If the predicted values do not match data well, then attempts are made to try to find model coefficients to produce better fit. In this case, the model is run and the coefficients are varied between maximum and minimum literature values specified in Table4.3 (Christian and Sheng, 2003). More than one thousand runs of light model simulations were conducted with this data set. The RMS errors were calculated for each run to test model performance of each set of light model coefficients. The root mean square error is an indication of the average discrepancy between observations and model results. In addition to root mean square error, model calibration was assessed via plots of model output and observation. Scatter plots of model output and observed data provide an indication of overall model performance. The best RMS errors for each of the tests is 0.6111 $^{-1}$ with best fit coefficients shown in Table 4.4 Dixon and Gray (1999) found the coefficients in Table 4.5 provided the best fit to all the data they examined. They applied σ_{400} *and* s_y as a function of color. The RMS error with this coefficient is 0.6511 m^{-1}. Even though, they reduced adjustable coefficients with relationship of σ_{400} *and* s_y with color, the RMS error is greater than that for adjusting all four coefficients. In this study, the best fit coefficients were used for simulating light attenuation. Figure 4.6 contains calibration period scattering plots with best fit of coefficient sets. The location of circles indicate the correlation between model predictions and observed data. A perfect match between model and observed data is indicated by the diagonal line on each graph. Circle above the line shows over prediction, while circles below the line indicate that under prediction.

Table 4.3 Coefficient ranges for use in stand along light model.

Coefficients	Minimum value	Maximum value
σ_{bl}	0.004	0.090
σ_{400}	0.255	0.600
s_d	0.011	0.019
s_y	0.011	0.019

Table 4.4 Best fit light model coefficients for Charlotte Harbor estuarine system.

Coefficient	Value
σ_{bl}	0.01 $m^{-1}NTU^{-1}$
σ_{400}	0.59 $m^{-1}NTU^{-1}$
s_d	0.014 nm^{-1}
s_y	0.013 nm^{-1}

Table 4.5 Dixon and Gray's model coefficients for the Charlotte Harbor estuarine system.

Coefficient	Value
σ_{bl}	0.064 $m^{-1}NTU^{-1}$
σ_{400}	0.0014×color+0.0731 $m^{-1}NTU^{-1}$
s_d	0.01125 nm^{-1}
s_y	0.00003×color+0.0178 nm^{-1}

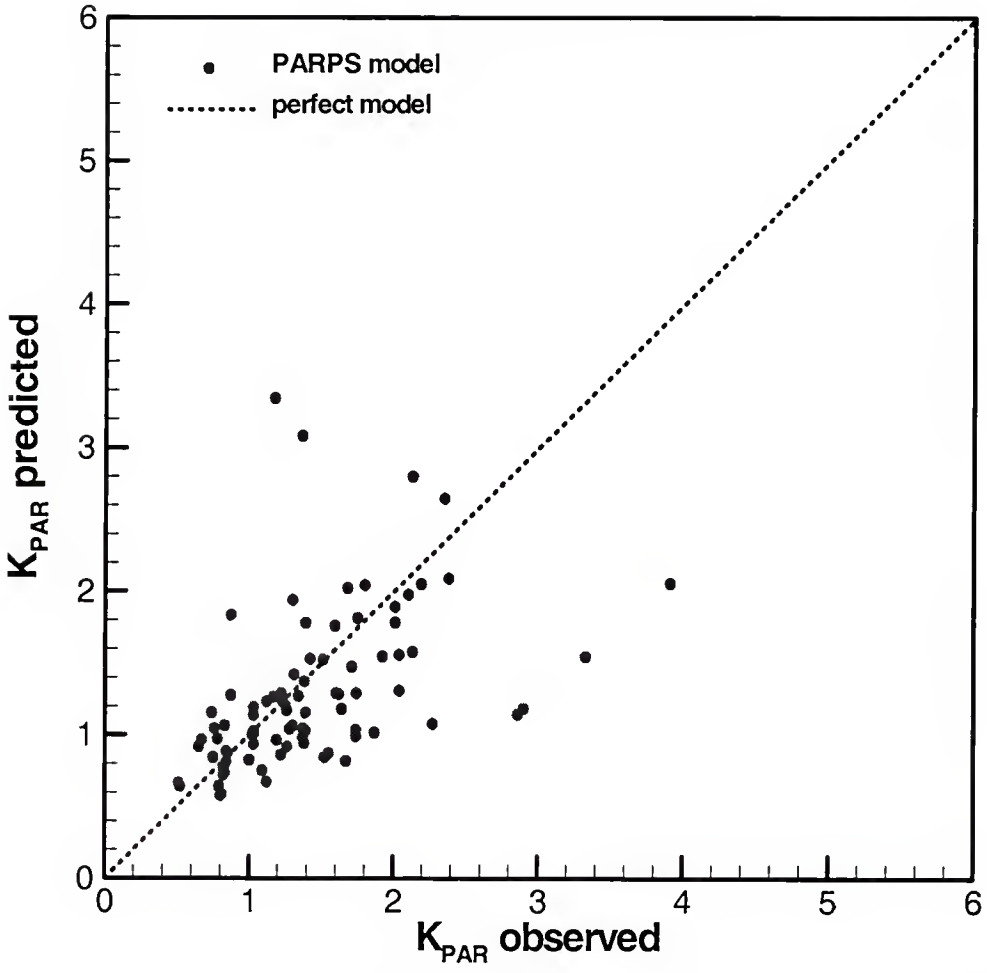

Figure 4.6 The scatter plots for Kd(PAR) during calibration period with best fit coefficients.

The water quality and sediment model outputs needed for the light model are turbidity in NTUs, chlorophyll_*a* concentration in μg/L, and color in Pt. Units. To calculate solar angle, this model needs the latitude and simulation day and time. Because the sediment model simulates the total suspended solids (TSS), it is necessary to develop a regression between TSS (mg/L) and turbidity (NTU) as follow:

$$Turbidity = 0.2677 \times TSS + 0.9665 \qquad \text{for 1996 data}$$
$$Turbidity = -0.0153 \times TSS + 2.602 \qquad \text{for 2000 data}$$

The stand alone light model was tested, calibrated, and then coupled with the models of hydrodynamics, sediment and water quality.

4.7 Model Parameters and Calibration Procedures

Reaction terms described in the previous section contain many model parameters which must be determined before using the model. The determination of model parameters is generally very difficult because they depend on many physical and biochemical factors, such as the location of the estuary, temperature and tidal variation, and point or non-point source loadings of nutrients and other chemical materials. In practice, parameters are selected from a range of feasible values, tested in the model, and adjusted until an optimal agreement between simulated and measured values is obtained. Two ways to determine feasible ranges of model parameters are field observation and laboratory experimentation. When field observations and laboratory experimentation are not available, the feasible ranges are obtained from literature or previous modeling studies. A list of the important kinetic parameters and their literature values are given in Table 4.6 ~ 4.11.

Table 4.6 Temperature adjustment functions for water quality parameters

Parameter	description	Unit	literature value	Reference
(θ_{phy})	temperature function for phytoplankton growth	-	1.01 ~ 1.2 1.09 1.08	Di Toro et al. (1980) Pribble et al.(1997) Sheng et al. (2001)
(θ_{kas})	temperature function for phytoplankton respiration and mortality	-	1.045 1.05 1.08	Ambrose (1991) Pribble et al.(1997) Sheng et al. (2001)
(θ_{zoo})	temperature function for zooplankton growth, respiration and mortality	-	1.01 ~ 1.2 1.04	Di Toro et al. (1980) Sheng et al. (2001)
(θ_{ONM})	temperature function for ammonification	-	1.0 ~ 1.04 1.07 1.02	Bowie et al. (1985) Pribble et al.(1997) Sheng et al. (2001)
(θ_{NN})	temperature function for nitrification	-	1.02 ~ 1.08 1.08 1.08	Bowie et al. (1985) Pribble et al.(1997) Sheng et al. (2001)
(θ_{DN})	temperature function for denitrification	-	1.02 ~ 1.09 1.04 1.045	Bowie et al. (1985) Pribble et al.(1997) Sheng et al. (2001)
(θ_{AI})	temperature function for ammonia instability	-	1.08	Sheng et al. (2001)
(θ_{OPM})	temperature function for mineralization	-	1.08	Sheng et al. (2001)
(θ_{SID})	temperature function for sorption/desorption	-	1.08	Sheng et al. (2001)
(θ_{D})	temperature function for oxidation	-	1.02 ~ 1.15 1.08	Bowie et al. (1985) Sheng et al. (2001)
(θ_{SOD})	temperature function for sediment oxygen demand	-	1.045 1.08	Bowie et al. (1985) Sheng et al. (2001)

Table 4.7 Water quality parameters related to conversion rate

Parameter	description	Unit	literature value	Reference
A_{OC}	Phytoplankton Carbon / Oxygen rate	gO_2/gC	2.67 2.67 2.67	Ambrose(1991) Cerco and Thomas (1995) Sheng et al. (2001)
ChlaC	Phytoplankton Carbon / Chlorophyll_*a* rate	gC/gChl a	10~ 112 100 60 50	Bowie et al. (1985) Pribble et al.(1997) Cerco and Thomas (1995) Sheng et al. (2001)
A_{CN}	Phytoplankton Carbon / Nitrogen rate	gN/gC	0.05 ~0.43 0.15 0.167 0.15	Jorgensen (1976) Pribble et al.(1997) Cerco and Thomas (1995) Sheng et al. (2001)
A_{CP}	Phytoplankton Carbon / Phosphorous rate	gP/gC	0.005~0.03 0.027 0.025	Jorgensen (1976) Cerco and Thomas (1995) Sheng et al. (2001)

Table 4.8 Water quality parameters related to phytoplankton and zooplankton

Parameter	description	Unit	literature value	Reference
$(\mu_{phy})_{\max}$	maximum phytoplankton growth rate	1/day	0.2 ~ 8 2.25 ~ 2.5 1.06~ 2.68	Bowie et al. (1985) Cerco and Thomas (1995) Sheng et al. (2001)
H_n	Nitrogen half saturation rate for phytoplankton uptake	µg/l	1.5 ~ 400 0.5 1 10	Bowie et al. (1985) Pribble et al.(1997) Cerco and Thomas (1995) Sheng et al. (2001)
H_p	Phosphorous half saturation rate for phytoplankton uptake	µg/l	1. ~ 105 1 1 2~4	Bowie et al. (1985) Pribble et al.(1997) Cerco and Thomas (1995) Sheng et al. (2001)

I_{opt}	optimum light intensity for phytoplankton growth	ly/day	225~600 300	Canale et al. (1976) Sheng et al. (2001)
K_{ax}	phytoplankton respiration rate	1/day	0.02~ 0.24 0.03~ 0.09 0.03~ 0.05	Jorgenson (1976) Cerco and Thomas (1995) Sheng et al. (2001)
K_{as}	phytoplankton non-predator mortality	1/day	0.01~ 0.22 0.03~ 0.09 0.02~ 0.06	Jorgenson (1976) Cerco and Thomas (1995) Sheng et al. (2001)
ws_{phy}	phytoplankton settling rate	m/day	0. ~ 3. 0. ~ 0.25 0.05 ~ 0.1	Bowie et al. (1985) Cerco and Thomas (1995) Sheng et al. (2001)
H_{phy}	phytoplankton half saturation rate for zooplankton uptake	µg/l	200~2000 800~1200	Bowie et al. (1985) Sheng et al. (2001)
Trs_{phy}	phytoplankton threshold for zooplankton uptake	µg/l	1~200 200	Bowie et al. (1985) Sheng et al. (2001)
$(\mu_z)_{\max}$	maximum zooplankton growth rate	1/day	0.15 ~0.5 0.18 ~0.2	Bowie et al. (1985) Sheng et al. (2001)
K_{zx}	zooplankton respiration rate	1/day	0.003~0.07 5 0.01	Bowie et al. (1985) Sheng et al. (2001)
K_{zs}	zooplankton non-predator mortality	1/day	0.001~0.36 0.015~0.05 5	Jorgensen (1976) Sheng et al. (2001)

Table 4.9 Water quality parameters in the nitrogen dynamics

Parameter	description	Unit	literature value	Reference
K_{ONM}	Ammonification rate	1/day	0.001~0.4 0.1 0.015 0.01	Bowie et al. (1985) Pribble et al. (1997) Cerco and Thomas (1995) Sheng et al. (2001)

K_{NN}	nitrification rate	1/day	0.004~0.11 0.08 0.07 0.01~0.02	Bowie et al. (1985) Pribble et al.(1997) Cerco and Thomas (1995) Sheng et al. (2001)
H_{nit}	DO saturation rate for nitrification	mg/l	0.1~2.0 2 2	Ambrose (1994) Pribble et al.(1997) Sheng et al. (2001)
K_{DN}	denitrification rate	1/day	0.02~ 1.0 0.09 0.09	Bowie et al. (1985) Pribble et al.(1997) Sheng et al. (2001)
H_{no3}	DO saturation rate for denitrification	mg/l	0.~ 1.0 0.1	Bowie et al. (1985) Sheng et al. (2001)
P_{on}	partition coefficient of PON/SON	-	1.E-5 1.E-6~9E-6	Simon (1989) Sheng et al. (2001)
P_{an}	partition coefficient of PIN/NH4	-	5.E-6~1.E-5 3.E-5~4.E-3	Simon (1989) Sheng et al. (2001)
d_{on}	sorption/desorption rate for SON/PON	1/day	0.02 0.08 0.01~0.02	Bowie et al. (1985) Cerco and Thomas (1995) Sheng et al. (2001)
d_{an}	sorption/desorption rate for PIN/NH4	1/day	0.01	Sheng et al. (2001)
K_{PDN}	preference partition coefficient of mortality for SON / PON	-	0.5 0.5	Cerco and Thomas (1995) Sheng et al. (2001)

Table 4.10 Water quality parameters in the phosphorous dynamics

Parameter	description	Unit	literature value	Reference
K_{OPM}	mineralization rate	1/day	0.001 ~ 0.6 2.27 0.1 0.1	Bowie et al. (1985) Pribble et al. (1997) Cerco and Thomas (1995) Sheng et al. (2001)
P_{op}	partition coefficient of POP/SOP	-	8.E-6 ~1.E-4	Sheng et al. (2001)

P_{ap}	partition coefficient of PIP/SRP	-	1.E-6 ~ 6E-4	Sheng et al. (2001)
d_{op}	sorption/desorption rate for SOP/POP	1/day	0.08 0.01	Cerco and Thomas (1995) Sheng et al. (2001)
d_{ap}	sorption/desorption rate for PIP/SRP	1/day	0.01	Sheng et al. (2001)
p_{PDP}	preference partition coefficient of mortality for SOP / POP	-	0.5 0.5	Cerco and Thomas (1995) Sheng et al. (2001)

Table 4.11 Water quality parameters in the oxygen balance

Parameter	description	Unit	literature value	Reference
K_D	oxidation rate	1/day	0.02 ~ 0.6 0.05	Bowie et al. (1985) Sheng et al. (2001)
H_{CBOD}	DO half saturation rate for oxidation	mg/l	1.5 ~ 400 0.5 1 10	Bowie et al. (1985) Pribble et al.(1997) Cerco and Thomas (1995) Sheng et al. (2001)
fd_{CBOD}	partition coefficient of particular/dissolved CBOD	-	0.5 0.3~0.5	Bowie et al. (1985) Sheng et al. (2001)
SOD	Sediment oxygen demand	gO_2/m^2-day	0.02~10. 0.0 ~ 10.7	Thomann (1972) Bowie et al. (1985)
H_{SOD}	DO half saturation rate for sediment oxygen demand	mg/l	0.01~ 0.22 0.03~ 0.09 0.02~ 0.06	Jorgenson (1979) Cerco and Thomas (1995) Sheng et al. (2001)
K_{AE}	reaeration rate	1/day	0. ~ 3. 0. ~ 0.25 0.05 ~ 0.1	Bowie et al. (1985) Cerco and Thomas (1995) Sheng et al. (2001)

Model calibration is the first stage testing or tuning of the model to a field data not used in the original construction of the model. Such tuning is to include consistent and rational set of theoretically defensible parameters and inputs (Thomann, 1992). Proper calibration of the water quality model requires having accurate representation of the inflow and loads of nutrients into the water body and selecting appropriate model parameters.

The reaction equation shown in previous section is a function of its concentration and the water quality parameters connected to it by the indicated processes. Within each reaction equation, there are numerous kinetic parameters and additional parameters. Water quality model in CH3D-IMS consists of 13 state variable equations with over 40 interrelated parameters. The interactions of water quality model parameters and the constituent equations as shown in Table 4.12 clearly indicate the complexity of the calibrating these types of models. The column of Table 4.12 show that each modeled constituent equation contains between 2 and 15 different water quality parameters. According to each row, each parameter can be found in up to 10 different constituent equations. Therefore, changing one parameter to improve the calibration of one constituent will simultaneously affect many other constituents. Traditionally, calibration of water quality models has been performed manually using a trial-and-error parameter adjustment procedure. The process of manual calibration depending on the number of model parameters and the degree of parameter interaction. With complexity of water quality model, the traditional process is a very tedious and time consuming task. It is necessary to apply more systematic and efficient calibration procedure for reducing calibration time and effort.

Based on the cascading effect of adjusting interrelated parameters, the efficient calibration of the water quality model should begin with the parameters that affect the more

constituents and the more sensitive parameters. First of all, each water quality parameter can be ranked with these sensitivity and relativity as parameterization. According to this order, high ranked parameters will be adjusted to reproduce major pattern of all constituents, and then lower ranked parameters will be calibrated for detail characteristics of local constituents. This procedure will reduce numerous calibration efforts and increase efficiency and effectiveness.

The calibration procedure involves optimization of numerical measures (objective functions) that compare observations of the state of the system with corresponding simulated values. The most commonly used objective function adopted in calibration is the root mean square errors between the observed and simulated model response. The root mean square error is an indication of the average discrepancy between observations and model results. It is computed as follow:

$$RMS = \sqrt{\frac{\sum (O - P)^2}{n}} \tag{4.45}$$

where RMS is root mean square error

O is observation

P is model prediction

n is number of observation

In addition with root mean square error, model calibration was assessed via plots of model output and observation with correlation coefficient R^2. Scatter plots of model output and observed data provide an indication of overall model performance. The correlation coefficient is defined by

$$R^2 = \frac{SS_{xy}^2}{SS_{xx} \cdot SS_{yy}} = \frac{(\sum O \cdot P - n \cdot \bar{O} \cdot \bar{P})^2}{(\sum O^2 - n \cdot \bar{O}^2) \cdot (\sum P^2 - n \cdot \bar{P}^2)}$$
$$SS_{xx} = \sum (O_i - \bar{O})^2 = \sum O^2 - n \cdot \bar{O}^2 \qquad (4.46)$$
$$SS_{yy} = \sum (P_i - \bar{P})^2 = \sum P^2 - n \cdot \bar{P}^2$$
$$SS_{xy} = \sum (O_i - \bar{O})(P_i - \bar{P}) = \sum O \cdot P - n \cdot \bar{O} \cdot \bar{P}$$

The process of model calibration is illustrated in Figure 4.7. In systematic calibration procedure, parameters are adjusted according to order of sensitivity and relativity according to parameterization for optimization of certain criteria (objective functions) that measure the goodness-of-fit of the simulation model. The process is repeated until a specified stopping criterion is satisfied.

Formation of a proper framework for systematic calibration involves the following key elements:

- Sensitivity analysis
- Model parameterization and choice of calibration parameters
- Specification of calibration criteria

The best way to calibrate water quality parameters is the automatic calibration, in which parameters are adjusted automatically according to a specific search scheme for optimization of certain calibration criteria. The process is repeated until a specified stopping criterion is satisfied. In this study, automatic calibration procedures have been developed and tested, using a Gauss-Newton method.

To test the automatic calibration procedure of the CH3D water quality model, a 1996 baseline run was adopted as representative of the true and valid field condition. All parameters from baseline run were considered representative of conditions that could hypothetically exist in the field. A small number of these parameters were perturbed slightly, and the automatic calibration procedure was employed. If the procedure is correct, these

perturbed parameters should converge on pre-perturbed values. The results of the test show that the changed parameters did converge on pre-perturbed baseline values, with the Gauss-Newton method. The method is therefore considered valid and accurate.

In real case, a trial run was conducted by using all the measured data to find best fit parameters. The calibration procedure continuously failed as calibration parameters were automatically adjusted outside the upper and lower bounds. The accuracy of the model calibration generated by this procedure, relies heavily on the quality and quantity of field observation, the model structure, and the nature of the system. Limited data, and uncertainties in water quality processes caused the procedure to fail to generated a valid calibration condition. To apply an automatic calibration procedure to this, or other water quality models, further investigation is required. These investigations should be focus on the optimization algorithm and refinement of the water quality processes.

Table 4.12 The relationship between water quality parameters and model constituents

	CA	CZ	PIN	NH4	NO3	SON	PON	PIP	SRP	SOP	POP	DO	CBOD	#of Eqns
AGRM	1			1	1				1			1		5
HALFN	1													1
HALFP	1													1
KAEX	1			1					1			1	1	5
KAS	1					1	1			1	1	1	1	7
WAS	1													1
HALFA	1	1												2
TRESHA	1	1												2
ZGRM	1	1												2
KZEX		1		1					1					3
KZS		1				1	1			1	1		1	6
SONM				1		1								2
NITR				1	1							1		3
DENR					1							1		2
PCON						1	1							2
DRON						1	1							2
KPDN						1	1							2
PCAN			1	1										2
DRAN			1	1										2
SOPM									1	1				2
PCOP										1	1			2
DROP										1	1			2
KPDP										1	1			2
PCIP								1	1					2
DRIP								1	1					2
SODM												1		1
FD5												1	1	2
AKD												1	1	2
AOC	1			1	1	1	1		1	1	1	1	1	10
CHLAC	1	1												2
CAN	1	1		1	1	1	1							6
ACP	1	1							1	1	1			5
TOPT	1													1
OPTL	1													1
AKNIT				1	1							1		3
AKDEN					1							1		2
AKBOD												1	1	2
AKSOD												1		1
AKAIR												1		1
# of Parameters	15	8	2	10	7	8	7	2	8	8	7	14	7	103

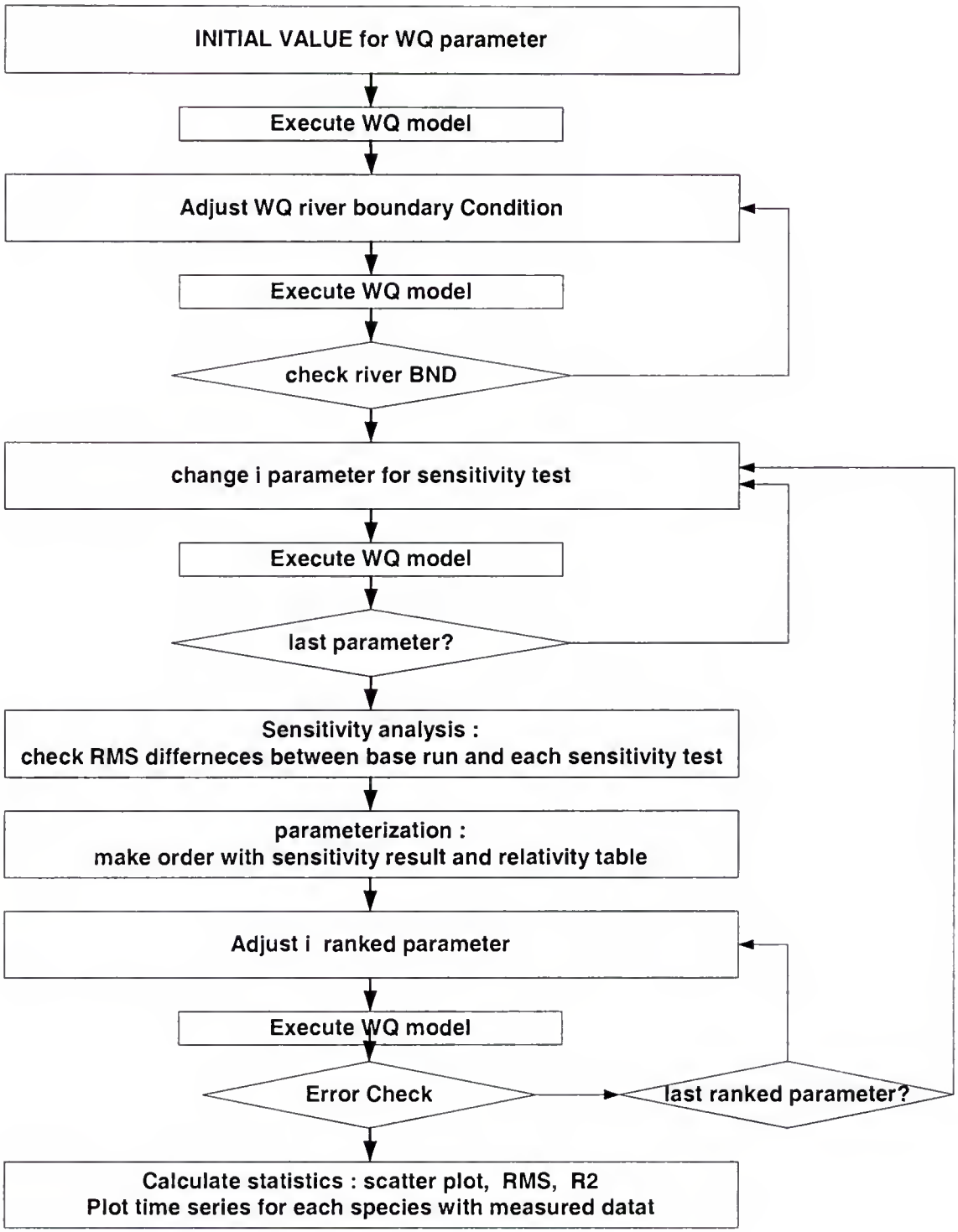
INITIAL VALUE for WQ parameter
Execute WQ model
Adjust WQ river boundary Condition
Execute WQ model
check river BND
change i parameter for sensitivity test
Execute WQ model
last parameter?
Sensitivity analysis :
check RMS differneces between base run and each sensitivity test
parameterization :
make order with sensitivity result and relativity table
Adjust i ranked parameter
Execute WQ model
Error Check
last ranked parameter?
Calculate statistics : scatter plot, RMS, R2
Plot time series for each species with measured datat

Figure 4.7 Systematic calibration procedure

CHAPTER 5
APPLICATION OF CIRCULATION AND TRANSPORT MODEL

Circulation in Charlotte Harbor is driven by tide, wind, and density gradient. The numerical model of circulation and transport described in Chapter 3 was applied to the Charlotte Harbor estuarine system, a large shallow estuary in southwest Florida. Model applications include 1) the simulation of three-dimensional circulation during summer 1986 2)one year simulation of flow, salinity, temperature, and sediment transport in 2000 and 3) simulation of the impact of removal of Sanibel Causeway on the circulation in San Carlos Bay and Pine Island Sound

A major purpose of the first two simulations is the calibration and validation of the Charlotte Harbor circulation and transport model using field data obtained by USGS, NOAA, SWFWMD, and SFWMD in Summer 1986 and January to December in 2000. During the calibration process, a few model coefficients and/or boundary/initial conditions are adjusted to produce more accurate overall simulation of observed data collected in July 1986 by USGS (Hammet, 1992; Stoker, 1992; Goodwin, 1996) covered the entire Charlotte Harbor estuarine system and include water level, horizontal currents and salinity. Hence July 1986 data were used for short-term calibration. To supplement the short-term calibration of July 1986, the long-term model calibration was conducted using one year water level and salinity data in Caloosahatchee River during 2000.

5.1 A High-Resolution Curvilinear Grid for Charlotte Harbor Estuarine System

To procedure a successful numerical simulation of the Charlotte Harbor estuarine system, it is necessary to design a numerical grid which represents the dominant geographic/ bathymetric features with sufficient spatial resolution. Since CH3D use a boundary-fitted curvilinear grid in the horizontal directions, it is possible to align the grid lines to coincide with shorelines, causeways, and bridges. The Charlotte Harbor estuarine system encompasses about 735 km^2 on Florida's southwest coast. The model domain includes all the sub-basins (Upper Charlotte Harbor, Lower Charlotte Harbor, Pine Island Sound, Matlatcha Pass, and San Carlos Bay), the major tributaries (Peace, Myakka, and Caloosahatchee up to the Franklin Dam), Estero Bay, and some offshore water. The model should be run with a spatial grid sufficiently fine to resolve the Sanibel Causeway. The eastern boundary includes many of the major rivers with specified flow rates, while the western boundaries and the western portion of north and south boundaries are open tidal boundaries where tidal elevations are prescribed. The interior of the model domain is represented with a boundary-fitted grid which is non-orthogonal but as orthogonal as possible, i.e. the grid analysis are usually between 60° and 120°.

The final boundary fitted grid used for the three-dimensional curvilinear-grid model (CH3D) of Charlotte Harbor estuarine system was generated using a grid generation program originally developed by Thompson et al. (1985) and further enhanced for this study. This grid (Figure 5.1) contains 92 x 129 horizontal cells and eight vertical layers, with a total of 11648 horizontal grid cells which include 5367 water cells and 6281 land cells. Grid spacing varies from 40 to 2876 meters (average 598 meters).

The bathymetry of the Charlotte Harbor estuarine system and the nearshore region

of the Gulf of Mexico is derived from data obtained from the Geophysical Data System of National Geophysical Data Center. Bathymetry of navigation channels in San Carlos Bay and the vicinity of Sanibel Causeway are based on the recent survey data provided by Lee County in December 1999. Bathymetry for Peace River and the upper Charlotte Harbor area was collected by SWFWMD and that for Caloosahatchee River was collected by SFWMD. All bathymetric data were converted to NAVD88 to unify vertical datum level (Appendix H). Charlotte Harbor grid bathymetry (Figure 5.2) was developed using all these bathymetric data. While an inverse distance interpolation followed by simple smoothing scheme was the primary method for determining bathymetry in the study area, several areas were added and the bathymetry further adjusted after the interpolation and smoothing was performed to ensure the proper passage of flow through a navigation channels.

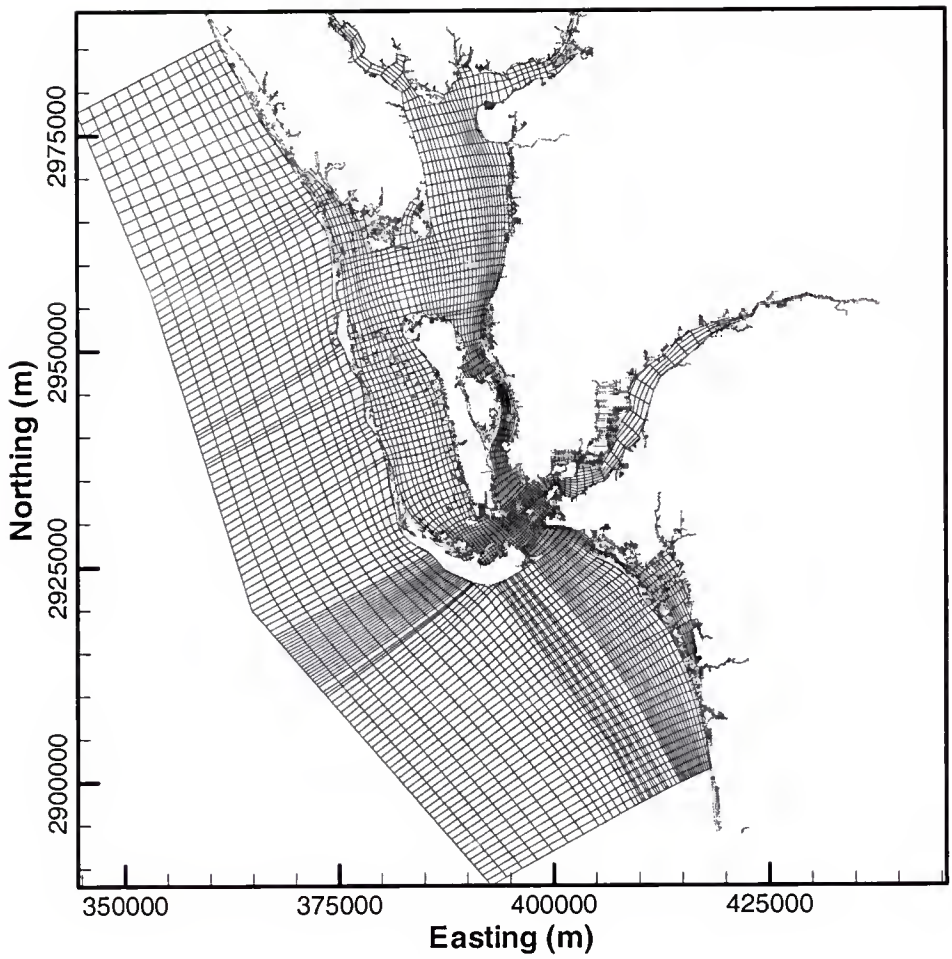

Figure 5.1 Boundary-fitted grid (92 x 129) used for numerical simulation for Charlotte Harbor estuarine system.

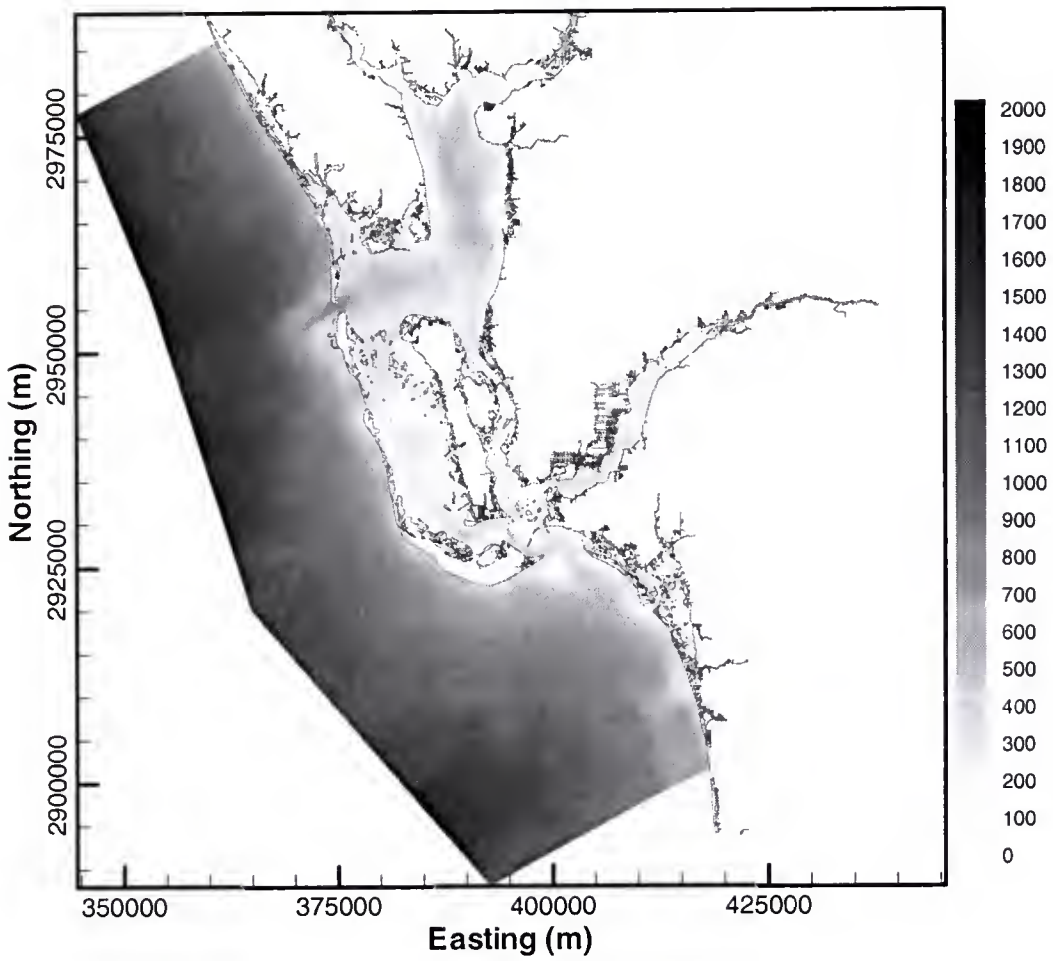

Figure 5.2 Bathymetry in boundary-fitted grid for Charlotte Harbor estuarine system (92 x 129).

5.2 Forcing Mechanism and Boundary Conditions

The forcing mechanisms for the hydrodynamic model include tide, wind, and density gradients. To incorporate these mechanisms in the model simulations, tides and oceanic salinity are specified along the offshore boundary, wind is specified at the air-sea interface, and river discharges are specified at the river boundaries.

The boundary between the Charlotte Harbor estuarine system and the Gulf of Mexico extends about 64 km from Gasparilla Pass on the north to San Carlos Pass on the south. One of the most important features is the similarity between the tidal curves at Venice and Cayo Costa which are located at northern end and near Boca Grande Pass (Figure 1.1). The phasing of the Gulf tides is nearly synchronous along the boundary of the estuarine system between Venice and Naples, which are located at the northern and southern ends.

For the 2000 simulation, tidal forcing along the Gulf of Mexico boundary was prescribed with water level data measured at the Naples station by the NOAA CO-OPS. For the 1986 simulation, water level data at Venice measured by USGS were used to provide the tidal boundary condition, since there was no data from the Naples station in this period. To unify the datum level with the bathymetry, these water level data were converted to NAVD88 datum level.

Discharge and runoff boundary conditions were imposed using the daily measured discharge data described in Table 4.1. Because no flow data were available for the Estero Bay and Caloosahatchee River except at S-79 in 1986, the discharges were assumed to be one half and a quarter of the Myakka River discharges, respectively.

The surface wind boundary condition is supplied using hourly wind magnitude and direction data collected at three stations, which are the National Data Buoy Center C-MAN

stations at Venice (27.07 N, 82.45 W), NOAA CO-OPS stations at Fort Myers (26° 36' N, 81° 52' W), and Naples (26.13 N, 81.807 W). For the 2000 simulation, hourly wind data from all three stations are available, while only the Venice and Fort Myers stations are available for 1986 simulation. The hourly wind magnitude and direction are converted into x-(East/West) and y- (North/South) velocity components using Garrat's formula (Garrat, 1977). These values are then interpolated to the entire computational grid, with a weighting function inversely proportional to the square of distances. Figures 5.3 shows the water level at Venice station for tidal boundary condition and the river flows at river boundaries in 1986. Figure 5.4 shows wind speed and direction at Venice and Fort Myers station in 1986. Figure 5.5 shows the water level at Naples station for tidal boundaries and the river flows at river boundaries in 2000. Figure 5.6 shows wind speed and direction at Venice, Fort Myers and Naples in 2000.

Table 5.1 Descriptions of 1986 and 2000 river boundary conditions for Charlotte Harbor estuarine system.

Station	Name	Agency	Latitude degree W	Longitude degree N	drainage area:mi^2	perio d
	Myakka River					
02298830	near Sarasota	USGS	27°14'25"	82°18'50"	229.0	daily
02299120	at Deer Prairie Slough	USGS	27°08'06"	82°15'24"	-	daily
02299410	at Big Slough Canal	USGS	27°11'35"	82°08'40"	36.5	daily
	Peace River					
02296750	at Arcade	USGS	27°13'19"	81°52'34"	1,376.0	daily
02297100	at Joshua Creek	USGS	27°09'59"	81°52'47"	132.0	daily
02297310	at Horse Creek	USGS	27°11'57"	81°59'19"	218.0	daily
02298202	Shell Creek	USGS	26°59'04"	81°56'09"	373.0	daily
	in Caloosahatchee River					
02292900	S79 spillway	USGS	26°43'25"	81°41'55"	-	daily
02293214	Cape Coral	USGS	26°38'10"	81°55'48"	-	daily
02293230	Whiskey Creek	USGS	26°34'29"	81°53'29"	-	daily
	in Estero Bay					
02291500	Imperial	USGS	26°20'07"	81°44'59"	65.0	daily
02291524	Spring Creek	USGS	26°21'42"	81°47'27"	-	daily
02291580	Estero River	USGS	26°26'30"	81°47'45"	-	daily
02291673	Mullock & Henry Creek	USGS	26°30'19"	81°51'00"	-	daily

Baroclinic simulations require realistic initial salinity and temperature fields in order to minimize the effects of the initial conditions on the solution, and to minimize the "spin-up" time. Salinity along the offshore boundary is assumed to be approximately constant at 36.5 ppt. Salinity at the river boundaries was set to 0 ppt. The near bottom salinity data measured at the nine USGS stations in 1986 were used to determine the initial salinity at the corresponding grid cells. These salinity data were interpolated over the entire computational grid, with a weighting function inversely proportional to the square of the distance to the three nearest stations. Initial temperature field for 2000 simulation was interpolated using water temperature data at Fort Myers and Naples stations measured by NOAA CO-OPS and Venice stations measured by National Data Buoy Center (NDBC). Air temperature data at the same locations were used to calculate heat flux for air-sea interface (Figure 5.7). These air temperature data were also interpolated over the study area.

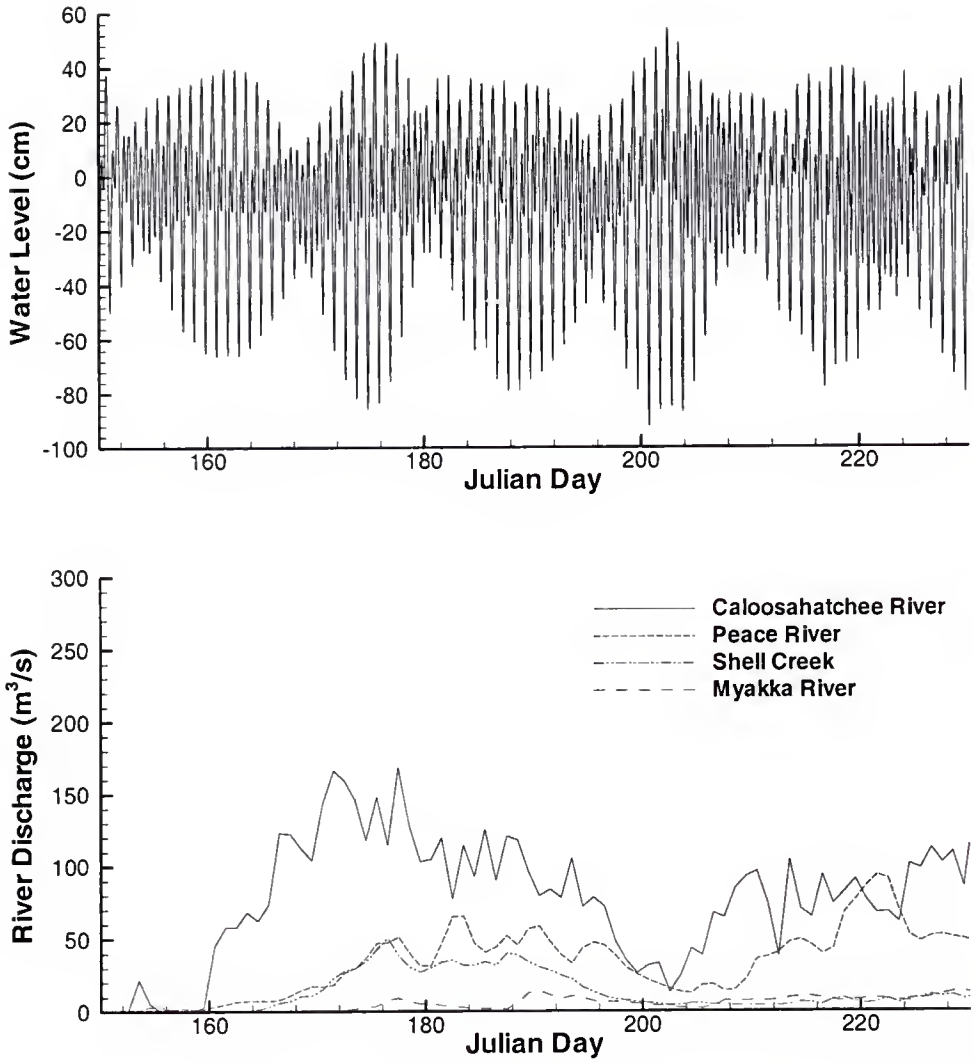

Figure 5.3 Tidal forcing and river discharges for 1986 simulation of Charlotte Harbor circulation.

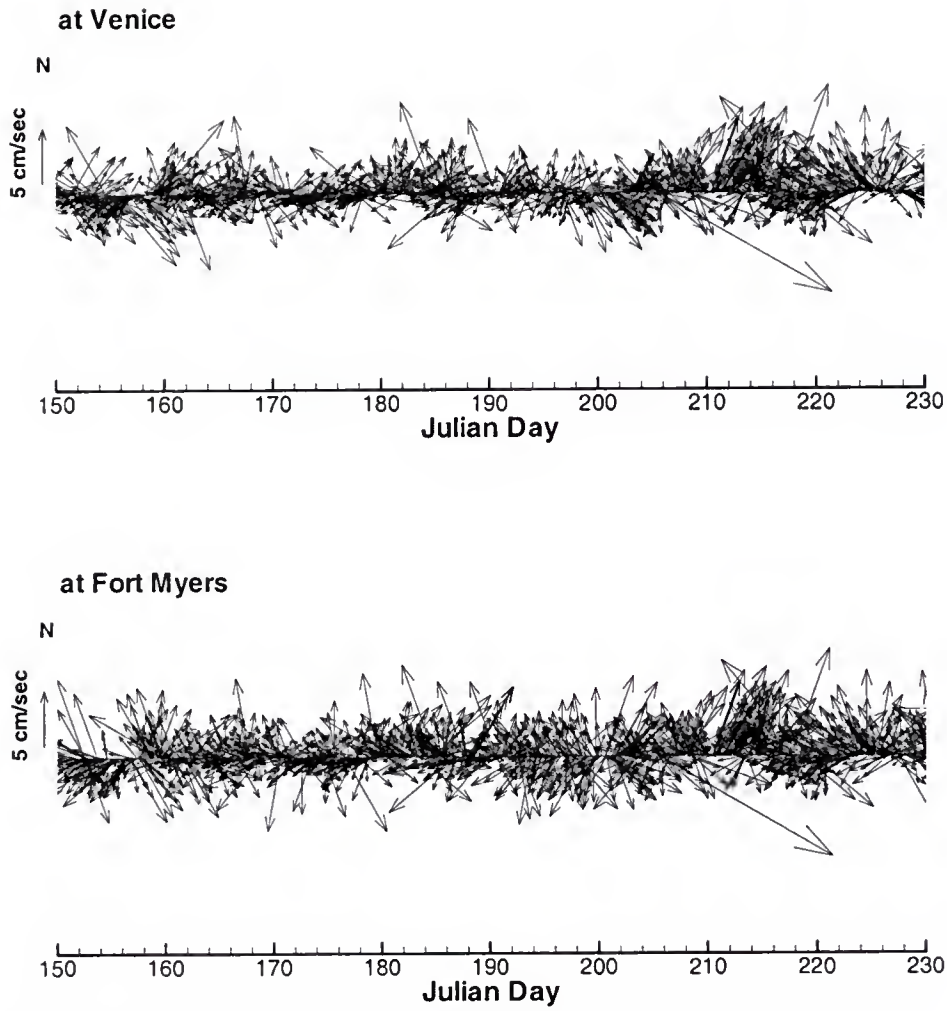

Figure 5.4 Wind velocity for 1986 simulation of Charlotte Harbor circulation.

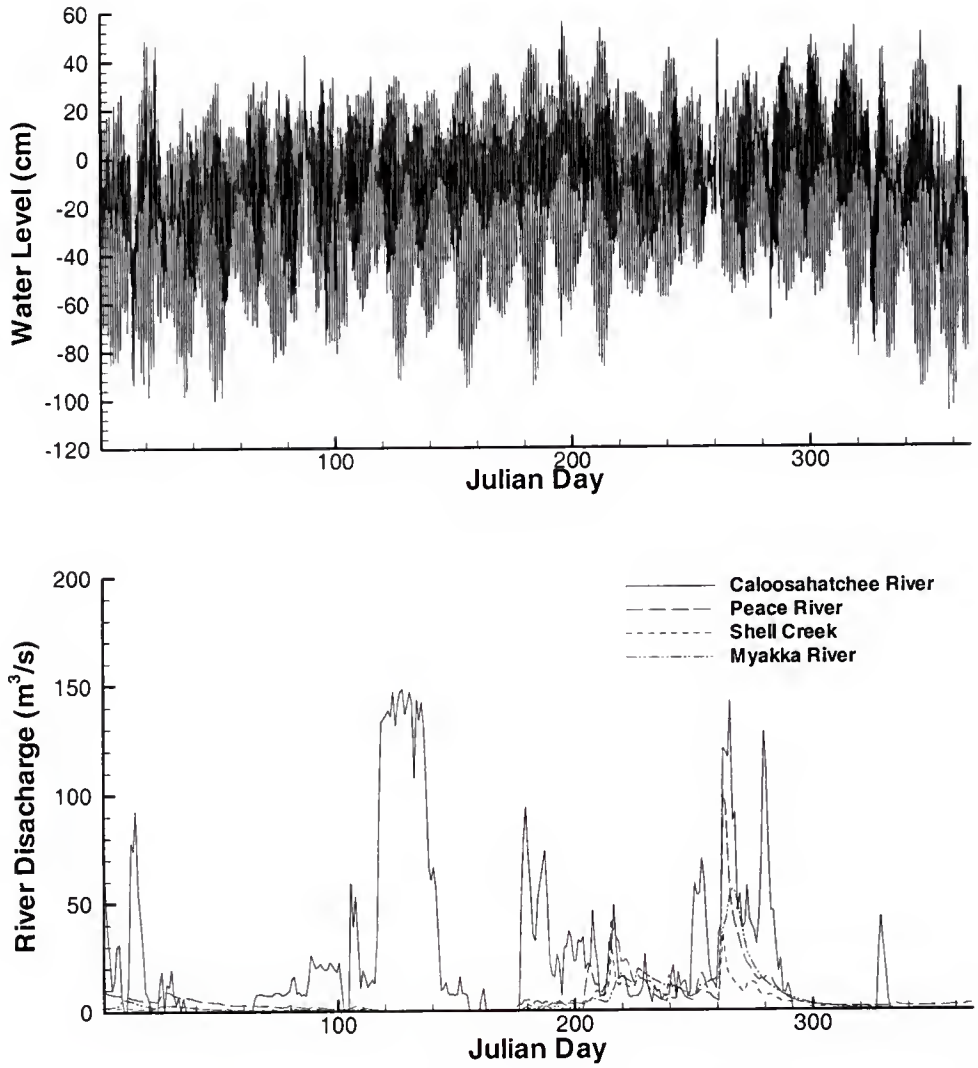

Figure 5.5 Tidal forcing and river discharges for 2000 simulation of Charlotte Harbor circulation

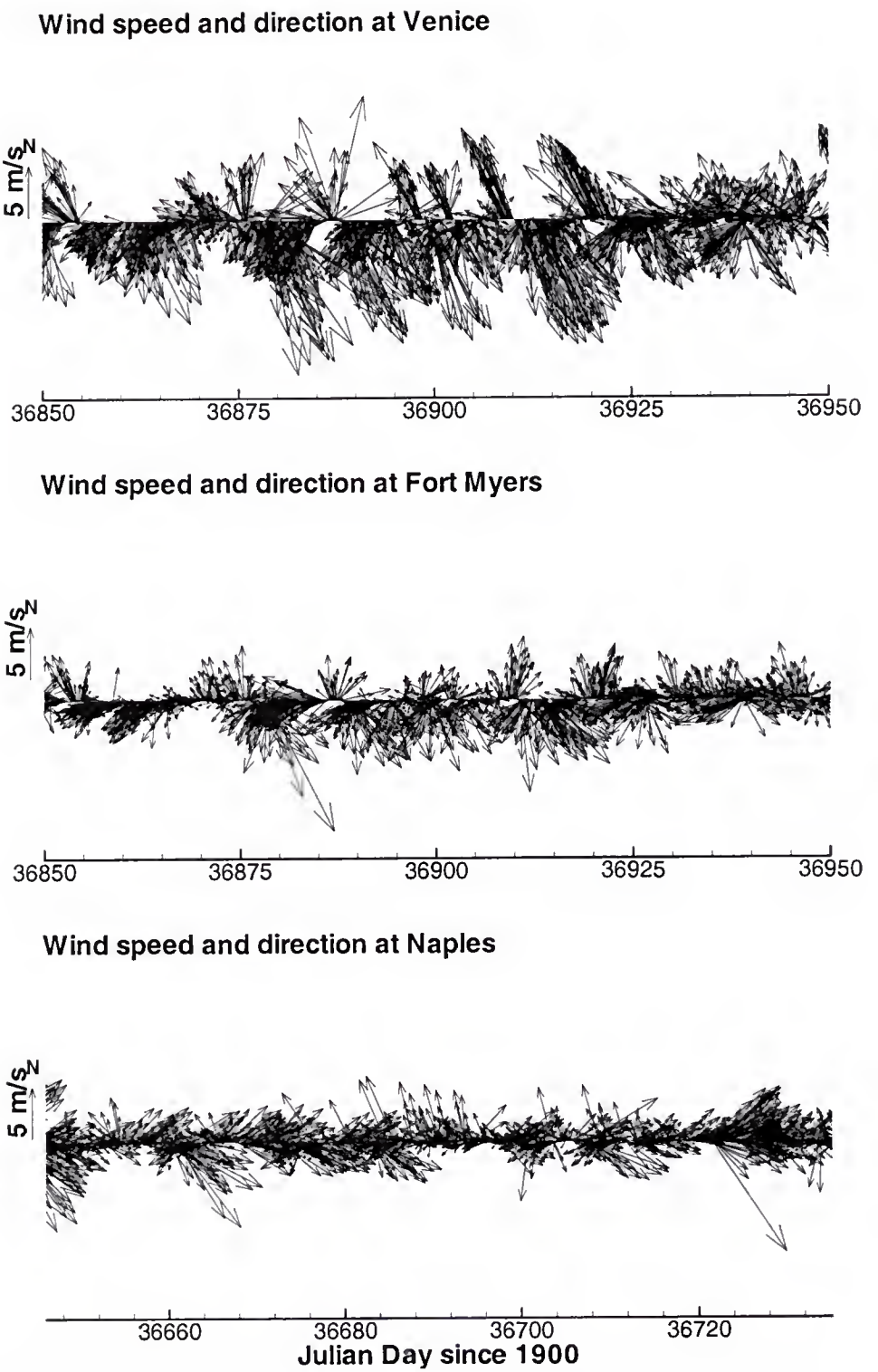

Figure 5.6 Wind velocity for 2000 simulation of Charlotte Harbor circulation.

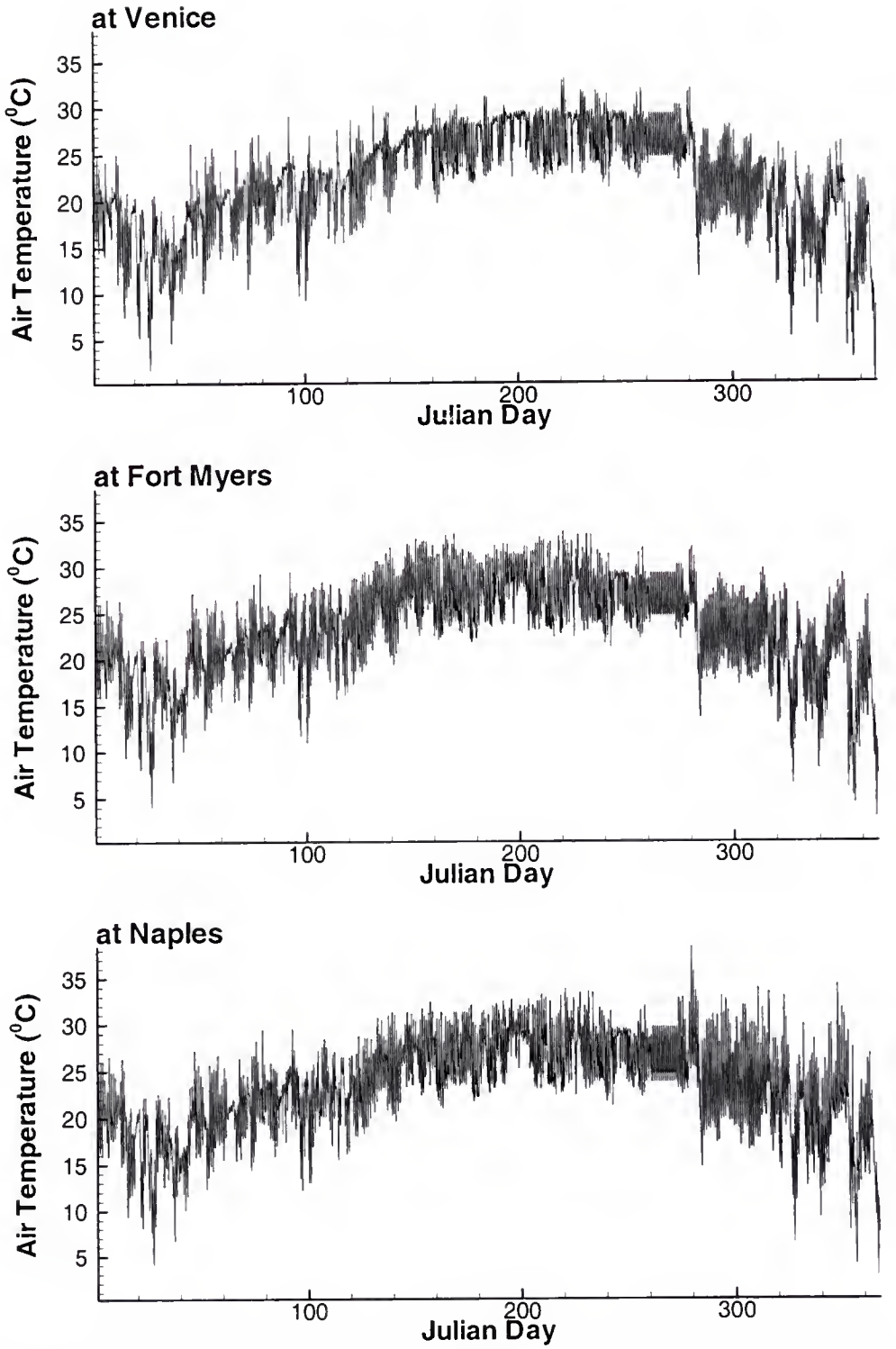

Figure 5.7 Air temperature for 2000 simulation of Charlotte Harbor circulation.

5.3 Simulations for 1986 Hydrodynamics

During the calibration process, a few model coefficients and/or boundary and initial conditions were adjusted to allow accurate simulation of observed data. As shown in Table 5.2, measured data of tidal stage, current, and salinity at several locations throughout the Charlotte Harbor were provided by USGS (Goodwin, 1992). Figure 5.8 shows the locations of tidal stages and Figure 5.9 shows the locations of current velocity and salinity measurement. Water elevation data at USGS station 4 (Venice) were compared with those at USGS stations 5 (Cayo Costa) and 8 (Gulf of Mexico at Fort Myers) which are located in the Gulf of Mexico (Figure 1.1). The tidal elevation and phase at stations 4 and 5 are almost identical. Tidal range at Fort Myers beach (station 8) is larger than those at stations. The reason for the larger tidal range at Fort Myers is probably due to the abrupt change in the direction of shoreline at the southern end of Sanibel Island, rather than different offshore tides. Therefore, water level data at Venice station were used as tidal boundary conditions along all open boundaries. All specific conductance measurements were converted to salinity concentrations in parts per thousand using the conversion equation by Miller (Goodwin. 1992). These data were used for comparison with model simulations of water level, velocity and salinity.

Before baroclinic simulations are performed, it is necessary to generate an initial salinity field because, in general, salinity is much slower to adjust to initial transients than water level or currents. The initial salinity field for the 1986 simulation is generated by "spinning up" a prescribed salinity field for a sufficiently long period. The salinity values at the end of the simulation are then used the initial values for the 1986 simulations. This process is discussed below in more detail.

First, a salinity field is created by linearly interpolating measured salinity onto the Charlotte Harbor grid. The bottom salinity data measured by USGS during 1986 are used to create this salinity field. Next, a salinity assimilation term is added to the salinity transport equation in the model. This term forces the salinity in a selected cell to approach a specific value, in this case, the initial value. The six USGS measured bottom salinity values shown in Figure 5.6 are chosen to be assimilated into the simulation. These values were chosen because they were measured closest to the July 9 starting date of the 1986 simulations. The assimilation term , which appears on the right side of the salinity equation, takes on the following form (Sheng and David, 2002):

$$-\frac{S^n_{i,j,k} - (S_A)_{i,j,k}}{T} \tag{5.1}$$

where $S^n_{i,j,k}$ is the simulated salinity at the n-th time level, $(S_A)_{i,j,k}$ is the value to be assimilated, i.e., the initial salinity values, and T is the assimilation period, which is set to 30 days for Charlotte Harbor simulation. It can be seen, when $S^n_{i,j,k}$ is not equal to $(S_A)_{i,j,k}$ a force is created to drive $S^n_{i,j,k}$, toward the value of $(S_A)_{i,j,k}$. Because of the addition of the salinity assimilation term, the salinity at the six USGS sites at the end of a simulation will be very close to their measured values at the beginning of the simulation.

A 30-day spin-up simulation was performed from May 28 to June 27 during a dry season with all barotrophic forcing mechanisms (tides, river discharges, wind) to allow water level, velocity and salinity field to reach a dynamic steady-state throughout the computational domain. Using the last time step surface elevation, velocity, and salinity of the spin-up simulation as the initial condition, the Charlotte Harbor circulation and salinity transport from June 27 to July 30 was simulated with tidal forcing, wind field and river discharges as boundary condition.

Table 5.2 Locations of tidal stage and velocity-salinity measured stations by USGS.

Site Number	(I ,J) Location in Computational domain	Duration	Data Type
1	(29,106)	6/15 ~ 8/31, 1986	Tidal Stage
2	(40,102)	7/15 ~ 8/31, 1986	Tidal Stage
3	(23, 81)	6/15 ~ 8/31, 1986	Tidal Stage
4	Outside, at Venice	6/30 ~ 8/31, 1986	Tidal Stage
5	(12, 81)	6/30 ~ 8/31, 1986	Tidal Stage
6	(14, 62)	7/10 ~ 8/31, 1986	Tidal Stage
7	(28, 47)	8/14 ~ 8/31, 1986	Tidal Stage
8	(33, 29)	6/26 ~ 8/20, 1986	Tidal Stage
SI-1	(33,100)	7/ 9 ~ 8/ 6, 1986	Velocity & Salinity
SI-2	(30, 90)	7/ 9 ~ 8/ 8, 1986	Velocity & Salinity
SI-3	(35, 86)	7/ 9 ~ 8/ 6, 1986	Velocity & Salinity
SI-4	(11, 96)	7/10 ~ 7/15, 1986	Velocity & Salinity
SI-6	(18, 76)	7/10 ~ 7/23, 1986	Velocity & Salinity
SI-7	(17, 65)	7/10 ~ 7/23, 1986	Velocity & Salinity
SI-8	(20, 51)	7/16 ~ 7/20, 1986	Velocity & Salinity

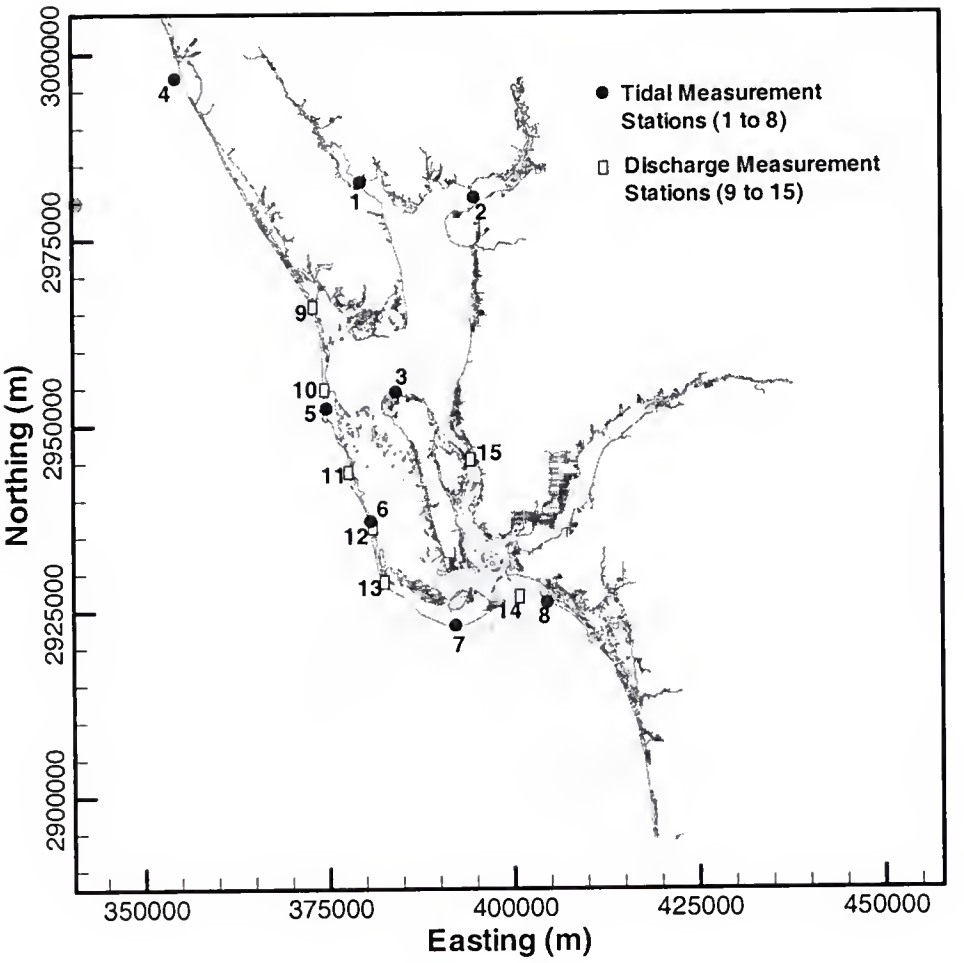

Figure 5.8 Locations of 1986 water level and discharge measurement stations of USGS (Goodwin, 1992).

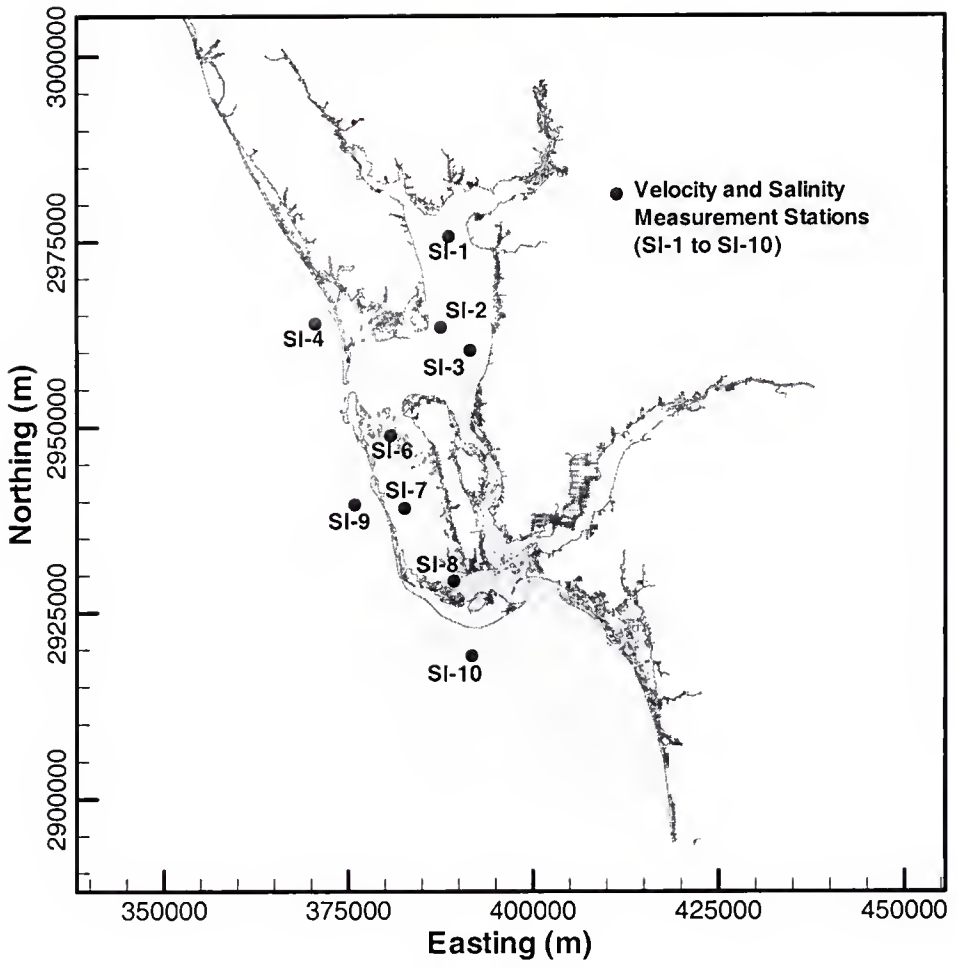

Figure 5.9 Locations of 1986 velocity and salinity measurement stations of USGS (Goodwin, 1992).

5.3.1 Sensitivity and Calibration Simulations

Several simulations were performed in order to test the consistency and sensitivity of numerical grid, bottom roughness, horizontal diffusion coefficient, and bathymetry. To quantify the model sensitivity to variations of these model parameters, time series statistics are presented in terms of the root-mean-square error (RMS) and normalize RMS error, define as the ratio between the RMS error and the observed range. The normalized RMS error gives a more meaningful indication on model's ability to reproduce the tidal signal and salinity at each station. The RMS error is calculated according to:

$$E_{rms} = \left[\frac{1}{N} \sum_{1}^{N} \left(S_{simulated} - S_{data} \right)^2 \right]^{1/2} \tag{5.2}$$

where N is the total number of measured data, $S_{simulated}$ is the model result, and S_{data} is measured data at each station.

To determine which non-tidal boundary and forcing conditions are most important to Charlotte Harbor estuarine system modeling, a series of 1986 simulations were performed with a different boundary and forcing conditions removed in each run (Table 5.3). These simulations show that baroclinc forcing is the most important factor in simulating water level, flow, and salinity at overall available measured stations.

Table 5.3 The effect of removing selected boundary conditions on the accuracy of simulated water level, velocity and salinity in July 1986. Values shown are average RMS differences vs. baseline simulation at all data stations.

Boundary and Forcing Condition Removed	Water level (cm)	U Velocity (cm^2/s)	V Velocity (cm^2/s)	Salinity (ppt)
Baroclinic Forcing	2.35	3.17	2.05	3.08
Wind	1.82	2.64	2.08	1.03
River Discharge	0.57	1.15	0.84	1.05

As shown in Equation 3.28, the bottom drag coefficient is defined as a function of

the bottom roughness, z_0. The default value of bottom roughness, z_0, used for Charlotte Harbor simulations is chosen to be a constant 0.3 cm over the entire domain based on running with the several bottom roughness values which range between 0.01 and 1 (Table 5.4). Because of the numerous different bottom types in the estuary, a constant value of bottom roughness may not be appropriate. To determine whether a spatially varying bottom roughness or a constant bottom roughness produces better simulated circulation and transport, a series of 1998 simulation was performed for the Indian River Lagoon (Davis and Sheng, 2001). The results show that simulations with the spatially varying bottom roughness have slightly smaller errors in water level but slight larger errors in salinity and flow. Since the varying bottom roughness does not improve the simulated circulation and transport significantly, the constant bottom roughness of 0.3 cm is used for all simulations in this study.

Table 5.4 The effects of varying bottom roughness, z_0, on the accuracy of simulated water level velocity, and salinity in July 1986. Values shown are average RMS errors at all data stations.

Bottom roughness (cm)	Water level (cm)	Velocity (cm^2/s)	Salinity (ppt)
0.1	8.11	7.87	1.71
0.3	8.12	7.88	1.71
1	8.11	7.87	1.71

As shown in Equations 3.2 and 3.3, the sub-grid scale motion is estimated with a horizontal diffusion coefficient, A_H. A default value of 10,000 cm^2/s was used for Charlotte Harbor simulations after performing several simulations using different coefficient values (Table 5.5). The results show little difference in water level and salinity.

Besides adjusting boundary conditions and model coefficients, it is also important to use more accurate grid and bathymetry. To improve the accuracy of bathymetry in Charlotte

Harbor, bathymetric surveys were performed in Caloosahatchee River and San Carlos Bay, and upper Charlotte Harbor by SFWMD and SWFWMD, respectively.

Table 5.5 The effect of varying horizontal diffusion, A_H, on the accuracy of simulated water level, velocity and salinity in July 1986. Values shown are average RMS errors at all data stations.

Horizontal diffusion Coefficient (cm2/s)	Water level (cm)	Velocity (cm^2/s)	Salinity (ppt)
5000	8.12	7.86	1.75
10000	8.12	7.88	1.71
20000	8.07	7.88	1.64

Overall, the model is able to simulate the surface elevation and salinity within 10% normalized error with maximum value. This provides validation that the hydrodynamic model reproduces the basic circulation of the Charlotte Harbor estuarine system.

To supplement this short term calibration of July 1986, long term model calibration was conducted using one year water level and salinity data in Caloosahatchee River during 2000. This 2000 model calibration include several test simulations to investigate effects of bottom roughness, salinity advection schemes, and grid resolution and bathymetry.

5.3.2 Results of the 1986 simulation

For the 1986 simulation, the 92x129 grid and updated bathymetry were used along with boundary conditions and model parameters described in Table 5.6. Water level, current velocity, and salinity are compared both qualitatively and quantitatively with measured data, where available.

Water Level

Calculated RMS errors between simulated and measured water level during the July 1986 simulation are shown in Table 5.7. The normalized RMS errors are less than 10% at all water level stations, demonstrating the model's ability to accurately reproduce surface

elevation in the system. The highest errors at stations 1 and 2 can be attributed to the relatively coarse horizontal grid near the river where the gages were located.

Table 5.6 A summary of boundary conditions and model parameters used in the 1986 simulation.

Boundary Condition or Model Parameter	Value
Tidal Forcing	Measured
Wind speed and direction	Measured at 2 stations
Fresh Water Discharge	Estimated (for Estero Bay) and Measured
Bottom Roughness	Constant (0.3 cm)
Horizontal Diffusion	Constant (10000 cm^2/s)
Horizontal grid	92 x 129
Vertical Layers	8

Table 5.7 Calculated RMS errors between simulated and measured water level in July 1986.

Station Number	RMS error (cm)	Range (cm)	% RMS error
1	9.59	104.24	9.20
2	9.61	104.55	9.19
3	6.61	90.83	7.28
5	9.55	117.05	8.16
6	7.56	107.90	7.00
7	5.78	144.48	4.00
Average	8.12	111.51	7.47

Figure 5.10 shows the comparison between measured and simulated water level at six Charlotte Harbor stations. The result shows a good agreement between data and model results, in both amplitude and phase. From these figures, it can be seen that tidal range decreases about 15% from Boca Grande Pass (site 5) to Peace and Myakka Rivers (sites 1 and 2). Also, the tidal wave takes about two to three hours to reach these rivers.

Figure 5.11 shows the spectra of water level (data and model results) for the same

stations. The spectral curves reveal major energy bands centered around two tidal frequencies: the diurnal band (between 0.8 to 1.2 cycle per day) and a semi-diurnal band (1.8 to 2.2 cycles per day). These two bands combined to represent the tides propagating from Gulf of Mexico into the estuarine system. The secondary energy bands, representing nonlinear interactions between diurnal and semi-diurnal tides with complex geometries and bathymetric features inside the estuary, are represented by the relatively small third and fourth diurnal peaks. Comparisons show that the model is able to capture both the amplitudes and phases well.

Velocity

The simulated and measured horizontal velocities at selected sites are shown in Figure 5.12. The angle of the vector shows the azimuth of the flow vector at a specific time, and the length of the vector represents the magnitude of the flow. It is important to point out that the observed velocity is measured at a discrete point in space and is subjected to many local influences that are not well represented in the model. These influences include physical features such as small channels, depression shoals, and mounds that are not resolvable at the model scale, but often influence the distribution of velocity at that location. Because of local influences, discrete measurement points are not consistently reliable indicators of the general velocity characteristics (Goodwin, 1996). The model results are spatially averaged values over a grid cell, hence are not expected to agree exactly with discrete data.

Site SI-1 is located in northern Charlotte Harbor in an area of converging river flow and having a complex bathymetry that creates a complex lateral distribution of velocity. The simulated velocity at SI-1 agrees well with measured data. However, some simulated velocity magnitudes were 50% smaller than measured magnitudes and there was some

deviation in the azimuth of more than 30 degrees. Since the current meter was located near the surface at this station, this station could be influenced by freshwater inflow, wind and any other effects as indicated by Goodwin (1996).

At Si-2 and Si-3, there is good agreement between simulated and measured velocities. In the Pine Island Sound, site-7 is located in the middle of several islands, and the observed data were strongly affected by local features that cannot be resolved at the scale modeled. However, agreement between simulated and measured data for this site is quite good.

Calculated RMS errors between simulated and measured current velocity are shown in Table 5.8. The average normalized RMS error is less than 20%. The RMS error is quite reasonable in comparison to the range of velocity, considering the fact that many local influences that are not well represented in the model.

Table 5.8 Calculated RMS errors between simulated and measured current velocity for 1986 simulation

Station Number		RMS error (cm/s)	Range (cm/s)	% RMS error
SI-1	U	4.38	30.54	14.34
	V	5.97		19.56
SI-2	U	11.70	55.19	21.20
	V	13.14		23.82
SI-3	U	7.16	38.25	18.72
	V	6.78		17.72
SI-6	U	3.06	34.79	8.79
	V	10.82		31.10
Average		7.88		19.40

Salinity

Figure 5.13 shows the near-bottom simulated and measured salinity at USGS stations

SI-1,2,3,6,7, and 8 inside of Charlotte Harbor. The difference between simulated and measured salinity does not exceed 2 ppt except at station SI-7.

Calculated RMS errors between simulated and measured salinity during July 1986 simulation are shown in Table 5.9. The results show the model's ability to simulate salinity within 10% accuracy. The highest error is at station SI-7. The measured salinity shows very strong daily fluctuation which is five times greater than simulated values. This location is near the Captiva pass which is possibly affected by local features such as small channels, depressions, shoals, and mounds as mentioned before.

Table 5.9 Calculated RMS errors between simulated and measured salinity for 1986 simulation

Station Number	RMS error (ppt)	Maximum (ppt)	% RMS error
SI-1	1.23	24.01	5.15
SI-2	1.47	25.42	5.77
SI-3	1.51	27.05	5.60
SI-6	0.61	33.83	1.81
SI-7	3.52	33.82	10.42
SI-8	1.90	25.38	7.50
Average	1.71	26.55	6.04

Flow Patterns

Typical averaged flow patterns during one tidal cycle, based on the water level at open boundary, for August, 6 on 1986 are shown in figure 5.14. Easterly flow on the western Florida shelf is dominant during the flood tide, whereas northerly and westerly shelf flows are dominant during the ebb tide. Two major passes in the Charlotte Harbor estuarine system are Boca Grande Pass and San Carlos Pass. The large flood and ebb flows through the Boca Grande Pass affects the tidal prism in upper and lower Charlotte Harbor and the flow through

San Carlos Pass satisfies the tidal prism in the Caloosahatchee River, San Carlos Bay, the lower part of Matacha Pass and lower extremity of Pine Island. The flow through Gasparilla, Captiva, and Redfish passes have effects that appear to be limited to the local area. In Pine Island Sound, the flow is very low during flood and ebb tide periods. However, there is some water transport through Pine Island Sound during high slack and low slack tide periods. During near high slack tide, there is northerly flow from San Carlos Bay, while there is southerly flow during near low slack tide.

Residual Flow and Salinity Patterns

Figure 5.15 show the 29-day residual circulation during July 2 to July 30, 1986. In the upper Charlotte Harbor, there are opposite direction surface residual flows which are the landward surface residual flow in relatively deep channel along the right side channel and seaward surface residual flow along the left side shoreline. In the bottom residual flow, the landward flow is dominant across the channel.

In the Pine Island Sound and Matlacha Pass, the northward residual flow is dominant in the surface, while there is a week southward flow in the bottom. The surface flow come from upper Charlotte Harbor, Pine Island Sound, and Matlacha Pass create a strong seaward surface residual flow at the lower Charlotte Harbor.

The offshore residual flow in the Gulf of Mexico is northward. The strong outflows from the Boca Grande Pass and San Carlos Pass create the clockwise gyres near the surface in the Gulf of Mexico.

The residual salinity has a uniform vertical and horizontal distribution in the lower Charlotte Harbor, while the salinity has horizontal inclination across the channel and vertically stratification in the upper Charlotte Harbor. In upper Charlotte Harbor, the surface

salinity along the right side shoreline has greater value than that along the left side shoreline because of the residual surface flow pattern. The residual salinity field shows a vertical stratification of 2 ppt at the Peace River mouth since the strong river discharge and mixed tide from Gulf of Mexico create two layered flow (seaward flow at surface and landward flow at bottom) in this area. A two layered flow and salinity stratification is often presented at the Charlotte Harbor estuarine system. The significant vertical stratification can suppress vertical mixing and lead to the formation of pycnocline and hypoxia in the upper Charlotte Harbor (Stoker, 1992; CDM, 1998). Therefore, understanding of the density-driven circulation is critical to the management of Charlotte Harbor estuarine system.

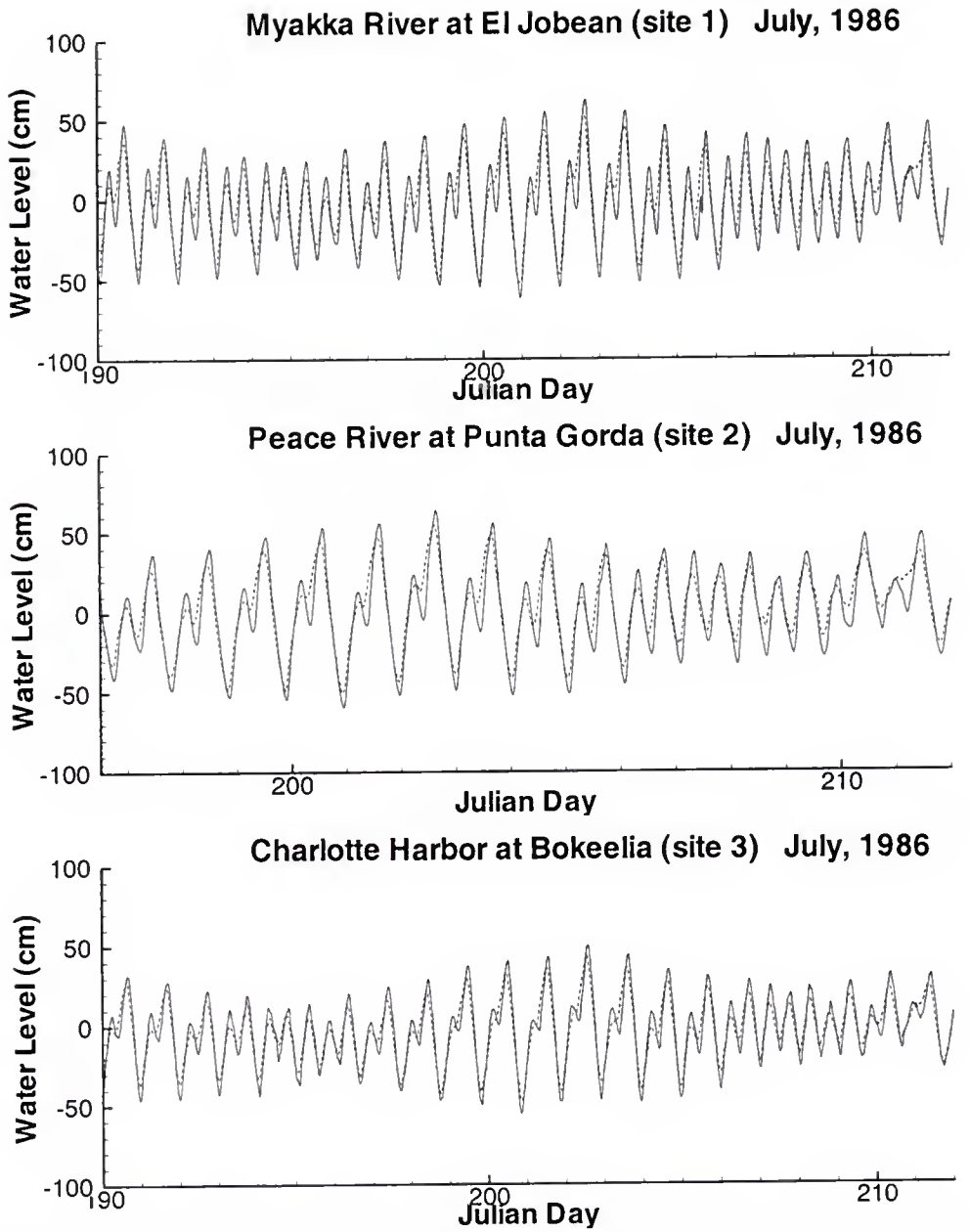

Figure 5.10 Comparison between simulated and measured water level in July 1986.

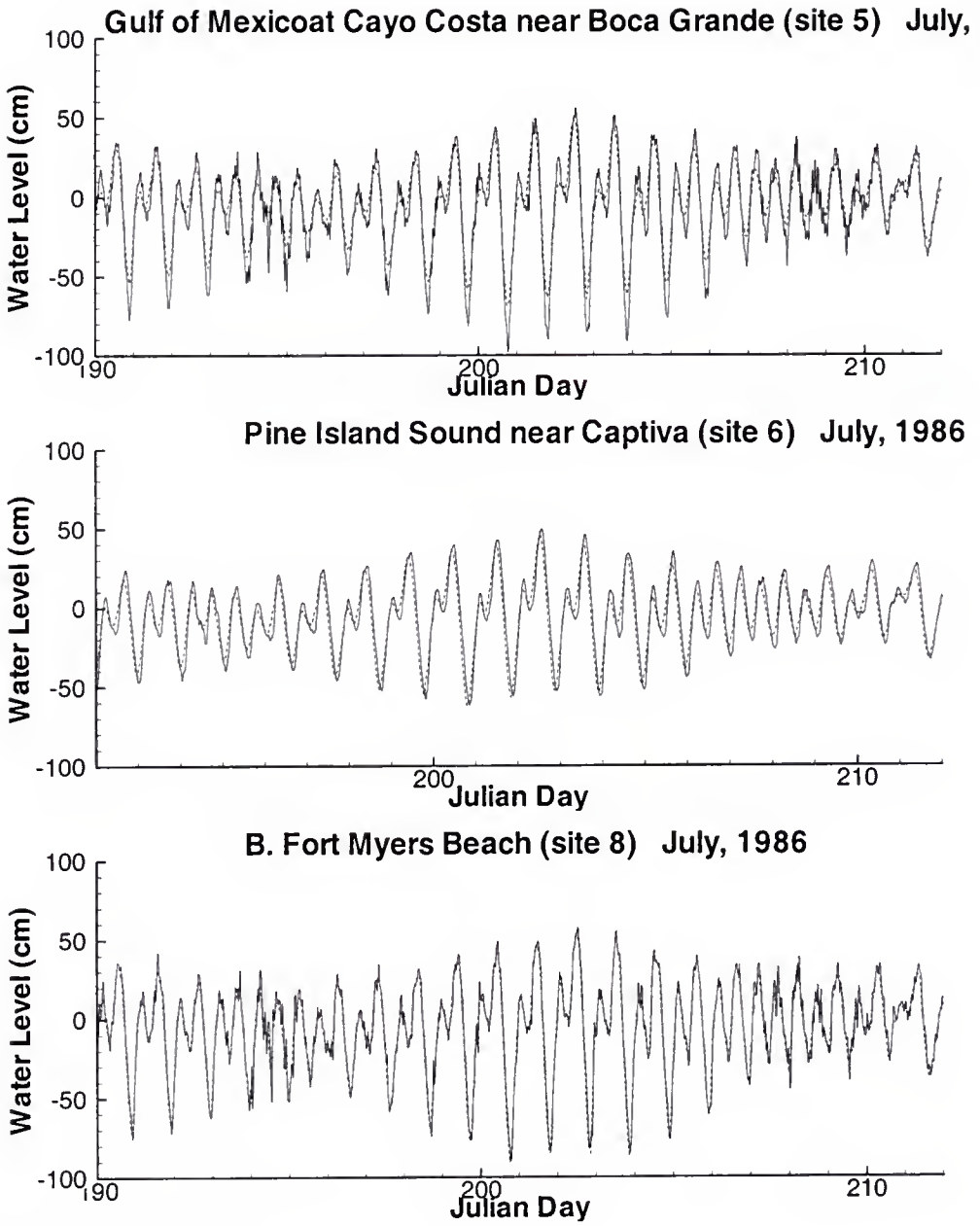

Figure 5.10 continued.

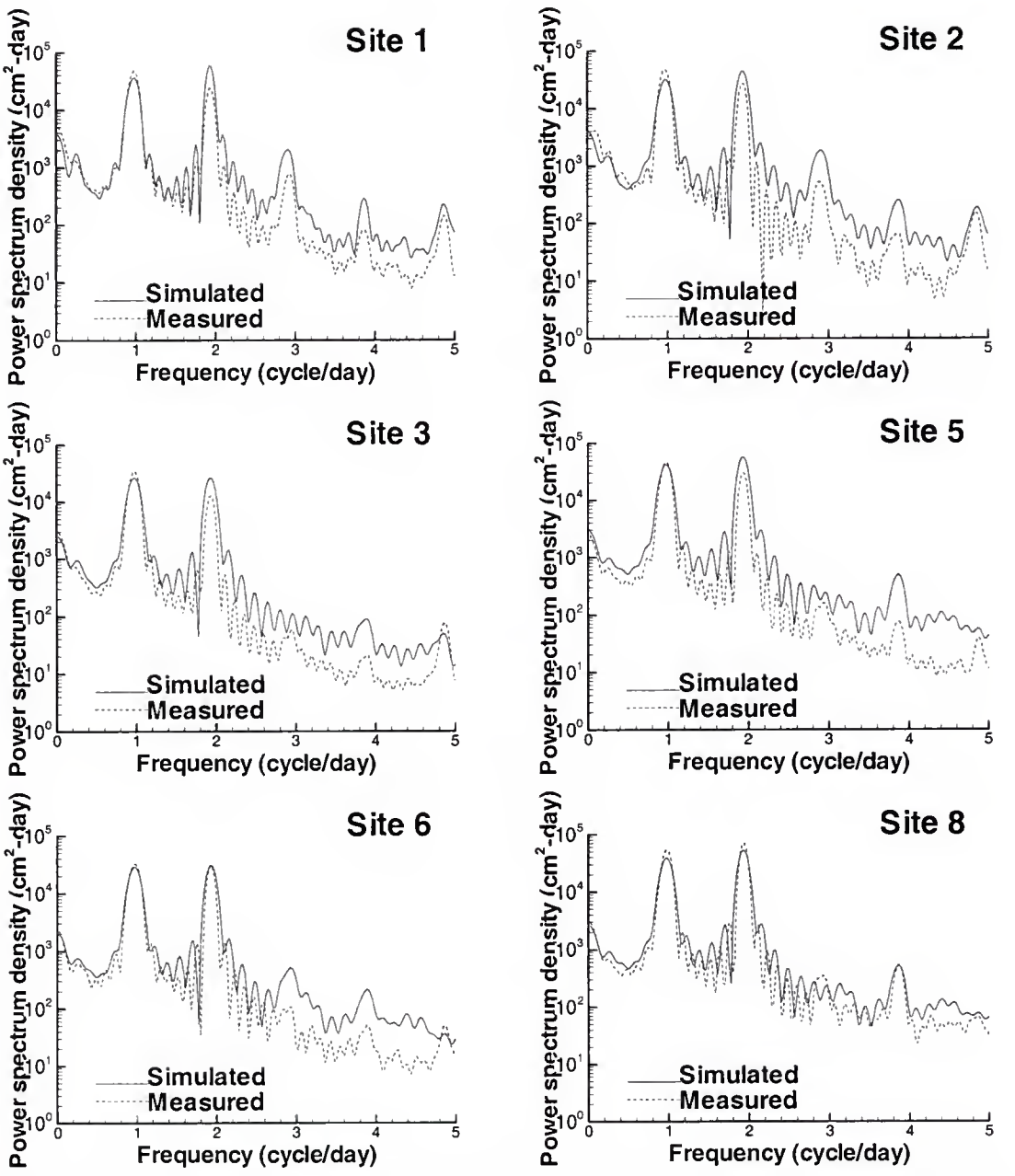

Figure 5.11 Comparison between simulated and measure spectra of water level in July 1986.

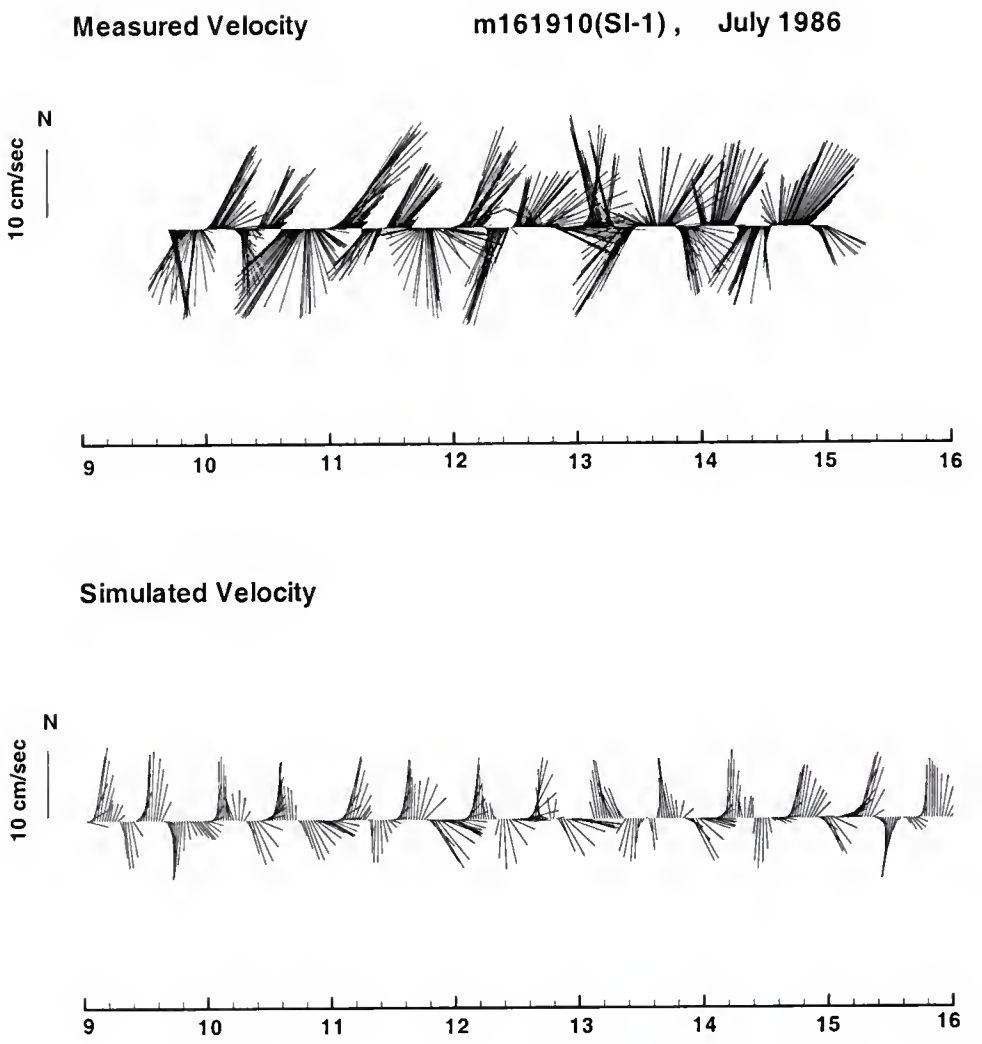

Figure 5.12 Comparison between simulated and measured velocity data in July 1986.

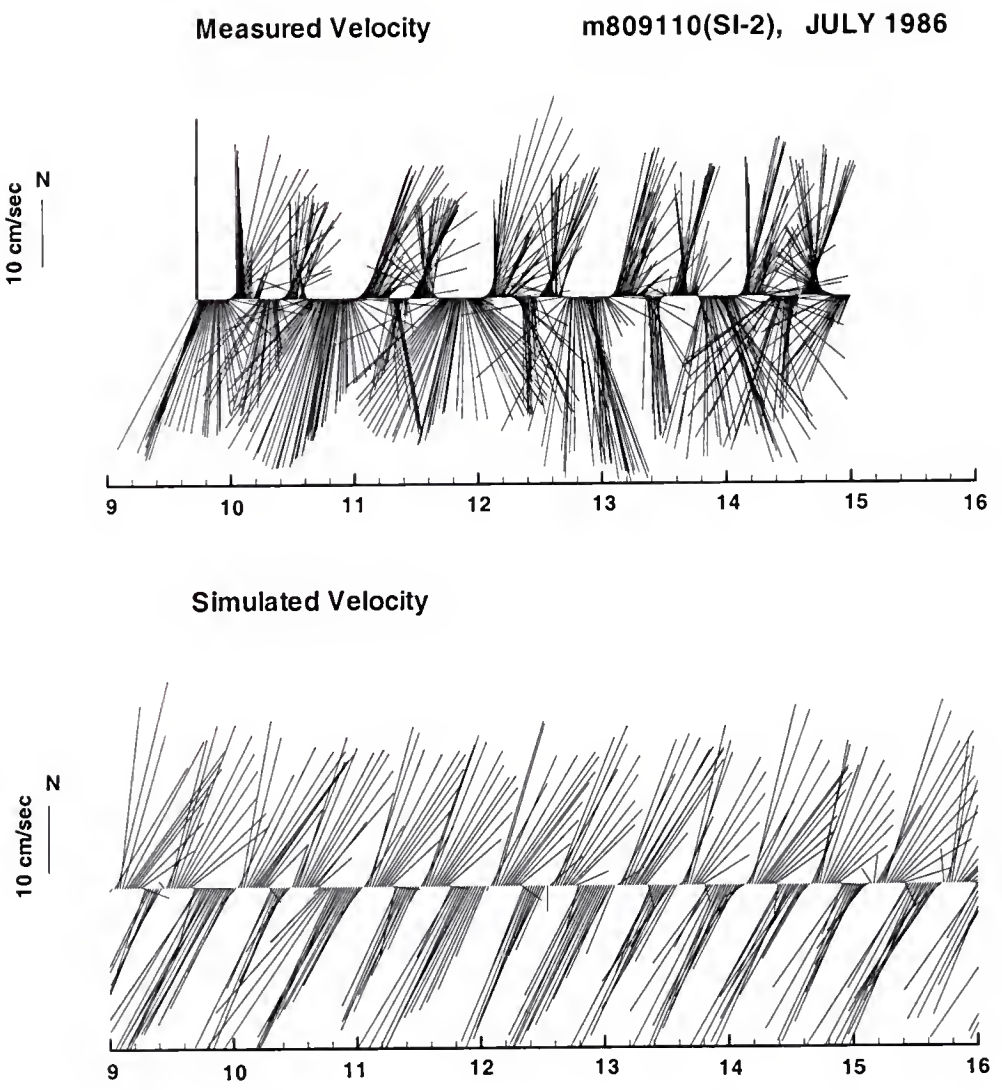

Figure 5.12 continued.

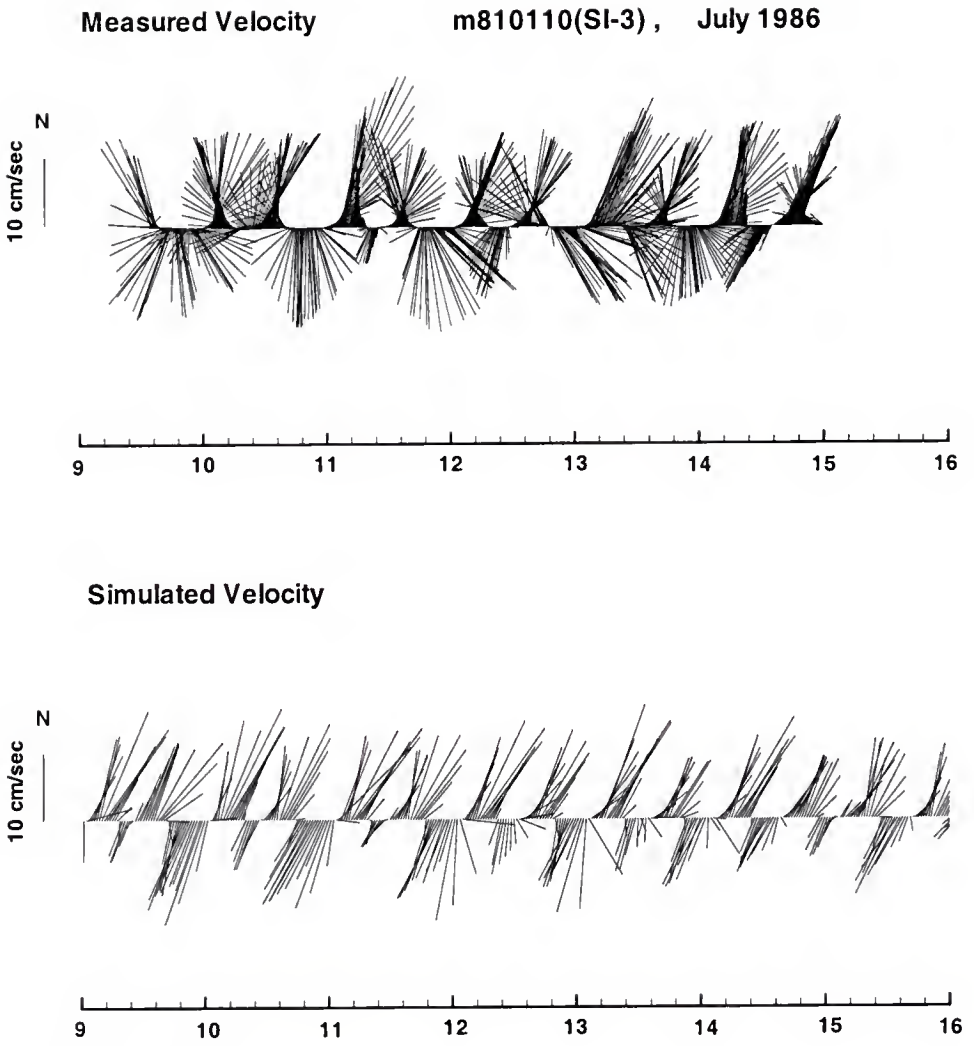

Figure 5.12 continued.

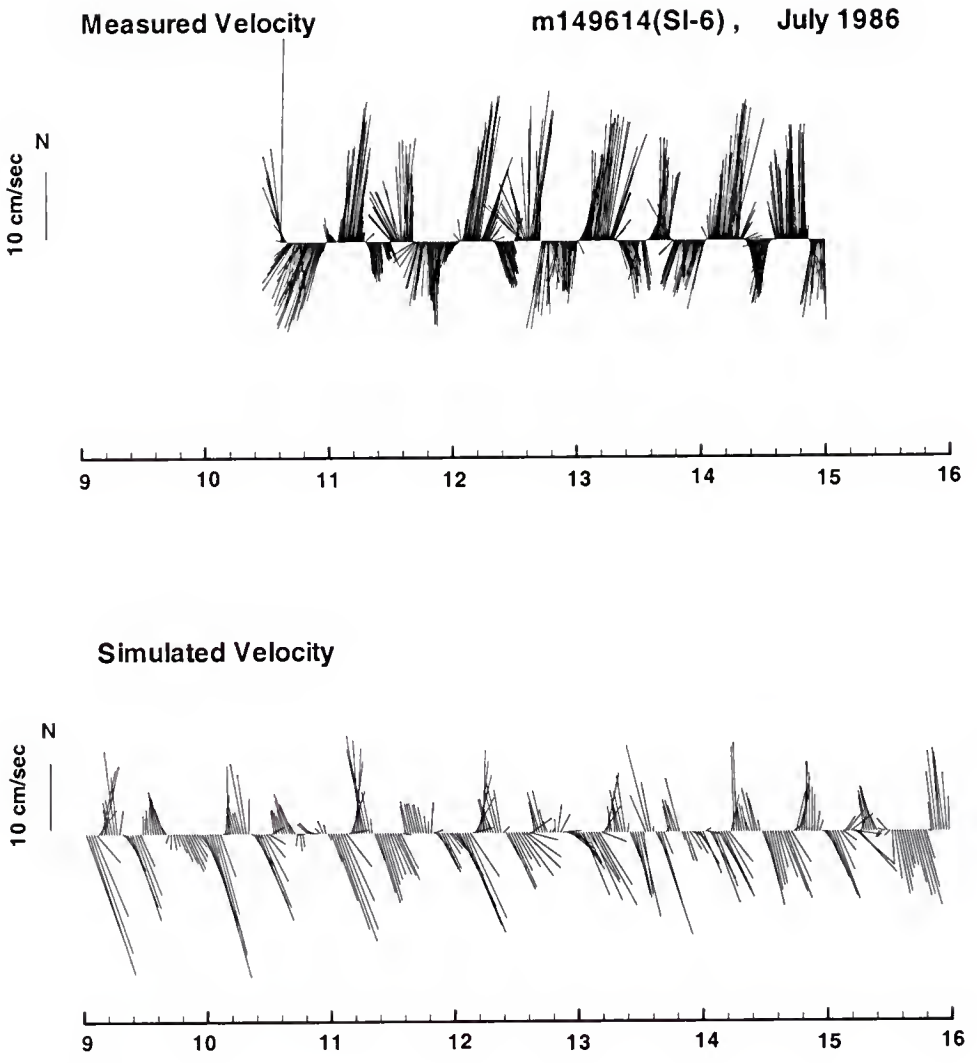

Figure 5.12 continued.

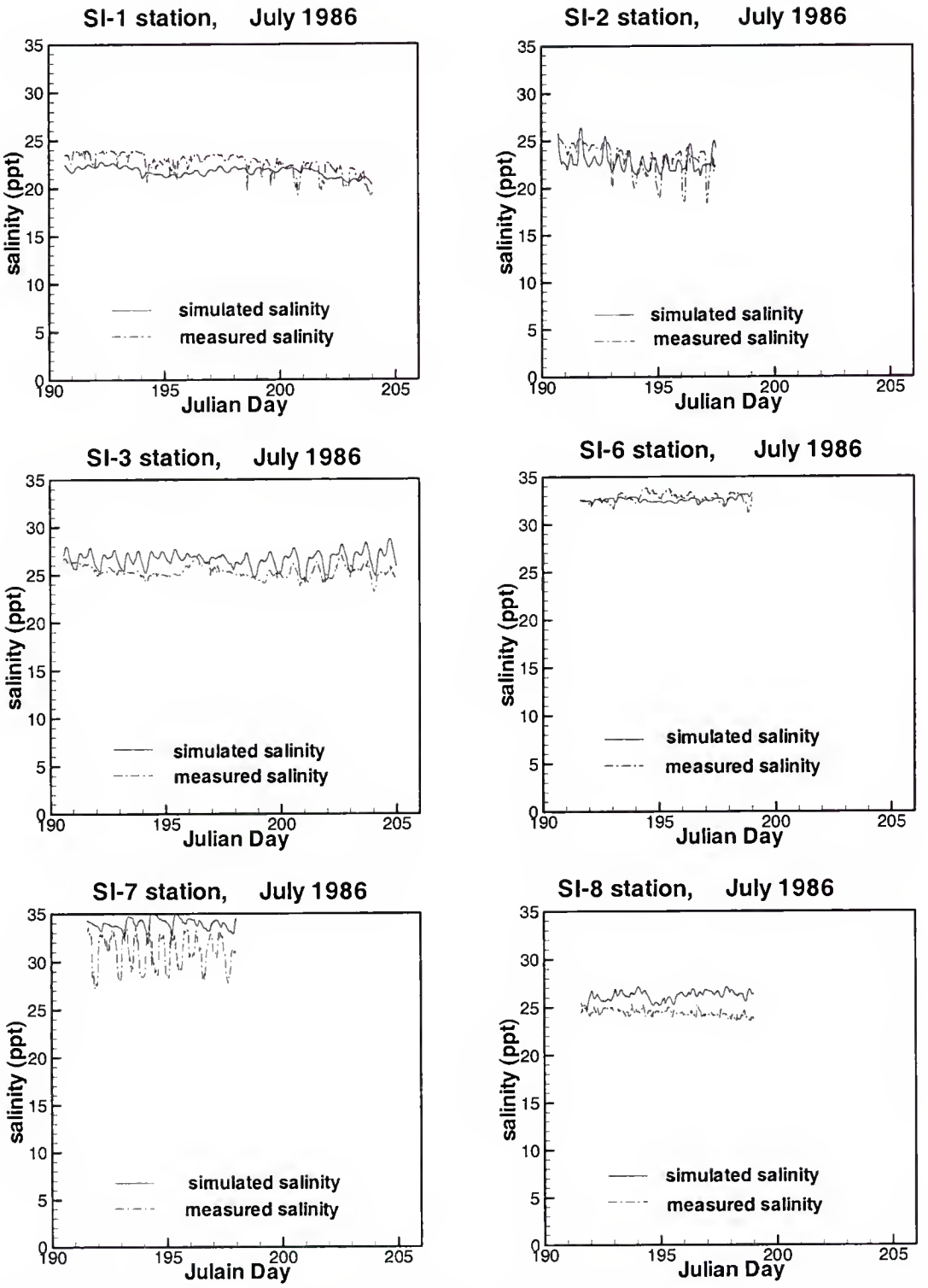

Figure 5.13 Comparison between simulated and measured salinity in July 1986.

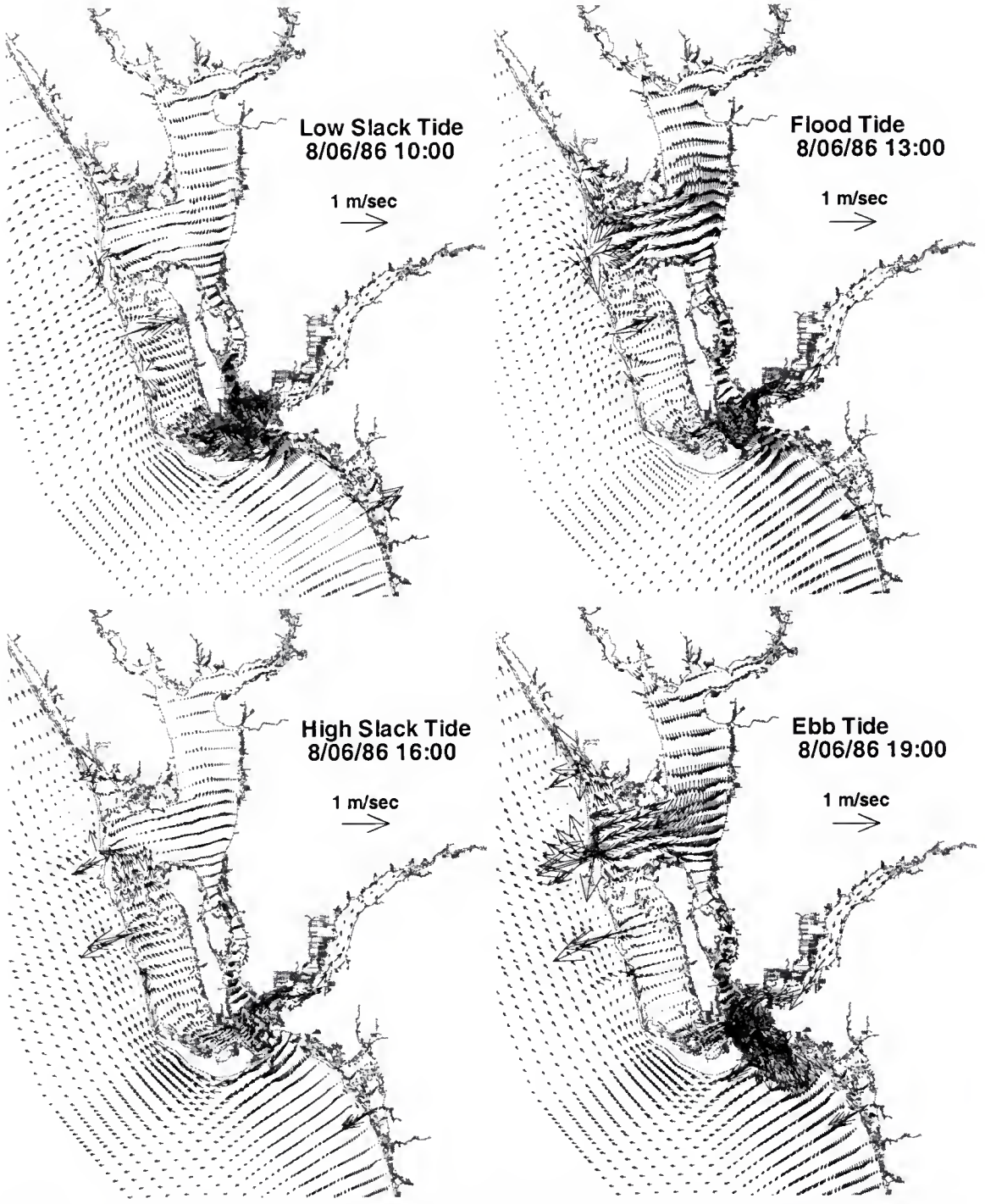

Figure 5.14 Typical flow pattern of Charlotte Harbor estuarine system during one tidal cycle for August 6, 1986.

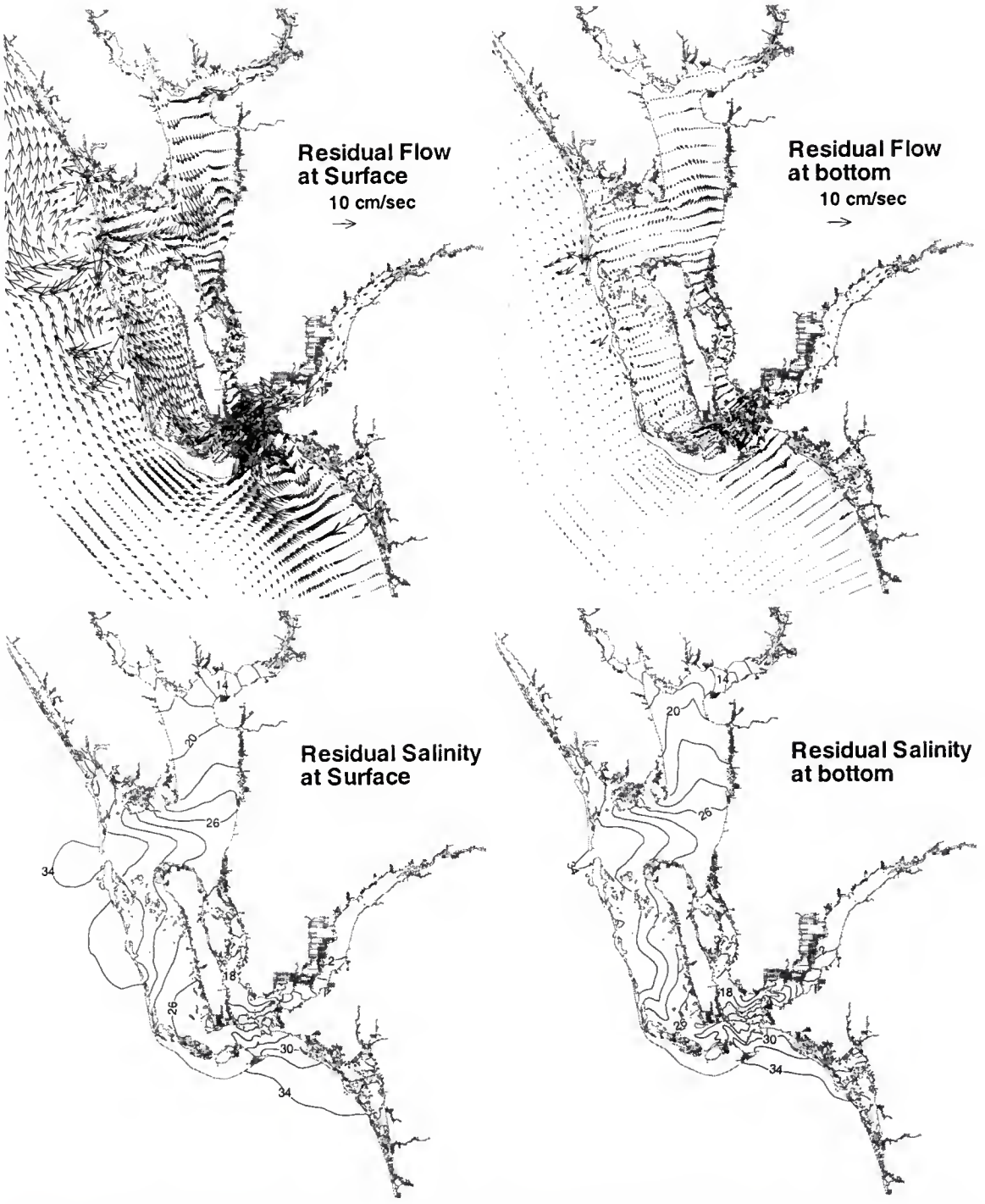

Figure 5.15 The 29-day residual flow and salinity for Charlotte Harbor estuarine system during July 2 to July 30, 1986

5.4 Simulations for 2000 Hydrodynamics

1986 hydrodynamic simulation of Charlotte Harbor estuarine system was conducted for 30 days to calibrate the major model coefficients and inputs. The field data did not cover the Caloosahatchee River which is a very important segment of the study area. To supplement 1986 calibration simulation, long-term model calibration was conducted using one year water level and salinity data in the Caloosahatchee River during 2000. Figure 5.16 shows the salinity measurement stations in Caloosahatchee River. Water levels were measured at Fort Myers and Shell Point. The validated CH3D model was then used to assess the effects of Sanibel Causeway and the navigation channel in San Carlos Bay, and to quantify the relationship between freshwater inflow and spatial and temporal salinity distribution in the Caloosahatchee River.

5.4.1 Sensitivity and Calibration Simulations

Several simulations were performed in order to test the effects of grid configuration, bottom roughness, bathymetry, and salinity advection scheme on salinity distribution in the Caloosahatchee River. To study how the horizontal grid resolution affects simulated circulation and transport within the estuarine system, two 2000 simulations are performed using two different grids. Figure 5.17 shows the comparison of the coarse grid (71x92) and the fine grid (92x129). The fine grid has about two times finer resolution than the coarse grid in San Carlos Bay and near the Caloosahatchee River mouth. Table 5.10 shows that the two different horizontal grids affected the salinity less significantly than the water level. The geometry and bathymetry at the river mouth play a very important role for water circulation inside the river. The coarse grid tends to produce more error in water level simulation than fine grid because the coarse grid does not accurately to represent the islands and navigation

channels in the San Carlos Bay and Caloosahatchee River mouth. The fine grid (92x129) is used for all simulations for Charlotte Harbor estuarine system.

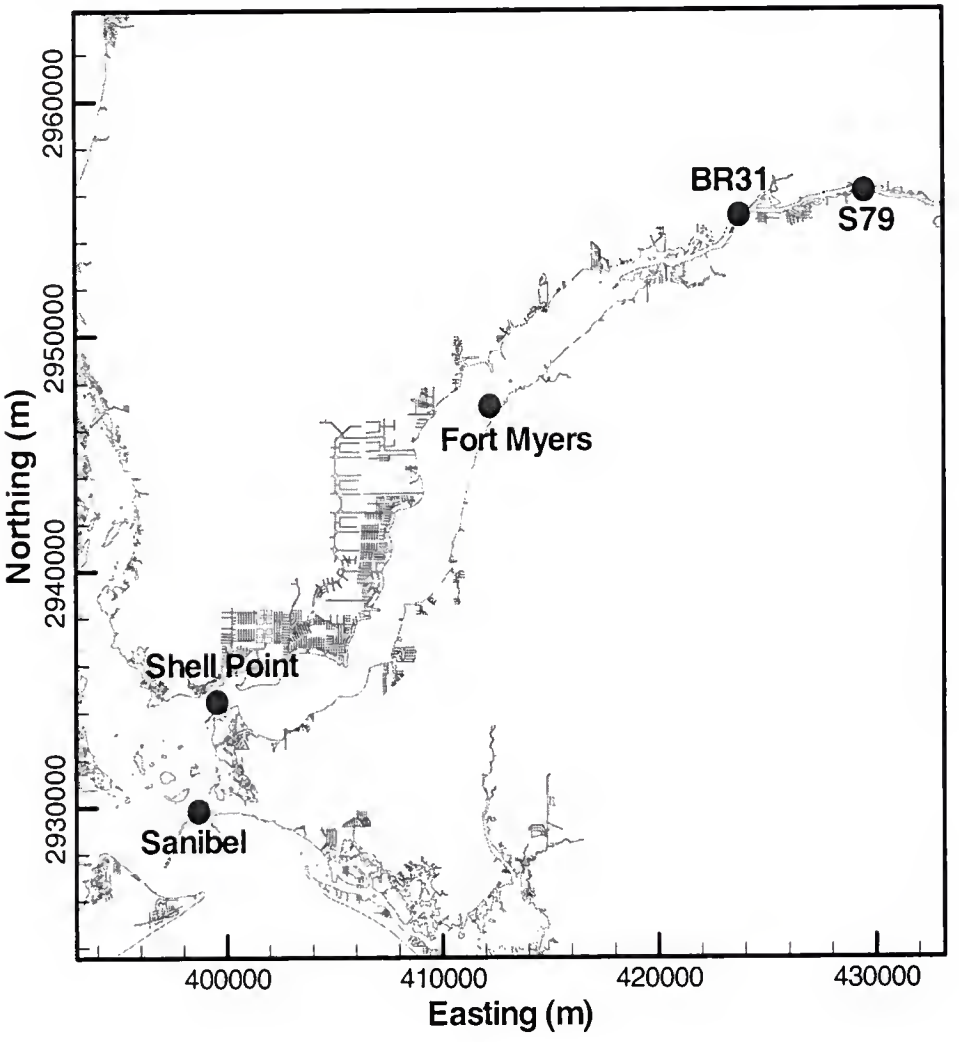

Figure 5.16 Locations of the available 2000 water level and salinity measured stations at Caloosahatchee River operated by SFWMD.

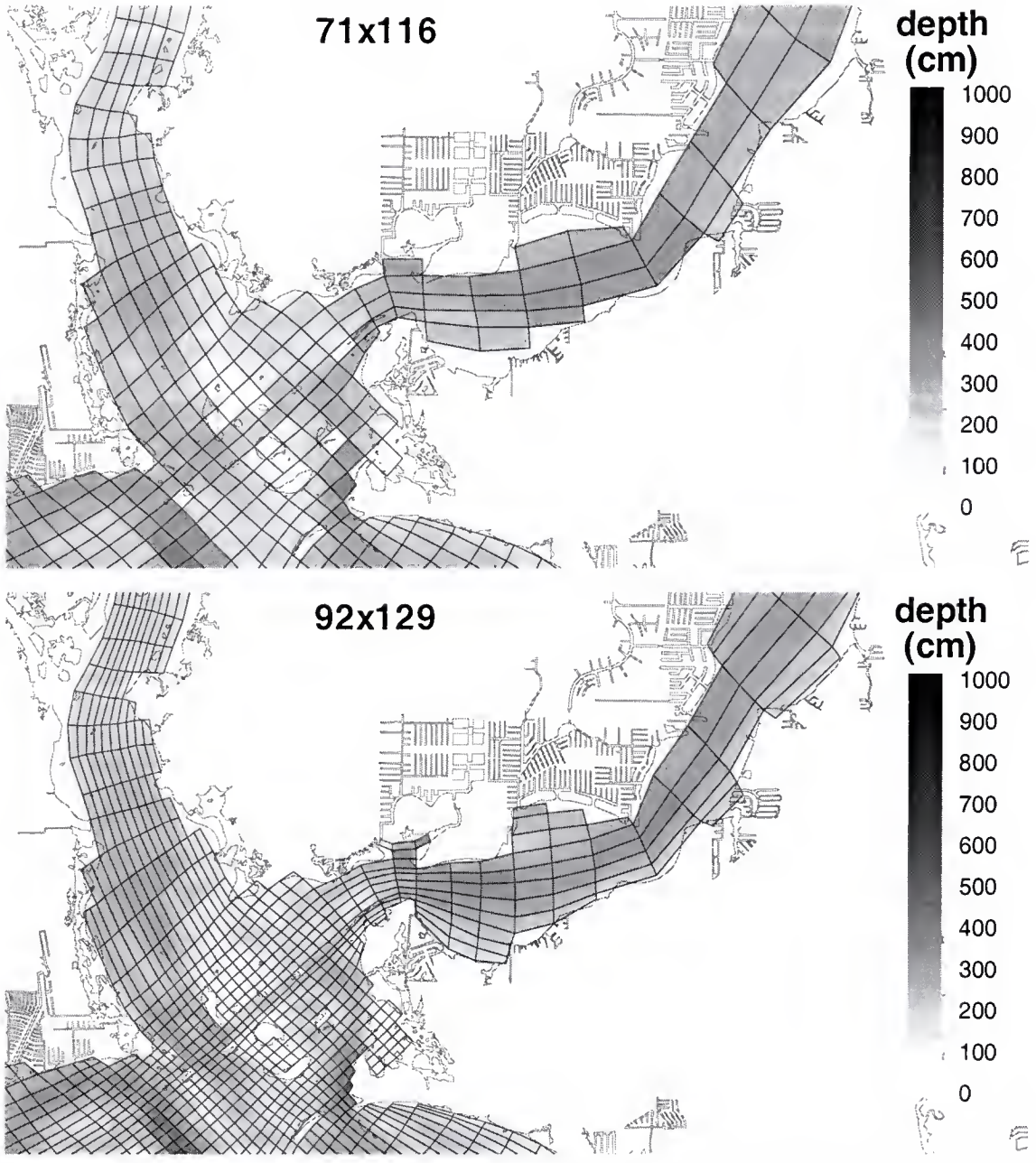

Figure 5.17 The comparison of the coarse grid (71x92) and the fine grid (92x129) for Charlotte Harbor estuarine system.

Table 5.10 The effect of horizontal grid resolution, on the accuracy of simulated water level and salinity. Values shown are average RMS errors for 2000 calibration at all available stations. Values shown in parenthesis are % RMS error normalized by maximum values.

Variables	Station		71 x 92	92 x 129
Salinity (ppt)	S79	S	1.69(4.62)	1.46(3.98)
		B	2.54(6.93)	1.84(5.03)
	BR31	S	1.17(3.20)	1.55(4.22)
		B	1.89(5.16)	2.06(5.61)
	Fort Myers	S	1.55(4.23)	1.85(5.03)
		B	2.07(5.63)	2.63(7.18)
	Shell Point	S	3.78(10.29)	3.76(10.25)
		B	3.37(9.17)	3.53(9.64)
	Sanibel	S	1.85(5.05)	1.94(5.28)
		B	2.05(5.59)	2.00(5.45)
	average		2.20(5.99)	2.26(6.17)
Water level (cm)	Fort Myers		9.08(5.44)	5.51(3.30)
	Shell Point		6.92(4.83)	4.25(2.96)
	average		8.00(5.14)	4.58(3.13)

Vertical salinity stratification in the Upper Charlotte Harbor and Caloosahatchee River is a common seasonal occurrence (Environmental Quality Laboratory, Inc., 1979). In high river inflow events, a stable vertical salinity gradient is created which suppresses vertical mixing unless there are sufficient mixing by wind or tide. Therefore, the vertical grid resolution is an important factor to reproduce vertical salinity distribution which is a one of major cause effects of hypoxia in upper Charlotte Harbor. To study the effect of varying the number of vertical layers used by CH3D model, 2000 simulations were performed with 4 and 8 vertical layers (Table 5.11). Since a one year simulation of hydrodynamics, sediment transport, and water quality took several days, the simulation with more than 8 vertical layers which required the additional computational time, is not feasible for this study. While the simulated water level RMS error changes little, the averaged simulated salinity RMS error

improves about 1 ppt with 8 layer simulation. The largest improvement in simulated salinity was achieved at Shell Point station with 3 ppt using 8 vertical layers. To reproduce vertical stratification for salinity and water quality simulation, eight layer simulations are deemed appropriate for the Charlotte Harbor estuarine system.

Table 5.11 The effect of vertical grid resolution, on the accuracy of simulated water level and salinity. Values shown are average RMS errors for 2000 calibration at all available stations. Values shown in parenthesis are % RMS error normalized by maximum values.

Variables	Station		4 layers	8 layers
Salinity (ppt)	S79	S	1.85(5.08)	1.46(3.98)
		B	2.09(5.73)	1.84(5.03)
	BR31	S	1.86(5.11)	1.55(4.22)
		B	2.37(6.51)	2.06(5.61)
	Fort Myers	S	2.34(6.43)	1.85(5.03)
		B	2.30(6.31)	2.63(7.18)
	Shell Point	S	6.82(18.70)	3.76(10.25)
		B	5.31(14.55)	3.53(9.64)
	Sanibel	S	2.48(6.80)	1.94(5.28)
		B	4.02(11.02)	2.00(5.45)
	average		3.14(8.63)	2.26(6.17)
Water level (cm)	Fort Myers		4.50(2.70)	5.51(3.30)
	Shell Point		4.42(3.08)	4.25(2.96)
	average		4.46(2.89)	4.58(3.13)

In Caloosahatchee River, water level and salinity are very sensitive with the varying bottom roughness while the varying bottom roughness does not affect the simulated circulation and transport significantly in the estuary in July 1986. However, several 2000 simulations were performed using different coefficient value to determined the effect of varying the bottom roughness on the accuracy of the simulation circulation and transport. (Table 5.12). With increasing bottom roughness, accuracy of water level is improved while that for salinity is worse. A constant bottom roughness of 0.3 cm is used for all simulations.

Table 5.12 The effect of varying bottom roughness, z_0, on the accuracy of simulated water level and salinity in 2000. Values shown are average RMS errors at all data stations.

Bottom roughness (cm)	Water level (cm)	Salinity (ppt)
0.2	4.94	2.28
0.3	4.87	2.29
0.4	4.88	2.31

Model sensitivity study was conducted to investigate the relative accuracy of the salinity advection schemes including upwind, QUICKEST, and Ultimate QUICKEST methods. Time series comparisons of measured and simulated surface salinity using three advection schemes at three stations, Shell Point, Fort Myers, and BR31, are shown in Figures 5.18 to 5.20. The salinity comparison at Shell point does not show much difference for all three schemes, while at Fort Myers and BR31, the simulated salinity with upwind scheme is much higher than those for the other advection schemes and measured salinity. The advection scheme plays a very important role for salinity simulation at cells inside river where there is usually very strong salinity gradient from the river mouth at Shell Point to the upstream. Lower order advection scheme such as upwind scheme tends to produce more error in salinity simulation because of its inherently high numerical diffusion. A series of vertical-longitudinal salinity profiles along the axis of the river during slack water is shown in Figure 5.21 to compare salinity distribution along the river simulated by various advection schemes. The salinity distribution obtained with the QUICKEST method shows similar pattern with that for Ultimate QUICKEST method. The upstream salinity near BR31 shows much higher value with upwind scheme because salinity is quickly diffused from river mouth to the upstream. With the upwind scheme, it is difficult to reproduce the vertical salinity stratification which often occurs during high river flow period, while the other advection schemes produced the stratification.

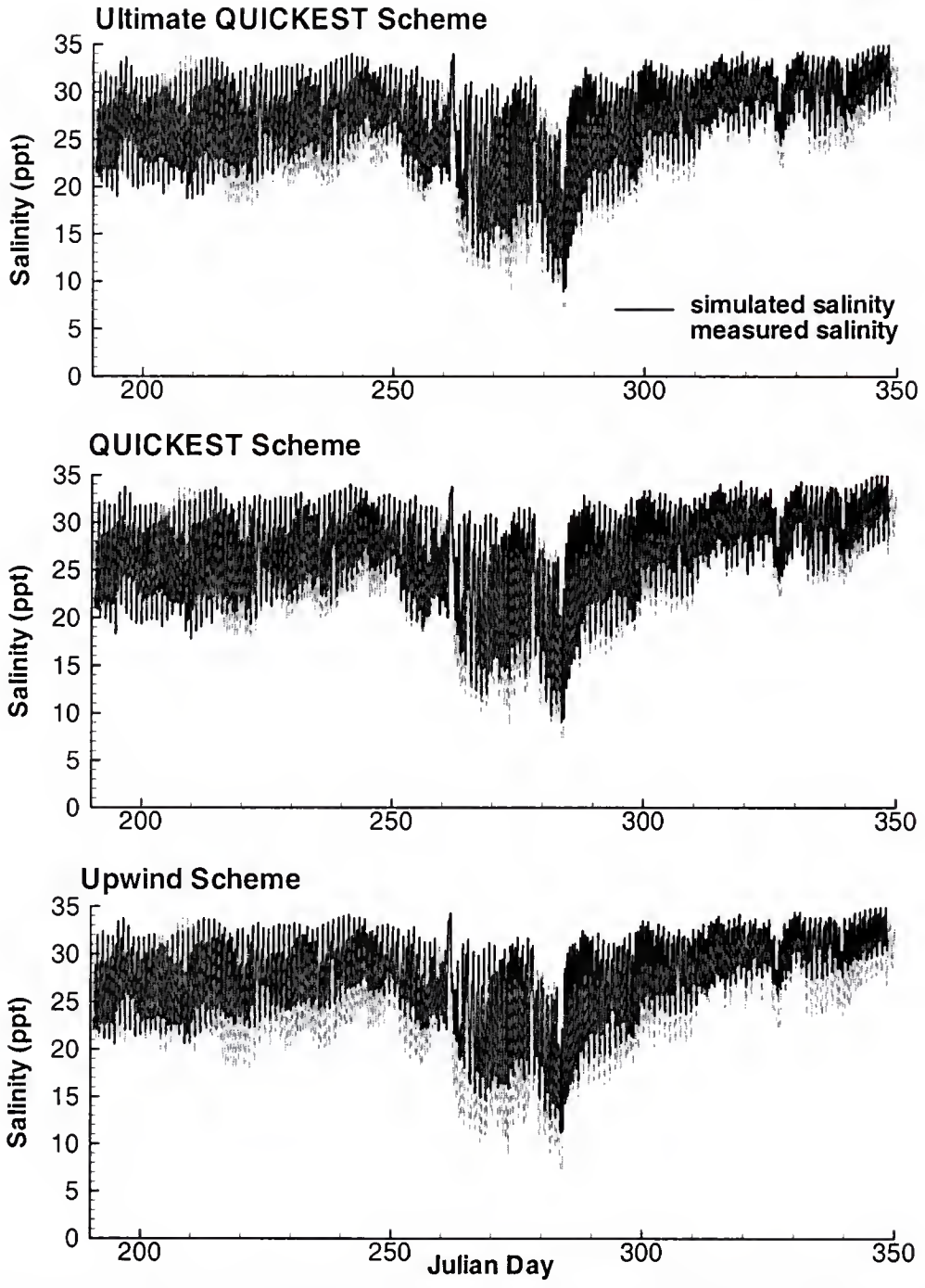

Figure 5.18 A comparison between simulated and measured salinity at Shell Point using Ultimate QUICKEST, QUICKEST, and upwind advection schemes.

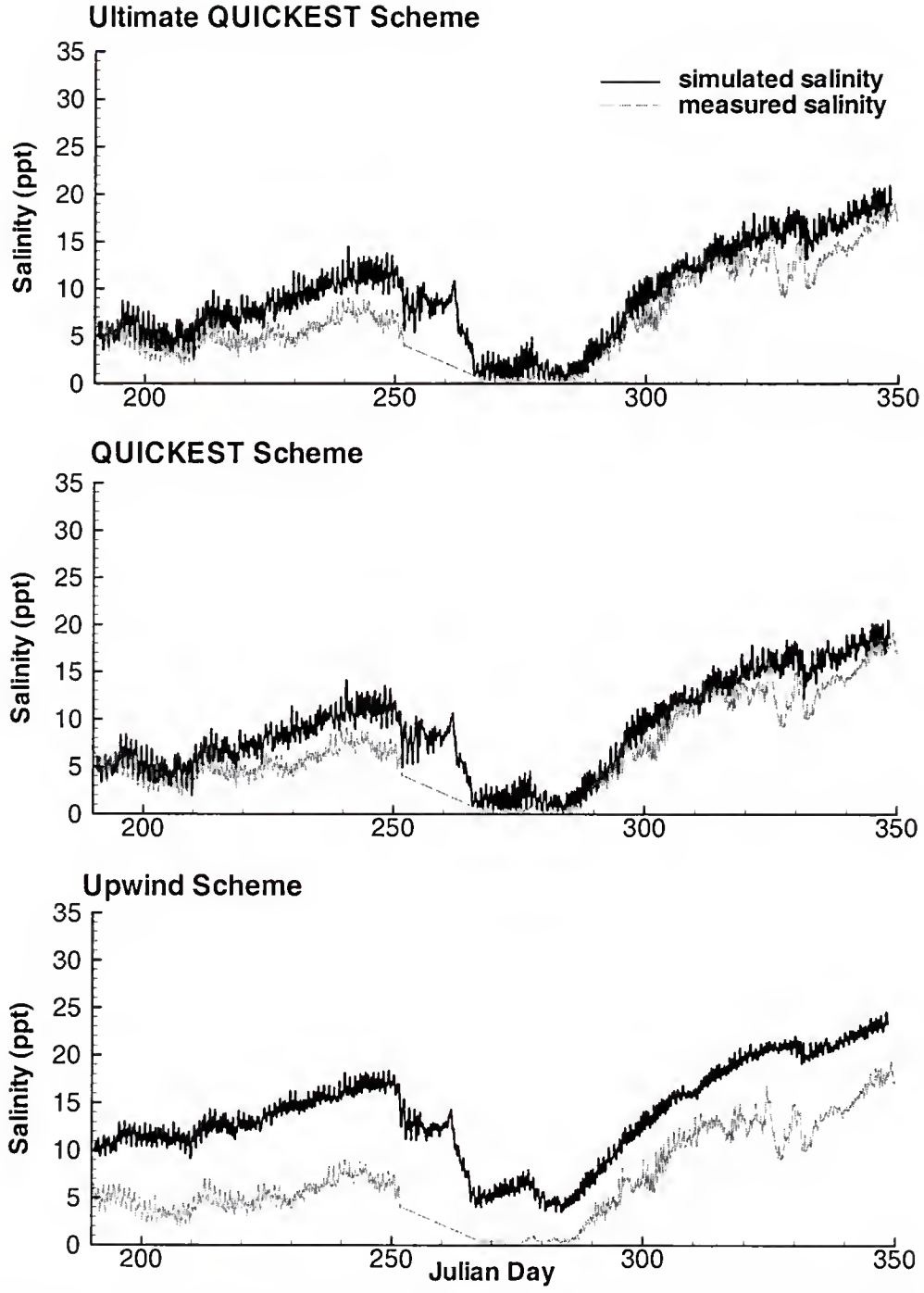

Figure 5.19 A comparison between simulated and measured salinity at Fort Myers using Ultimate QUICKEST, QUICKEST, and upwind advection schemes.

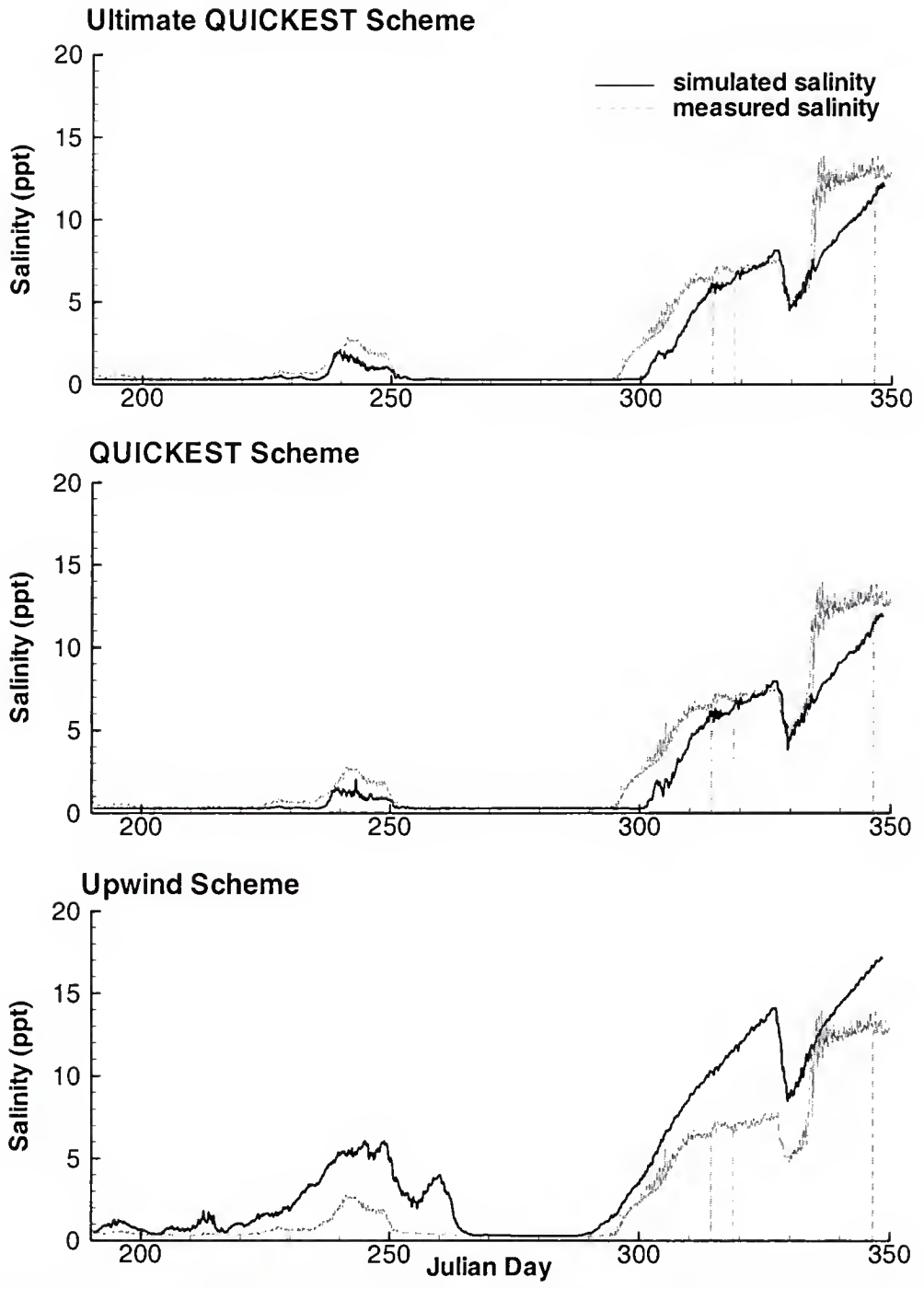

Figure 5.20 A comparison between simulated and measured salinity at BR31 using Ultimate QUICKEST, QUICKEST, and upwind advection schemes.

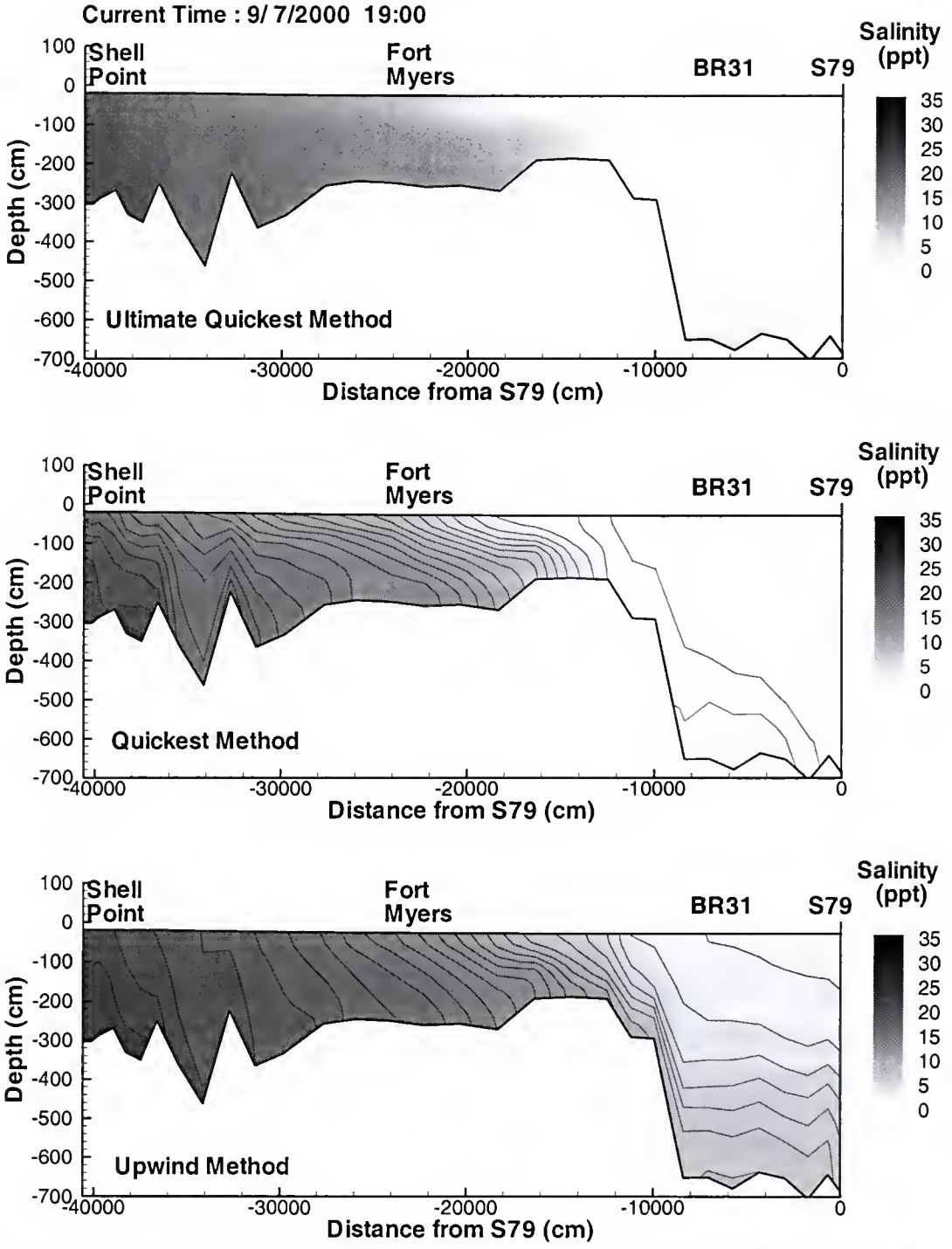

Figure 5.21 Simulated longitudinal-vertical salinity along the Caloosahatchee River at slack water before flood on September 7, 2000.

Table 5.13 shows the effect of salinity advection scheme on the accuracy of simulated water level and salinity. The results show slight difference between water level and salinity simulated with the Ultimate QUICKEST scheme and the QUICKEST scheme, while the simulated salinity RMS errors with upwind scheme is much greater. Maximum improvement in simulated salinity is achieved when the QUICKEST scheme is used because most of the model parameters and boundary conditions are calibrated using the QUICKEST scheme. However, because of the higher cost of model simulations using the Ultimate QUICKEST scheme, coupled with only a marginal improvement in the simulated results, the QUICKEST scheme is deemed appropriate for this study.

Table 5.13 The effect of varying salinity advection scheme on the accuracy of simulated water level and salinity in 2000. Values shown are average RMS errors at all data stations.

Advection scheme	Water level (cm)	Salinity (ppt)
Ultimate QUICKEST	5.56	2.35
QUICKEST	5.63	2.34
Upwind	5.36	3.73

Beside adjusting boundary condition and model coefficients, it is also interesting to see how varying the model grid and bathymetry affects simulated circulation and transport within the estuary. Because flow through the Caloosahatchee River mouth is crucial to the water level and salinity inside the river basin, it is useful to perform a numerical simulation to study how the flow through the river mouth is affected by its cross-sectional area. As was discussed in the previous section, the Charlotte Harbor grid bathymetry was developed by interpolating measured bathymetry onto the entire grid followed by a simple smoothing scheme. Although the bathymetry in upper Charlotte Harbor and inside Caloosahatchee River were updated by measured data by SWFWMD and SFWMD, the resolution of bathymetry in San Carlos Bay area, including the Caloosahatchee River mouth, is very coarse

(about 300 m resolution). To study how the accuracy of grid bathymetry affects simulated the circulation and transport, several 2000 simulations were performed using grid systems with modified bathymetry data. The first simulation used a modified grid bathymetry which had a minimum depth of 2.5 m (1.5 m for baseline simulation). This simulation was performed to determine how important the "shallowness" of the river is to the circulation and transport. The second simulation used a bathymetry that included an artificially dredged channel through out the entire river. The navigation channel included in the grid bathymetry at a depth of 3.5 m (NAVD88). Since the grid system is too coarse to adequately resolve the navigation channel, forcing a channel into the grid system resulted in over estimation of the cross-sectional areas within the river. Table 5.14 compares the results of the year-long simulations performed using the original and two modified grid bathymetries. While forcing an deeper navigation channel into the grid system had little effect, imposing a 2.5 m minimum cell depth slightly improved simulated salinity and greatly worsened water level through the Caloosahatchee River. Since neither modified grid system improved the 2000 simulation, the standard bathymetry is used for all subsequent simulations.

Table 5.14 The effect of modifying bathymetry on the accuracy of simulated water level and salinity in 2000. Values shown are average RMS errors at all data stations.

Simulation description	Water level (cm)	Salinity (ppt)
Standard bathymetry	4.88	2.29
Minimum depth of 2.5 m	6.14	1.90
Deeper navigation channel	4.90	2.32

Overall, the model is able to simulate water level and salinity within 10 % normalized RMS error with the maximum measured values. This indicates that the hydrodynamic model reproduces the basic circulation and salinity transport of the Caloosahatchee River so that

this model can be used to simulate water quality processes.

5.4.1 Results of the 2000 Simulation

This section summarizes the calibration of the long term Charlotte Harbor circulation and transport model using the field data collected in January to December 2000. In addition, the mathematical model of the temperature transport with heat flux model as surface boundary condition was applied to improve the simulation of circulation in the study area. Based on the results, it is apparent that the model accurately simulated the observed water level, salinity, and temperature distribution in the Caloosahatchee River. Table 5.15 summarizes the boundary conditions and model parameters for 2000 simulation.

Table 5.15 A summary of boundary conditions and model parameters used in 2000 simulation.

Boundary Condition or Model Parameter	Value
Tidal Forcing	Measured at Naples
Wind speed and direction	Measured at 3 stations
Fresh Water Discharge	Estimated for Estero Bay and Measured at Peace, Myakka, and Caloosahatchee Rivers
Bottom Roughness	Constant (0.3 cm)
Horizontal Diffusion	Constant (10000 cm^2/s)
Horizontal grid	92 x 129
Vertical Layers	8

Water Level

When measured water level at an open sea is used as a tidal boundary condition, it is necessary to unify datum level with bathymetry and water level measured in the estuary. For the 2000 simulation of Charlotte Harbor, the datum level for all measured water levels and the bathymetry were converted to NAVD88. Water level at the Naples station, which is the tidal boundary condition, was leveled to MLW by NOAA CO-OPS and converted to

NAVD88 according to tidal bench mark at Naples (26° 7.8'N, 81° 48.4W).

Calculated RMS errors between simulated and measured water level for 2000 simulations are shown in Table 5.16. The normalized RMS errors are less than 3% at all available water level stations, demonstrating the model's ability to accurately reproduce surface elevation in the system.

Table 5.16 Calculated RMS errors between simulated and measured water level for 2000 simulation

Station Name	RMS error (cm)	Maximum Range (cm)	% RMS error
Fort Myers	5.51	166.80	3.30
Shell Point	4.25	143.26	2.96
Average	4.88	155.03	3.13

Figure 5.22 shows a year long and 20 days' comparison between simulated and measured water level at Shell point and Fort Myers. Although the normalized RMS errors are very small, the model constantly overestimated at Fort Myers and underestimated at Shell Point station. A probable sources of these differences could be the bathymetry, grid resolution, bottom roughness, and open boundary condition. In the Caloosahatchee River, there is a very narrow navigation channel which the current grid system could not resolved. The bottom roughness is a very sensitive parameter, specially in the river environment, as shown in previous calibration. This study uses a constant bottom roughness of 0.3 value, but there is no direct measurement of the bottom roughness for this estuarine system. This might cause some error in model simulation. In this study, CH3D does not include calculation of flooding/drying cell. Therefore, this study uses a minimum depth of 1.5 m which could not resolve any shallow water below this depth. Once again, it has been demonstrated that model is sensitive to the bathymetry and grid resolution, and the model accuracy will improve if

more accurate bathymetry and grid are used.

Salinity and Temperature

The circulation in Charlotte Harbor estuarine system is driven primarily by the mixed (diurnal and semi-diurnal) tides from the Gulf of Mexico, as well as by wind and density gradient. During periods of high freshwater inflow from the rivers, significant vertical salinity stratification can be found in the Upper Charlotte Harbor and Caloosahatchee River. A two layered flow and salinity structure characteristic of the "classic estuarine circulation" is often present (Sheng, 1998). Therefore, understanding of vertical salinity distribution is a very important part of hydrodynamic and transport simulations. The salinity is measured at two locations in the water column referred to as "upper" and "lower". The vertical positions of the salinity measurements taken by SFWMD are given in Table 5.17. For this study, eight vertical layers are used by the CH3D model. The simulated salinity values at eight vertical layers are interpolated vertically to allow comparison of salinity at the exact location of the measured stations.

Table 5.17 presents the maximum and minimum measured salinity, the RMS error, and the normalized RMS error (with respect to maximum salinity) for all stations during 2000. The results show the model's ability to simulate salinity is within 7% error except at the Shell Point station. The Shell Point station is located at the Caloosahatchee River mouth, which is very sensitive to bathymetry and grid resolution. As mentioned before, to improve salinity at this point, finer grid resolution and bathymetry data will be needed. It should be pointed out that % RMS error is not a good measure of model accuracy. At S79 and BR31, although the % RMS error is low, the actual error is quite significant.

Figure 5.23 to 5.27 show the near-bottom and near-surface simulated and measured

salinity at SFWMD stations in Caloosahatchee River. The results show reasonable agreement with measured data for both wet season and dry season except at S-79 and BR31. S-79 and BR31 stations are directly affected by the river boundary condition because these two stations are located within a few grid cells from S-79. The water level and discharge at the Lock and S-79 is controlled by 8 tainter gates and 2 sector gates whereas the river boundary condition in CH3D is specified by the averaged flow rate. At these two stations, there is only one grid cell across the relatively narrow width. Therefore, the current boundary condition and grid resolution at S-79 and BR31 stations could not resolve the detail characteristics of circulation and salinity transport. Furthermore, the bathymetry in this area was produced from only a few cross sectional bathymetry data provided by SFWMD.

Table 5.17 Calculated RMS errors between simulated and measured salinity for 2000 simulation

Station Name	Mean depth (cm)	Layers	Location from bottom (cm)	RMS error (ppt)	Minimum Salinity (ppt)	Maximum Salinity (ppt)	% RMS error
S-79	591	upper	298	1.49	0.3	13.85	4.07
		lower	103	1.88	0.3	14.55	5.11
BR31	678	upper	386	1.60	0.3	13.96	4.36
		lower	251	2.11	0.3	15.51	5.76
Fort Myers	261	upper	227	1.84	0.3	18.66	5.01
		lower	101	2.56	0.3	20.83	6.98
Shell Point	304	upper	209	3.82	2.4	34.50	10.41
		lower	93	3.57	3.1	36.13	9.72
Sanibel	254	upper	135	1.96	11.2	36.69	5.34
		lower	19	2.05	14.3	36.45	5.59
Average				2.29			6.23

Seasonal salinity patterns occurred in response to the variation in volume of

freshwater inflow. The highest measured salinity occurred during an extended period of low flow in December 2000. During the wet season, the fresh water from S-79 reached into San Carlos Bay. The salinity in San Carlos Bay was directly affected by the variation of river discharge from S-79 station.

Figure 5.28 shows the simulated and measured temperature near the surface at the Fort Myers station. The measured and simulated temperature show significant annual variations in the Charlotte Harbor estuarine system. Water temperature ranges from an average of about 30 °C during the summer to about 15 °C in December and January. The daily fluctuation of water temperature is about 1 to 3 °C. The simulation result shows very good agreement with measured data over seasonal and daily scales. The RMS error is less than 2.5 °C at the Fort Myers station which is about 7% RMS error of the maximum temperature of 32.20 °C.

Flow Patterns

Typical flow pattern (vertically averaged flow) in San Carlos Bay during flood tide and ebb tide on August, 7 2000 are shown in figure 5.29. The large flood and ebb flows through San Carlos Pass satisfy the tidal prism in the Caloosahatchee River, San Carlos Bay, the lower part of Matacha Pass and lower extremity of Pine Island Sound. Due to Sanibel Causeway and three navigation channels, the flood tide is separated into three major flows along the navigation channel. The flow through the right side of causeway moves toward the Caloosahatchee River , the flow through left side of causeway moves to Pine Island Sound, and flood tide across the center channel of causeway follows navigation channel toward the Matlacha Pass. During ebb tide, the flows are relatively weak and follow the opposite directions. Along the East-West direction navigation channel, there are two direction flows:

the eastward flow during flood tide and the westward flow during ebb tide.

Residual Flow and Salinity Patterns

Figures 5.30 and 5.31 show the one year residual flow and salinity in 2000. In the San Carlos Bay, the westward residual flow is dominant in the surface and bottom, while there is a relatively week northward flow along the left and right side of shoreline. The strong outflows from the left side of San Carlos Pass create the anti-clockwise gyres near the surface at the outside of Sanibel Causeway. This anti-clockwise gyre is associated with the clockwise gyre in the Gulf of Mexico which is shown in Figure 5.15 for the1986 simulation.

The residual salinity has a relatively uniform vertical and horizontal distribution in the San Carlos Bay, while the salinity has a strong vertical stratification at the Caloosahatchee River mouth due to the strong river discharge and mixed tide from Gulf of Mexico. Therefore, the density-driven circulation is a very important factor for understanding the circulation near such large rivers as Peace and Caloosahatchee.

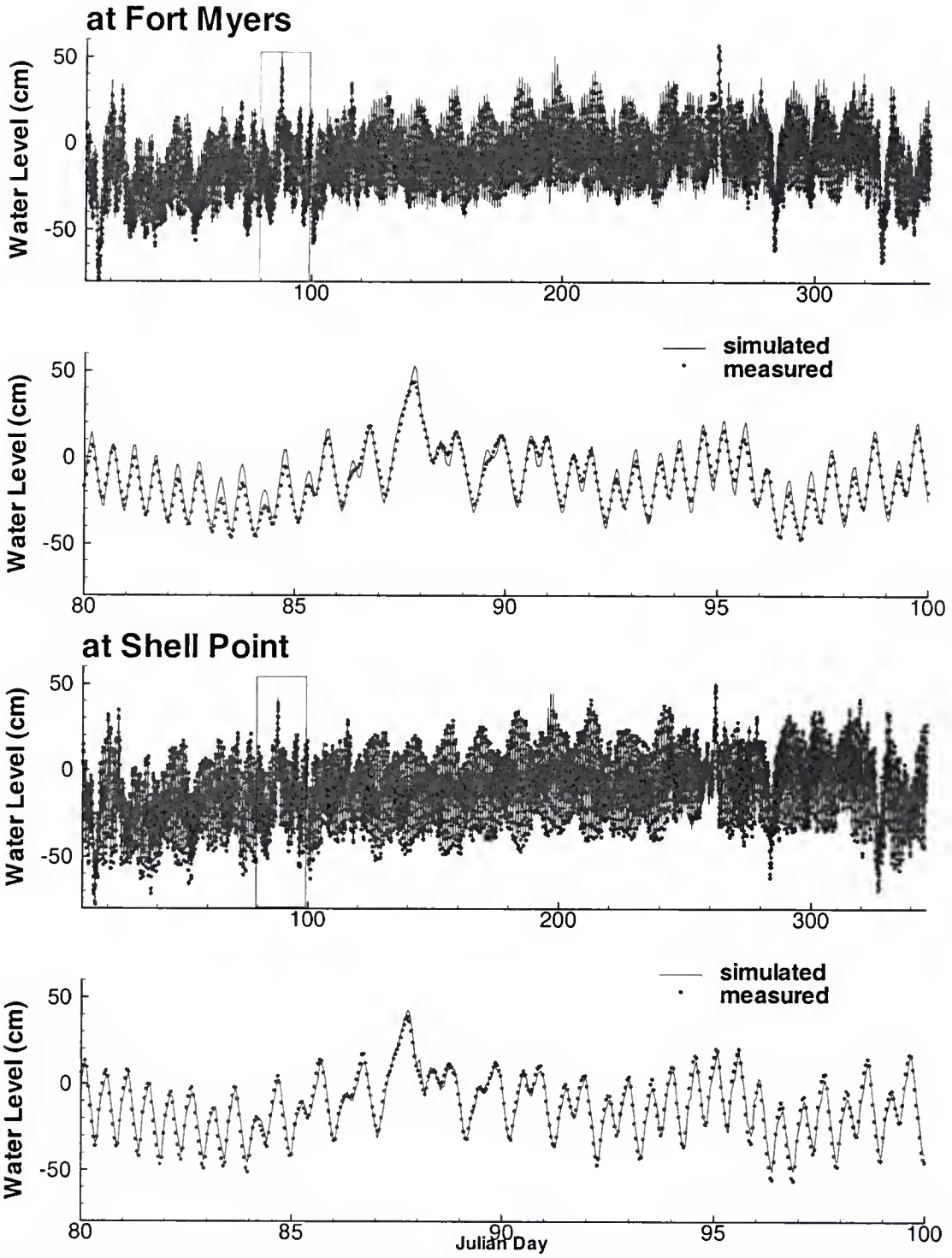

Figure 5.22 Comparison between simulated and measured water level for 2000 simulation.

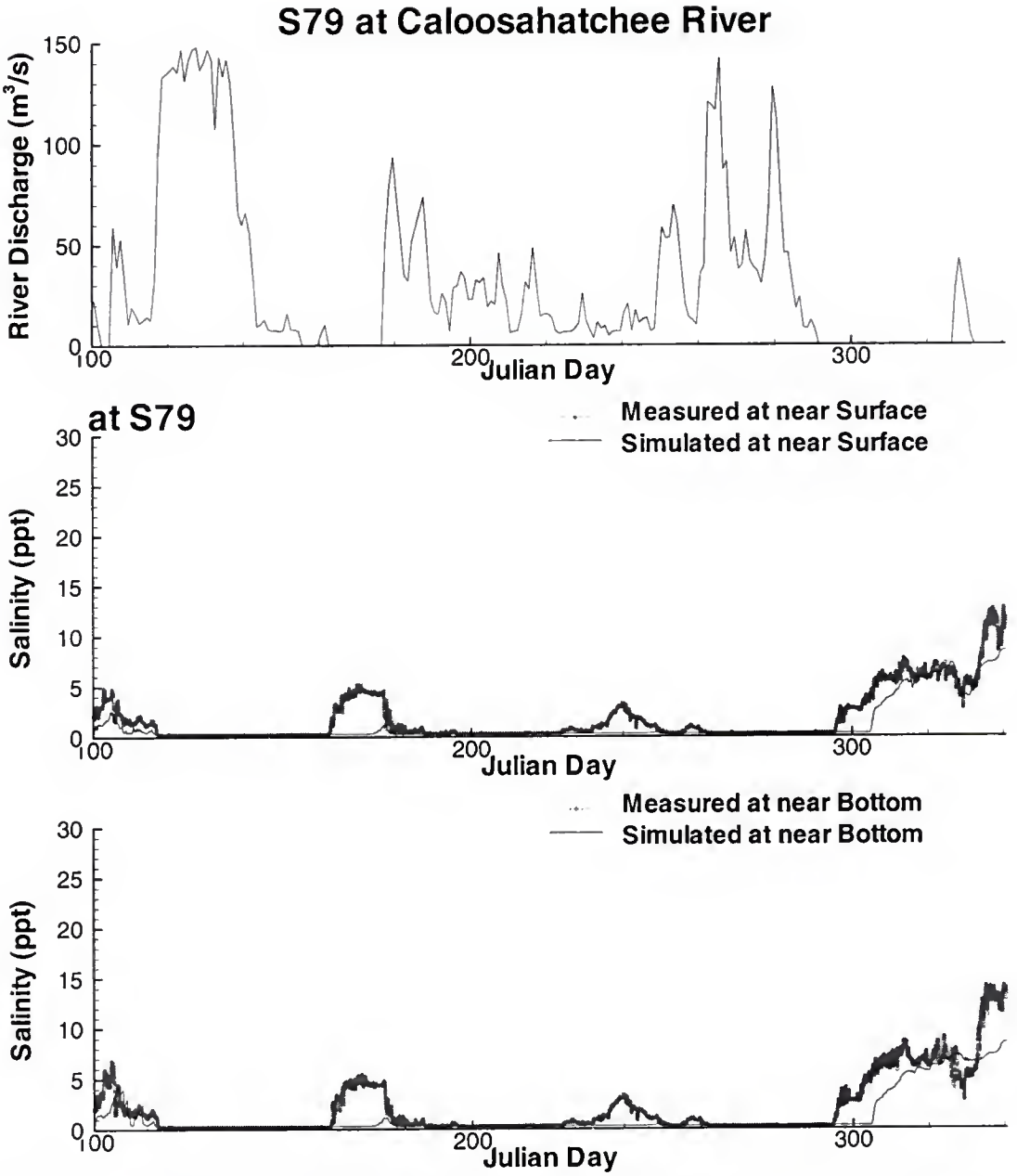

Figure 5.23 Comparison between simulated and measured salinity at S-79 in 2000.

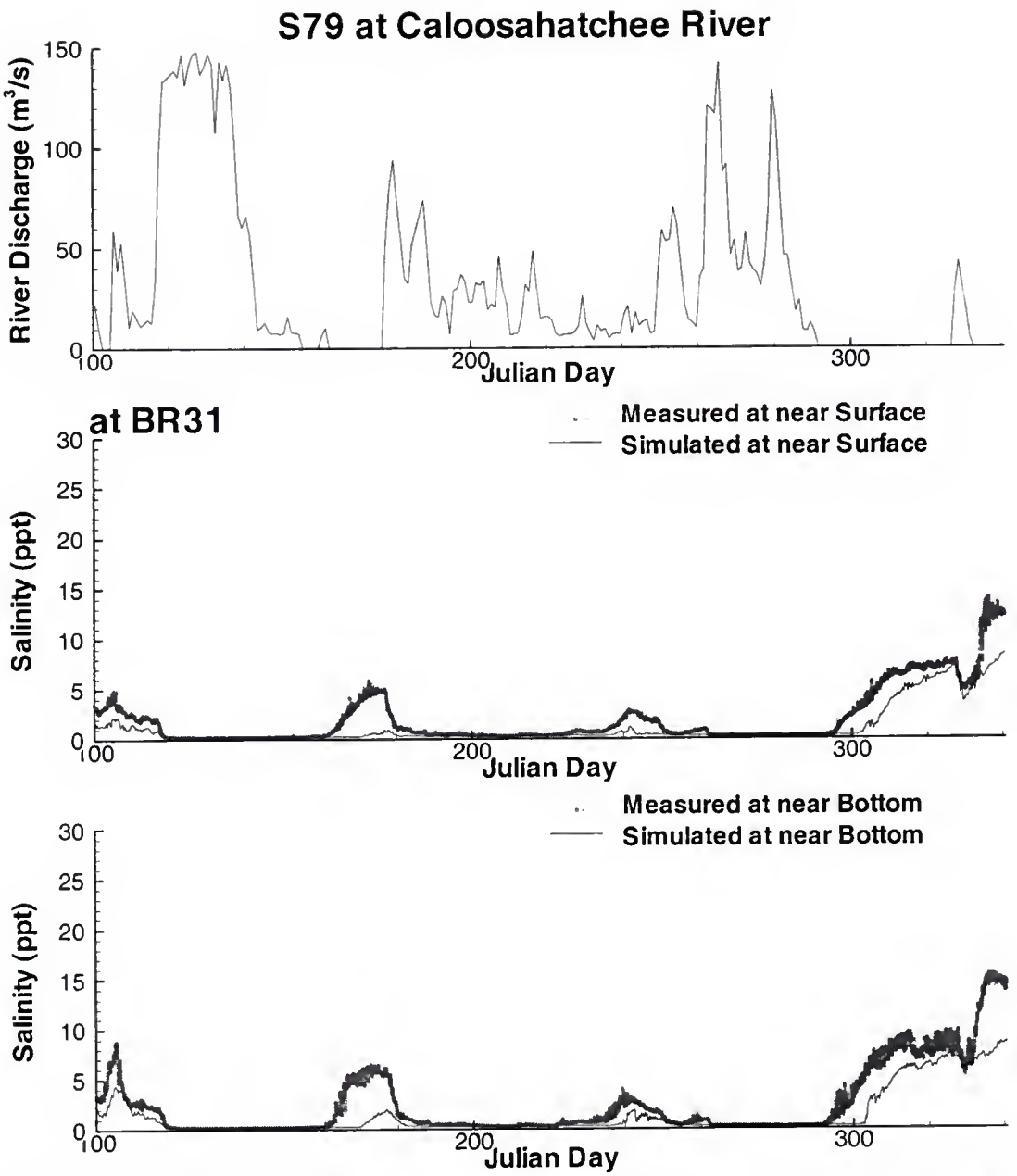

Figure 5.24 Comparison between simulated and measured salinity at BR31 in 2000.

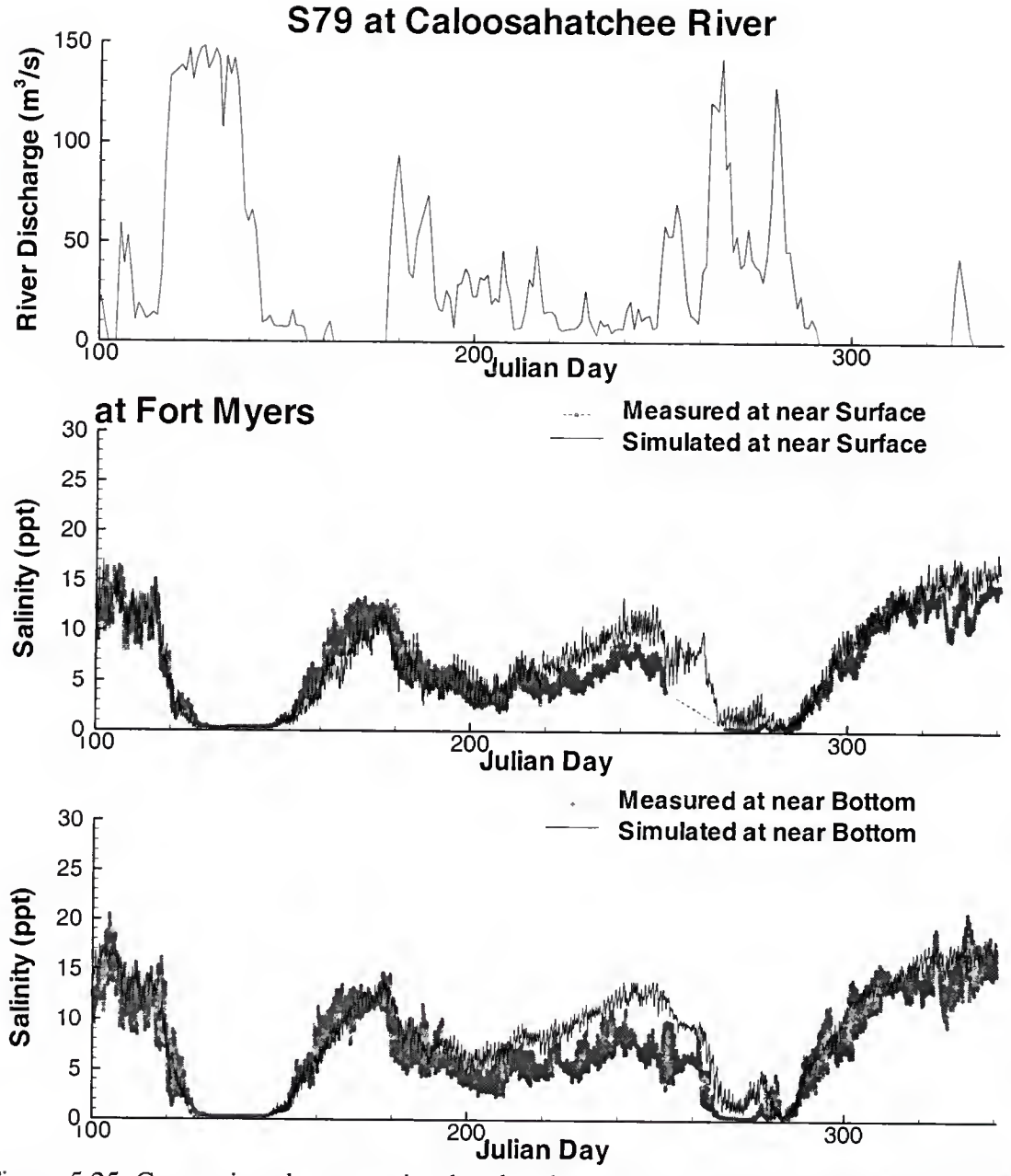

Figure 5.25 Comparison between simulated and measured salinity at Fort Myers in 2000.

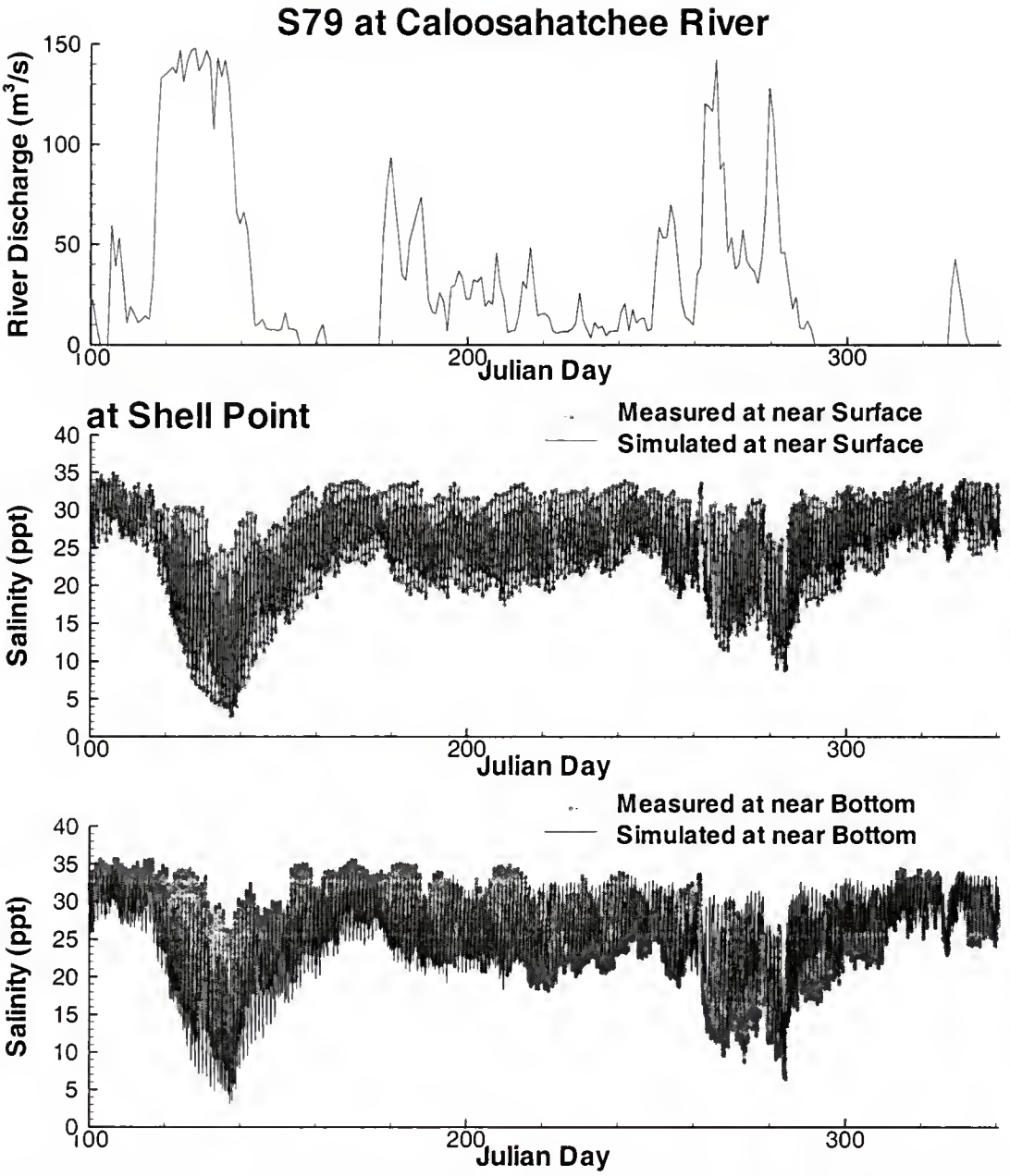

Figure 5.26 Comparison between simulated and measured salinity at Shell Point in 2000.

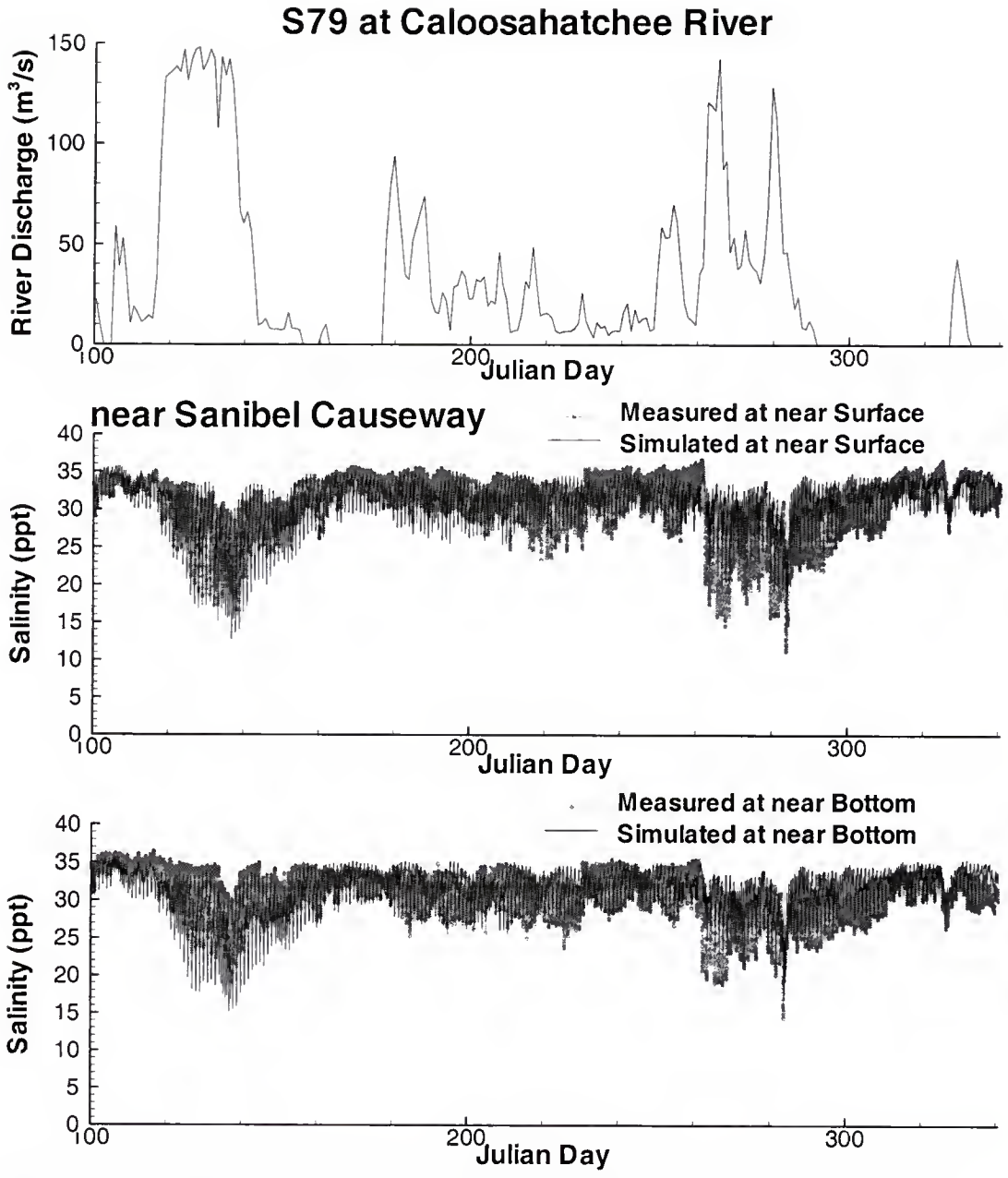

Figure 5.27 Comparison between simulated and measured salinity near Sanibel Causeway in 2000.

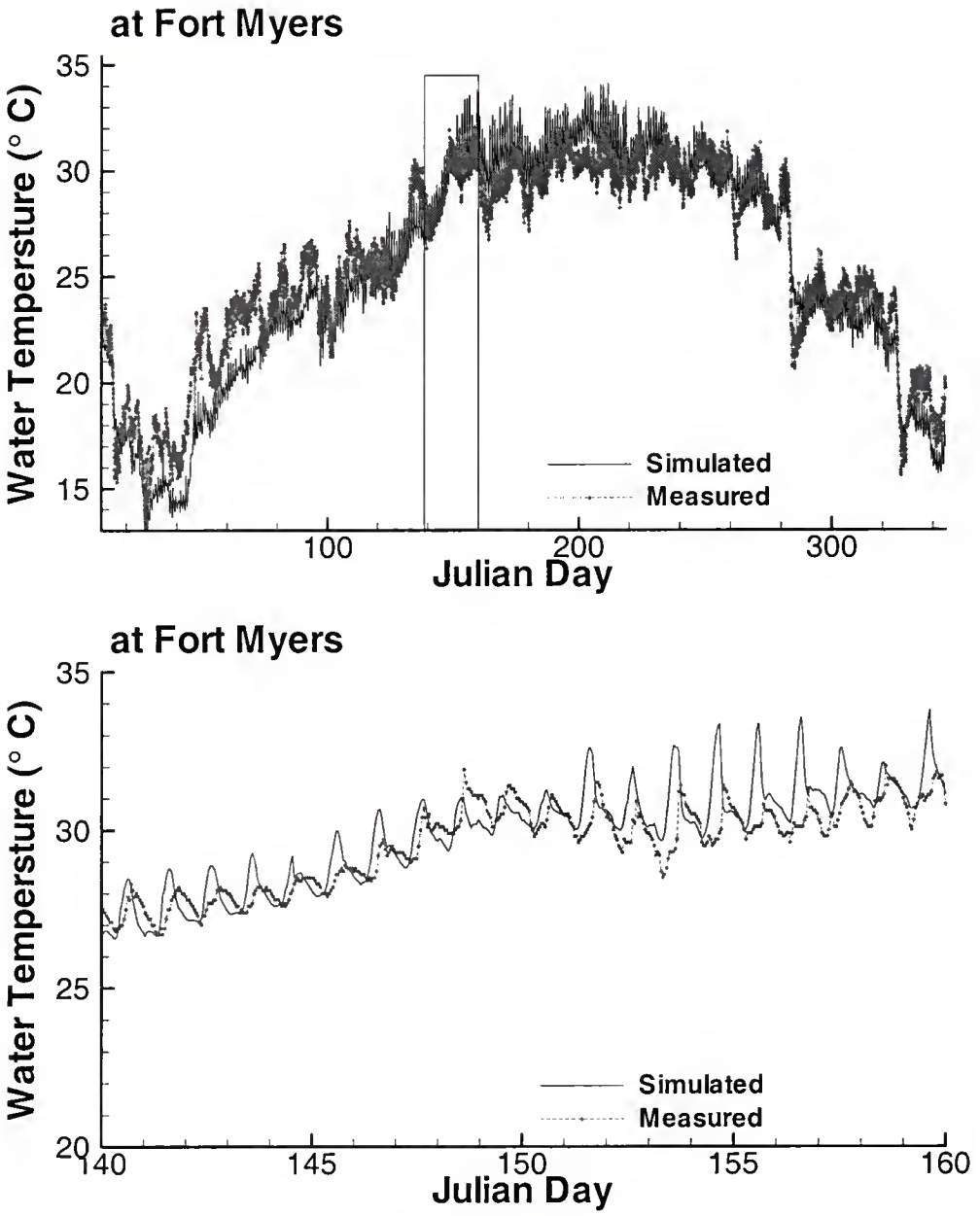

Figure 5.28 Comparison between simulated and measured temperature at Fort Myers in 2000.

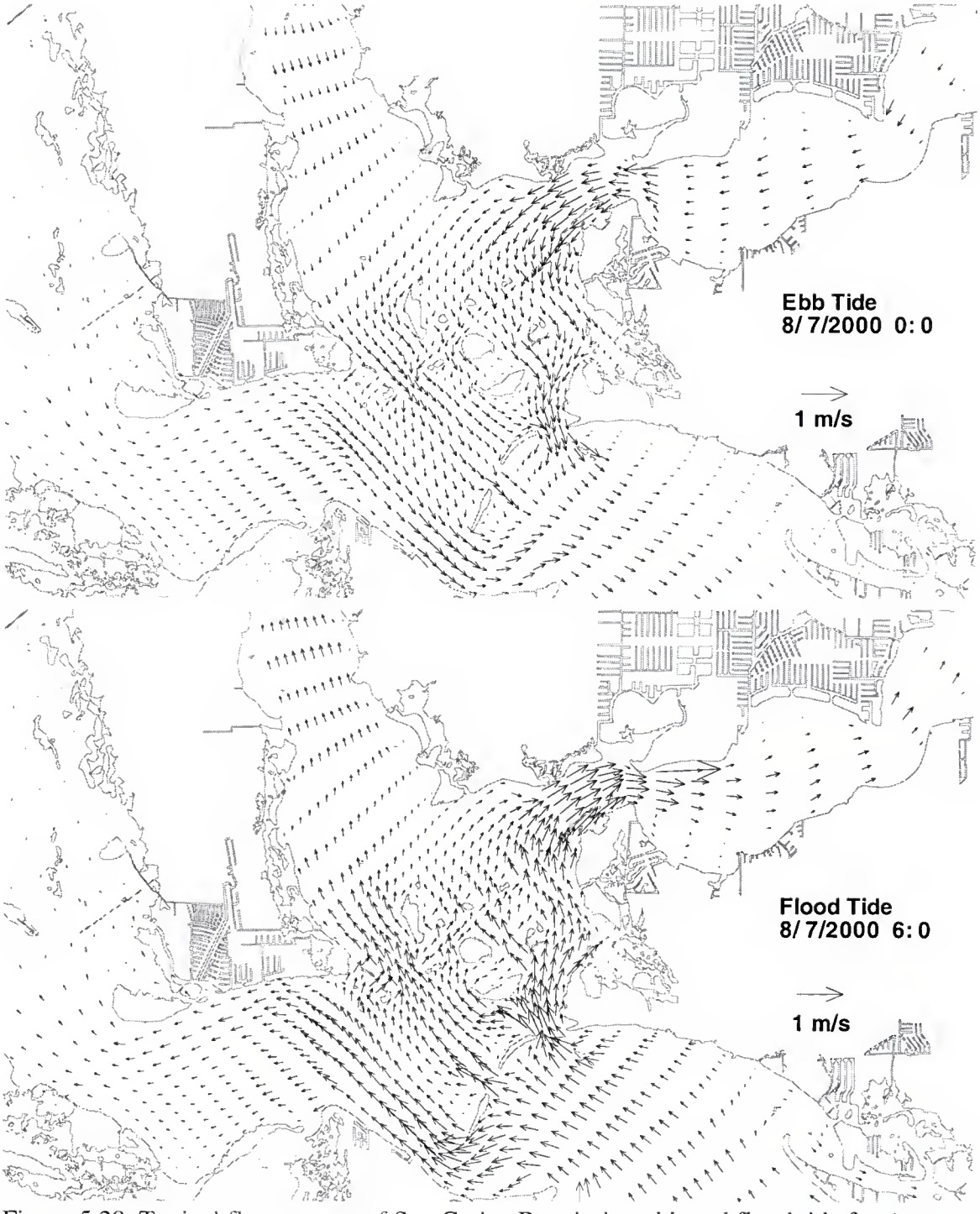

Figure 5.29 Typical flow pattern of San Carlos Bay during ebb and flood tide for August, 7 on 2000.

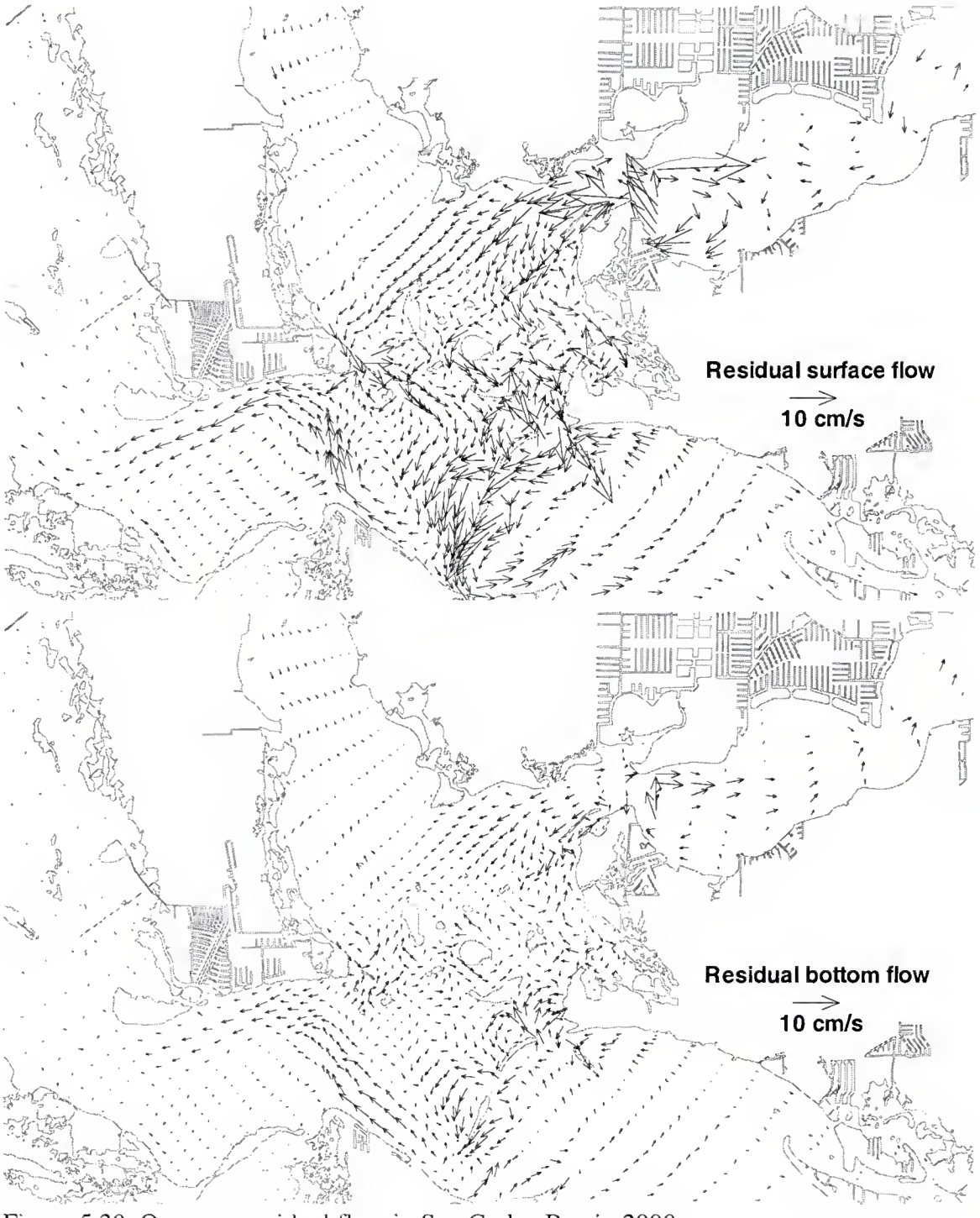

Figure 5.30 One-year residual flow in San Carlos Bay in 2000.

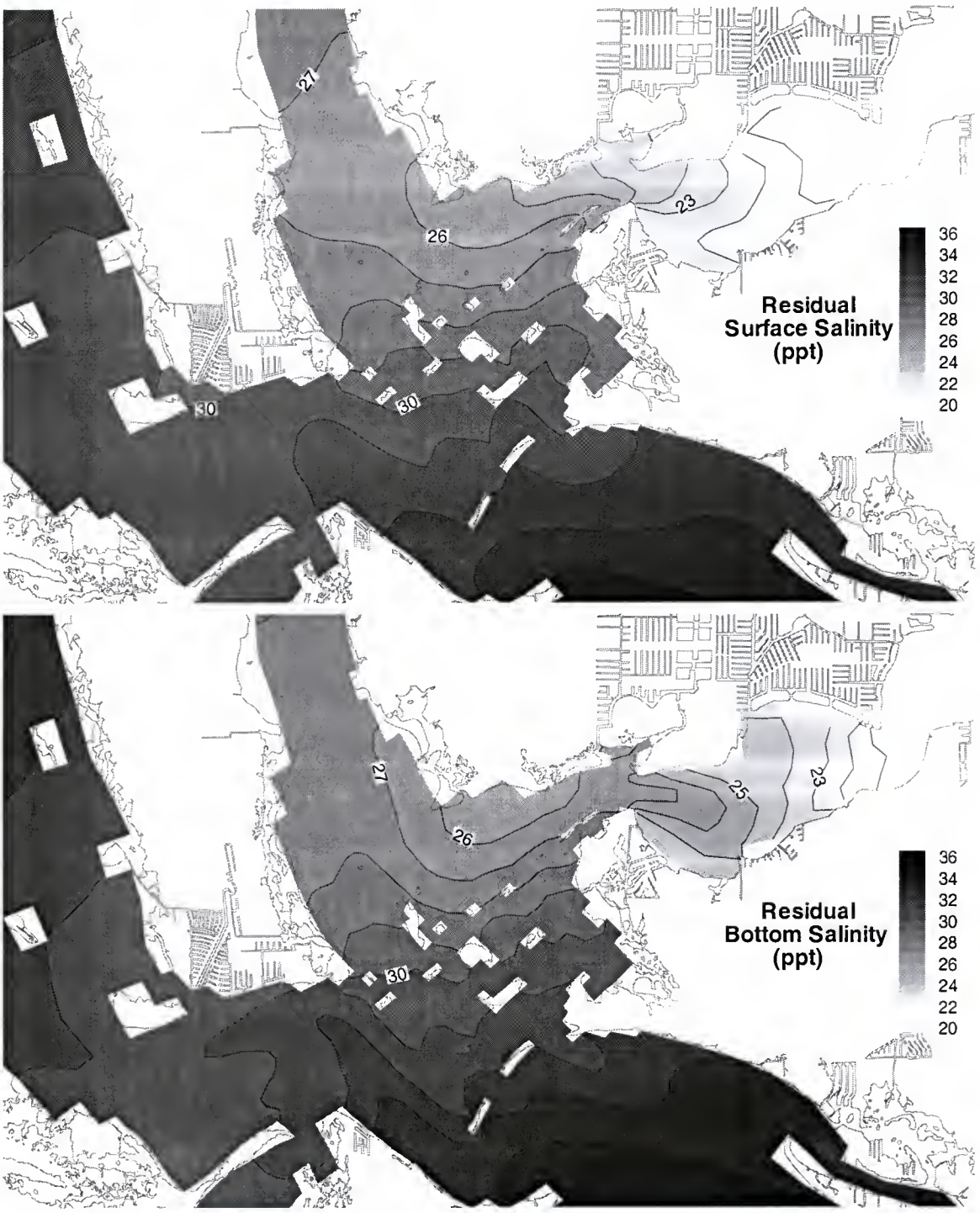

Figure 5.31 One year residual salinity distribution in San Carlos Bay in 2000.

5.4.2 Applications of 2000 Hydrodynamic Simulations

Hydrologic Alterations

Hydrologic alterations in the San Carlos Bay and Caloosahatchee River have taken many forms such as navigation channel and causeway. It has been suggested such large transportation projects as the dredging of the IntraCoastal Waterway (ICW) and the construction of Sanibel Causeway (SC) are linked to the decline of scallop populations in Pine Island Sound (Estevez, 1998). A quantitative assessment of this suggestion is long overdue. Moreover, to improve the natural environment of this area, it is necessary to quantify the effects of these artificial hydrologic alterations. In this study, the calibrated Charlotte Harbor model is used to evaluate the effects of these hydrologic alterations.

Figure 5.32 shows the location of eleven stations which are selected to quantify the hydrologic alteration, and the locations of Sanibel Causeway (A) and IntraCoastal Waterway (B). Three month simulations from April 9 to July 8, 2000 were conducted with two hydrologic alterations in the Charlotte Harbor estuarine system. To test these effects, three cases were considered: (1) present condition with Sanibel Causeway and existing bathymetry (BASELINE), (2) hypothetical condition with Sanibel Causeway removed (NSC), (3) hypothetical condition with ICW removed (NICW). Figure 5.33 shows the bathymetry and shoreline for each case.

The simulated Charlotte Harbor circulation in the presence of and in the absence of the Sanibel Causeway and IntraCoastal Waterway are compared in terms of the instantaneous flow from July 3 to July 8, 2000. Figures 5.34 and 5.35 show the comparisons of water level and salinity for each case at three selected stations: ST05 (Pine Island Sound), ST08 (San Carlos Bay), and ST10 (Caloosahatchee River mouth).

The water level at all three stations show little difference among the three cases. The salinity at Pine Island Sound (ST05) show little difference among the three cases, because the impacts of these hydrologic alterations are very small and local. The results show that water level and salinity transport are more affected by the absence of Intracoastal Waterway (NICW) than by the absence of the Sanibel Causeway (NSC) except salinity at ST08 which is located near the Sanibel Causeway. The freshwater from Caloosahatchee River and saltwater from Gulf of Mexico are exchanged through the ICW. In the absence of the ICW, salinity at San Carlos Bay (ST08) is increased, while salinity at Caloosahatchee River Mouth (ST10) is decreased at both surface and bottom layers because of the reduced flow and salinity transport between the Caloosahatchee River and San Carlos Bay.

Calculated water level RMS differences between the baseline simulation and two alteration cases from April to July 2000 are shown in Table 5.18 for 11 selected stations. The RMS differences are less than 2 cm at all selected stations. The highest difference is found at station 10 which is located at the Caloosahatchee River mouth. Calculated salinity RMS differences between baseline simulation and the two cases during this period are shown in Table 5.19. Salinity for the two alteration runs did not show much difference with the baseline simulation except at station 10.

The 29-day residual flow and salinity patterns in San Carlos Bay are shown in Figure 5.36 (at a surface) and Figure 5.37 (at a bottom) during June 9 to July 8, 2000. Although the results show some slight impact of the causeway on the residual flow as manifested by the circulation gyres in the immediate vicinity of the causeway, there is no noticeable impact on the salinity distribution in the San Carlos Bay area. The causeway islands did not block the flow of saline ocean water from entering into the San Carlos Bay and reaching Pine Island

Sound because the causeway islands are already located in a very shallow region. While there is strong residual flow along the IntraCoastal Waterway for the baseline simulation, this strong residual flow vanished without this waterway. This can explain the effect of the absence of IntraCoastal Waterway, which reduced the flow and salinity transport between Caloosahatchee River and San Carlos Bay. Overall, the IntraCoastal Waterway and Sanibel Causeway did not appear to show noticeable impact on the flow and salinity patterns in the San Carlos Bay and Pine Island Sound.

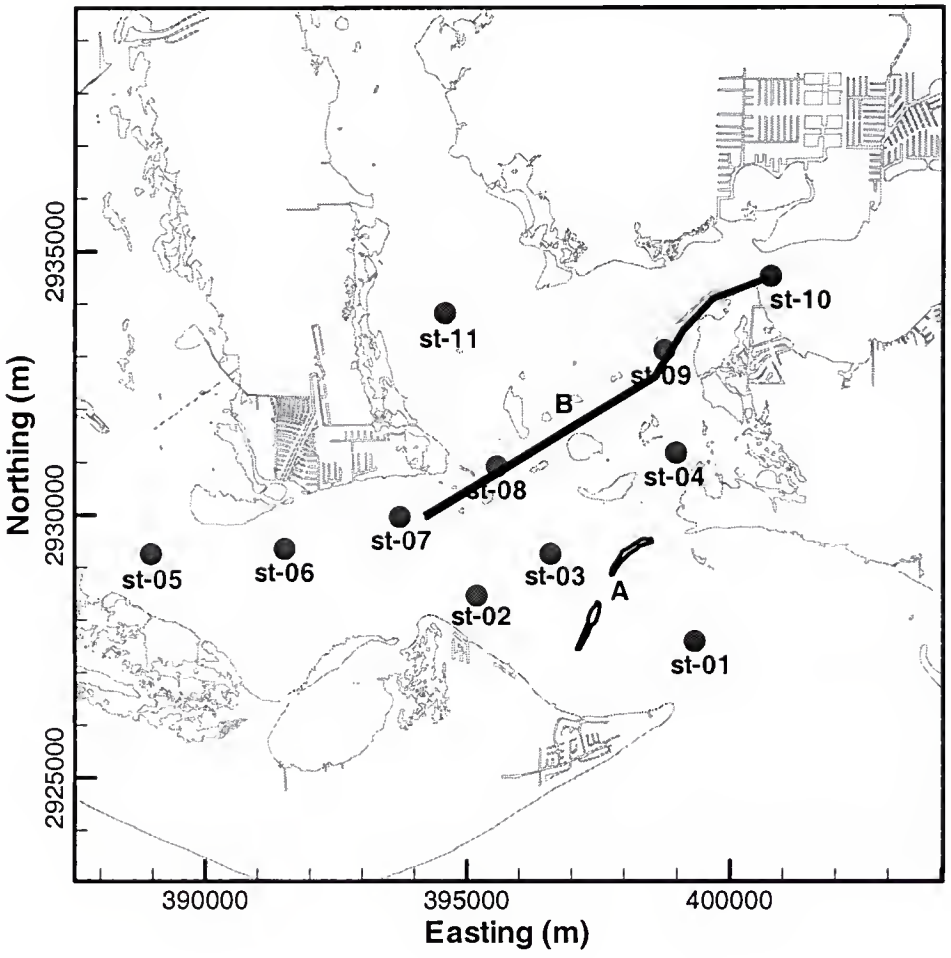

Figure 5.32 The locations of Sanibel Causeway and Intracoastal Waterway and stations for comparing the effects of hydrologic alterations.

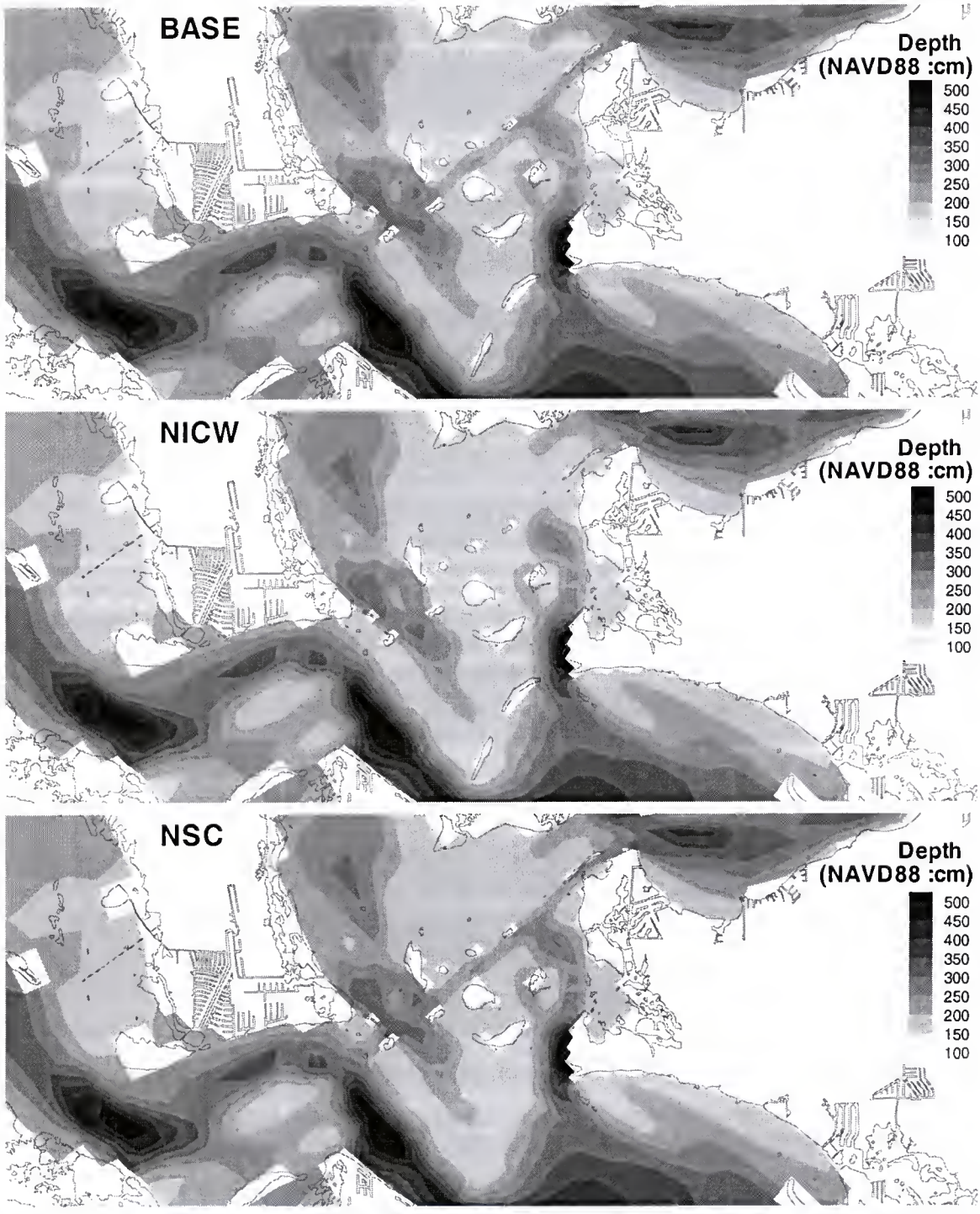

Figure 5.33 The comparison of bathymetry and shoreline for each hydrologic alteration case scenarios which are Baseline, the absence of IntraCoastal Waterway, and the absence of causeway.

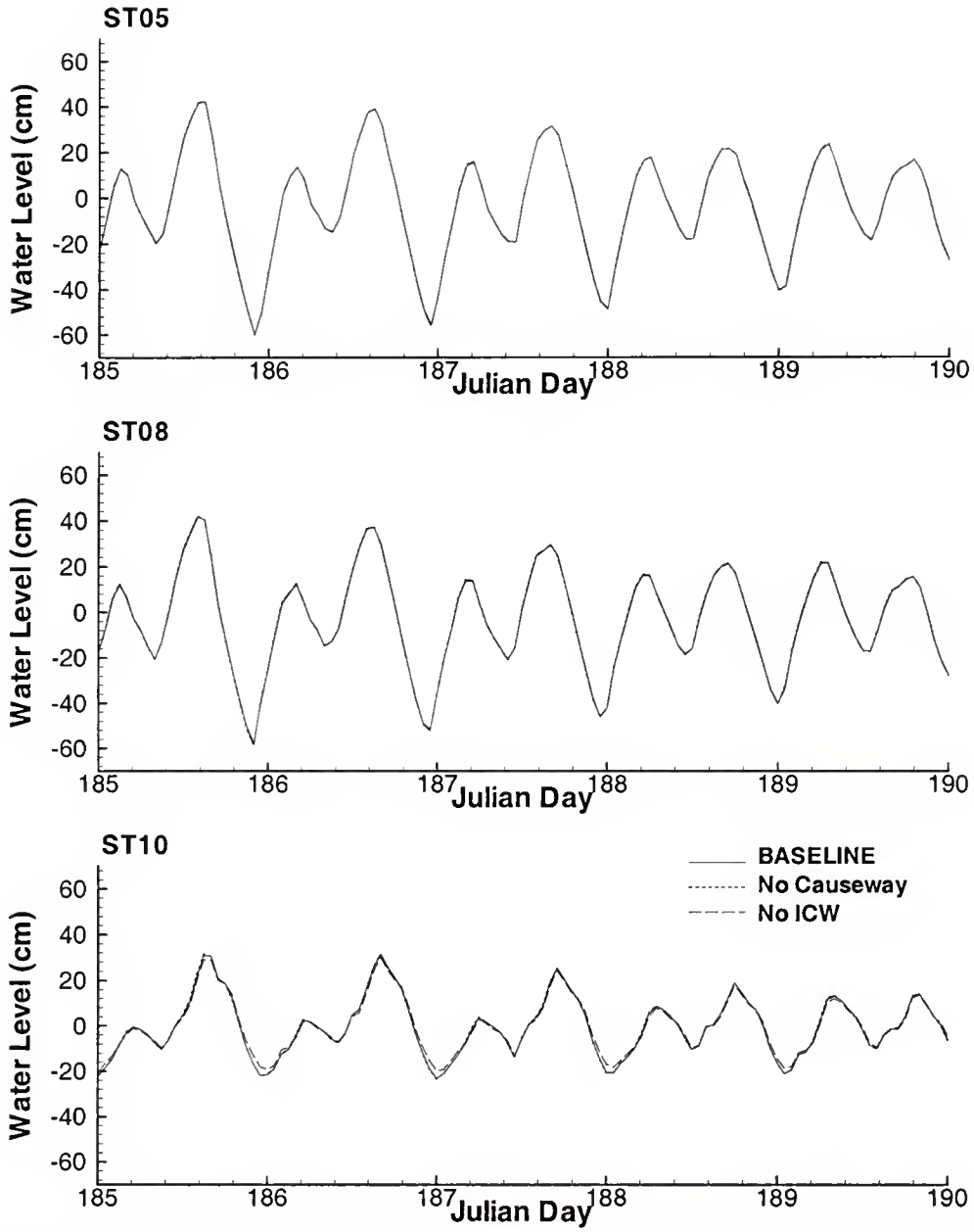

Figure 5.34 The comparisons of water level for three cases at three selected stations: ST05 (Pine Island Sound), ST08 (San Carlos Bay), and ST10 (Caloosahatchee River mouth).

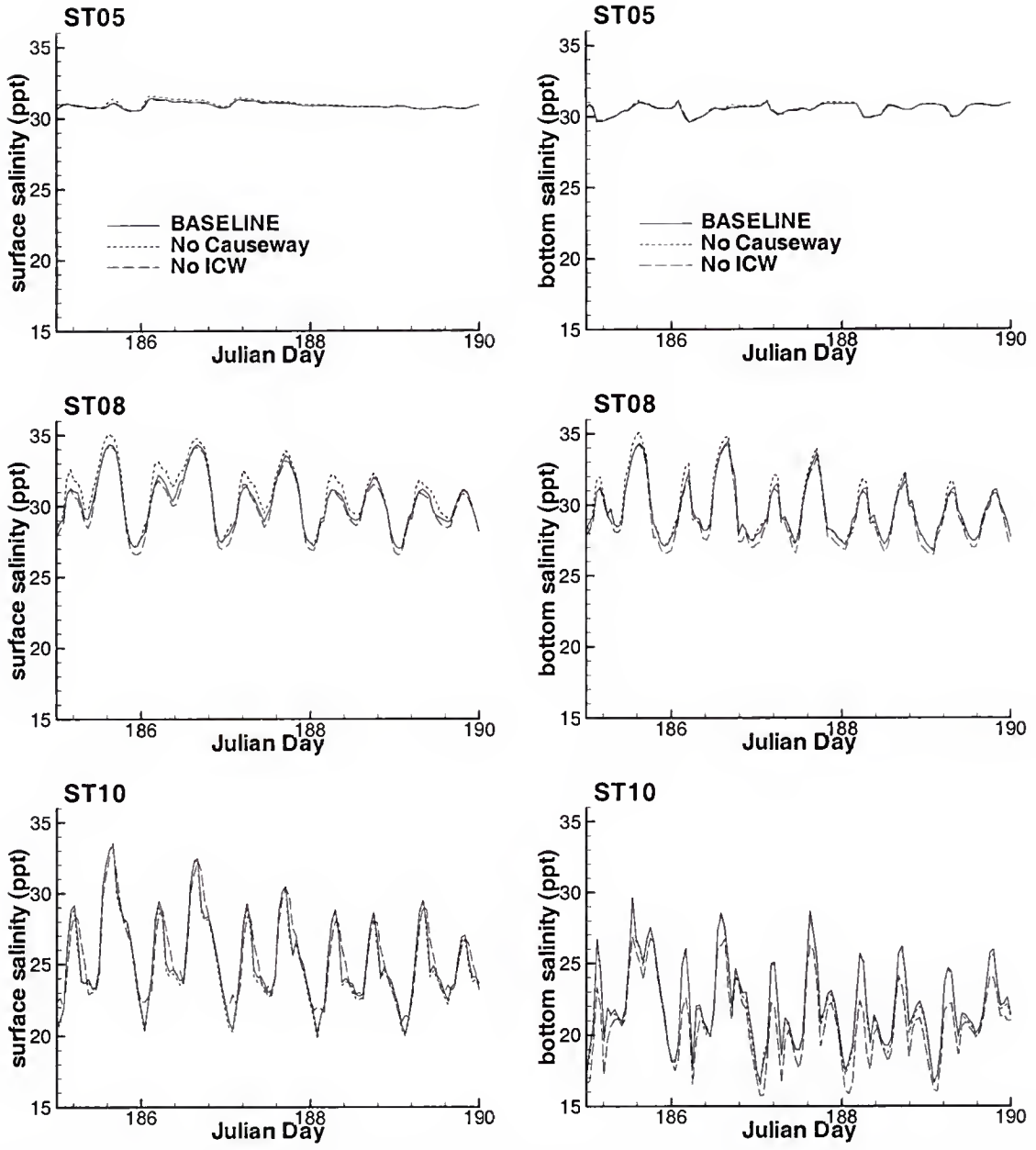

Figure 5.35 The comparisons of surface and bottom salinity for three cases at three selected stations: ST05 (Pine Island Sound), ST08 (San Carlos Bay), and ST10 (Caloosahatchee River mouth).

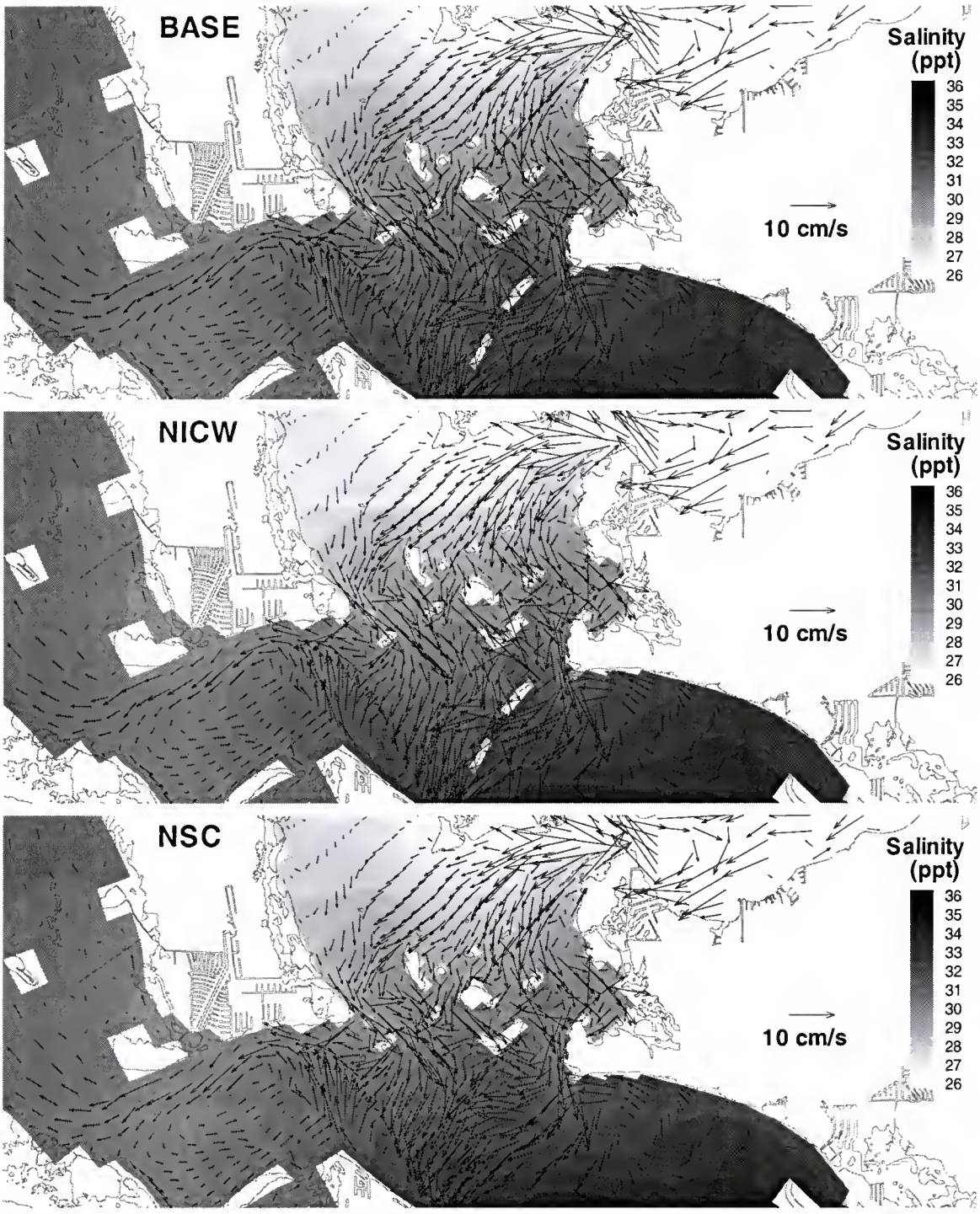

Figure 5.36 The comparisons of surface residual flow and salinity fields for three cases.

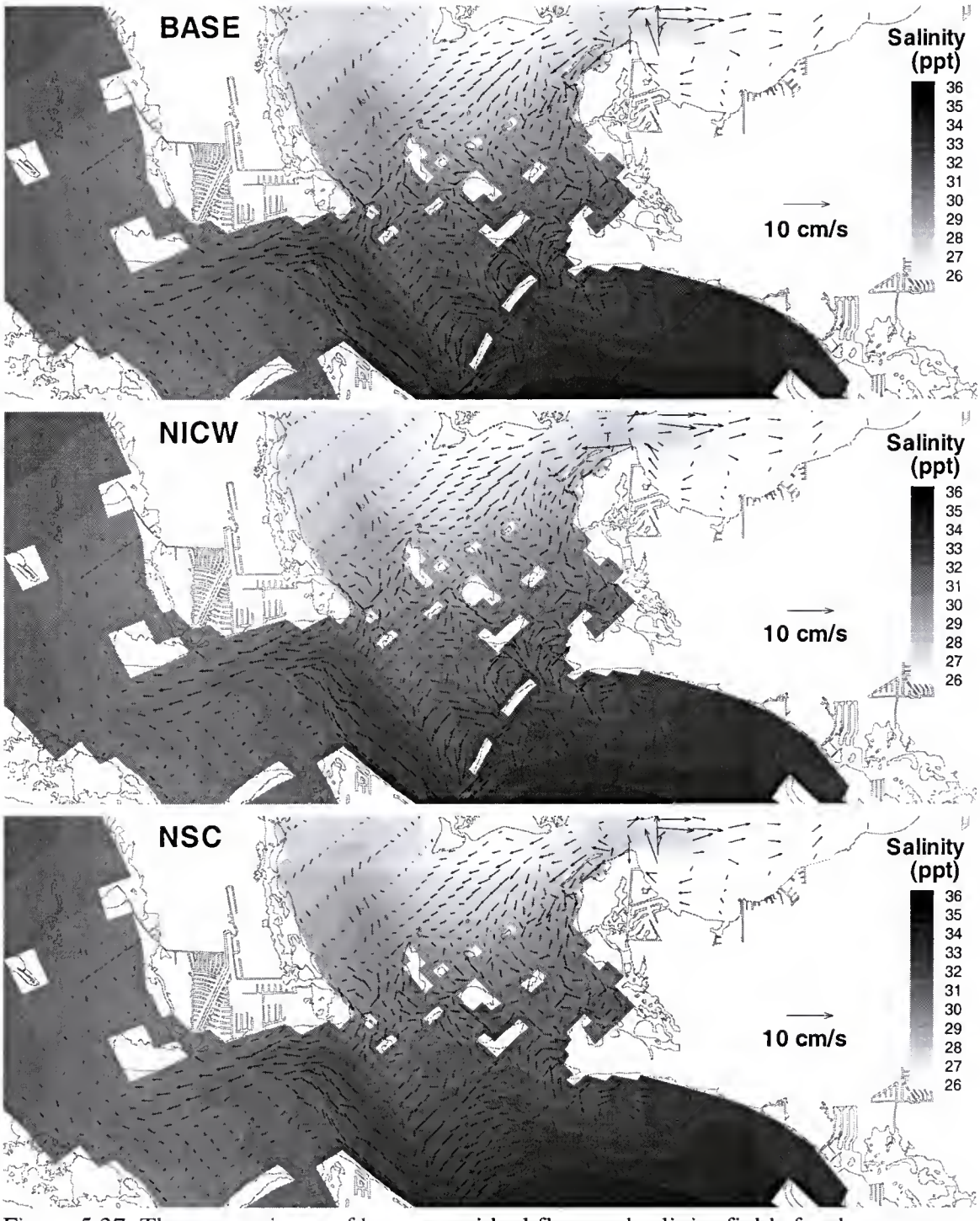

Figure 5.37 The comparisons of bottom residual flow and salinity fields for three cases.

Table 5.18 The effects of hydrologic alteration on 2000 water levels. Values shown are average RMS differences with baseline simulation for all selected stations.

Station Number	Range (cm)	RMS error for NSC	RMS error for NICW	RMS error for NSCICW
1	126.58	0.41	0.16	0.38
2	115.75	0.76	0.31	0.93
3	115.01	1.11	0.40	1.31
4	115.19	0.55	0.44	0.92
5	116.69	0.36	0.19	0.49
6	114.70	0.43	0.23	0.60
7	114.53	0.55	0.30	0.80
8	112.49	0.63	0.33	0.90
9	110.60	0.62	0.68	1.15
10	84.55	0.40	1.36	1.22
11	111.49	0.61	0.39	0.94
Average	126.58	0.58	0.44	0.88

Table 5.19 The effects of hydrologic alteration on 2000 salinity. Values shown are average RMS differences with baseline simulation for all selected stations.

Station Name	Layers	Range (ppt)	RMS error for NSC	RMS error for NICW	RMS error for NSCICW
1	surface	19.48	0.51	0.21	0.49
	bottom	11.07	0.32	0.08	0.34
2	surface	18.16	0.78	0.20	0.80
	bottom	11.80	0.24	0.06	0.24
3	surface	19.90	0.66	0.33	0.70
	bottom	18.46	0.39	0.20	0.44
4	surface	28.45	0.40	0.41	0.50
	bottom	26.58	0.32	0.21	0.31
5	surface	14.42	0.22	0.09	0.21
	bottom	9.53	0.25	0.07	0.29
6	surface	16.46	0.27	0.14	0.28
	bottom	12.07	0.23	0.08	0.24
7	surface	20.69	0.44	0.23	0.50
	bottom	11.92	0.25	0.10	0.28
8	surface	20.95	0.44	0.43	0.61
	bottom	20.26	0.42	0.40	0.57
9	surface	30.44	0.44	0.71	0.69
	bottom	30.37	0.33	0.51	0.66
10	surface	30.01	0.32	1.62	1.79
	bottom	30.45	0.38	1.33	1.24
11	surface	20.83	0.21	0.69	0.80
	bottom	18.18	0.33	0.37	0.42
Average	surface		0.43	0.46	0.67
	bottom		0.32	0.31	0.46

Freshwater Inflow and Salinity in the Caloosahatchee River

The Caloosahatchee River has been drastically altered for channelized flood-control and navigational waterway. These changes have caused large fluctuations in freshwater inflow volume, frequency of inflow events, timing of discharges, and water quality in the downstream estuary (Chamberlin and Doering, 1998). Therefore, it is necessary to quantify the impacts of freshwater inflow from S-79 on downstream estuarine system.

A minimum flow is defined by Ch.373.042(1) F.S (Florida State Law) as "the limit at which further withdrawals would be significantly harmful to the water resources or ecology of the area." Significant harm is defined in Chapter 40E-8 F.S. as "the degree of impact requiring more than two years for the water (or biological) resource to recover". Establishing quantifying relationship between freshwater inflow and the temporal and spatial distribution of salinity in the river is the first step to determine MFL condition.

Salinity distribution in San Carlos Bay and adjoining water directly responds to the fresh water inflow from Caloosahatchee River (Sheng and Park, 2001). In this study, the calibrated Charlotte Harbor model is used to evaluate the effects of the fresh water inflow from S79 to the salinity distribution in Caloosahatchee River. Using this calibrated model, a series of vertical-longitudinal salinity profiles along the axis of the Caloosahatchee River during one tidal cycle for wet and dry periods of river discharge at S-79 in 2000 are shown in Figures 5.38 and 5.39, respectively. The fresh water (less than 1 ppt salinity) from S-79 reached the river mouth near Shell Point in wet season, while the fresh water stayed upstream near BR31 during dry season. The salinity distribution at Caloosahatchee River shows much difference corresponding to river discharge from S-79.

To quantify this relationship for Caloosahatchee River, the locations of specific

salinity values were calculated during the 2000 simulation periods. Figure 5.40 shows the time histories of the river discharge rate and the locations of 1, 10, and 20 ppt surface salinity along the Caloosahatchee River. As the river discharge varied, the 1 ppt location is varied from S79 to near Shell Point. The tidal excursion of the salinity location is about 2 km for 1ppt salinity and 5 km for 20 ppt salinity. The salinity locations result from a combination of river discharge and tide and wind driven water circulation.

To test the relationship between river discharge and salinity distribution, the river discharge at S79 was reduced 50% and increased 50% of current river discharge condition. To remove tidal effect, 1-day averaged salinity location was compared. Figure 5.41 shows the locations of 1-day averaged 1 ppt salinity location during the simulation period in response to varying river discharge. The results show that 1 ppt salinity location move 3.4 km downstream and 8.5 km upstream, corresponding to a 50% reduction and a 50% increase in river discharge, respectively.

The Caloosahatchee MFL rule (SFWMD) states that: "A MFL exceedance occurs during a 365-day period, when (a) 30-day average salinity concentration exceeds 10 parts per thousand at the Fort Myers salinity station or (b) a single daily averaged salinity exceeds a concentration of 20 parts per thousand at the Fort Myers salinity station. Exceedance of either subsection (a) or subsection (b), for two consecutive years are a violation." Figure 5.42 show current conditions of salinity distribution to compare MFL rule for Caloosahatchee River during 2000 simulation periods. According to this result, the salinity does not exceed the Caloosahatchee MFL rule during 2000 simulation periods except winter dry season.

To quantify the Caloosahatchee MFL rule due to river discharge, the locations of 10

ppt surface salinity values were calculated during the 2000 simulation periods. Figure 5.43 shows the locations of 10 ppt surface salinity along the Caloosahatchee River due to river discharge rate. The polynomial regression line was calculated from the relationship between the locations of 10 ppt salinity and river discharge rate. According to this regression line, a total river discharge of 15 m^3/s at S79 produces 10 ppt salinity at the Fort Myers station.

An alternative and more acceptable approach to determine if the MFL has been exceeded, is to use a numerical mass-balanced model in which flows from different sources can be specified (Edwards et al., 2000). Therefore, the total river discharge at S79 required to produce a given salinity at Caloosahatchee River can be estimated with a calibrated model. Using the calibrated model, a diagram describing the relationship between river discharge and the locations of two salinity values (1-day averaged 20 ppt and 30-day averaged 10 ppt) in the river were generated in Figure 5.44. Twelve scenarios with constant river discharges of 5, 10, 15, 20, 30, 50, 75, 100, 150, 200 m^3/s at S79 were simulated for 60 days. The 60 day simulations allowed the model salinity to reach equilibrium condition for all specified river discharges. To compare current Caloosahatchee MFL rule with simulated salinity results, 30-day averaged 10 ppt salinity location and 1-day averaged 20 ppt salinity location were calculated for each case. According to this diagram, a total river discharge of 18 m^3/s at S79 produces 30-day averaged 10 ppt salinity at the Fort Myers station.

To quantify the relationship between salinity at Fort Myers station and river discharge, 1-day and 30-days averaged salinity at Fort Myers station were plotted vs. the fresh water inflow at S79 (Figure 5.45). The result show the minimum flow to produce a salinity of a 10 ppt at Fort Myers is about 18 m^3/s, which is the same as that obtained form Figure 5.44. The contribution of river discharge at S79 to spatial and temporal salinity

distribution was successfully quantified with the integrated model for Charlotte Harbor estuarine system. This modeling approach would develop a management tool to establish the MFL criteria, with long term salinity and river discharge data.

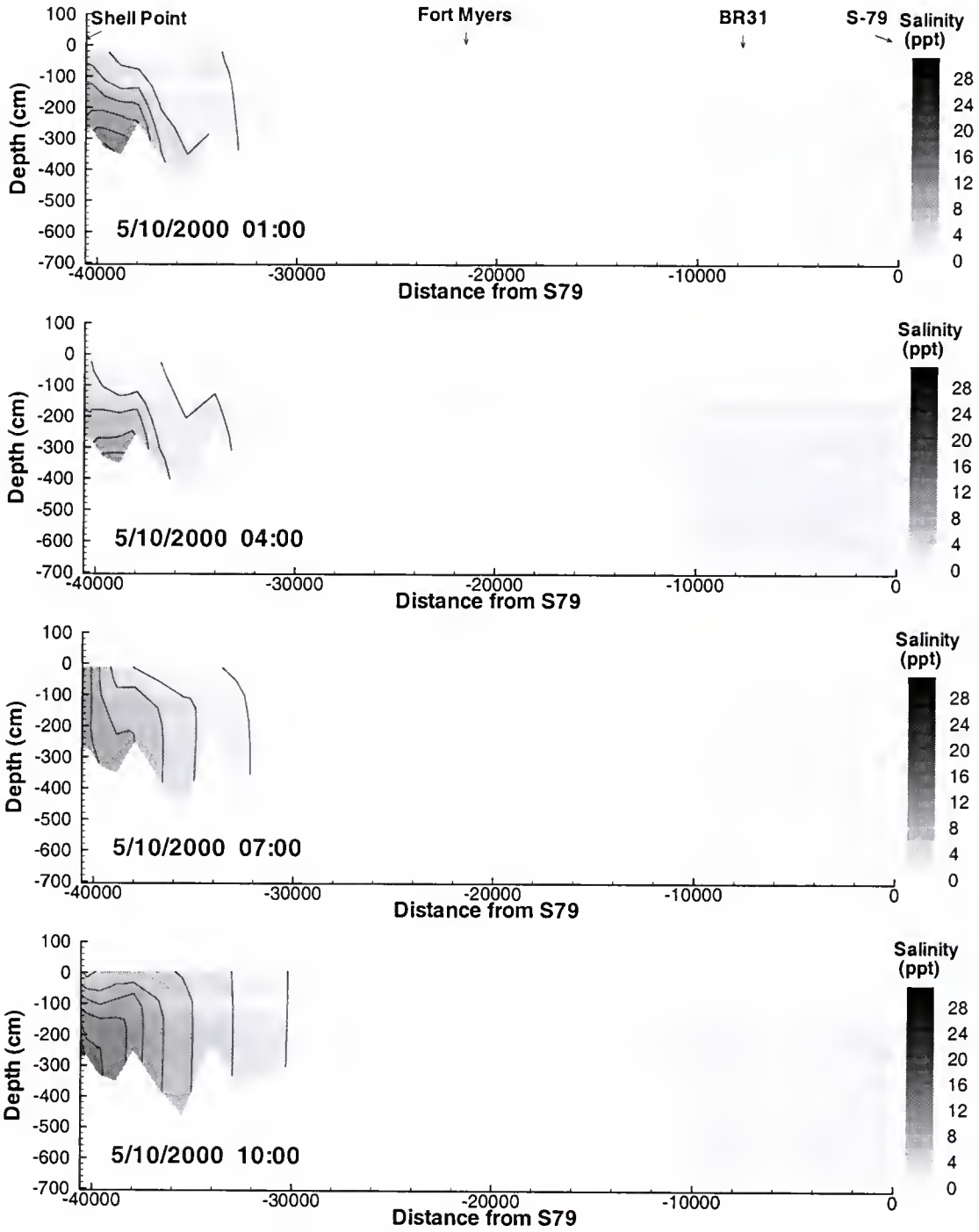

Figure 5.38 The vertical-longitudinal salinity profiles along the axis of the Caloosahatchee River during wet season in 2000

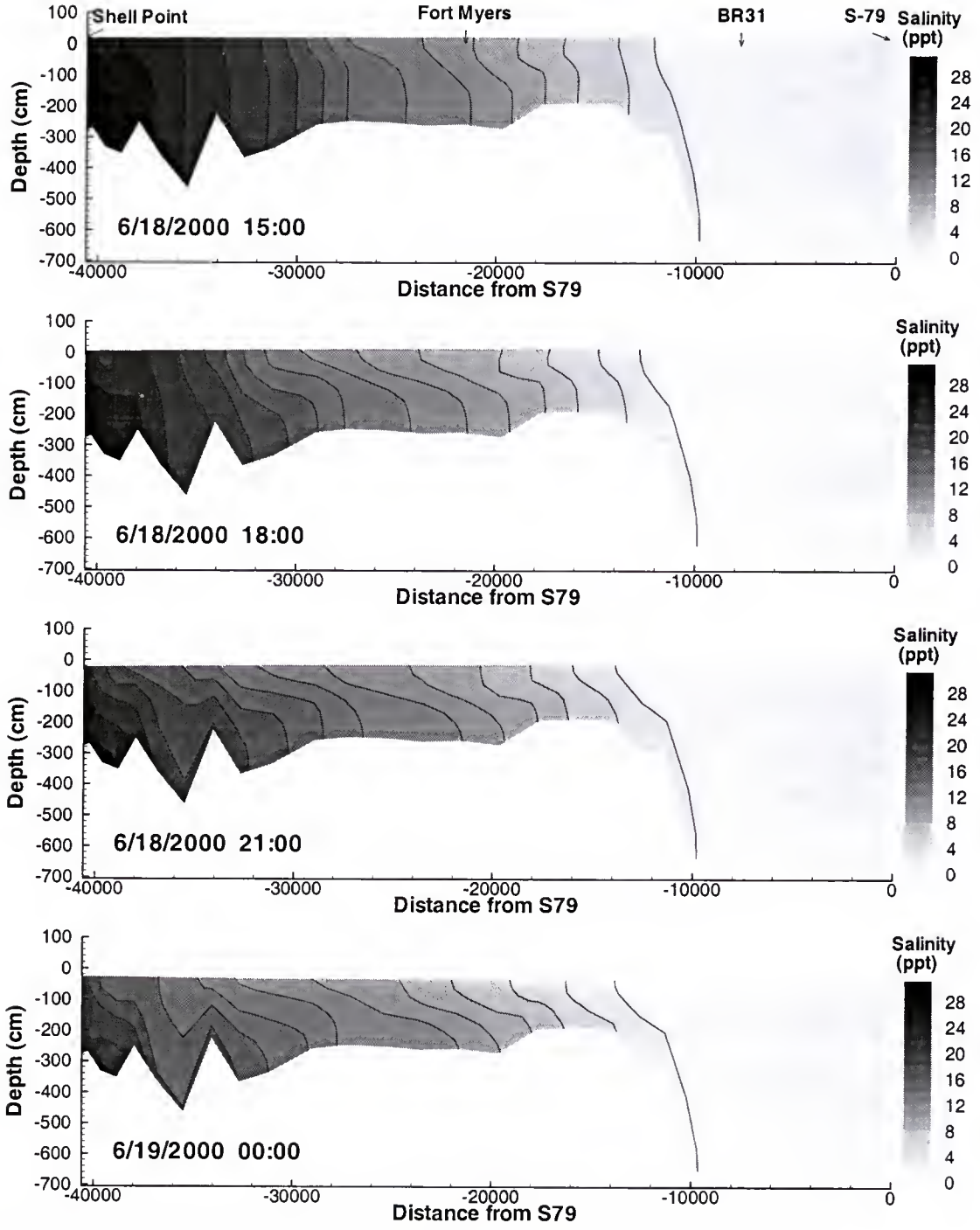

Figure 5.39 The vertical-longitudinal salinity profiles along the axis of the Caloosahatchee River during dry season in 2000

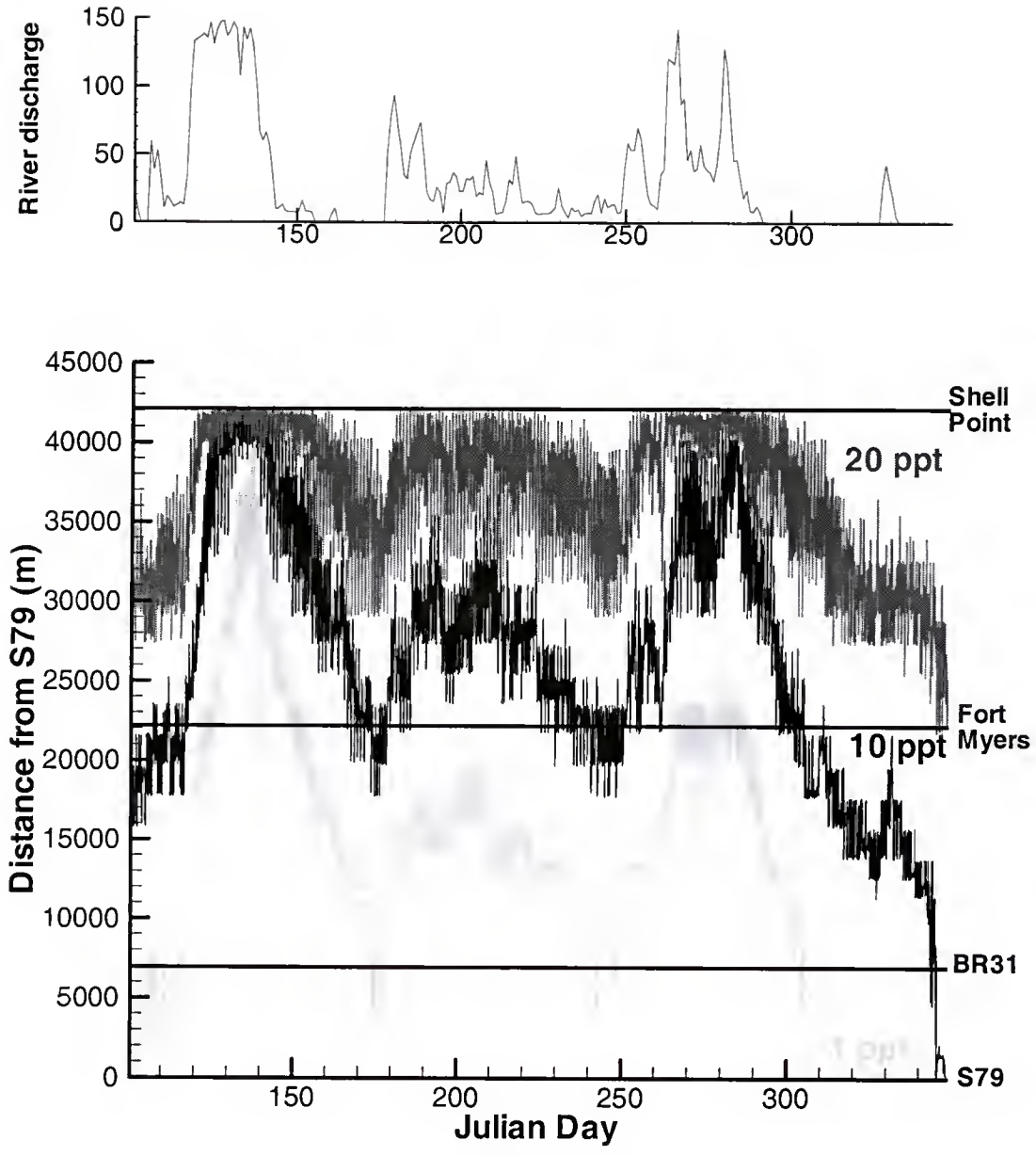

Figure 5.40 Time histories of river discharge at S79 and the locations of 1, 10, and 20 ppt surface salinity along the Caloosahatchee River during 2000 simulation period.

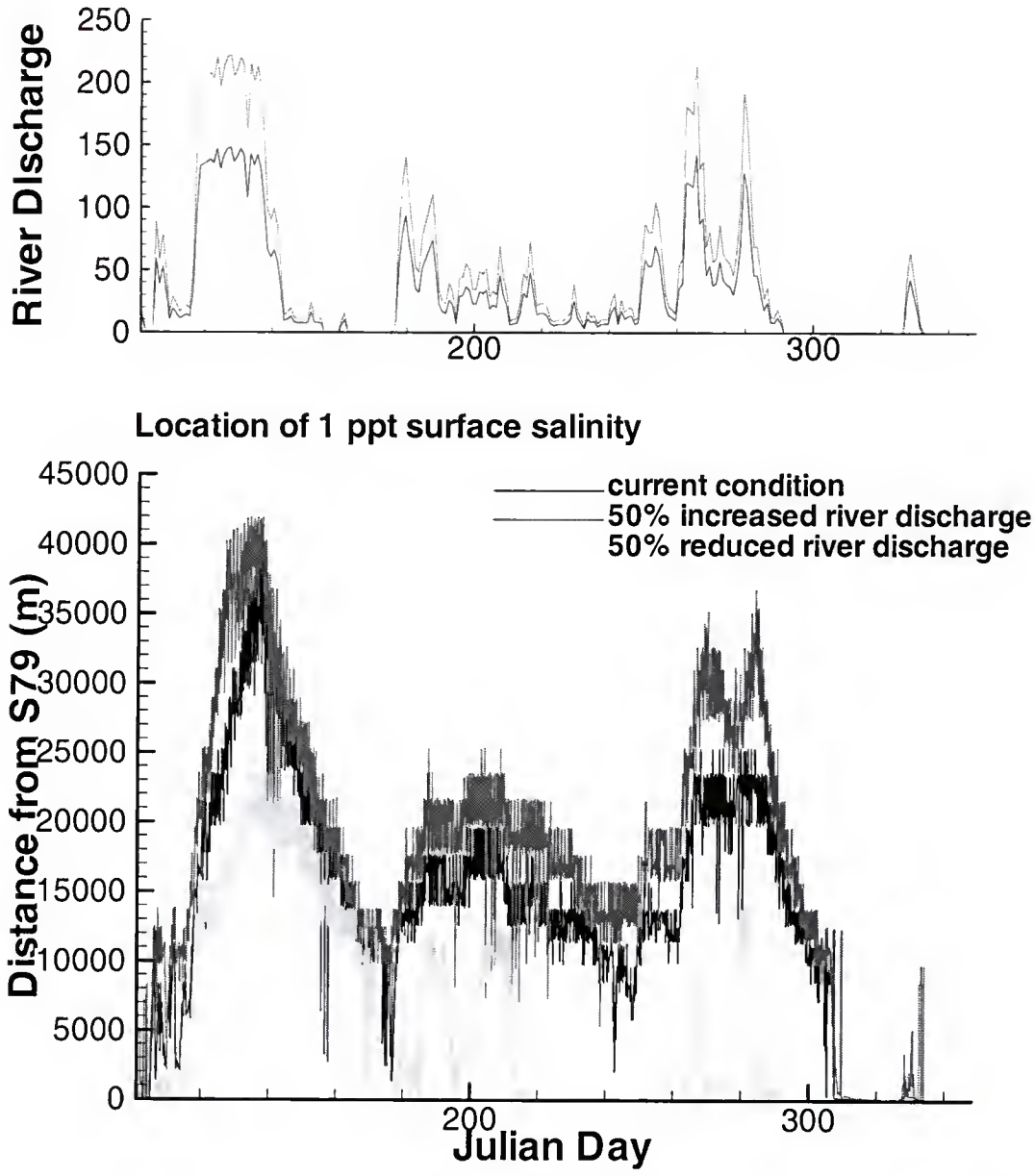

Figure 5.41 Time histories of river discharge at S79 and the 1 ppt salinity location along Caloosahatchee River.

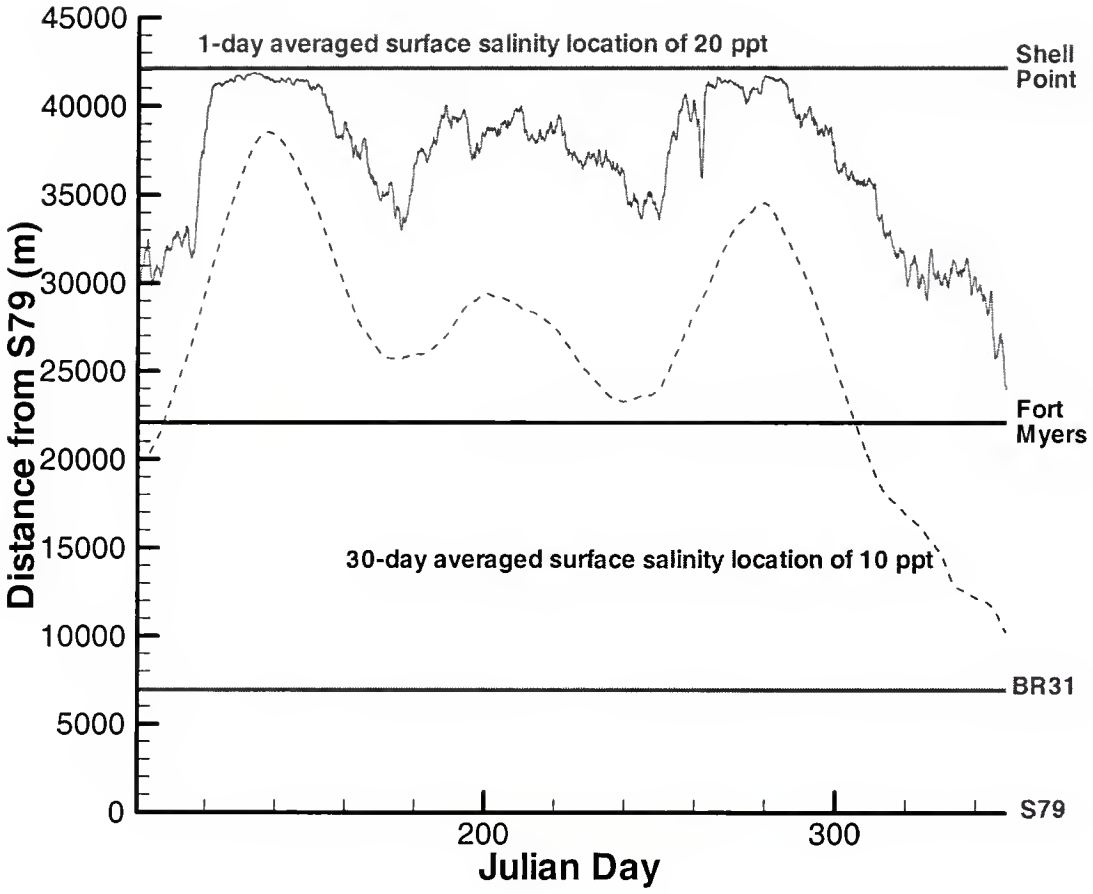

Figure 5.42 The 1-day averaged 20 ppt surface salinity location and 30-day averaged 10 ppt surface salinity location during the 2000 simulation period.

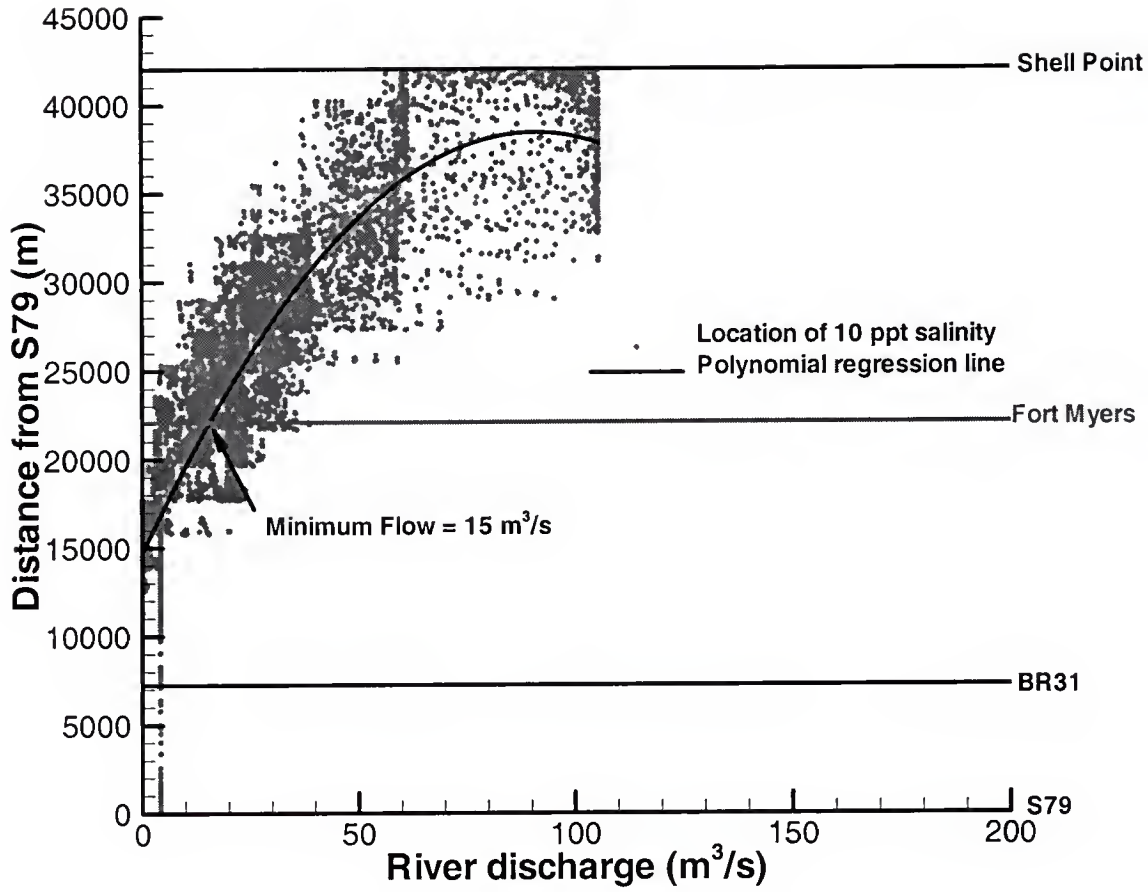

Figure 5.43 The locations of 10 ppt surface salinity due to river discharge rate at S-79 during 2000 baseline simulation.

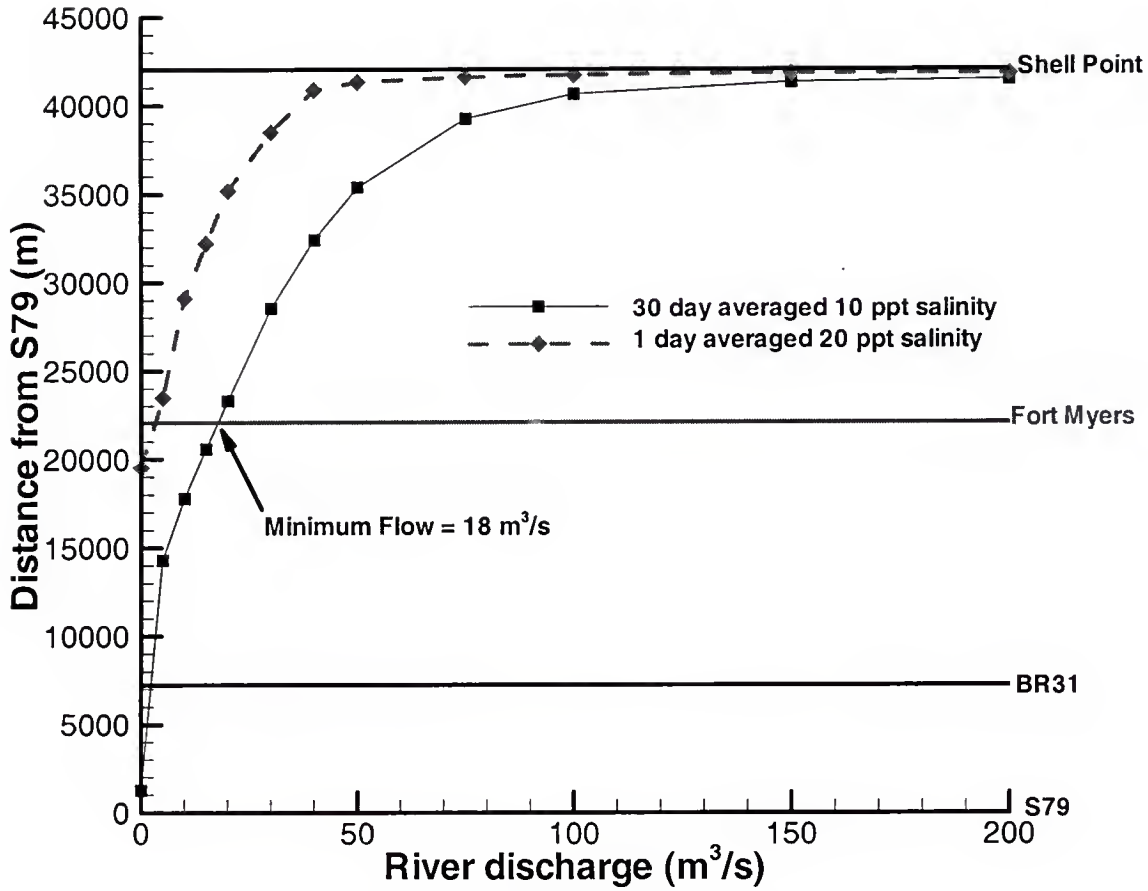

Figure 5.44 The relationship between locations of specific salinity value vs. river discharge at S-79.

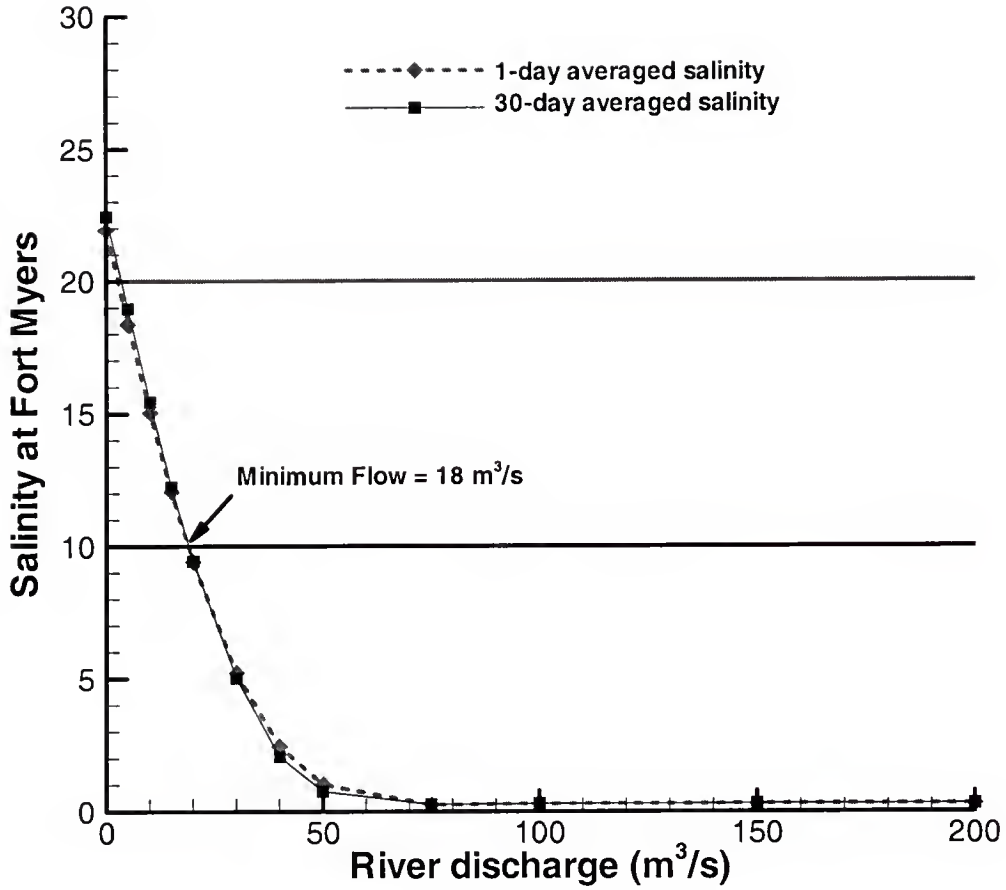

Figure 5.45 The relationship between salinity at Fort Myers station vs. river discharge at S-79

CHAPTER 6
APPLICATION OF WATER QUALITY MODEL

The water quality model described in Chapter 4 was applied to the Charlotte Harbor estuarine system. Model applications include the simulation of the three-dimensional circulation, sediment transport and water quality processes during summer 1996, the entire 2000. These simulations provide calibration and validation of the Charlotte Harbor water quality model using field data obtained by USGS, SWFWMD, and SFWMD. In addition, model simulation provide assessment of (1) the effects of hydrologic alteration of causeway and navigation channels, (2) the impact of river pollutant loading and its reduction on the water quality in the Charlotte Harbor estuarine system, and (3) the causes for hypoxia of bottom water in the upper Charlotte Harbor.

To reduce the computational time necessary to simulate annual response of the Charlotte Harbor estuarine system, the parallel CH3D model developed by Sheng et al. (2003) is used. The detail description of validation, CPU time, and speedup of the parallel CH3D code are given in Appendix G.

6.1 Forcing Mechanism and Boundary Condition of Circulation

The tidal forcing along the Gulf of Mexico boundary is prescribed by the water level data measured at Naples by NOS (http://www.co-ops.nos.noaa.gov/data_res.html). The surface wind boundary condition is produced by using the hourly wind magnitude and direction data collected at the National Data Buoy Center C-MAN stations at Venice and

USGS station at Naples and Fort Myers. The hourly wind magnitude and direction are converted into East/West(-x) and North/South (-y) wind velocity components and then interpolated onto the entire computational grid.

Daily river discharges for Peace River, Shell Creek, Myakka River, Caloosahatchee River (S-79 spillway, Cape Coral and Whiskey Creek) and Estero Bay (Mullock & Hendry Creek, Estero River, Spring Creek, and Imperial River) were measured by the USGS daily (Table 5.1). Figures 6.1 to 6.3 show the water level at the tidal boundary, river flows at the river boundary, wind speed and direction at the surface boundary, and air temperature for the air-sea heat flux in 1996. The forcing mechanism and boundary condition for circulation of 2000 simulation were explained at Chapter 5.

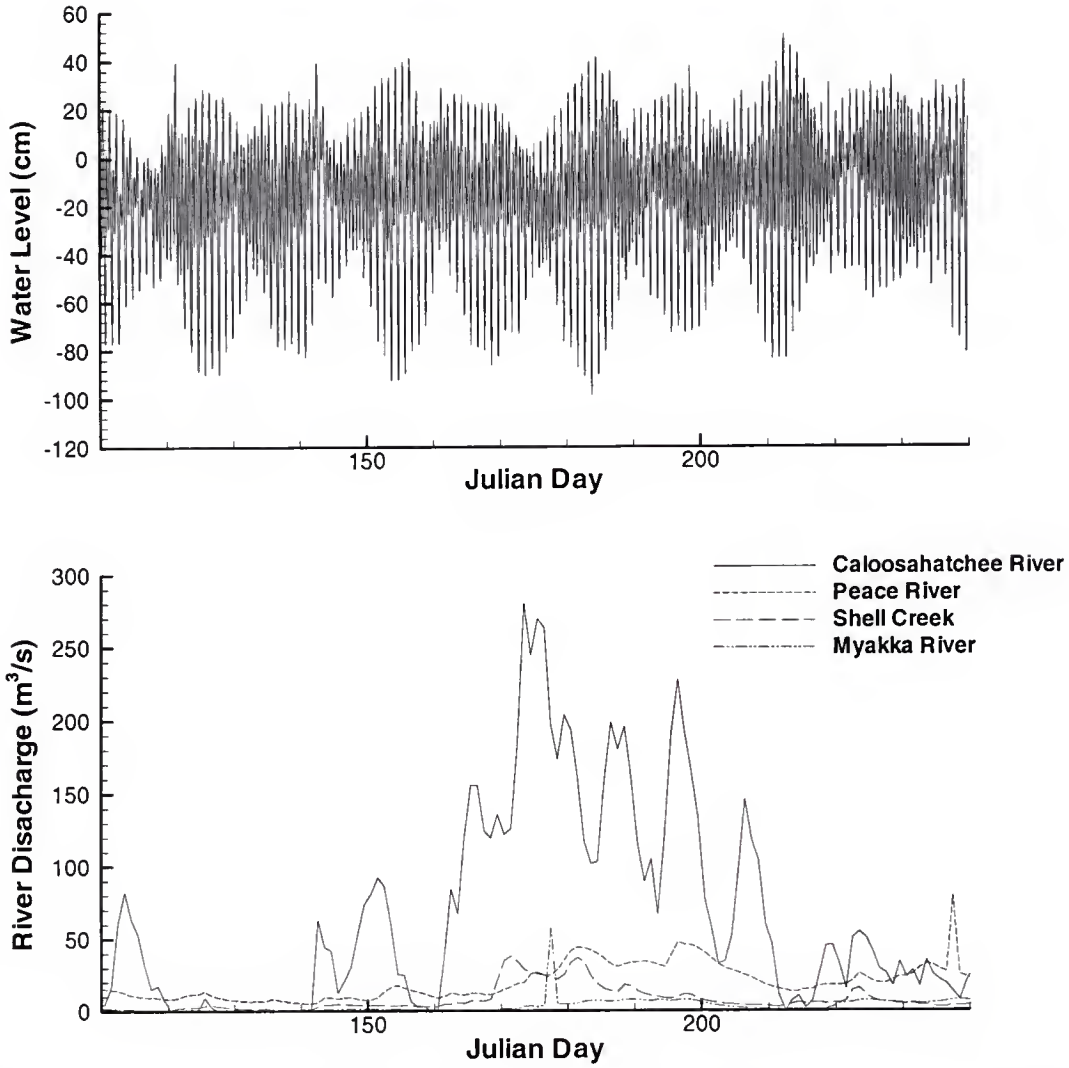

Figure 6.1 Tidal forcing and river discharges for 1996 simulations of Charlotte Harbor.

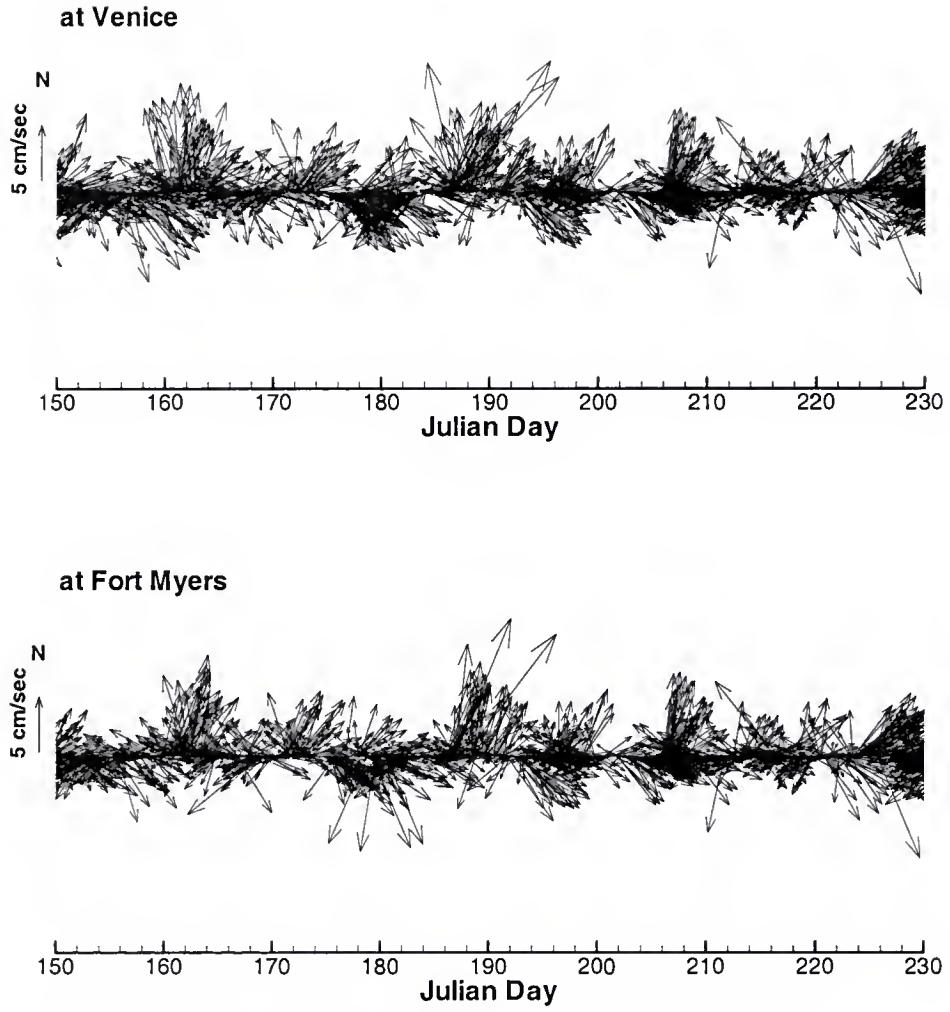

Figure 6.2 Wind velocity for 1996 simulations of Charlotte Harbor.

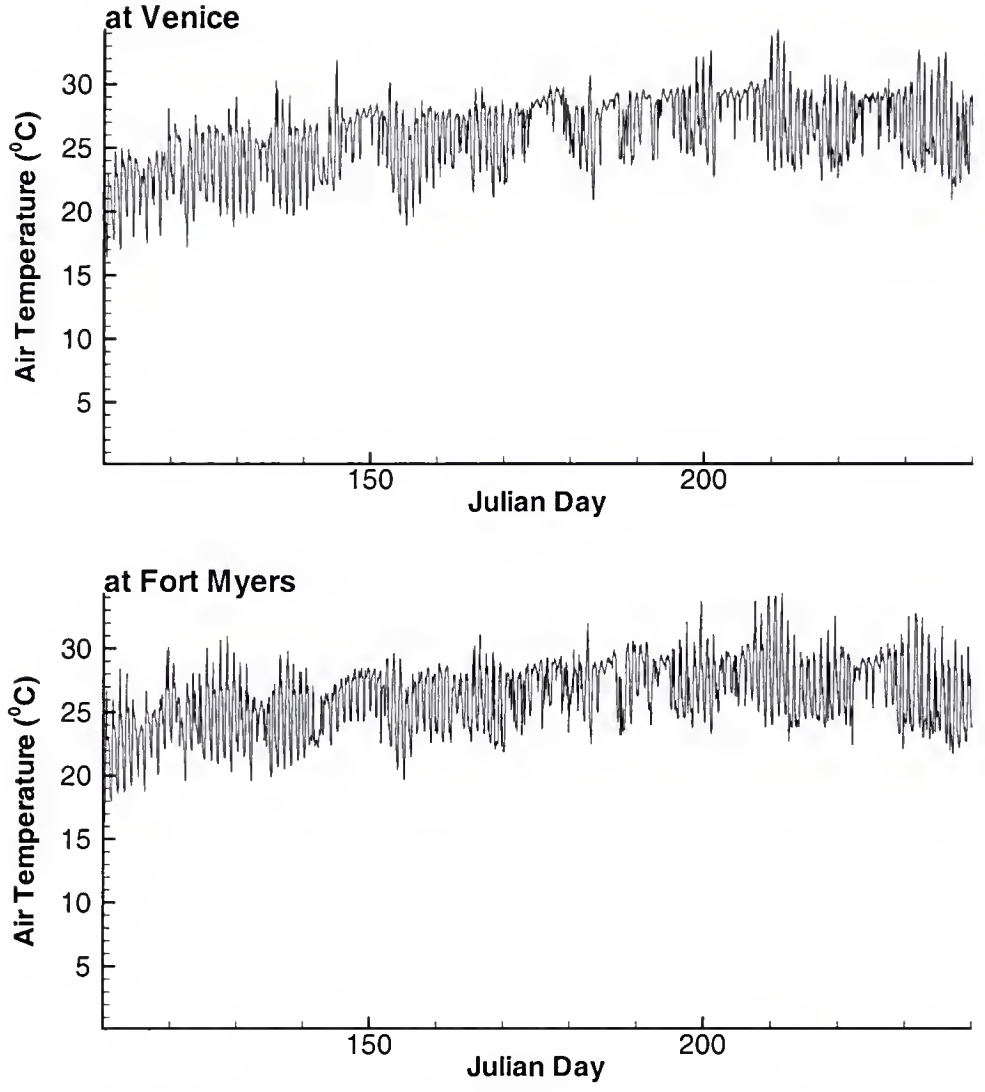

Figure 6.3 Air temperature for 1996 simulations of Charlotte Harbor.

6.2 Initial and Boundary Condition for the Water Quality Model

For 1996 simulations, there were 21 stations sampled monthly for water quality data in 1996 by SWFWMD and SFWMD (Table 6.1). The locations of the measurement sites are shown in Figure 6.4. Most of the data were collected from May to July 1996. For Estero Bay, there were 14 sites sampled for total nitrogen, total phosphorous, pH, dissolved oxygen, temperature, turbidity and chlorophyll_a data in June 1996 by SFWMD. The initial water column concentrations of several water quality parameters are determined from the EPA data. The water quality data for May are used to produce the initial condition of 1996 simulations. The water quality data at each grid cell are calculated by interpolation of the data at the three closest data stations, with a weighting function inversely proportional to the distance from each of the three stations. Data collected at station CH001, CH029, and CH004 are used to provide river loading data of Myakka River, Peace River, and Horse Greek, respectively. There are three river boundary conditions at Caloosahatchee River, which are S-79 spillway, Cape Coral, and Whiskey Creek. For these three river boundary conditions, data at HB01, HB03, and HB04 were used. The water quality data at stations EB002, EB004 EB013 and EB012 are used for four river boundary conditions of Estero Bay.

For 2000 simulation, the initial water column concentrations of several water quality parameters were determined from SWFWMD and SFWMD data of January 2000. Figure 6.5 shows the locations of SWFWMD (CH-001 to CH-014) and SFWMD (CES01 to CES08) water quality monitoring stations (Table 6.1). Data collected at station CH001, CH029, CH004, CES01, CES05, and CES08 are used to provide river loading data of each river boundary.

Table 6.1 Locations of water quality measured stations

station	Latitude	Longitude	X UTM	Y UTM	(I,J) in Grid	Agency
CH-001	27 00 072	82 15 108	375674.130	2987267.910	(38,123)	SWFWMD
CH-002	26 57 216	82 12 300	380063.200	2982147.510	(37,120)	SWFWMD
CH-02B	26 58 048	82 11 048	382419.400	2983448.440	(42,119)	SWFWMD
CH-029	27 00 588	81 59 030	402367.040	2988631.380	(71,117)	SWFWMD
CH-004	26 56 396	82 03 324	394887.010	2980722.130	(60,116)	SWFWMD
CH-005	26 55 558	82 06 156	390352.680	2979406.960	(53,116)	SWFWMD
CH-05B	26 57 114	82 06 330	389904.080	2981718.790	(54,118)	SWFWMD
CH-006	26 54 006	82 07 090	388859.690	2975881.310	(47,113)	SWFWMD
CH-007	26 52 396	82 04 072	393859.500	2973345.640	(57,111)	SWFWMD
CH-009	26 49 132	82 05 294	391542.120	2966995.710	(47,106)	SWFWMD
CH-09B	26 53 132	82 09 288	384983.960	2974439.100	(38,113)	SWFWMD
CH-011	26 44 120	82 10 000	383975.740	2957800.680	(29,97)	SWFWMD
CH-013	26 41 300	82 18 010	370636.040	2952944.680	(9,98)	SWFWMD
CH-014	26 39 310	82 19 210	368386.980	2949305.790	(7,95)	SWFWMD
HB-001	26 41 480	81 49 277	417982.560	2953104.130	(79,58)	SFWMD
HB-002	26 40 007	81 52 213	413179.170	2949843.840	(76,58)	SFWMD
HB-003	26 38 090	81 54 294	409616.420	2946422.590	(73,58)	SFWMD
HB-004	26 33 576	81 54 534	408897.610	2938704.790	(70,55)	SFWMD
HB-005	26 30 570	81 59 024	401965.780	2933186.980	(63,50)	SFWMD
HB-006	26 29 250	82 01 150	398261.910	2930385.140	(45,43)	SFWMD
HB-007	26 32 264	82 07 324	387873.180	2936041.360	(24,70)	SFWMD
CES01	26 43 199	81 41 233	431400.582	2955824.308	(91,56)	SFWMD
CES02	26 43 354	81 42 284	429607.466	2956326.423	(89,56)	SFWMD
CES03	26 43 001	81 45 382	424351.809	2955279.834	(84,56)	SFWMD
CES04	26 40 541	81 50 017	417059.745	2951448.633	(78,57)	SFWMD
CES05	26 38 118	81 53 193	411552.356	2946470.516	(74,56)	SFWMD
CES06	26 34 563	81 54 367	409380.629	2940485.917	(71,55)	SFWMD
CES07	26 31 488	81 57 562	403804.420	2934742.217	(65,54)	SFWMD
CES08	26 31 239	82 00 312	399508.606	2934006.048	(58,51)	SFWMD

Light and temperature are the main limiting factors for the phytoplankton growth rate. Temperature is calculated by solving the heat equation with the heat flux model as a surface boundary condition, which was explained in chapter 3 and 4. The input data for the temperature model include an air temperature and cloud cover rate. Continuous hourly air temperature data collected at the NOS data collection platforms (DCP) and stored in the CO-OPS databases are available for the Naples and Vince stations. Since there is no available data for cloud cover, a constant cloud cover of 0.2 is used for all simulations.

To calculate PAR (Photosynthetically Active Radiance) in the light attenuation model, the light intensity at the surface is used as the surface boundary condition. The light intensity data (Langleys/day) are converted from the global and diffuse horizontal solar irradiance data (W/m^2) which were processed at the National Renewable Energy Laboratory (NREL). Figure 6.6 shows the light intensity data used in the 1996 and 2000 water quality model simulations.

A total of 215 sediment grab samples and 28 shallow cores were collected from the Charlotte Harbor estuarine system during the period of December 27, 1964, to January 1, 1965 by Huang (1965). Based on the sediment size distribution, the entire study area is characterized into five sediment types (Table 6.2).

Table 6.2 Sediment types for Charlotte Harbor water quality simulations

Type	D_{50} Range (mm)	Category	Remark
very coarse	D_{50} >0.50	5	
coarse	0.25 > D_{50} > 0.50	4	
medium	0.125 > D_{50} > 0.25	3	
fine	0.0625 > D_{50} > 0.125	2	
silts or clay	0.0625 > D_{50}	1	

Sediments were predominantly sand, with low amounts of silt, clay, and organic

matter. Silt or clay deposits were only observed at the mouth of Peace River. This type of sediment can be considered fine or cohesive sediment. Fine sediments exist in upper Charlotte Harbor, the southern part of Pine Island Sound, and the northern part of San Carlos Bay due to weak wave actions there. Sediment nutrient analyses were performed by the FDEP Sediment Contaminant Survey with data from 33 sample stations from 1985 to 1989 (Schropp, 1998). These data include organic carbon, total nitrogen, and total phosphorous.

Based on water quality data, sediment data, bathymetry, and geometry, the Charlotte Harbor study area is divided into 15 segments as shown in Figure 6.7 for the water quality simulations.

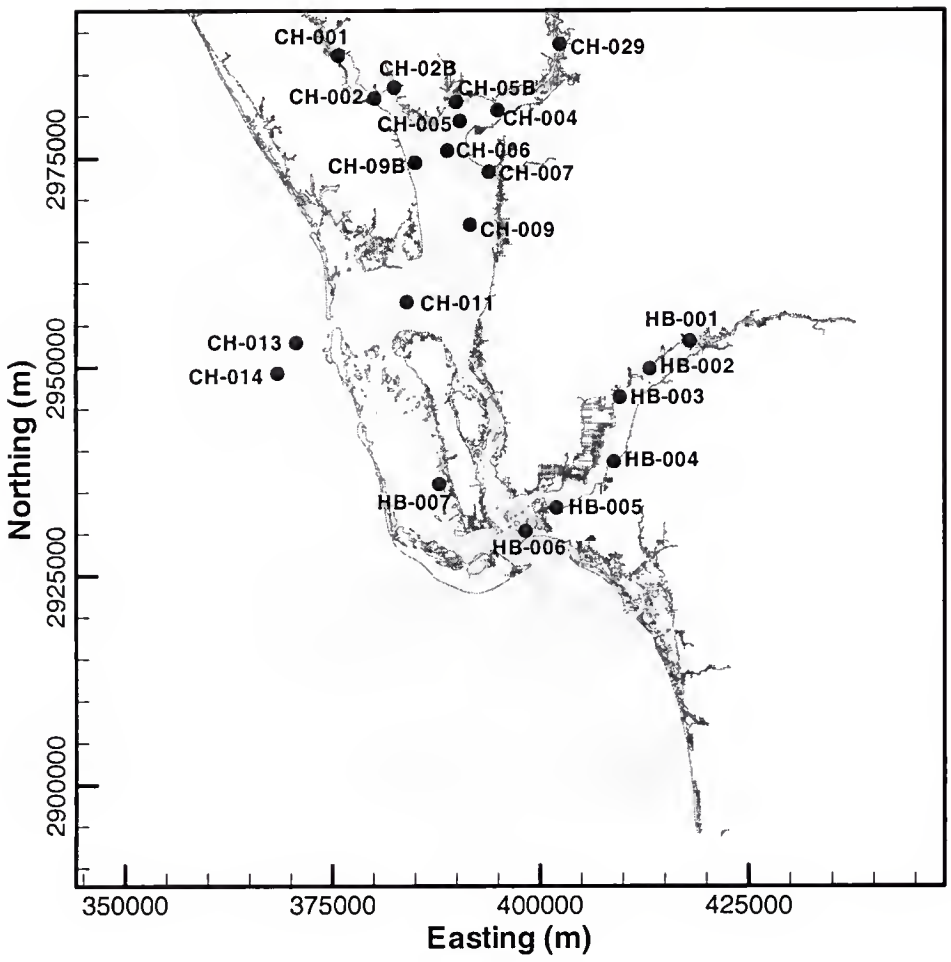

Figure 6.4 Locations of 1996 water quality measurement stations operated by EPA

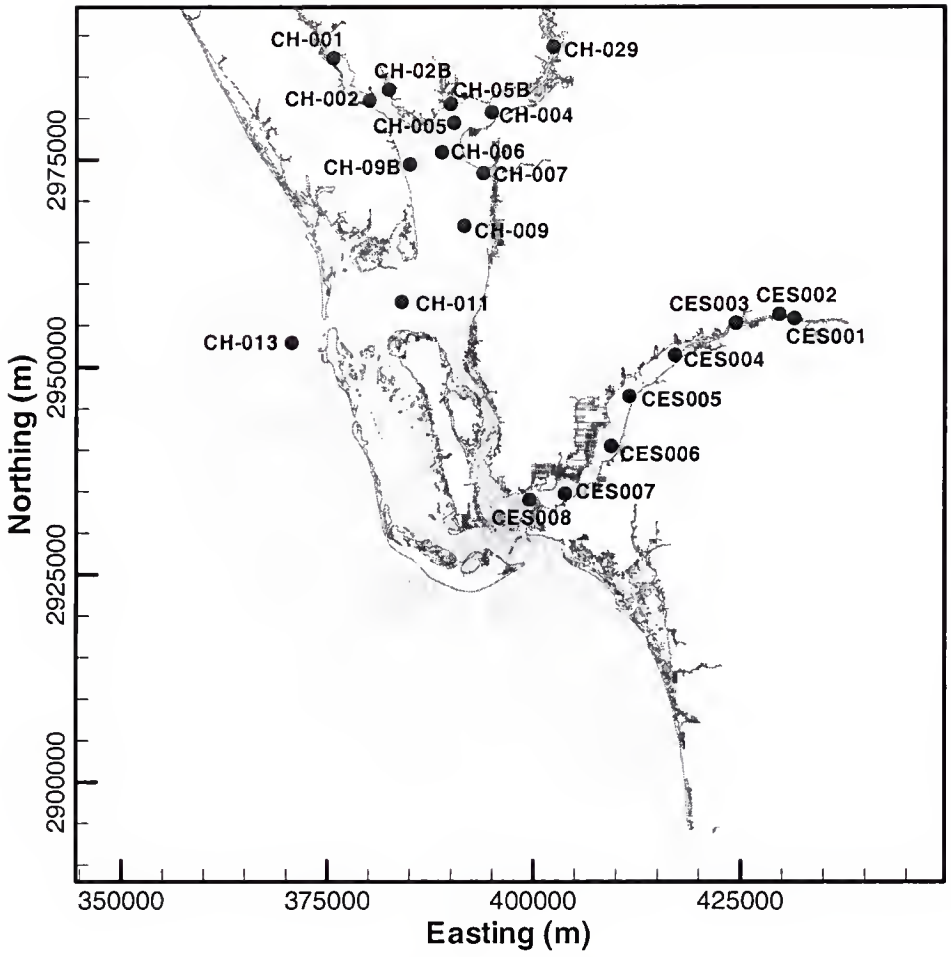

Figure 6.5 Locations of 2000 water quality measurement stations operated by SFWMD and SWFWMD

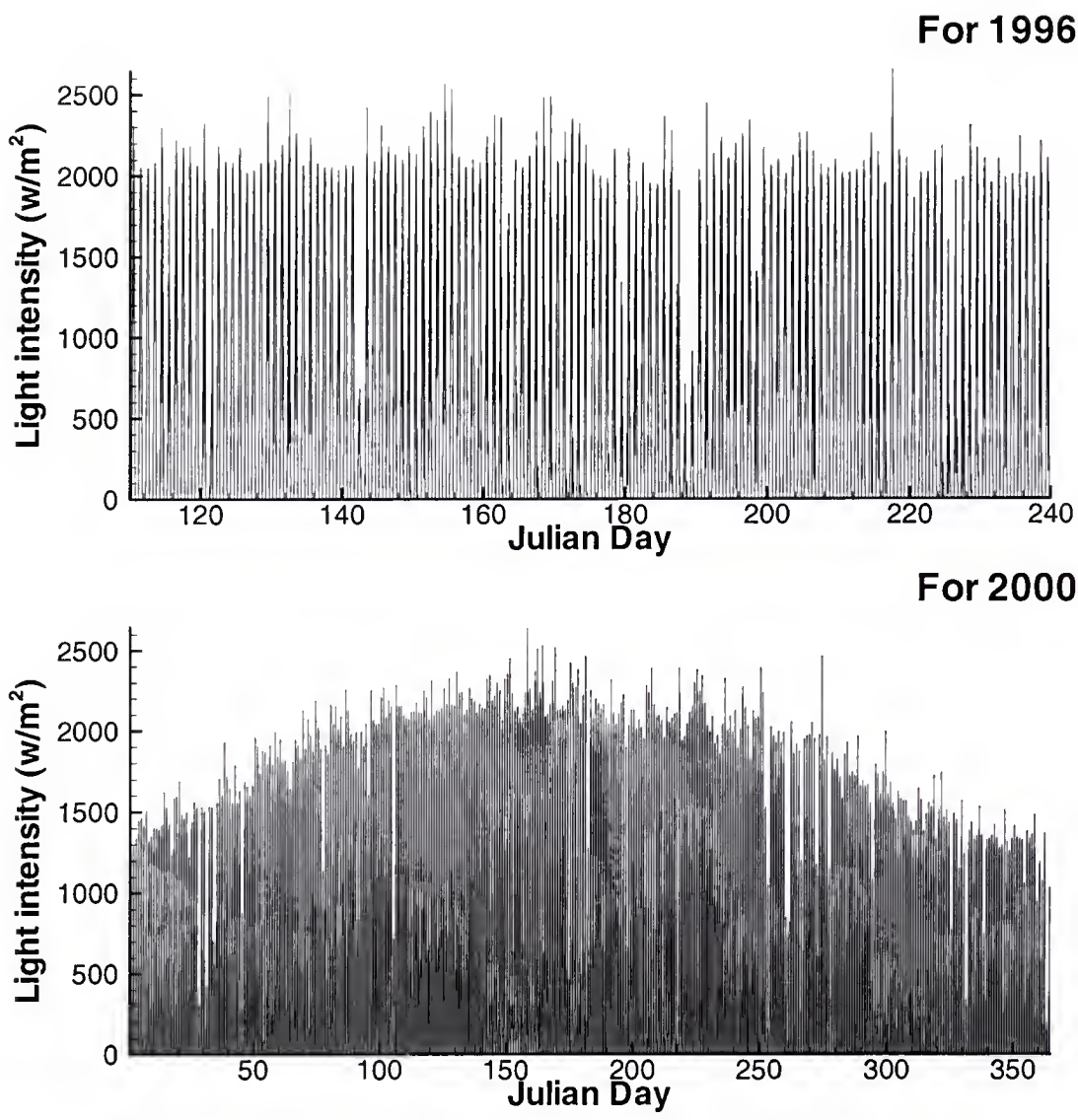

Figure 6.6 Light intensity at water surface for 1996 and 2000 simulations

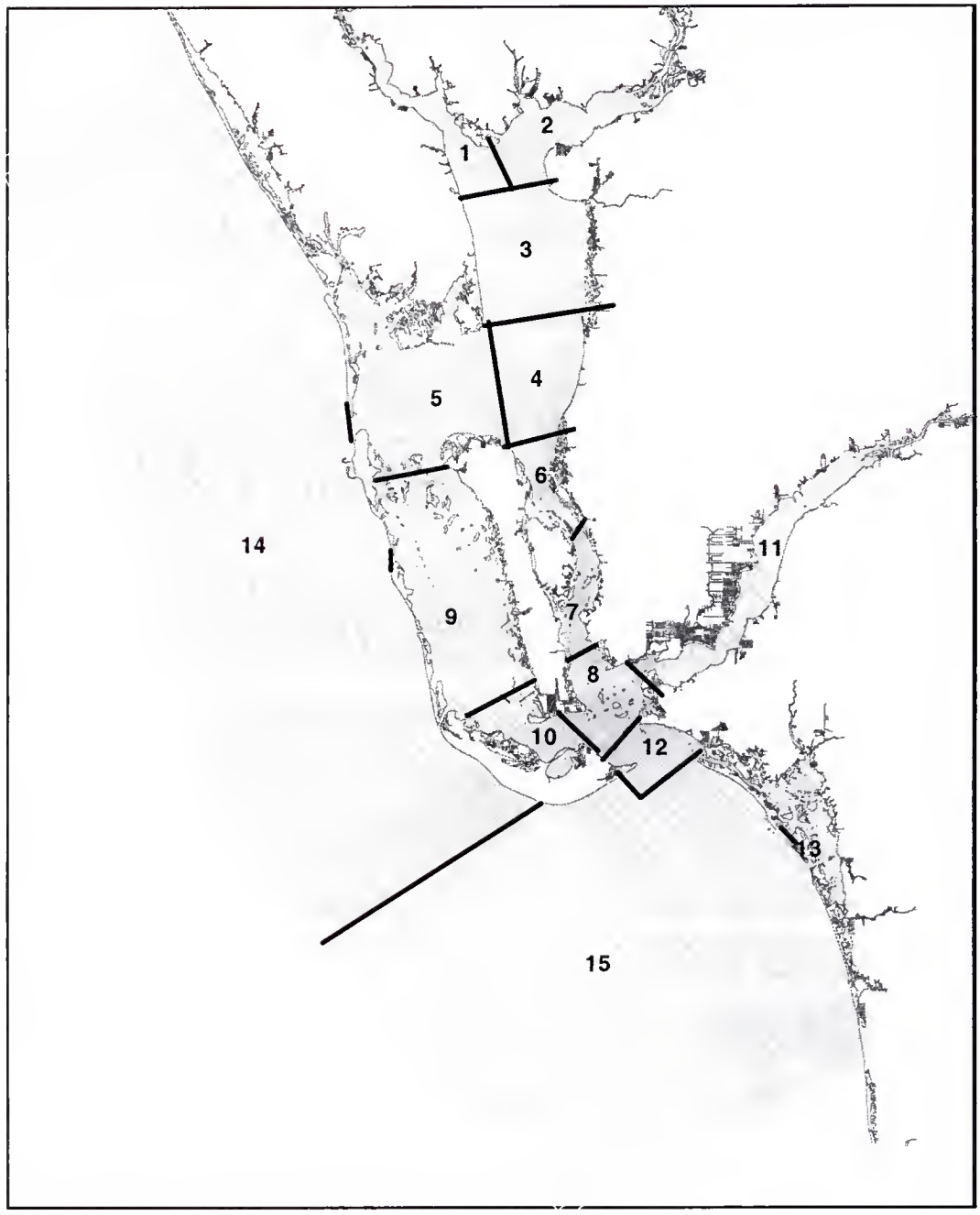

Figure 6.7 Segments for Charlotte Harbor estuarine system.

6.3 Simulations of Water Quality in 1996

CH3D-IMS are used to simulate the circulation, sediment transport, and water quality dynamics of the Charlotte Harbor estuarine system during May 23 to August 21, 1996. To create an appropriate initial condition throughout the computational domain, a spin-up simulation was executed until the flow and salinity field reached a dynamic steady state. The river discharge data for this area showed that the simulation period can be divided into a dry season which lasts from January 1 until June 8 and a wet season which spans from June 9 until July 22 (Sheng and Park, 2002). A 30-day spin-up simulation was performed from April 23 to May 23 (dry season) with all forcing mechanisms (tides, river discharges, wind) to allow water level, velocity and salinity field to reach dynamic steady-state throughout the computational domain. Using the surface elevation, velocity, and salinity at the end of the spin-up simulation as the initial condition, the Charlotte Harbor circulation and water quality models are then run from May 23 to August 21 with hydrodynamic, sediment and water quality input data.

6.3.1 Calibrations

The calibration of water quality model was conducted using the monthly water quality data obtained from the EPA STORET database. To compare the water quality results with measured data, fourteen stations were selected: CH002 (near Myakka), CH005 (near Peace), HB02, HB03 and HB06 (near Caloosahatchee), CH006, CH007, CH09B and CH009 in upper Charlotte Harbor, CH011 in lower Charlotte Harbor, HB007 in Pine Island Sound, HB006 in San Carlos Bay, and CH013 and CH014 in the open sea.

Several initial water quality parameters for the Charlotte Harbor simulation are obtained from "A Mechanistic Water Quality Model for the Tidal Peace and Myakka Rivers"

(Pribble et al, 1997) and Indian River Lagoon simulations (Sheng et al., 2001) shown in Chapter 4.

In order to test the model response to variation of these specific parameters, the sensitivity test was conducted for each water quality parameter by performing 90-day simulations and comparison with the baseline simulation. These simulations used the same initial and boundary conditions, and external forcing as those for the baseline simulation. Therefore, variations in nutrient concentrations between the sensitivity test and the baseline simulation can be directly related to variation of each parameter in a sensitivity test. Table 6.3 shows the parameters considered in the sensitivity analysis, baseline values in the simulations and the parameter variations of each sensitivity test. The tests were performed by varying each parameter within reasonable ranges according to literature survey. Table 6.4 shows the sensitivity analysis results which are presented in terms of percent RMS difference in concentration, normalized by concentrations of each water quality species in the baseline simulation. The SUM in Table 6.4 is linearly averaged value of RMS errors for each sensitivity test.

The results of the tests showed the nitrogen half saturation constant (HALN) for uptake as the most sensitive parameter in the water quality model, followed by the maximum algae growth rate (AGRM). These two parameters are related and their major impact should be detected in the phytoplankton biomass. However, the chlorophyll_a concentration is more sensitive to ammonification than maximum algae growth rate or nitrogen half saturation constant, which reveals the extension of nitrogen limitation to phytoplankton growth. Morever, the effect of reducing the maximum growth rate (AGRM0.5) is more pronounced in chlorophyll_a concentration than increasing this rate (AGRM2.0). Result of test

AGRM2.0 show that ammonia nitrogen (NH4) and nitrate+nitrite (NO3) is rapidly uptaked by phytoplankton and phytoplankton is increased due to increasing growth rate. If more ammonia nitrogen and nitrate+nitrite are available in the system, phytoplankton will increase more than that for this sensitivity test simulation. Related with algae growth rate and nitrogen half saturation constant, algae respiration rate and algae mortality are also important parameters. Therefore, the coefficients related with algae growth rate are most important factors for overall water quality processes.

The third most important parameter revealed by the sensitivity test is an ammonification rate. Soluble organic nitrogen (SON) is rapidly mineralized to ammonium nitrogen. Nitrate (NO3) level also increased due to nitrification. Due to high concentrations of inorganic nitrogen, which is a food for phytoplankton growth, chlorophyll_a concentration increased. On the opposite side, decreasing an ammonification rate promoted an increase in SON, and decrease in NH4, NO3, and chlorophyll_a.

The information obtained from the sensitivity tests enabled a more systematic and efficient calibration of model coefficients described in Table 4.9 of Chapter 4. According to the sensitivity test, the six most important parameters, which include maximum algae growth rate, nitrogen half saturation constant, ammonification rate, algae mortality, algae respiration rate, and sorption/desorption rate for SON and PON, are adjusted first for all water quality species as part of the systematic calibration procedure. The other parameters are adjusted as partially sensitive parameters for each specific water quality species. More than 100 simulations were made during calibrations which include all the sensitivity analyses. During these simulations, kinetic coefficients were adjusted within accepted tolerances, estimated loads were reviewed and adjusted, and new processes were added or

modified in water quality model, if necessary. Listed in Table 6.5 are values for the calibration parameters described in Chapter 4 and Table 4.3.

Table 6.3 Water quality parameters, baseline values, and range used in the sensitivity analysis

Test Run	Parameter	Literature Range	Baseline Parameter	Test run parameter =Baseline parameter ***multiplier**
AGRM2.0 AGRM0.5	Maximum algae growth rate	0.2 - 8	2.0 - 2.2	2.0 0.5
HALN10.0 HALN0.5	Nitrogen half saturation rate	1.5 - 400	25	10.0 0.5
HALP10.0 HALP0.5	Phosphorous half saturation rate	1.0 - 105	2	10.0 0.5
KAEX2.0 KAEX0.5	Algae respiration rate	0.02 - 0.24	0.06	2.0 0.5
KAS2.0 KAS0.5	Algae mortality	0.01 - 0.22	0.07	2.0 0.5
WAS10.0 WAS0.1	Algae settling velocity	0.0 - 300	10	10.0 0.1
HALA2.0 HALA0.5	Algae half saturation rate	200 - 2000	200	2.0 0.5
SONM2.0 SONM0.2	Ammonification rate	0.001 - 1.0	0.015	2.0 0.2
NITR2.0 NITR0.5	Nitrification Rate	0.004 - 0.11	0.08	2.0 0.5
DRON2.0 DRON0.5	Sorption/desorption rate of SON/PON	0.02 - 0.08	0.03	2.0 0.5
DRAN2.0 DRAN0.5	Sorption/desorption rate of PIN/NH4	0.02 - 0.08	0.03	2.0 0.5
SOPM2.0 SOPM0.2	Mineralization rate	0.001 - 0.6	0.02	2.0 0.2
DROP2.0 DROP0.5	Sorption/desorption rate of SOP/POP	-	0.02	2.0 0.5
DRIP2.0 DRIP0.5	Sorption/desorption rate of SRP/PIP	-	0.02	2.0 0.5
SODM2.0	Sediment oxygen demand	0 - 10.7	0.5 - 2.0	2.0
AKD2.0 AKD0.5	Oxidation rate	0.02 - 0.6	0.05	2.0 0.5

Table 6.4 Sensitivity analysis results in RMS difference w.r.t. baseline for 1996 water quality calibration simulations

	ChlA	DO	NH4	NOX	TKN	PO4	PHOS	TOC	SUM
BASE	0.00	0.00	0.00	0.00	0.00	0.00	0.00	0.00	0.00
AGRM0.5	17.63	4.29	55.20	171.6	3.31	25.53	8.47	9.51	**36.9**
AGRM2.0	5.68	2.54	12.68	12.72	0.97	5.00	1.91	1.81	5.42
HALN0.5	2.03	0.73	6.23	5.92	0.47	1.99	0.78	0.89	2.38
HALN10.0	18.56	4.26	65.73	204.0	3.71	37.54	10.61	10.99	**44.4**
HALP0.5	0.31	0.07	0.35	0.67	0.03	0.56	0.10	0.11	0.28
HALP10.0	4.02	0.77	6.07	13.27	0.45	12.03	1.89	1.76	5.03
KAEX0.5	2.13	0.92	7.17	5.24	0.54	2.58	0.87	0.92	2.55
KAEX2.0	5.43	2.08	18.59	17.27	1.35	6.87	2.33	2.55	**7.06**
KASS0.5	14.75	6.23	2.64	4.69	3.47	1.93	1.49	9.11	5.54
KASS2.0	19.58	5.59	7.56	13.49	3.99	2.47	2.20	9.29	**8.02**
WASS0.1	0.57	0.08	0.22	0.26	0.04	0.08	0.05	0.17	0.18
WASS010	5.51	0.81	2.43	2.94	0.47	0.84	0.50	1.67	1.90
HALA0.5	13.47	3.03	7.88	16.84	0.81	2.89	0.84	4.09	6.23
HALA2.0	13.13	3.11	2.76	4.54	1.00	1.20	0.28	3.62	3.70
SONM0.2	22.22	3.25	22.71	15.43	19.75	72.50	16.26	17.26	**23.6**
SONM2.0	12.47	3.66	32.01	42.19	13.49	19.84	7.96	8.96	17.5
NITR0.5	0.12	0.11	2.51	10.39	0.35	0.17	0.06	0.07	1.72
NITR2.0	0.20	0.17	4.09	17.36	0.55	0.29	0.11	0.12	2.86
DRON0.5	3.19	0.90	6.03	6.27	10.87	6.46	2.44	3.13	4.91
DRON2.0	4.47	1.60	11.52	15.81	17.05	9.31	3.58	4.42	**8.47**
DRAN0.5	1.46	0.40	1.74	1.65	0.71	2.94	1.12	1.31	1.42
DRAN2.0	2.32	0.68	2.96	3.01	1.12	4.58	1.74	1.99	2.30
SOPM0.2	2.24	0.29	3.42	7.15	0.29	10.14	2.96	1.07	3.44
SOPM2.0	1.68	0.21	2.68	4.21	0.23	9.15	2.68	0.91	2.72
DROP0.5	0.70	0.08	1.07	1.94	0.09	2.61	2.73	0.37	1.20
DROP2.0	0.55	0.07	0.83	1.61	0.07	2.13	2.21	0.29	0.97
DRIP0.5	1.99	0.27	3.16	6.42	0.27	8.43	3.32	0.94	3.10
DRIP2.0	2.34	0.31	3.94	5.74	0.34	14.75	5.73	1.28	4.30
SODM2.0	0.01	13.06	0.24	1.72	0.03	0.02	0.01	0.58	1.96
AKDD0.5	0.00	3.26	0.05	0.26	0.01	0.00	0.00	6.14	1.21
SUM	5.96	2.09	9.82	20.49	2.86	8.83	2.84	3.51	7.05

Table 6.5 The water quality model coefficients used for the Charlotte Harbor simulation

Coefficient	Description	Units	Literature Range	Charlotte Harbor
$(\theta_{AD})^{T-20}$	temperature coefficient for NH4 desorption	-	1.08	1.08
$(\theta_{a})^{T-20}$	temperature coefficient for algae growth	-	1.01~1.2	1.08
$(\theta_{AI})^{T-20}$	temperature coefficient for ammonium instability	-	1.08	1.08
$(\theta_{BOD})^{T-20}$	temperature coefficient for CBOD oxidation	-	1.02~1.15	1.08
$(\theta_{DN})^{T-20}$	temperature coefficient for denitrification	-	1.02~1.09	1.08
$(\theta_{NN})^{T-20}$	temperature coefficient for nitrification	-	1.02~1.08	1.04
$(\theta_{OD})^{T-20}$	temperature coefficient for SON desorption	-	1.08	1.045
$(\theta_{ONM})^{T-20}$	temperature coefficient for mineralization	-	1.02~1.09	1.08
$(\theta_{RESP})^{T-20}$	temperature coefficient for algae respiration	-	1.045	1.08
$(\theta_{z})^{T-20}$	temperature coefficient for zooplankton growth	-	1.01~1.2	1.04
$(\mu_a)_{max}$	algae maximum growth rate	1/day	0.2~8.	2.0~2.1
$(\mu_z)_{max}$	zooplankton maximum growth rate	1/day	0.15~0.5	0.16
$(NH_3)_{air}$	ammonia concentration in the air	μg /L	0.1	0.1
a_{chla}	algal carbon-chlorophyll-a ratio	mg C/mg Chla	10 ~ 112	100
a_{nc}	algal nitrogen-carbon ratio	mg N /mg C	0.05~0.43	0.16
a_{pc}	algal phosphorous-carbon ratio	mg N /mg C	0.005-0.03	0.025
a_{oc}	algal oxygen-carbon ratio	mg O_2 /mg C	2.67	2.667

Coefficient	Description	Units	Literature Range	Charlotte Harbor
d_{an}	desorption rate of adsorbed ammonium nitrogen	1/day	-	0.03
d_{on}	desorption rate of adsorbed organic nitrogen	1/day	-	0.03
d_{ip}	desorption rate of adsorbed inorganic phosphorous	1/day	-	0.02
d_{op}	desorption rate of adsorbed organic phosphorous	1/day	-	0.02
d_{mol}	molecular diffusion coefficient for dissolved species	cm^2/s	4.E-6~1.E-5	1.E-5
H_{bod}	half-saturation constant for CBOD oxidation	mg O_2	0.02~5.6	0.5
H_n	half-saturation constant for algae uptake nitrogen	g/L	1.5~400	25
H_p	half-saturation constant for algae uptake phosphorous	g/L	1.~105	2
H_{nit}	half-saturation constant for nitrification	mg O_2	0.1~2.0	2.0
h_v	Henry's constant	mg/L-atm	43.8	45
I_s	optimum light intensity for algal growth	$\mu E/m^2/s$	300-350	350
K_{ax}	excretion rate by algae	1/day	0.02~0.24	0.06
K_{as}	mortality rate of algae	1/day	0.2~0.22	0.07
K_{AI}	ammonia conversion rate constant	1/day	0.01-0.1	0.01~0.02
K_D	CBOD oxidation rate	1/day	0.02~0.6	0.05
K_{DN}	denitrification rate constant	1/day	0.02~1.0	0.09
K_{NN}	nitrification rate constant	1/day	0.004~0.11	0.08
K_{on}	rate of ammonification of SON	1/day	0.001~1.0	0.015

Coefficient	Description	Units	Literature Range	Charlotte Harbor
K_{op}	rate of mineralization of SOP	1/day	0.001~0.6	0.02
K_{Vol}	rate constant for nitrogen volatilization	1/day	3.5~9.0	7.
K_{zs}	mortality rate of zooplankton	1/day	0.001~0.36	0.02
K_{zx}	excretion rate of zooplankton	1/day	0.003~0.075	0.01
P_{an}	partition coefficient between SAN and PIN	l/μg	.5E-7~1.E-5	1E-4
P_{on}	partition coefficient between SON and PON	l/μg	1.0E-5	1E-5
P_{ip}	partition coefficient between SRP and PIP	l/μg	-	1E-5
P_{op}	partition coefficient of SOP and POP	l/μg	-	E-4
WS_{CBOD}	CBOD settling velocity	cm/s	-	0.01
WS_{algae}	algae settling velocity	cm/s	0.0~300.	10.

Figure 6.8 contains the scattering plots for the calibration period. The location of circles indicates the correlation between model predictions and observed data. A perfect match between model and observed data is indicated by the diagonal line on each graph. The circle above the line is over predicting the observation. Circles below the line indicate that the model is under predicting the observation. Shown with each plot are the root mean square (RMS) error and correlation coefficient (R^2) mentioned before. Values shown in parenthesis are RMS errors normalized with maximum measured data.

Overall, the model results show reasonable RMS errors for all constituents, although the R^2 values are not very high. The normalized RMS errors are less than 50%, except NH4, PO4, and TSS. Dissolved oxygen has the best agreement with measured data as shown by

the RMS error. Total suspended sediment concentration changed quickly with time on the order of minutes and hours, hence comparison with monthly data did not show reasonable RMS error. Dissolved ammonium nitrogen and soluble reactive phosphorous are strongly affected by sorption and desorption processes, while particulate species are affected by dynamic processes of settling and erosion of suspended sediment. The water quality model calculates CBOD instead of total organic carbon. The simulated CBOD was compared with measured total organic carbon because there is no measured CBOD data. Hence, the amount of CBOD was under predicted as shown in the scatter plot, due to the difference between CBOD and total organic carbon concentration in the system.

The correlation coefficient (R^2) measures the strength of linear association between simulated and measured data. Correlation coefficients for all species vary form 0.2 to 0.88.

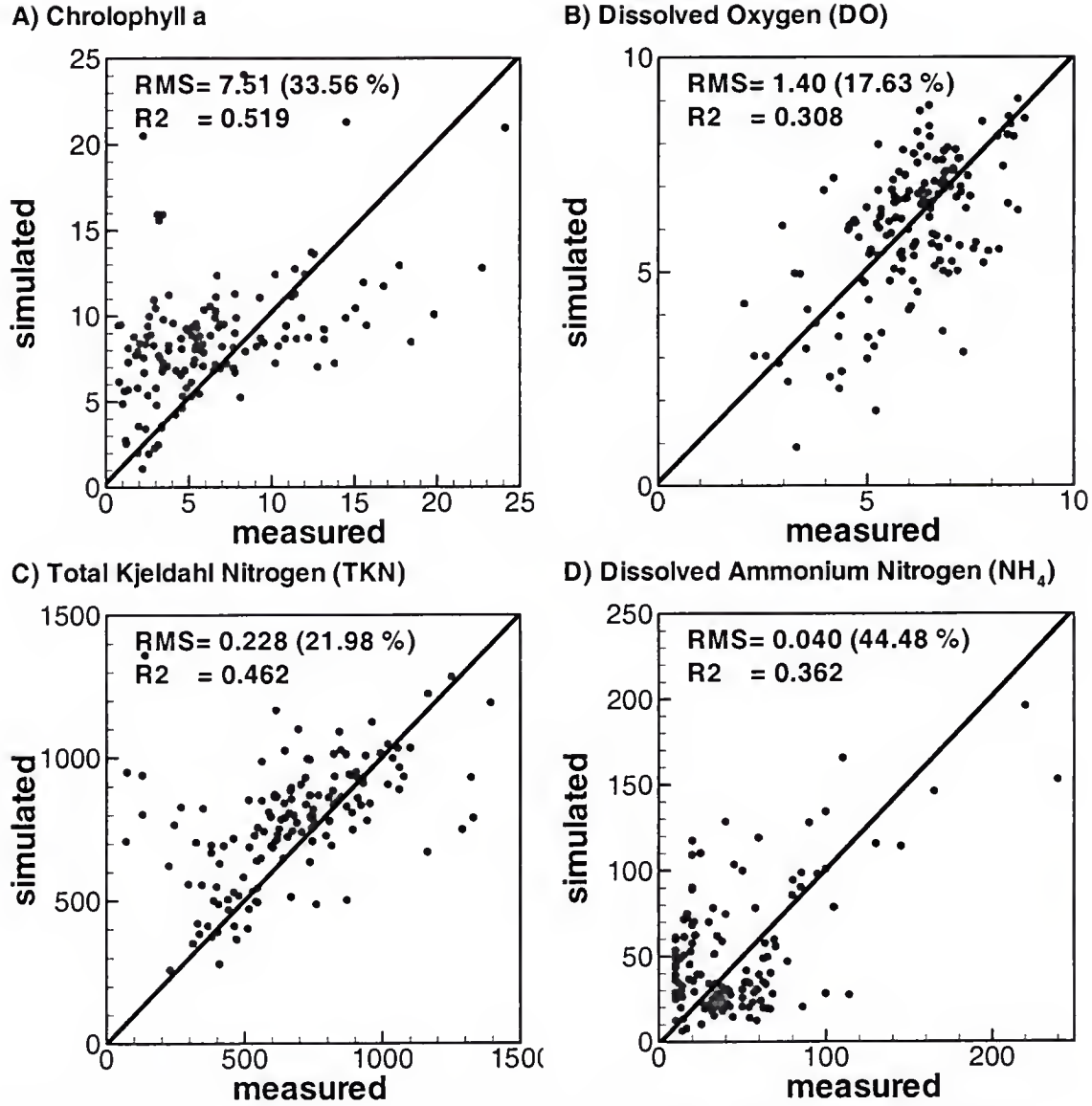

Figure 6.8 The scatter plots for water quality constituents during calibration period

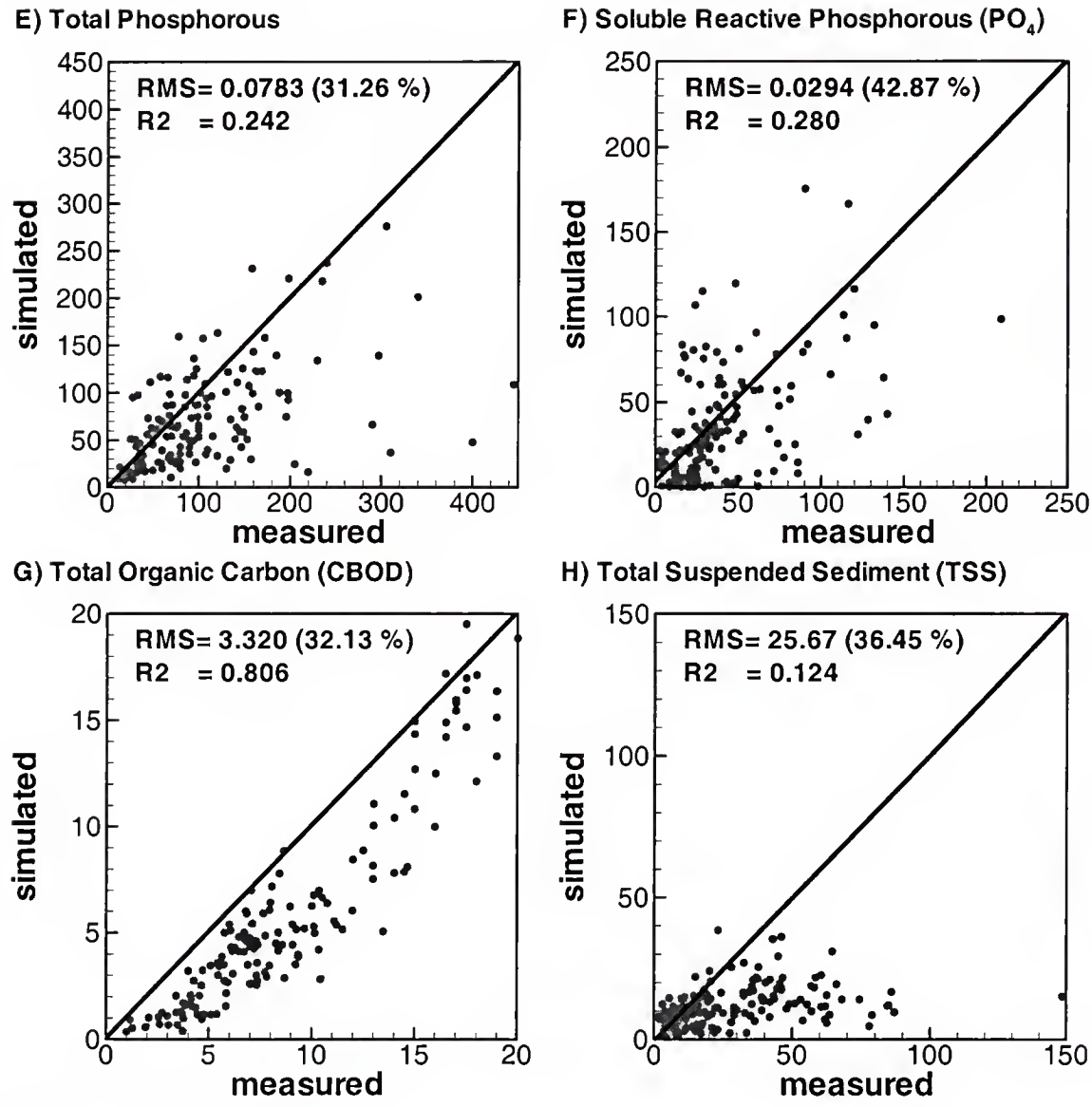

Figure 6.8 Continued

6.3.2 Results of 1996 Water Quality Simulation

The temporal variation of water quality species at each measured station is compared with measured data in Figures 6.9 to 6.20. The thicker solid lines represent the simulated water quality parameters near surface and dashed lines are those for bottom layer. The measured water quality parameters are represented with rectangular symbols which represent several vertical layers. The numbers of vertical layer of measured data are all different for each species and each station. The measured data were plotted at all available vertical measured location. The results show simulated and measured Chlorophyll_a, dissolved oxygen, TKN, dissolved ammonium nitrogen, total phosphorous, and soluble reactive phosphorous. During the simulation period, there was relatively little temporal variation in the water quality parameters. One major exception is at the CH-005 and CH-006 station which showed a significant vertical stratification of dissolved oxygen concentration.

The dissolved oxygen processes are important in any aquatic environment, because living organisms depend on oxygen in one form or another to maintain their metabolic processes. In Charlotte Harbor estuarine system, bottom water hypoxia has been reported periodically by Environmental Quality Laboratory (EQL) since the mid-1970 (Heyl, 1996). In the water quality model, dissolved oxygen is a function of photosynthesis and respiration by phytoplankton organisms, sediment oxygen demand, reaeration, nitrification and denitrification, decomposition of organic matter, tide and wind mixing, and river loading. As shown in Figures 6.9 to 6.20, concentrations of dissolved oxygen exhibit a temporal and vertical variation in response to variations in phytoplankton biomass and nitrogen species in the northern part of Charlotte Harbor, while relatively little variation in the southern part of Charlotte Harbor during the simulation period. Figure 6-21 shows the snapshots of the near

simulated bottom dissolved oxygen distribution in the study area on August 22, 1996 (at the end of 90-day simulation). The result corresponds well with the measured low (< 2mg/L) dissolved oxygen in the bottom water at the Peace River mouth. The rest of estuary does not show low dissolved oxygen less than 2 mg/l.

Due to wind and tidal mixing and the shallow water depth, the Charlotte Harbor estuarine system generally exhibits a vertically well mixed distribution of DO. In the upper Charlotte Harbor, where the lowest DO in the system is usually found, stratification may occur and a pycnocline may form if the condition is right - high river inflow from the Peace river and low wind mixing (Sheng and Park, 2002). With this strong stratification, surface water DO from reaeration would be blocked and high sediment oxygen demand in summer season could create the hypoxia observed in this area. Model results showed that strong stratification and low DO developed during the simulation period.

Phytoplankton dynamics are very important processes simulated in this study. It is closely related to the nutrient recycling through uptake during growth, and excretion/decay during respiration. The measured phytoplankton as algal mass per volume, was converted to phytoplankton carbon with an algae to carbon ratio of 100. The chlorophyll_a concentrations of Myakka and Peace River have maximum value of on July 23 (Julian Day 204) and those for the other stations have no trends during the simulation periods. The highest daily fluctuation of chlorophyll_a is occurred in HB006 due to strong tidal fluctuation and high chlorophyll_a concentration from the Caloosahatchee River.

In order to compare the nitrogen cycle simulations with the nitrogen species data provided by EPA, simulated soluble organic nitrogen, dissolved ammonium and ammonia nitrogen concentrations are combined and compared with the EPA total Kjeld nitrogen data.

The dissolved ammonium nitrogen data were also compared with measured data. For phosphorous species, total phosphorous concentration and soluble reactive phosphorous are used to compare with the EPA data. According to time series plot of each species in Figures 6.9 to 6.20, model results appear to capture the overall trend of the EPA data.

Figure 6-22 shows the snapshots of the near surface chlorophyll_a distribution in study area for August 22 (the end of 90-day simulation). Only the Peace River mouth area exhibits very high chlorophyll_a concentration of 3000μg (phytoplankton carbon). Higher phytoplankton concentrations are generally found near the river mouths and low concentrations are found in the Gulf of Mexico.

Figures 6.23 to 6.26 show the snapshots of the near surface dissolved ammonium nitrogen, soluble organic nitrogen, soluble reactive phosphorous, and soluble organic phosphorous distributions in the study area at 2 pm on August 21, 1996 (at the end of 90-day simulation). It is interesting to note that high dissolved ammonia concentrations but low dissolved organic nitrogen concentrations are found in the area between upper Charlotte Harbor and the Boca Grande Pass. High concentrations of particulate organic nitrogen and adsorbed ammonium are first resuspended by the strong currents in the Boca Grande Pass area, causing high dissolved ammonium concentration in the water column which are then transported towards the upper Charlotte Harbor area. High concentrations of phosphorous species are found in the upper Charlotte Harbor because Peace River drains the Hawthorn phosphatic formations.

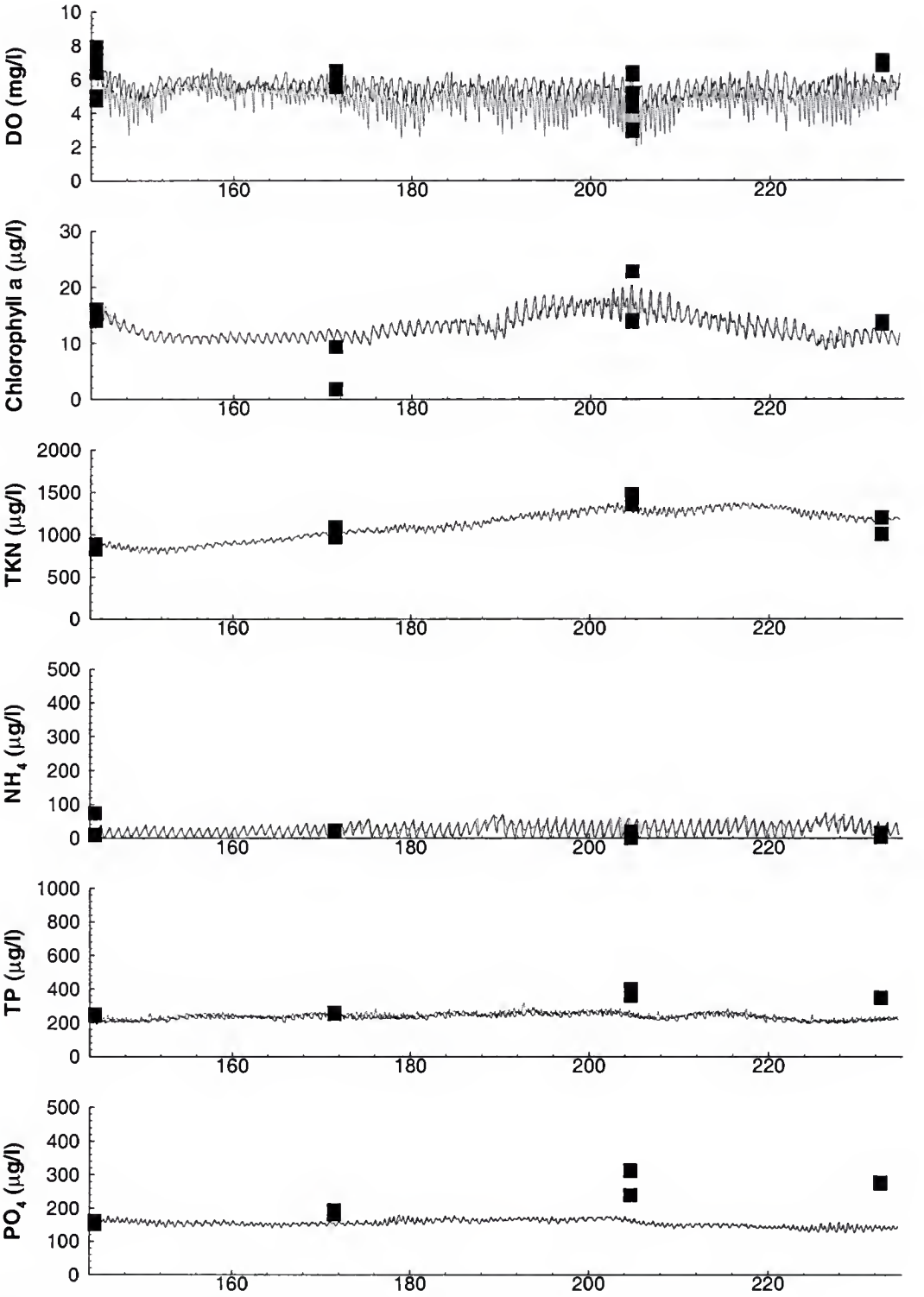

Figure 6.9 Temporal water quality variations at CH002 station in 1996.

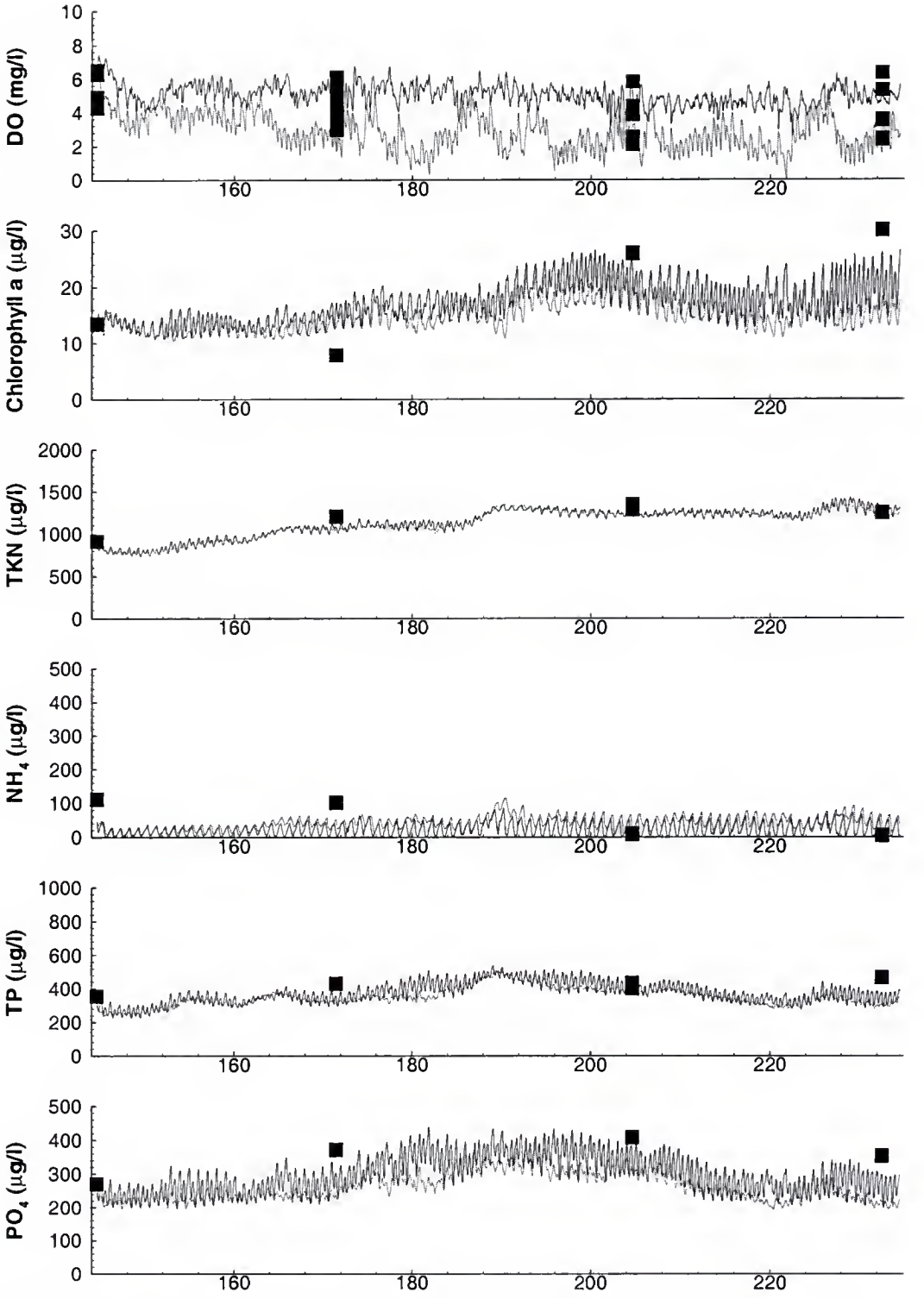

Figure 6.10 Temporal water quality variations at CH004 station in 1996.

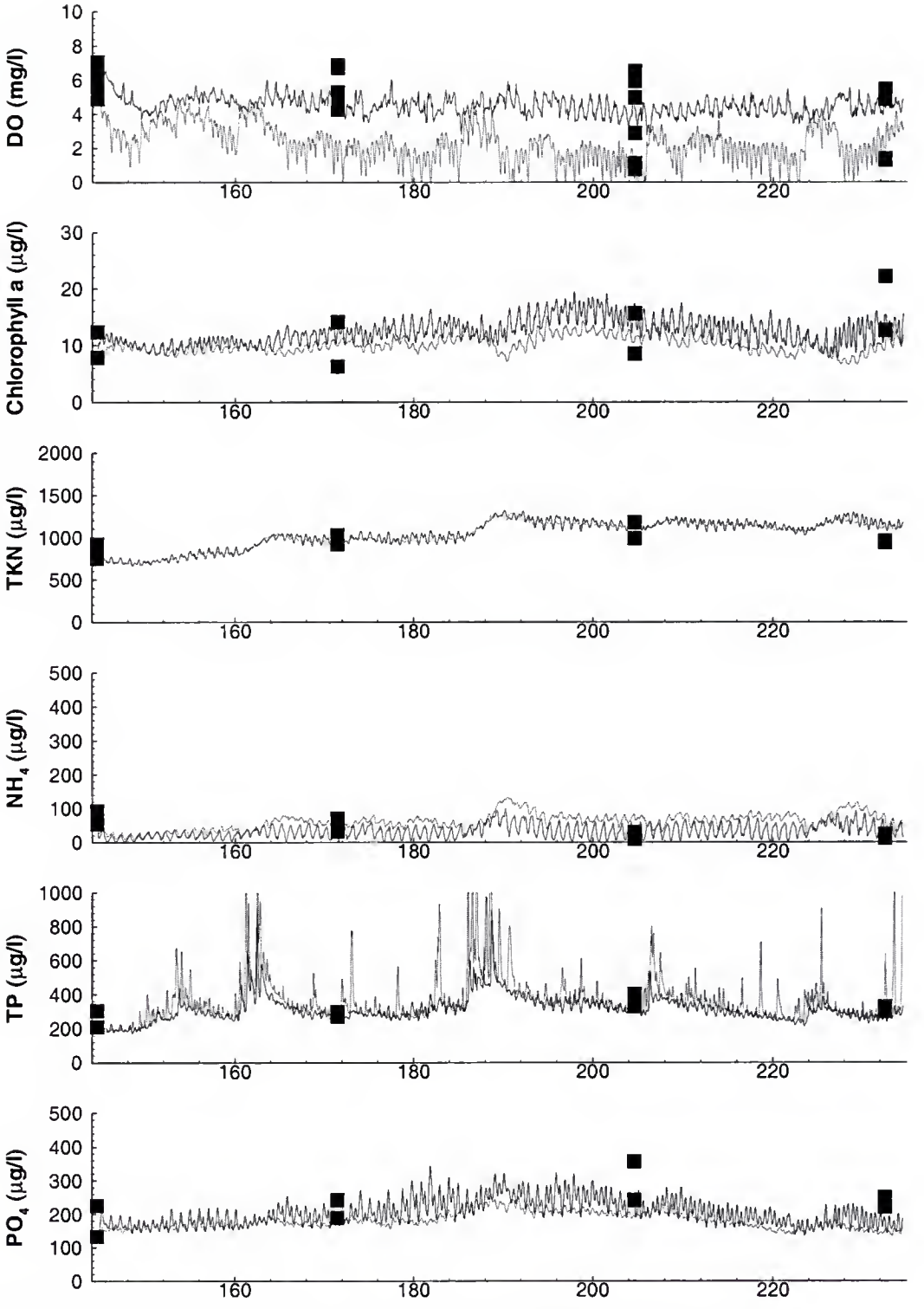

Figure 6.11 Temporal water quality variations at CH005 station in 1996.

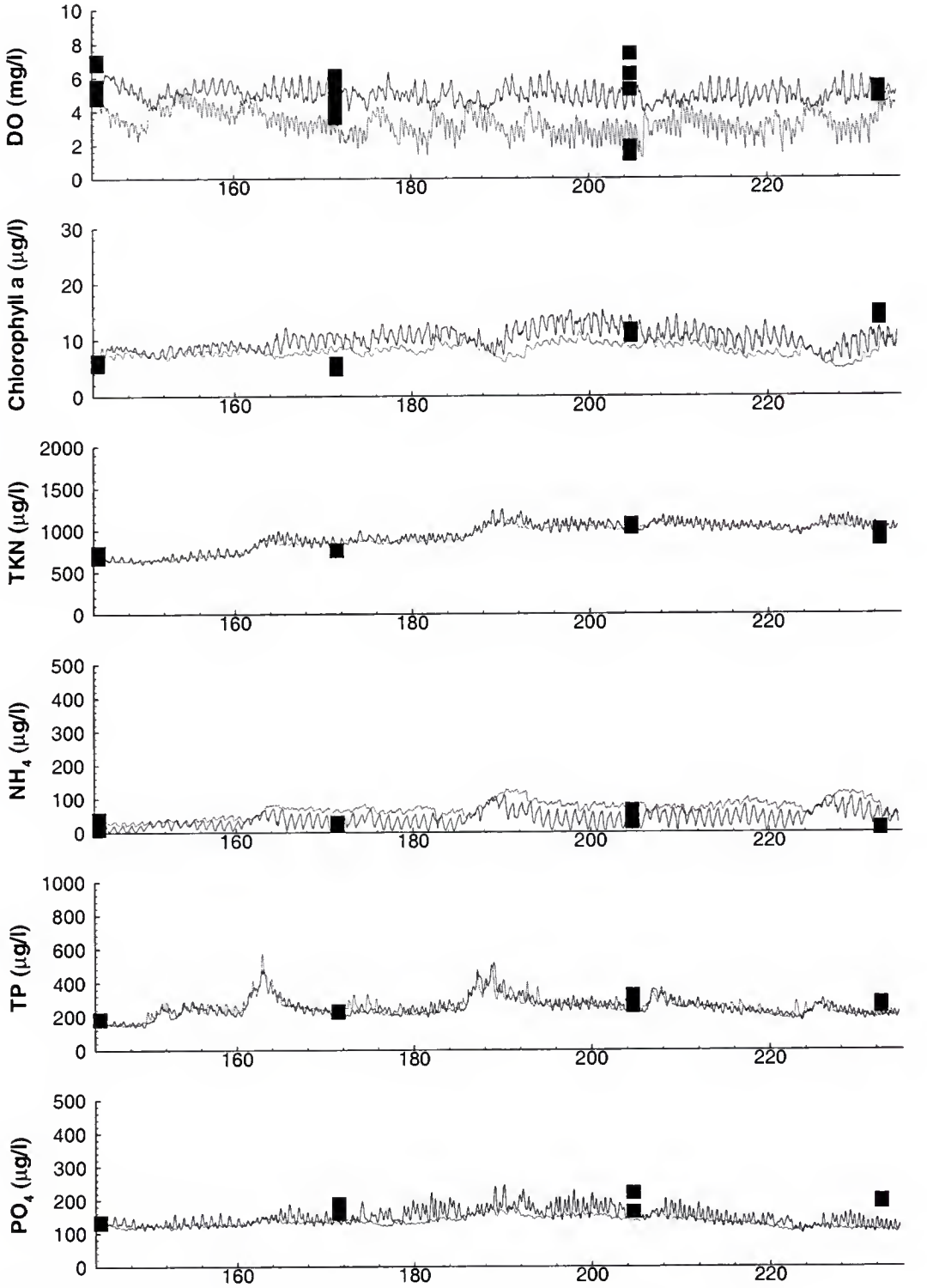

Figure 6.12 Temporal water quality variations at CH006 station in 1996.

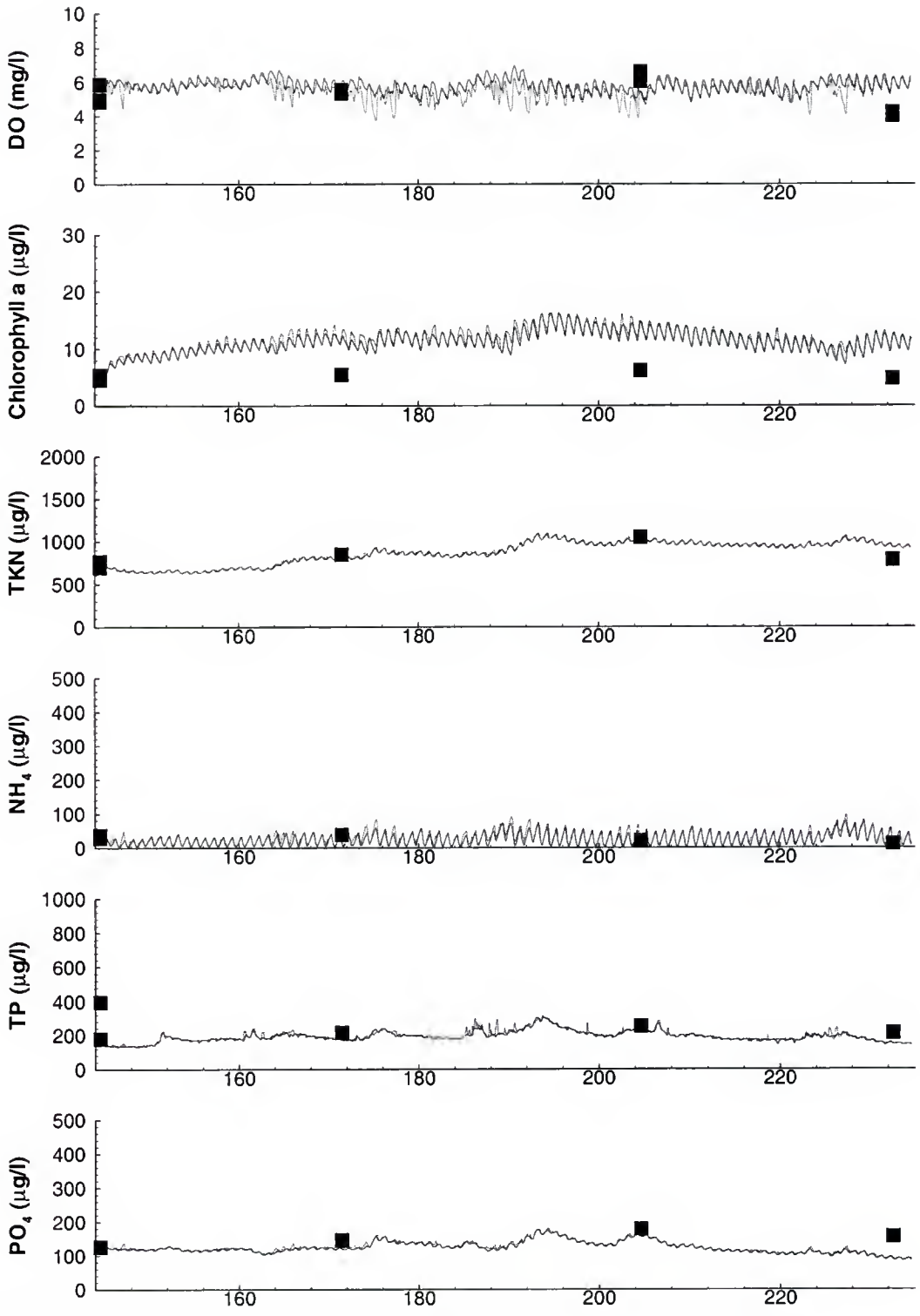

Figure 6.13 Temporal water quality variations at CH007 station in 1996.

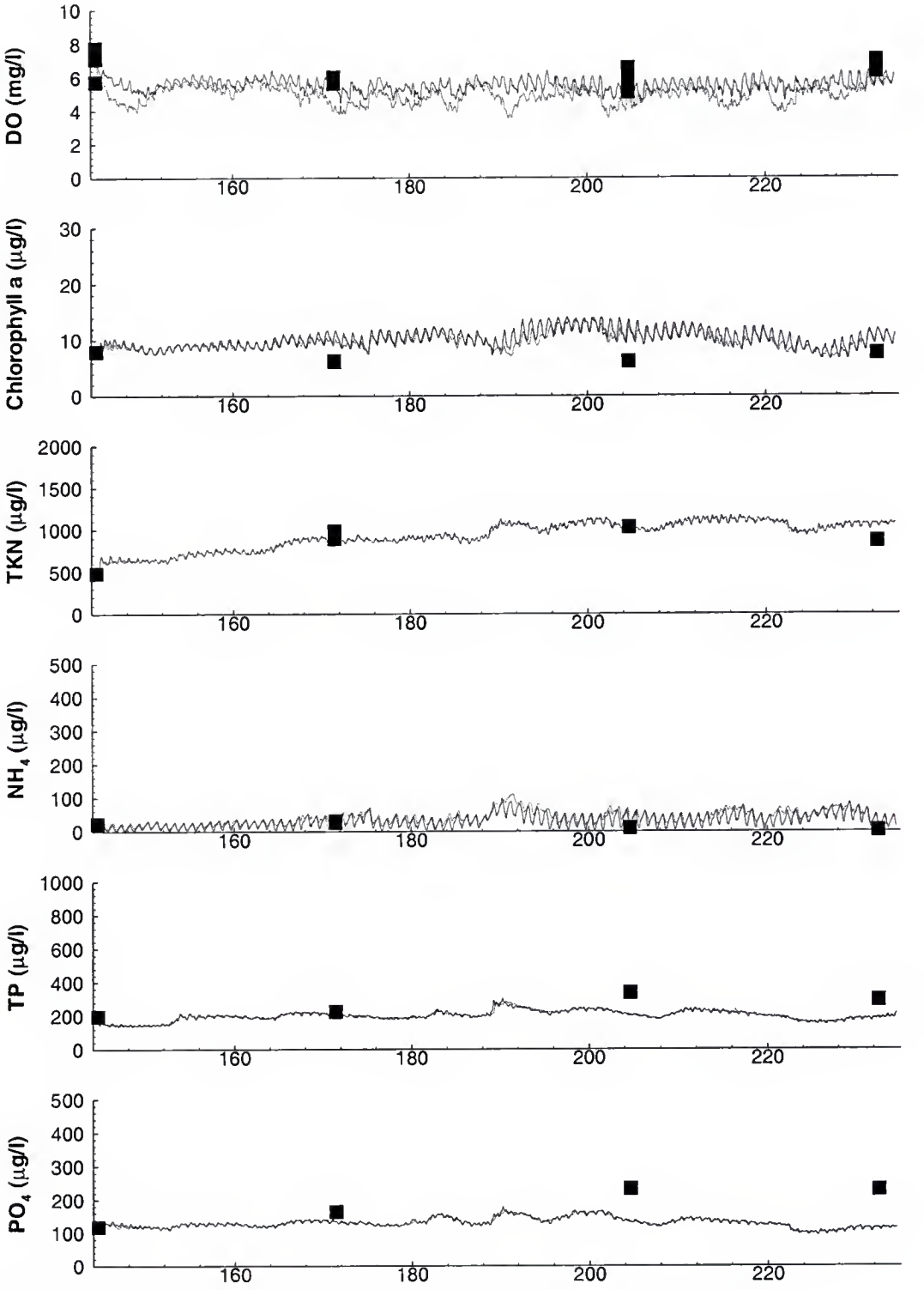

Figure 6.14 Temporal water quality variations at CH09B station in 1996.

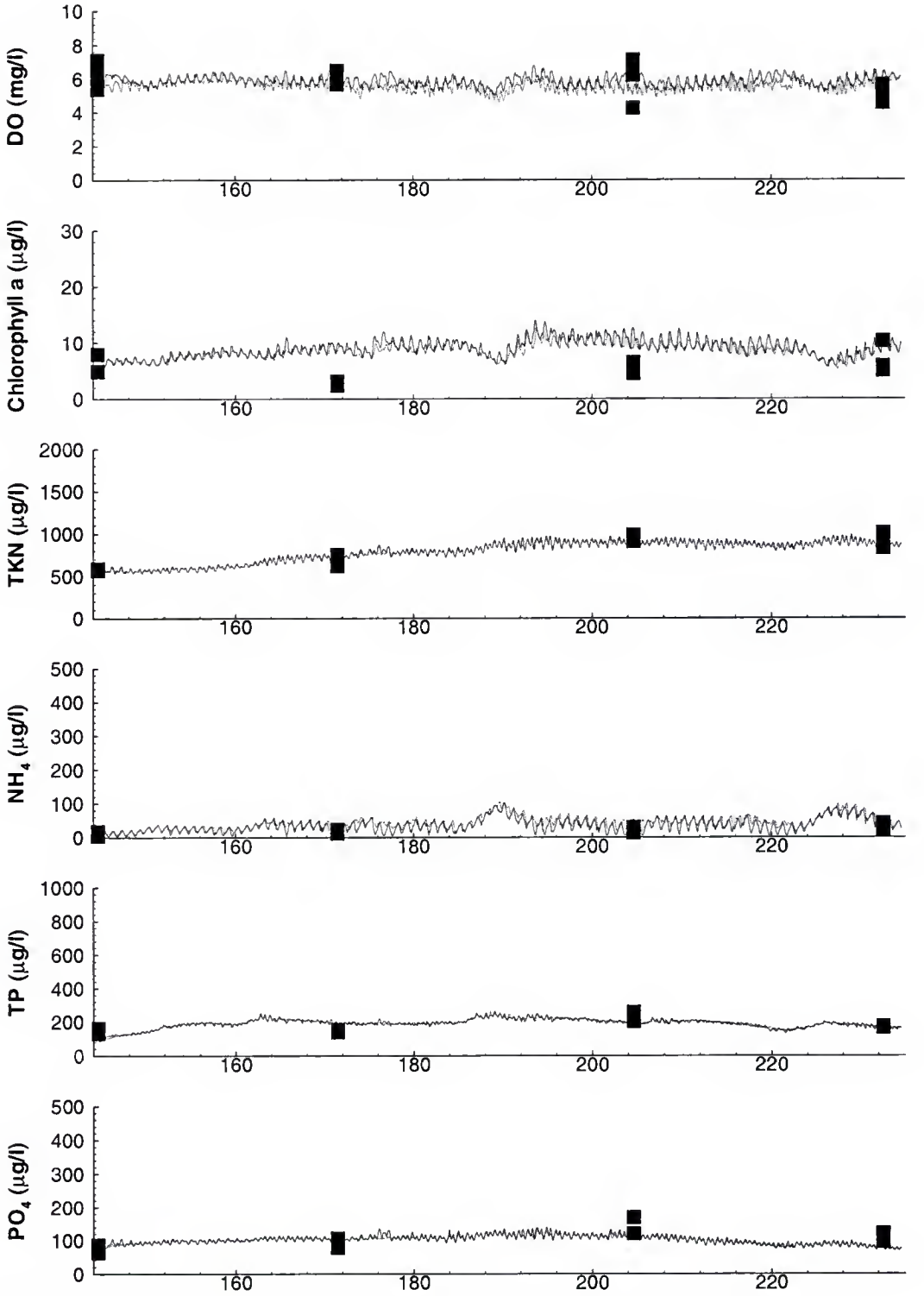

Figure 6.15 Temporal water quality variations at CH009 station in 1996.

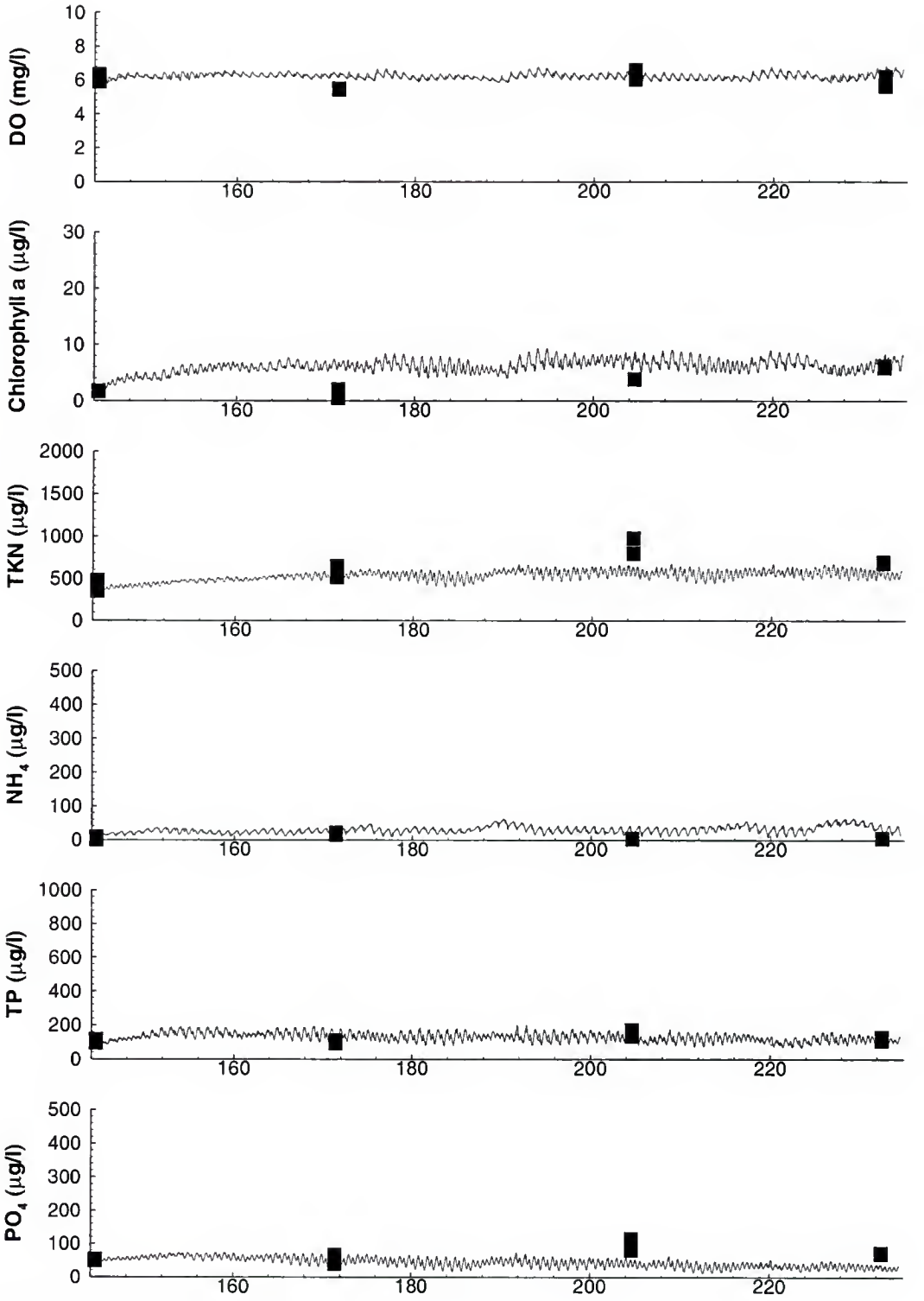

Figure 6.15 Temporal water quality variations at CH010 station in 1996.

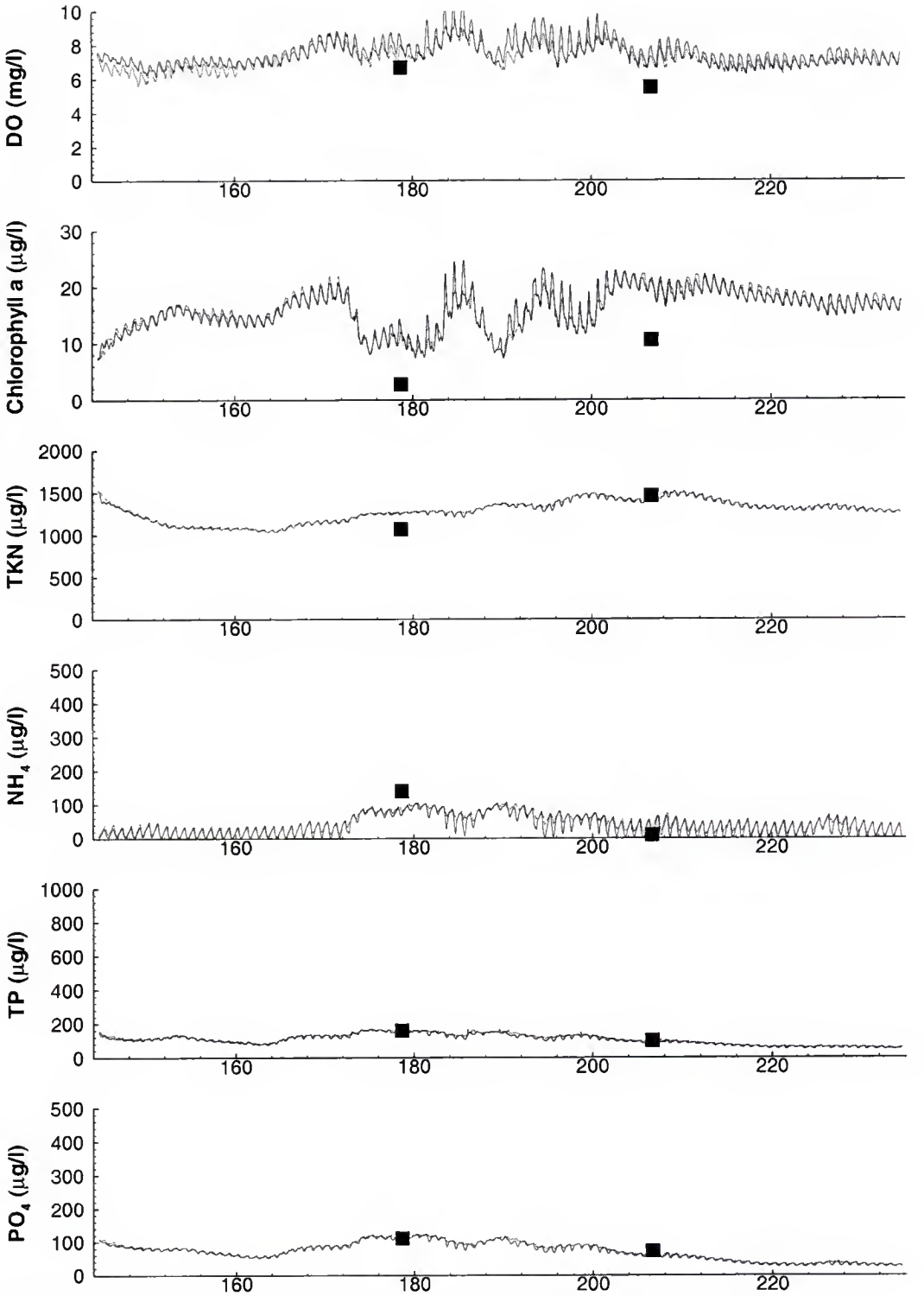

Figure 6.17 Temporal water quality variations at HB002 station in 1996.

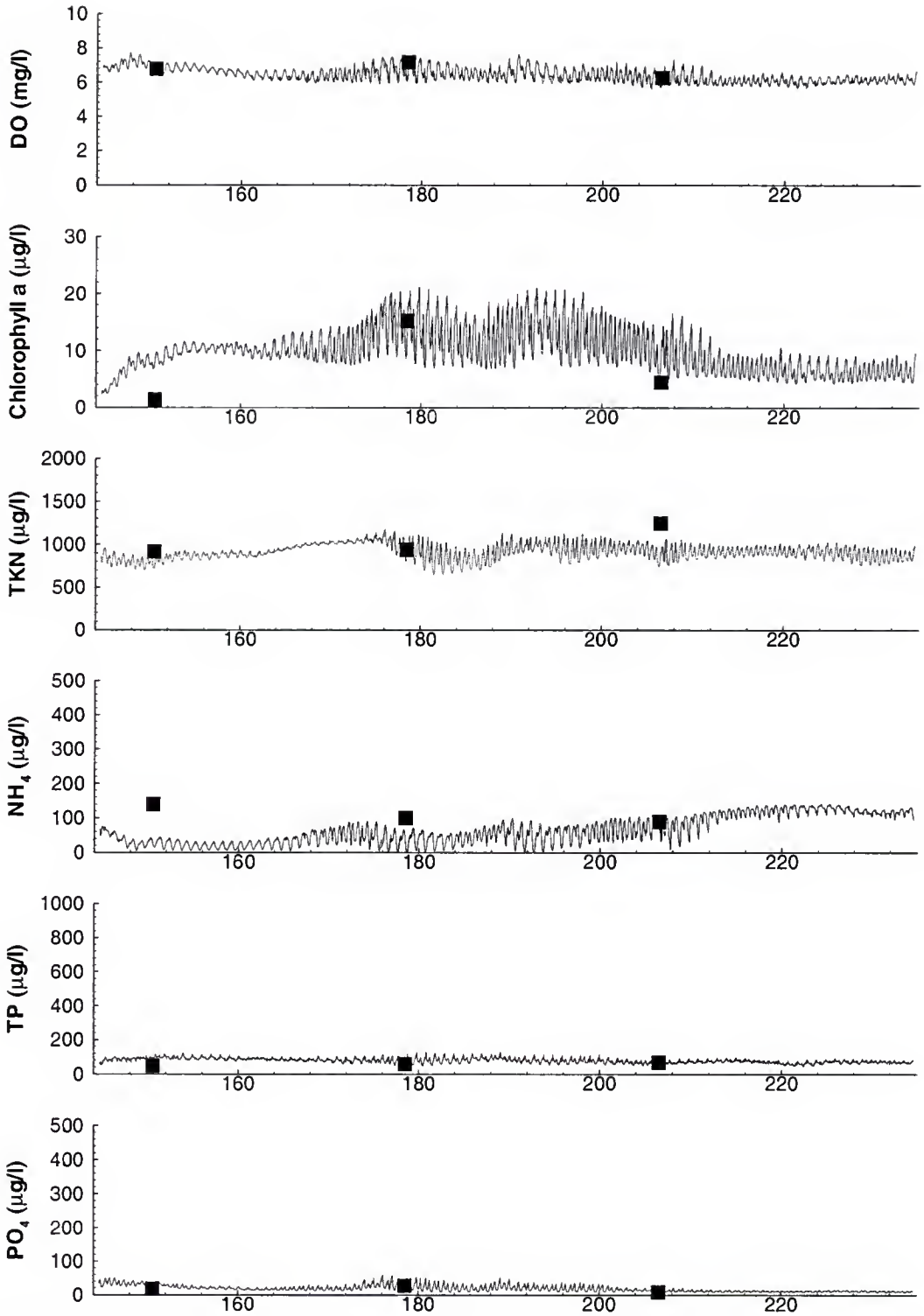

Figure 6.18 Temporal water quality variations at HB006 station in 1996.

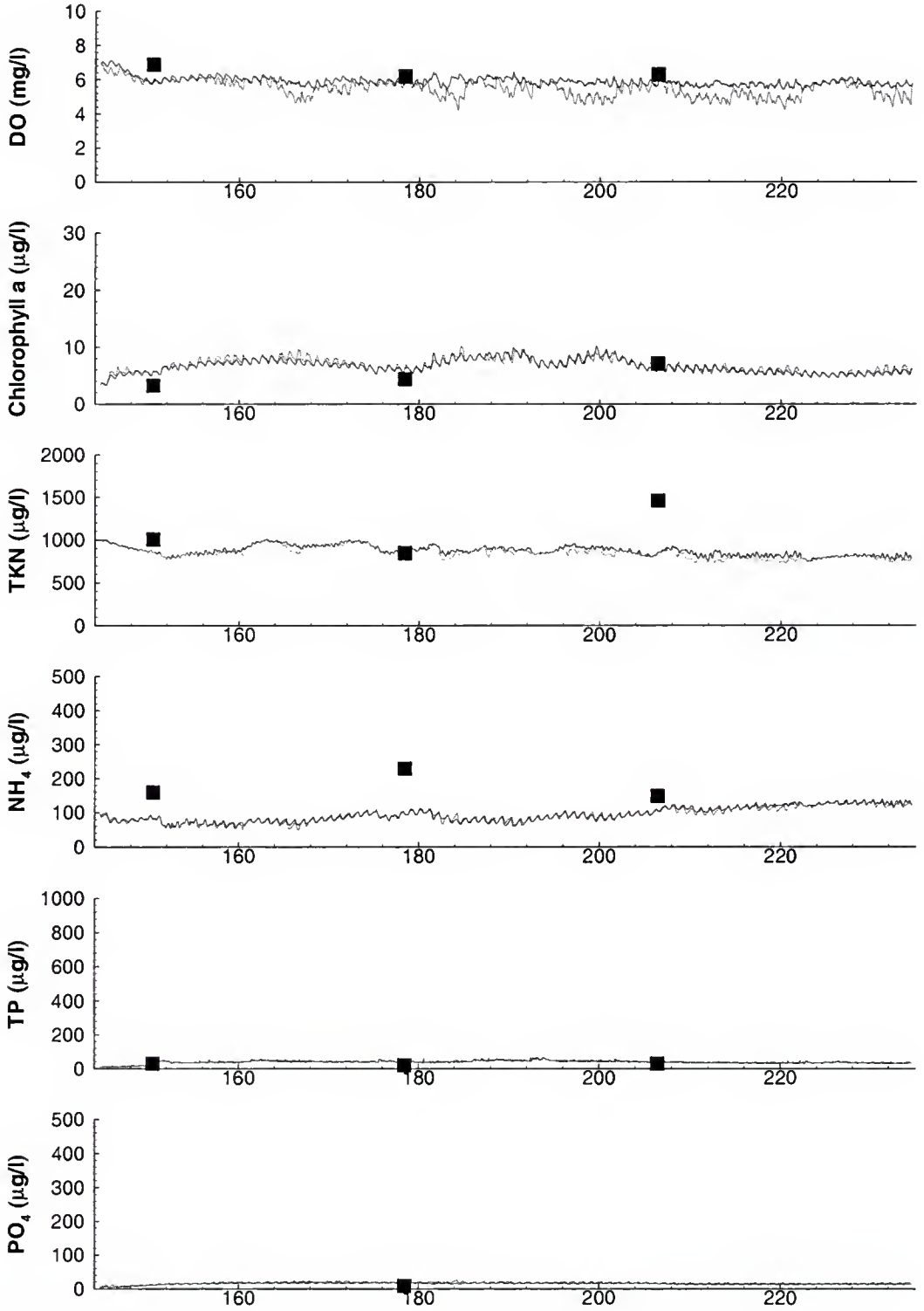

Figure 6.19 Temporal water quality variations at HB007 station in 1996.

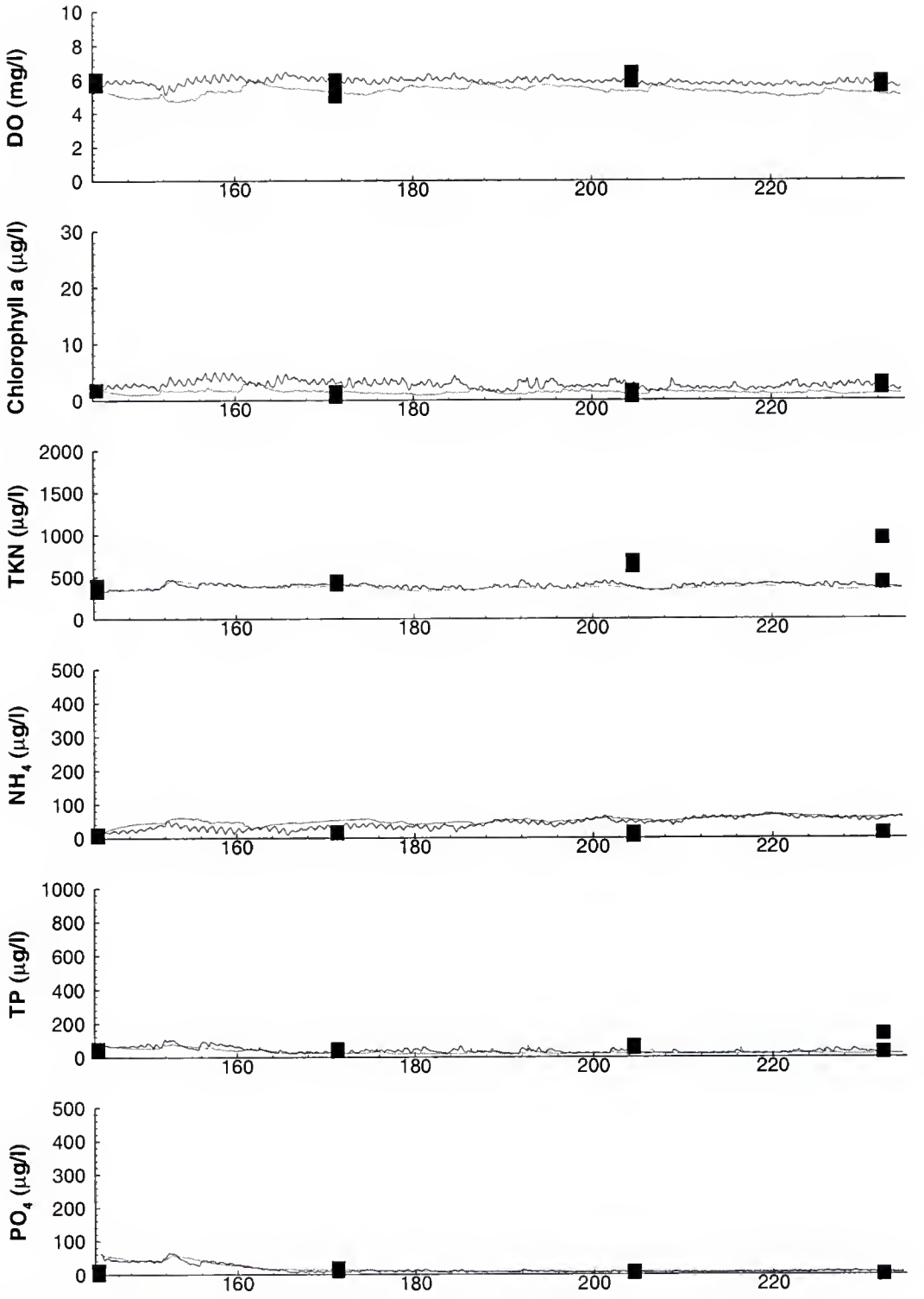

Figure 6.20 Temporal water quality variations at CH013 station in 1996.

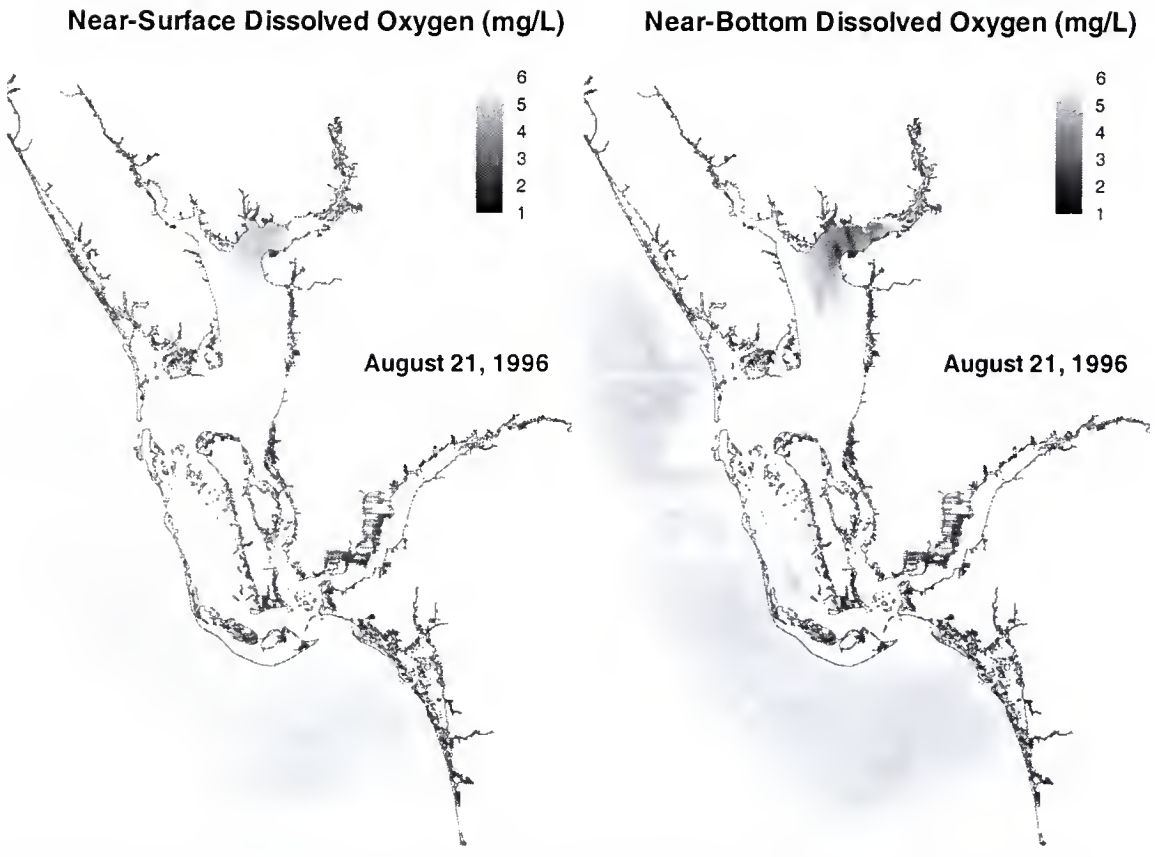

Figure 6.21 Simulated dissolved oxygen concentration in Charlotte Harbor estuarine system on August 21, 1996.

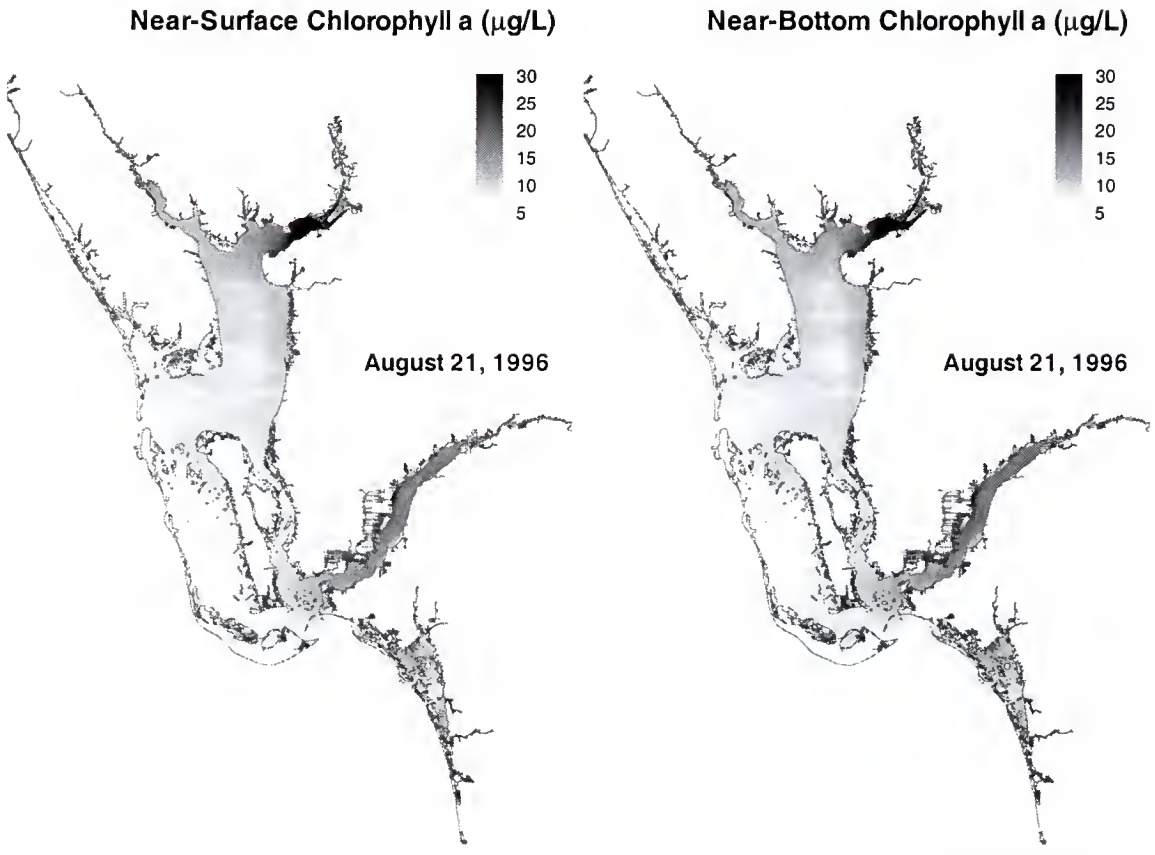

Figure 6.22 Simulated Chlorophyll_a concentration in Charlotte Harbor estuarine system on August 21, 1996.

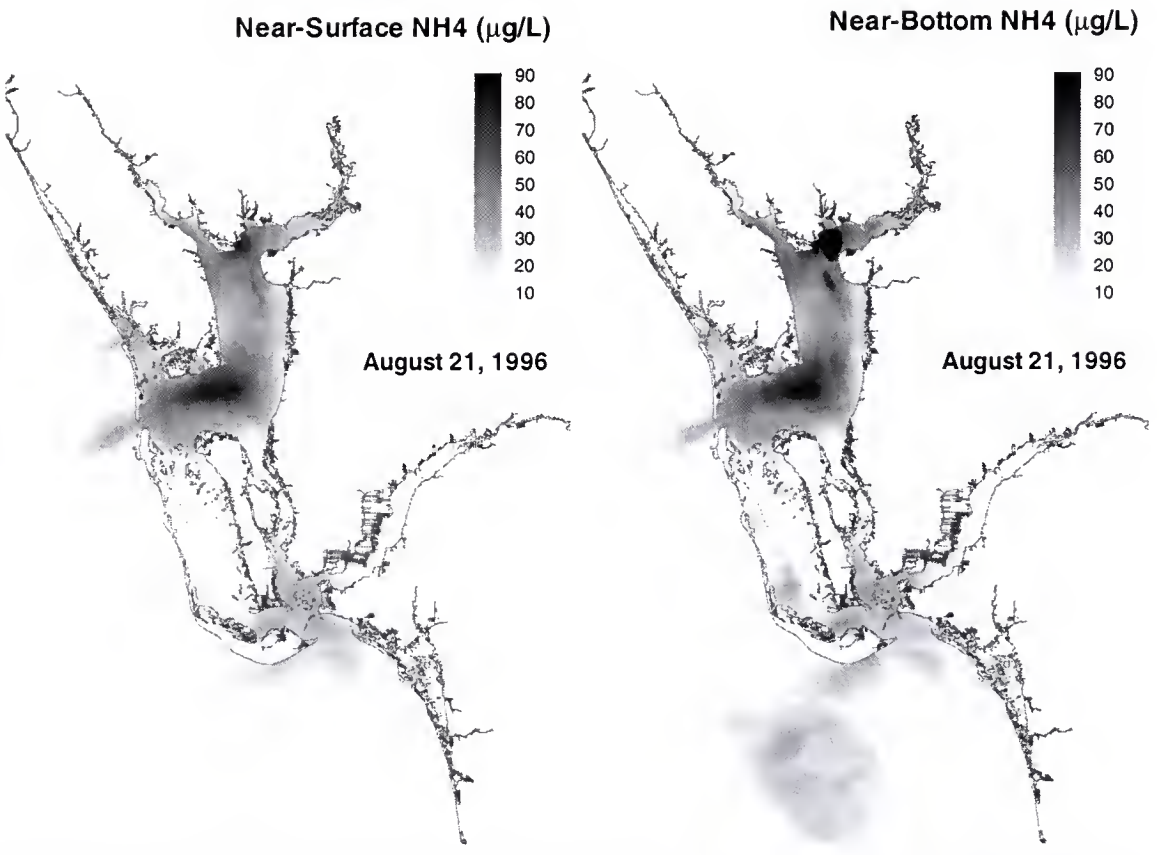

Figure 6.23 Simulated dissolved ammonium nitrogen concentration in Charlotte Harbor estuarine system on August 21, 1996.

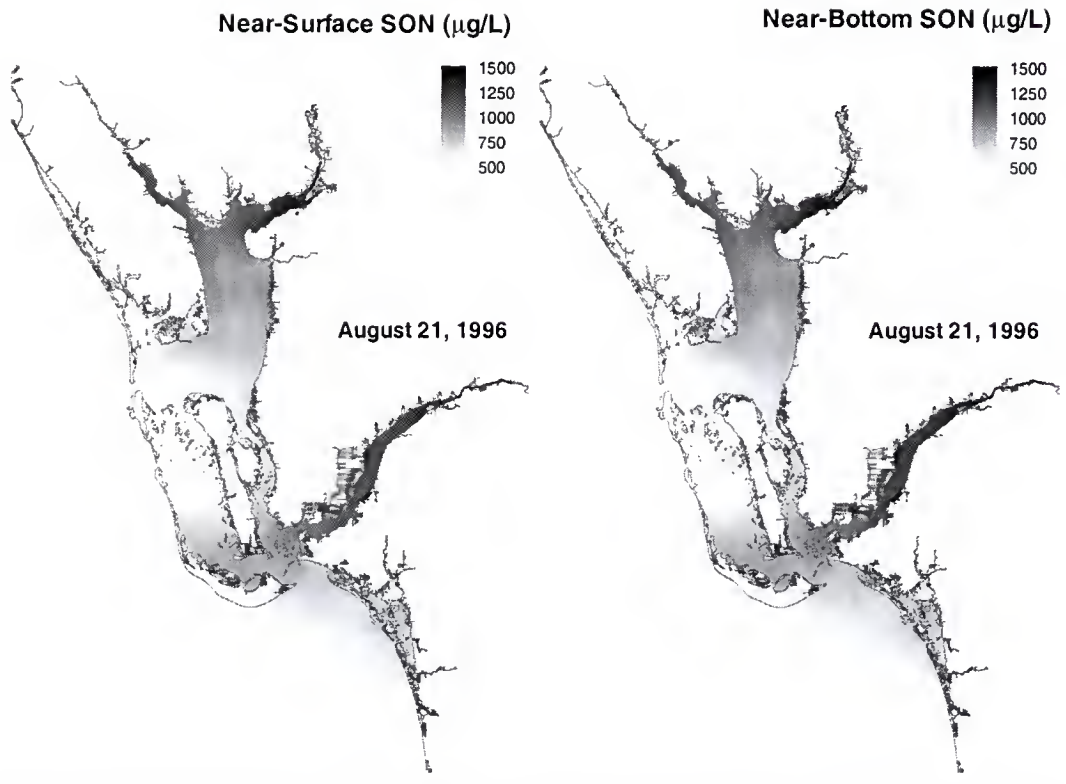

Figure 6.24 Simulated soluble organic nitrogen concentration in Charlotte Harbor estuarine system on August 21, 1996.

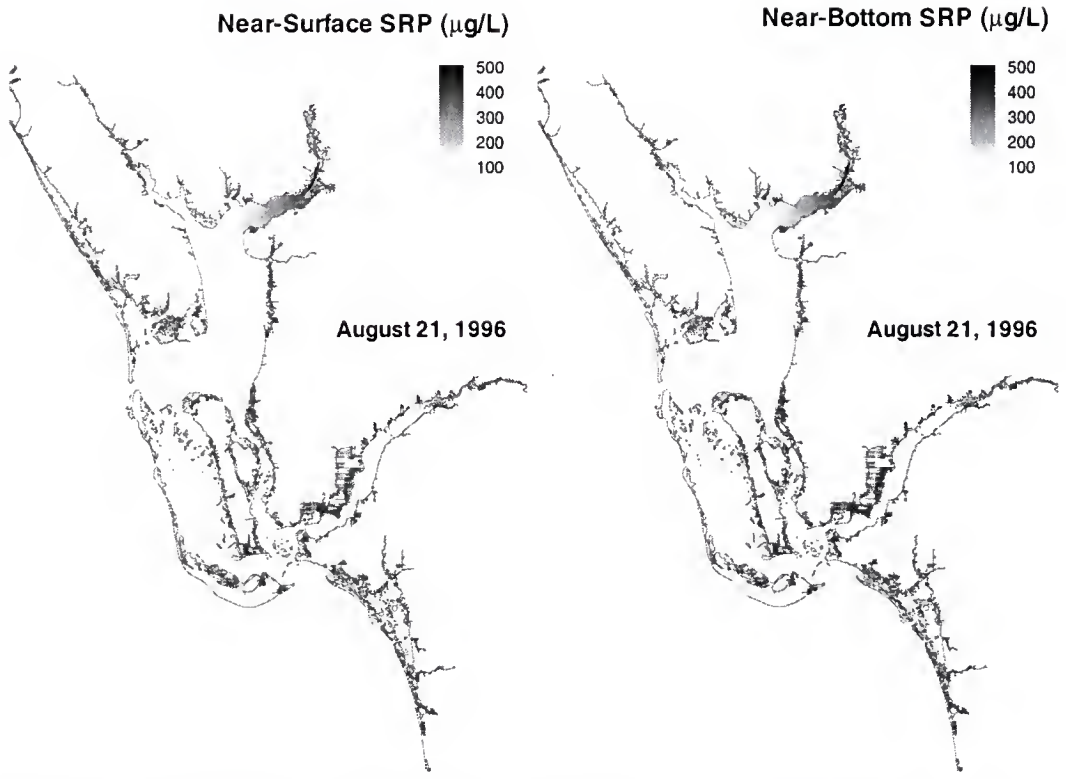

Figure 6.25 Simulated soluble reactive phosphorous concentration in Charlotte Harbor estuarine system on August 21, 1996.

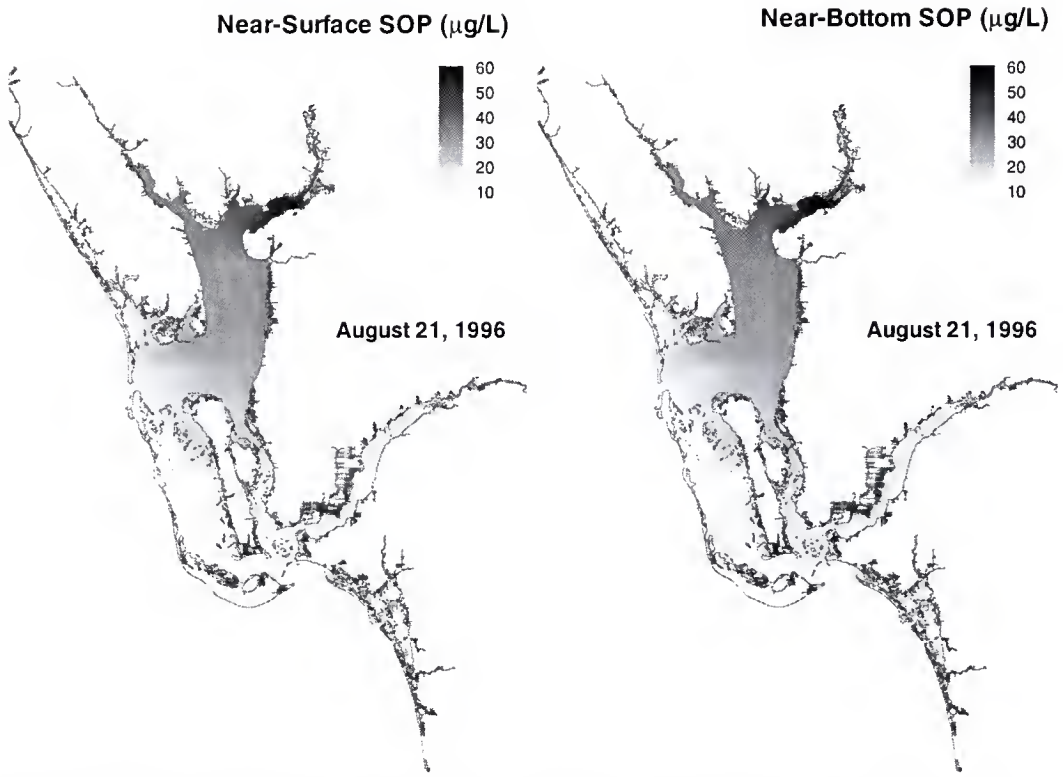

Figure 6.26 Simulated soluble organic phosphorous concentration in Charlotte Harbor estuarine system on August 21, 1996.

6.4 Simulations of Water Quality in 2000

Model simulation of circulation, sediment transport and water quality dynamics in Charlotte Harbor estuarine system during the summer 1996 was conducted as calibration process tunning of model parameters and inputs followed systematic calibration procedure. Based on the results presented, the water quality model was considered calibrated and validated, and additional one year simulation was performed to validate the model. This validated model was used to assess the effects of Sanibel Causeway and the navigation channel in San Carlos Bay as well as river load reductions.

6.4.1 Validation

For validation runs, hydrodynamic and water quality model coefficients were held fixed at the calibration values, and results of a one-year 2000 simulation were compared with field data collected in January to December 2000. The data include phytoplankton, nitrogen, phosphorous, dissolved oxygen at several locations in the Charlotte Harbor estuarine system.

Figure 6.27 contains calibration period scattering plots which include the root mean square (RMS) error and correlation coefficient (R^2). Values shown in parenthesis are normalized RMS errors with maximum measured data. Without adjusting any water quality model coefficients, the normalized RMS errors are less than 45%. Dissolved oxygen has the best agreement with measured data as shown by the RMS error. Correlation coefficients for all species vary form 0.124 to 0.80. These plots allow us to assess weaknesses of the model, and to suggest areas needing further improvement.

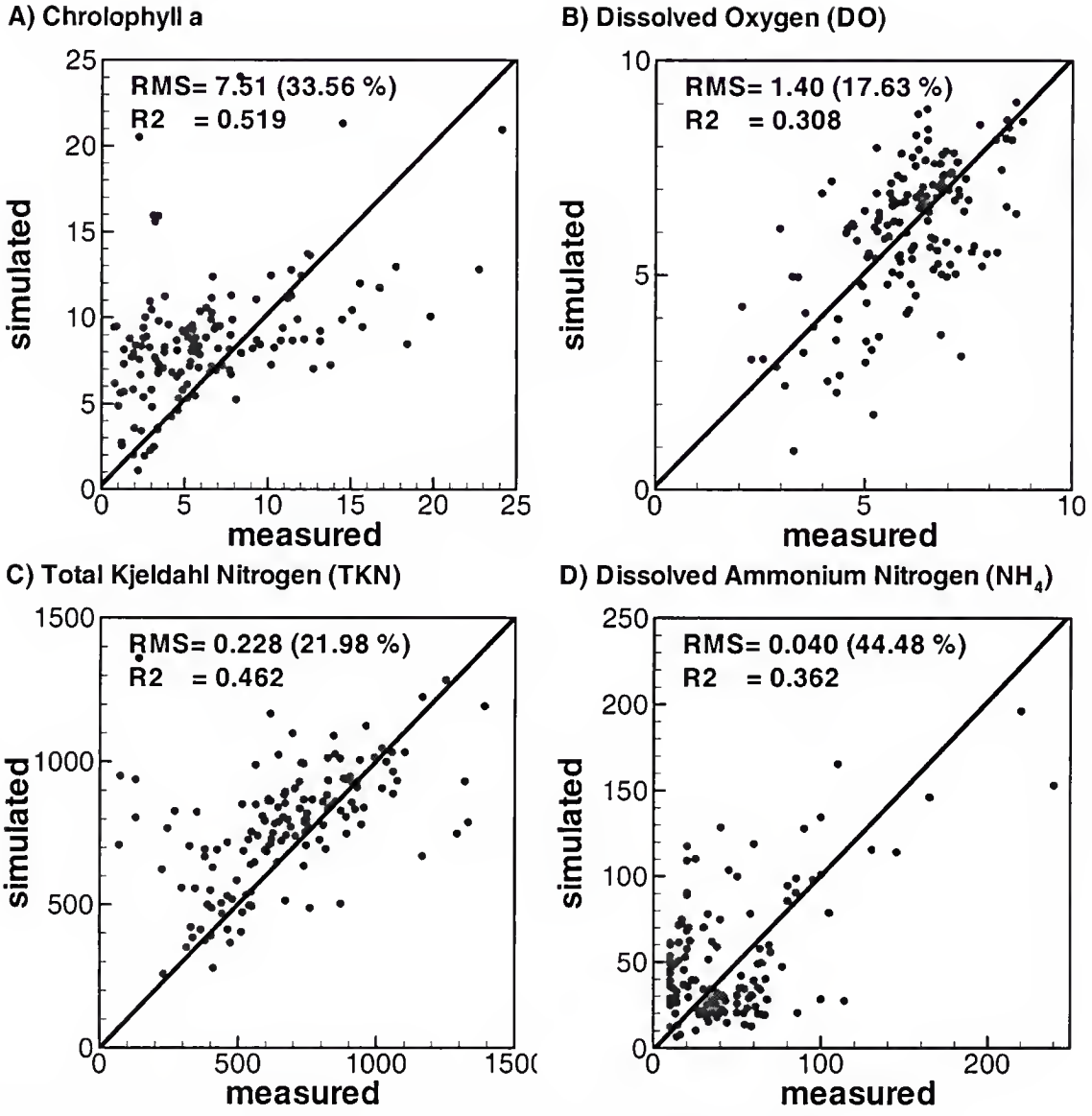

Figure 6.27 The scatter plots for water quality constituents in 2000.

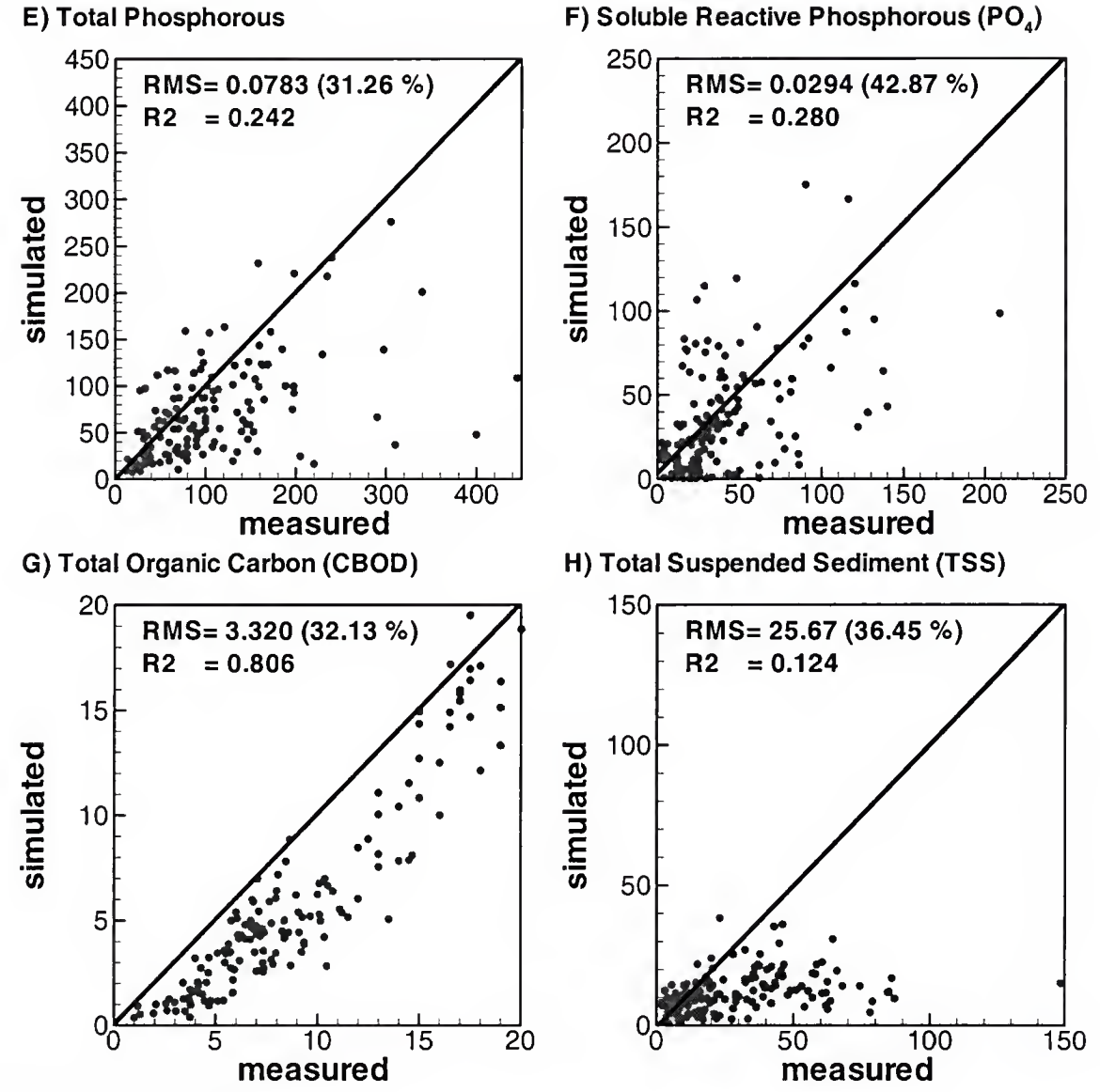

Figure 6.27 continued

6.4.2 Results of 2000 Water Quality Simulation

The simulated water quality species at each measured station in 2000 as shown with measured data in Figure 6.28 to Figure 6.39. During the simulation period, the water quality data show the seasonal variation, and these seasonal variations are produced quite well by the water quality model. In the water quality model, dissolved oxygen is a function of photosynthesis and respiration by phytoplankton organisms, sediment oxygen demand, reaeration, nitrification and denitrification, decomposition of organic matter, tide and wind mixing, and river loading. As shown in Figures 6.28 to 6.39, simulated dissolved oxygen concentrations show spatial and temporal variations in reasonable agreement with measured data. The average monthly near-surface concentrations declined from 8.5 to 6.7 mg/L from January to July and then began to rise in upper Charlotte Harbor. Near-bottom average monthly concentrations in this area were highest in February, declined slowly through May, and then declined more rapidly until September. The hypoxia conditions during summer are attributed to strong stratification, which cause restricted re-aeration, and SOD. After the breakup of the stratification, the DO concentration increased from October to December.

Algae photosynthesis and re-aeration maintain surface dissolved oxygen level, while vertical mixing controls the transfer of dissolved oxygen to bottom water. Sediment oxygen demand is a function of temperature which has strong seasonal variation. The high water temperature in summer season will increase SOD in bottom sediment. If there is no stratification, surface water dissolved oxygen will become mixed with bottom water dissolved oxygen quickly. The Charlotte Harbor estuarine system generally exhibits a vertically well mixed distribution of DO due to wind and tidal mixing and the shallow water depth. The dissolved oxygen in most part of the estuary does not show any strong

stratification except in Peace and Caloosahatchee Rivers. In the upper Charlotte Harbor, which usually has the lowest level of DO, some stratification may occur due to high consumption by SOD near the bottom and super-saturation near the surface with strong river discharge from Peace River. To quantify the causes of the bottom water hypoxia in this area, dissolved oxygen concentration at CH006 was compared with river discharge at Peace River, salinity, temperature and, reaeration and SOD fluxes in Figure 6.40. Although, the SOD flux is higher than the reaeration flux in summer (Julian Day 120 to 280) due to high temperature, the DO stratification did not occur during this period. The DO stratification period (Julian Day 220-280) matches with the salinity stratification caused by strong river discharge from Peace River.

To compare salinity stratification and vertical DO distribution, Simulated longitudinal-vertical salinity and dissolved oxygen concentration along the Peace River at 1 pm on June 18 (Julian Day 170) and October 6 (Julian Day 280), 2000 were plotted in Figures 6.41 and 6.42, respectively. The salinity at these two time period represent the effect of salinity stratification on vertical DO distribution since the SOD and re-aeration fluxes are similar at these periods. The results show the strong relationship between salinity and DO stratifications. Therefore, the hypoxia in the upper Charlotte Harbor is primarily caused by the combination effects of SOD and stratification with strong river discharge and high temperature.

In the Caloosahatchee River upstream near the S79 (CES02), there is very strong daily fluctuation in the surface dissolved oxygen concentration due to tidal fluctuation and high dissolved oxygen concentration from the Caloosahatchee River. Chlorophyll_a concentrations ranged from 1 to 100 mg/L and averaged 8.5 mg/L. Both productivity and

biomass were greater during summer near the mouth of tidal rivers which has middle range salinity of 6 to 12 ppt. The chlorophyll_a concentration of Caloosahatchee River has a maximum value of 98 mg/L on July 12 (Julian Day 193), 2000 and then quickly drop to 5 mg/L because of low chlorophyll_a concentration of river loading and fast flushing due to strong river discharge from Caloosahatchee River. Simulated nitrogen and phosphorous concentrations appear to capture the overall trend of the measured data collected by SFWMD and SWFWMD.

Figures 6.43 and 6.44 show the snapshots of the near surface chlorophyll_a and the near bottom dissolved oxygen concentration distribution in the study area on February 9, May 9, August 7, and November 5, to represent seasonal characteristics. In February, phytoplankton was low in the entire estuary and DO was a generally high. In May, phytoplankton significantly increased in the Caloosahatchee River due to strong river discharge with high nutrient concentrations. Hence, DO was reduced substantially in all portions but was higher in the north than in the south, except in Pine Island Sound. In August, there was significant increase in phytoplankton and decrease in dissolved oxygen concentration in the bottom water. This low dissolved oxygen in bottom water reached the north portion of upper Charlotte Harbor. The new water quality model, which contains improved dissolved oxygen processes at the air/sea interface and water-sediment interface, successfully reproduced the bottom water hypoxia in both temporal and spatial plots.

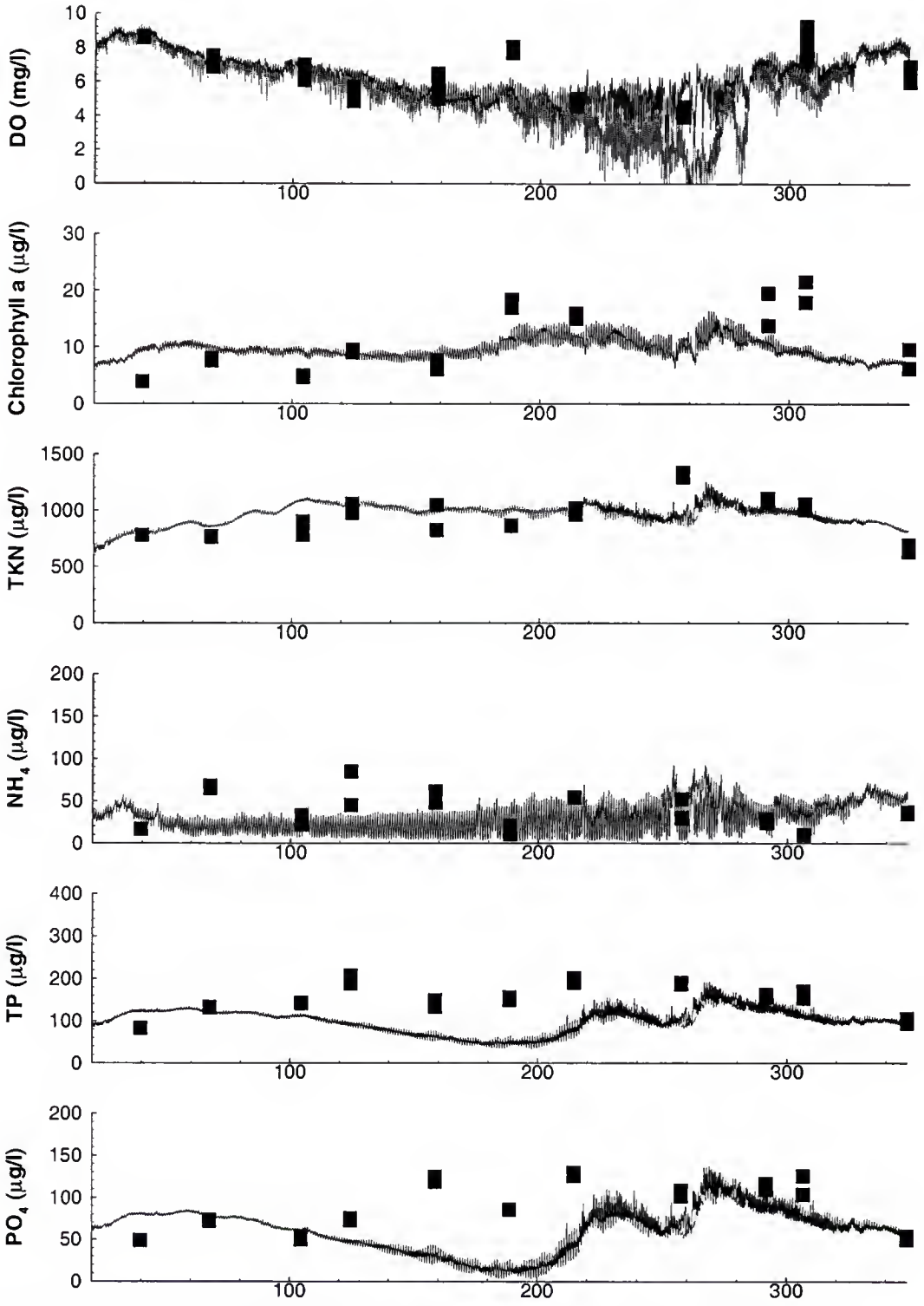

Figure 6.28 Temporal water quality variations at CH002 station in 2000.

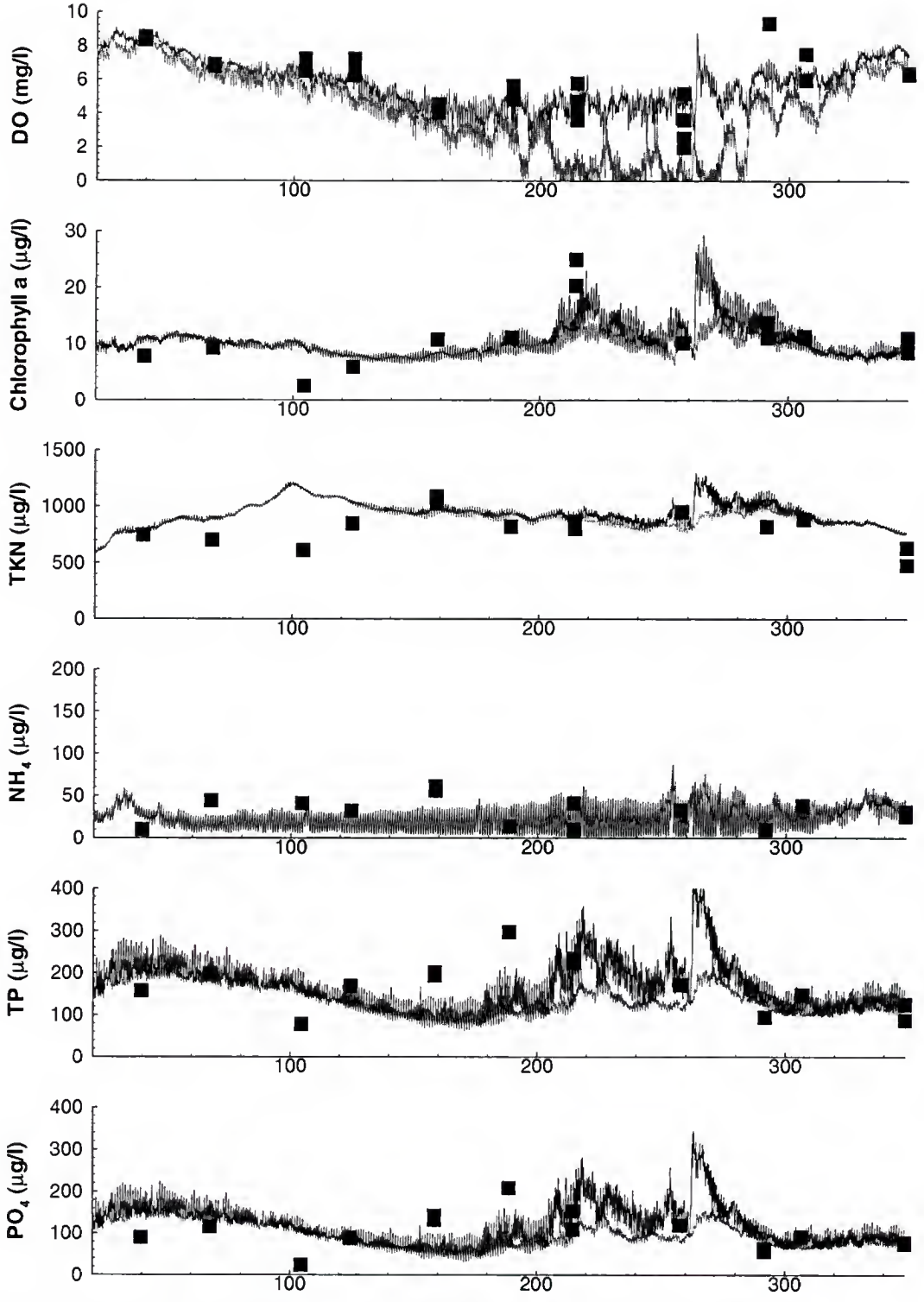

Figure 6.29 Temporal water quality variations at CH004 station in 2000.

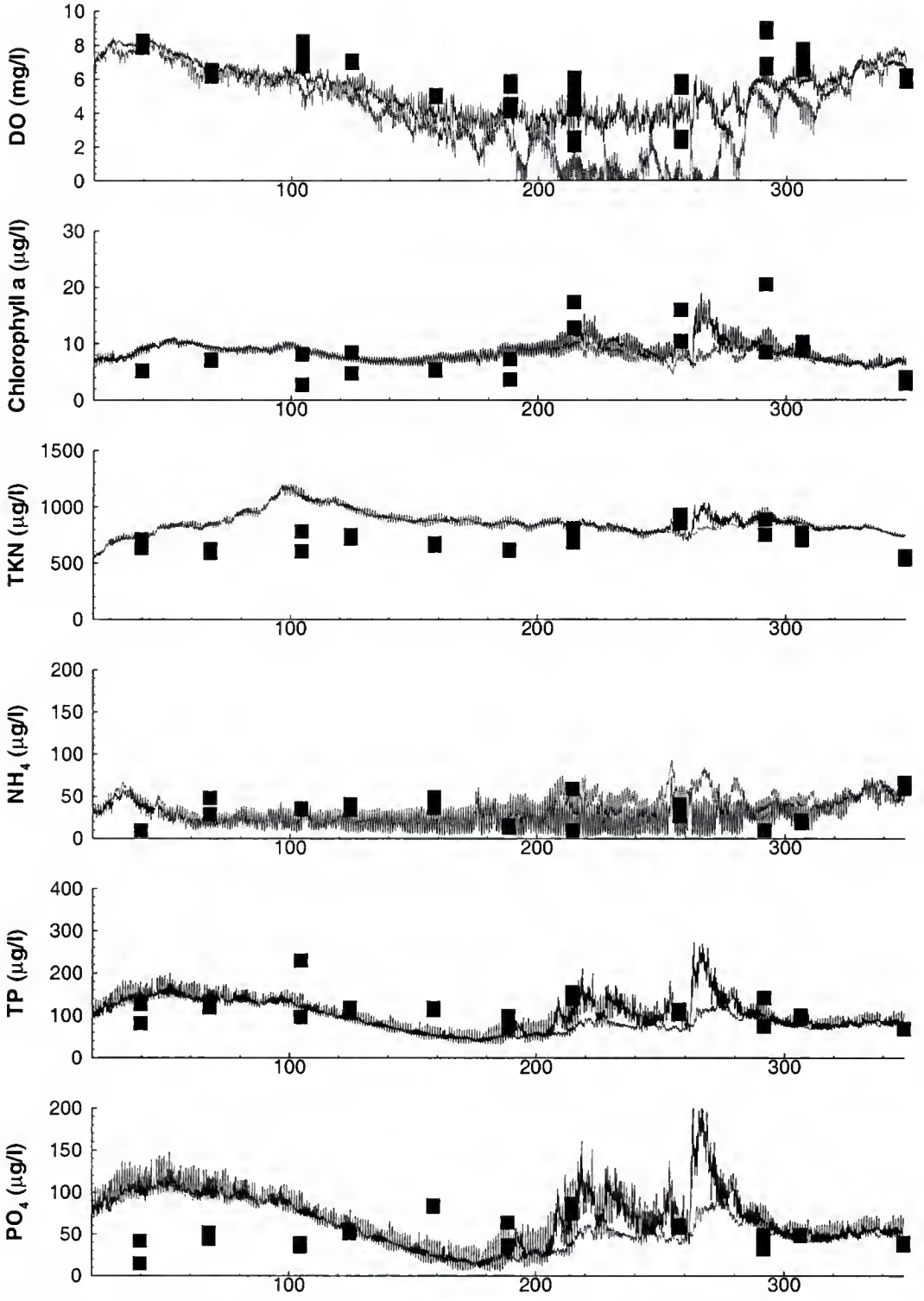

Figure 6.30 Temporal water quality variations at CH005 station in 2000.

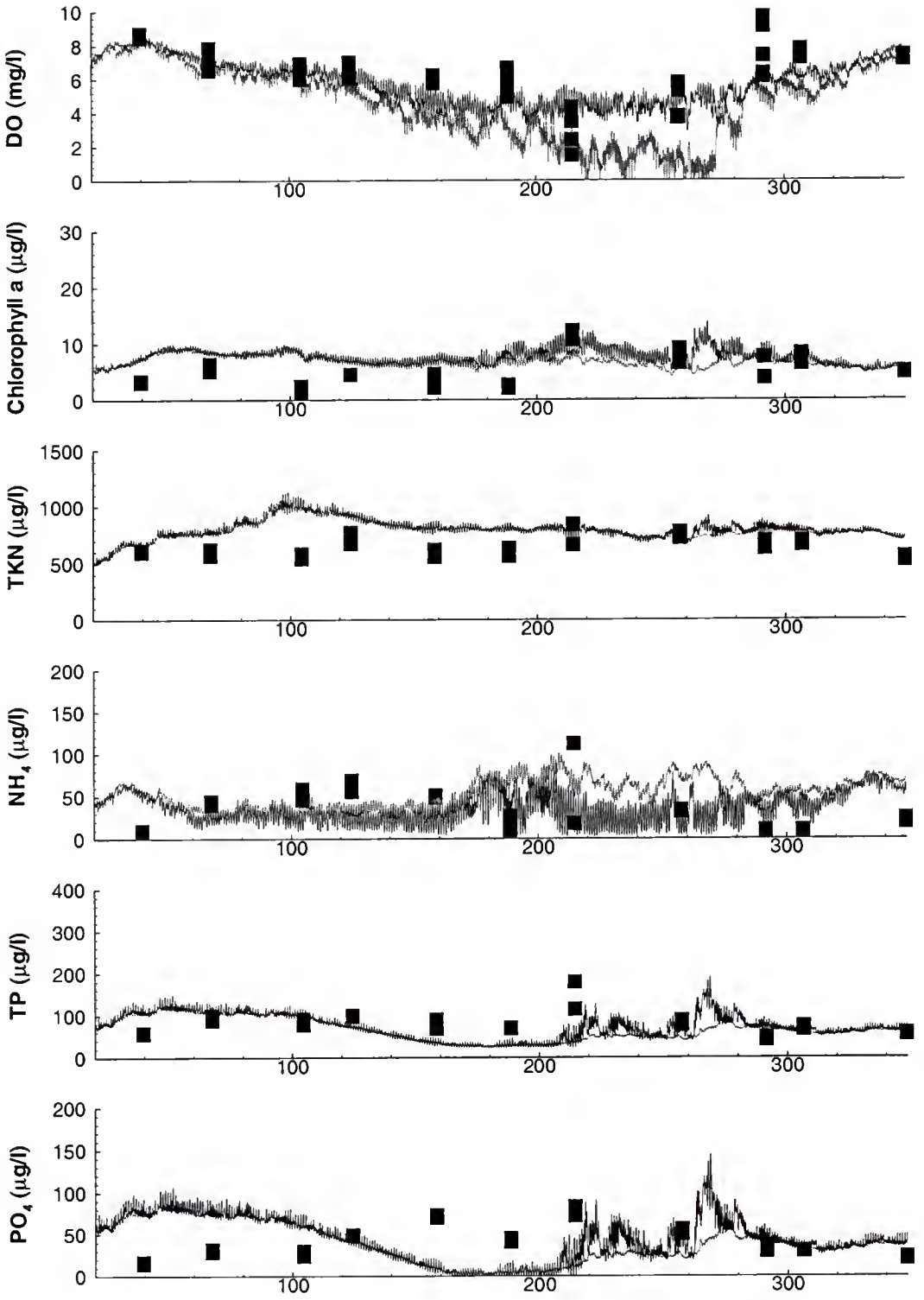

Figure 6.31 Temporal water quality variations at CH006 station in 2000.

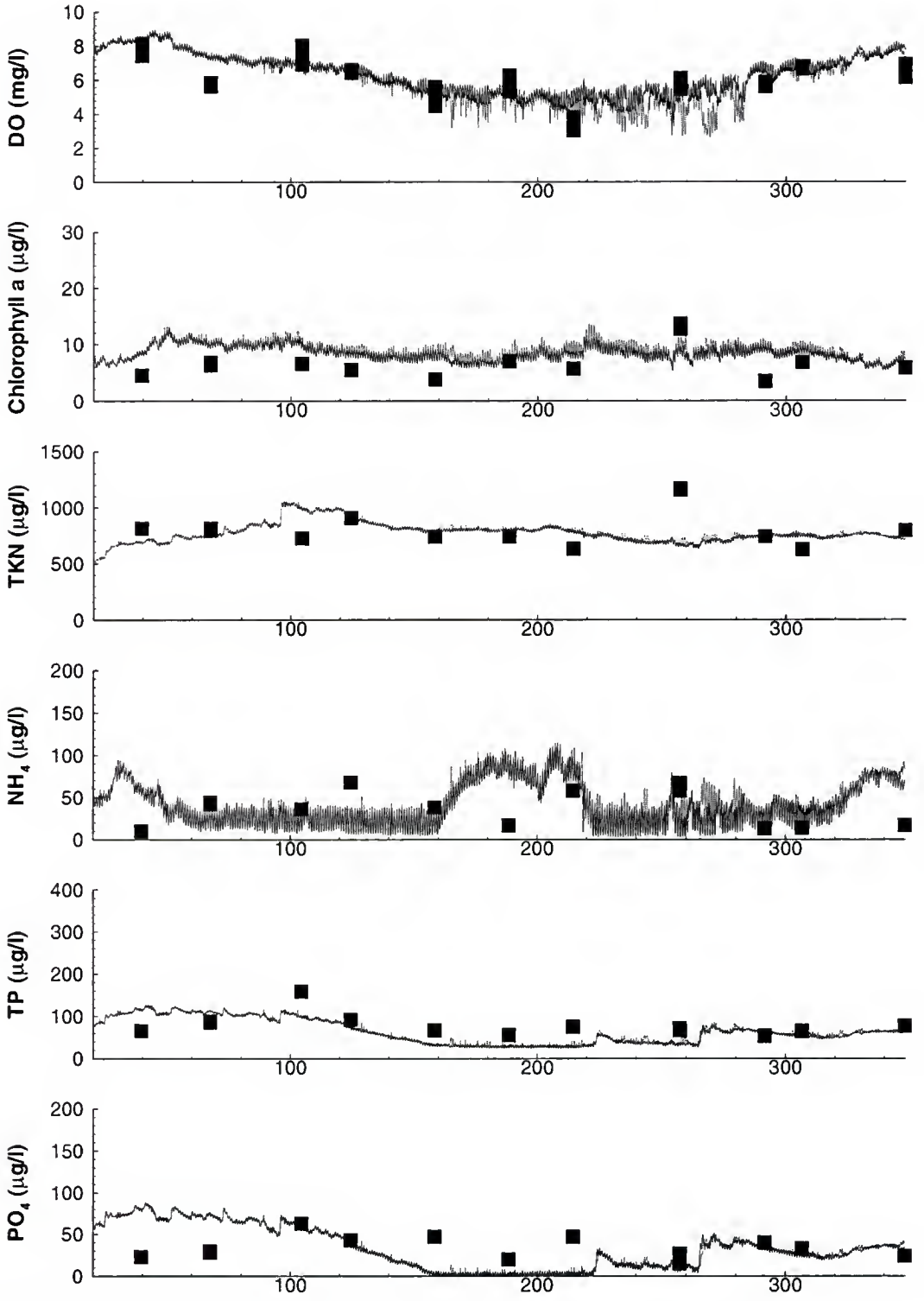

Figure 6.32 Temporal water quality variations at CH007 station in 2000.

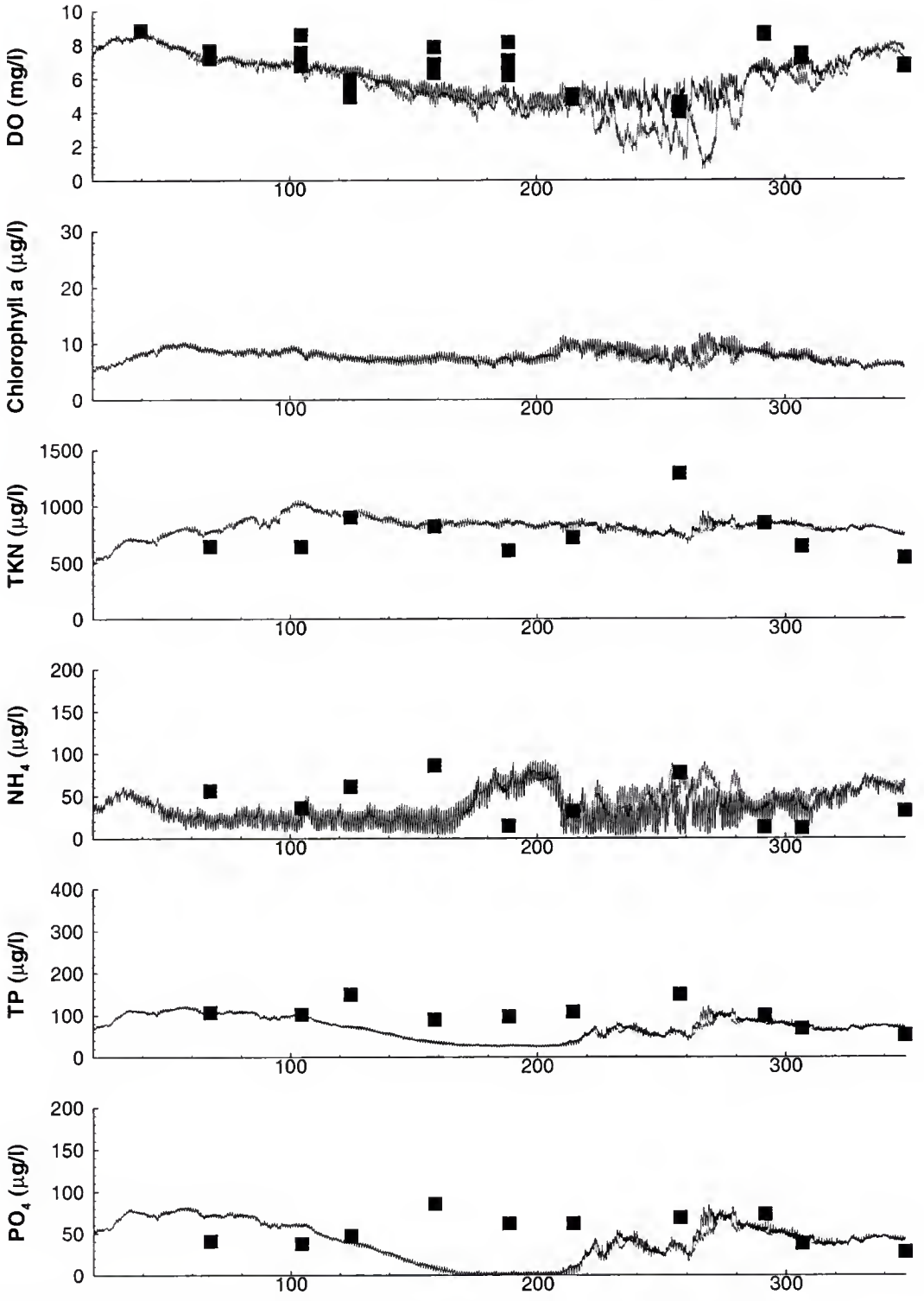

Figure 6.33 Temporal water quality variations at CH008 station in 2000.

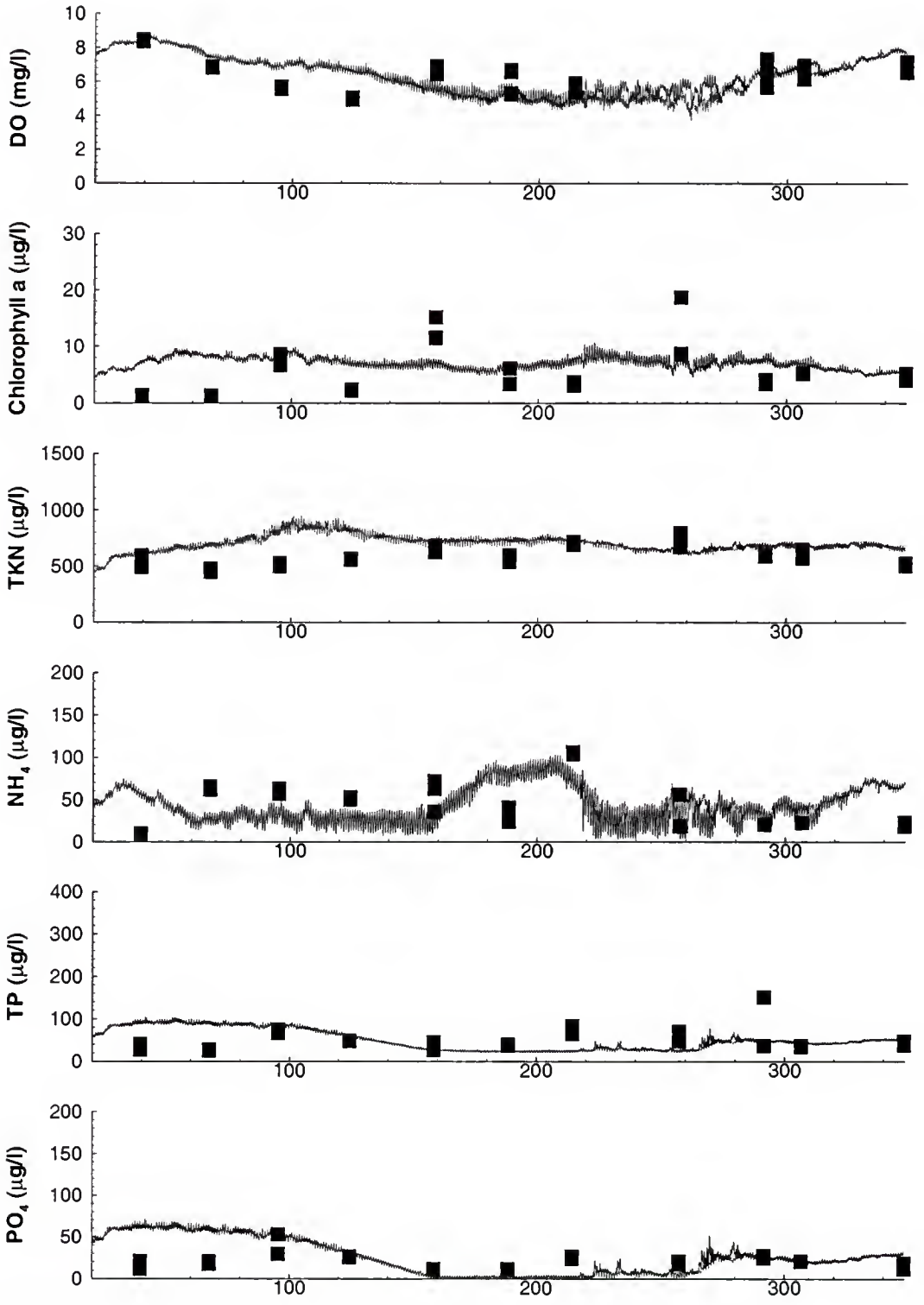

Figure 6.34 Temporal water quality variations at CH009 station in 2000.

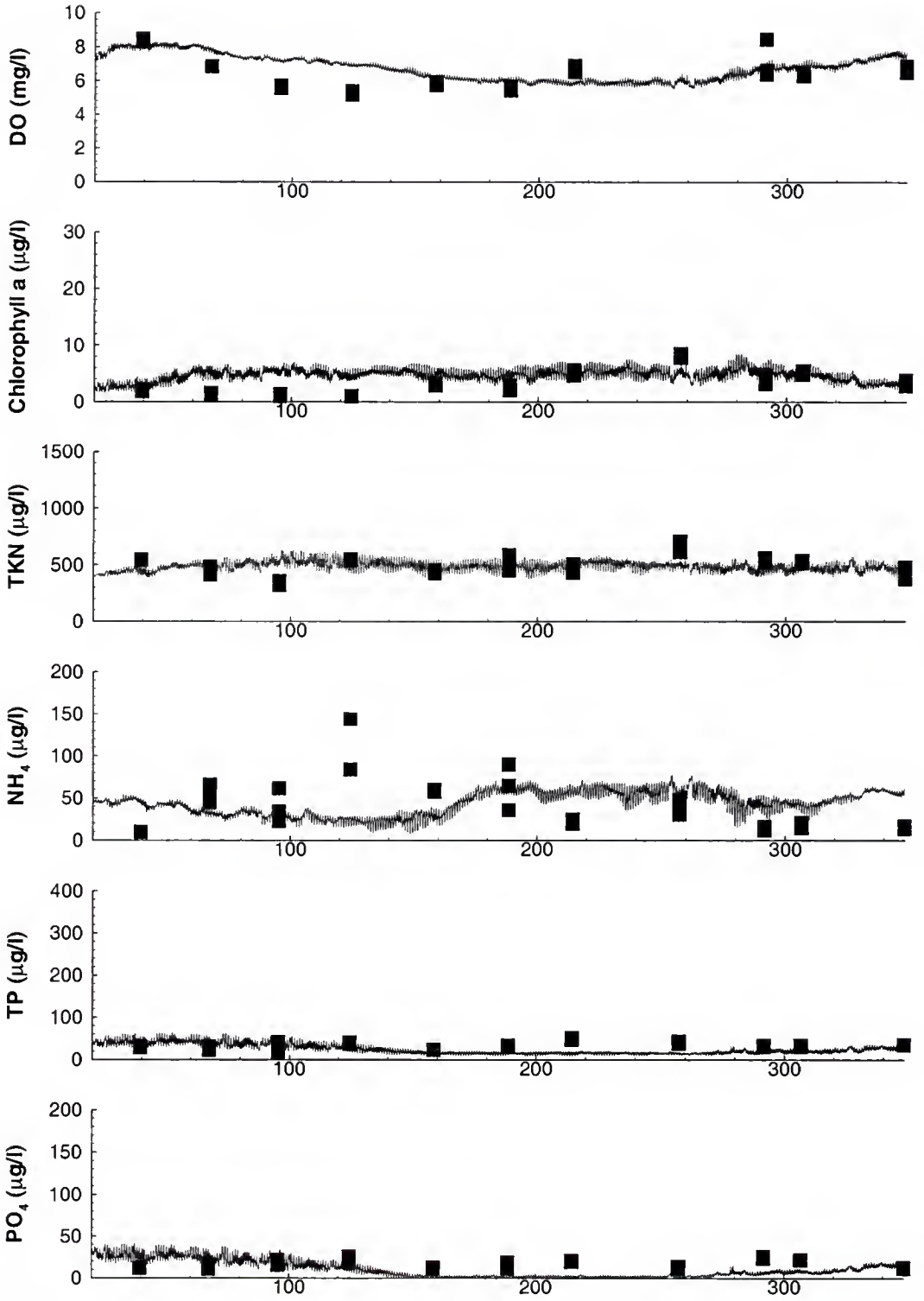

Figure 6.35 Temporal water quality variations at CH010 station in 2000.

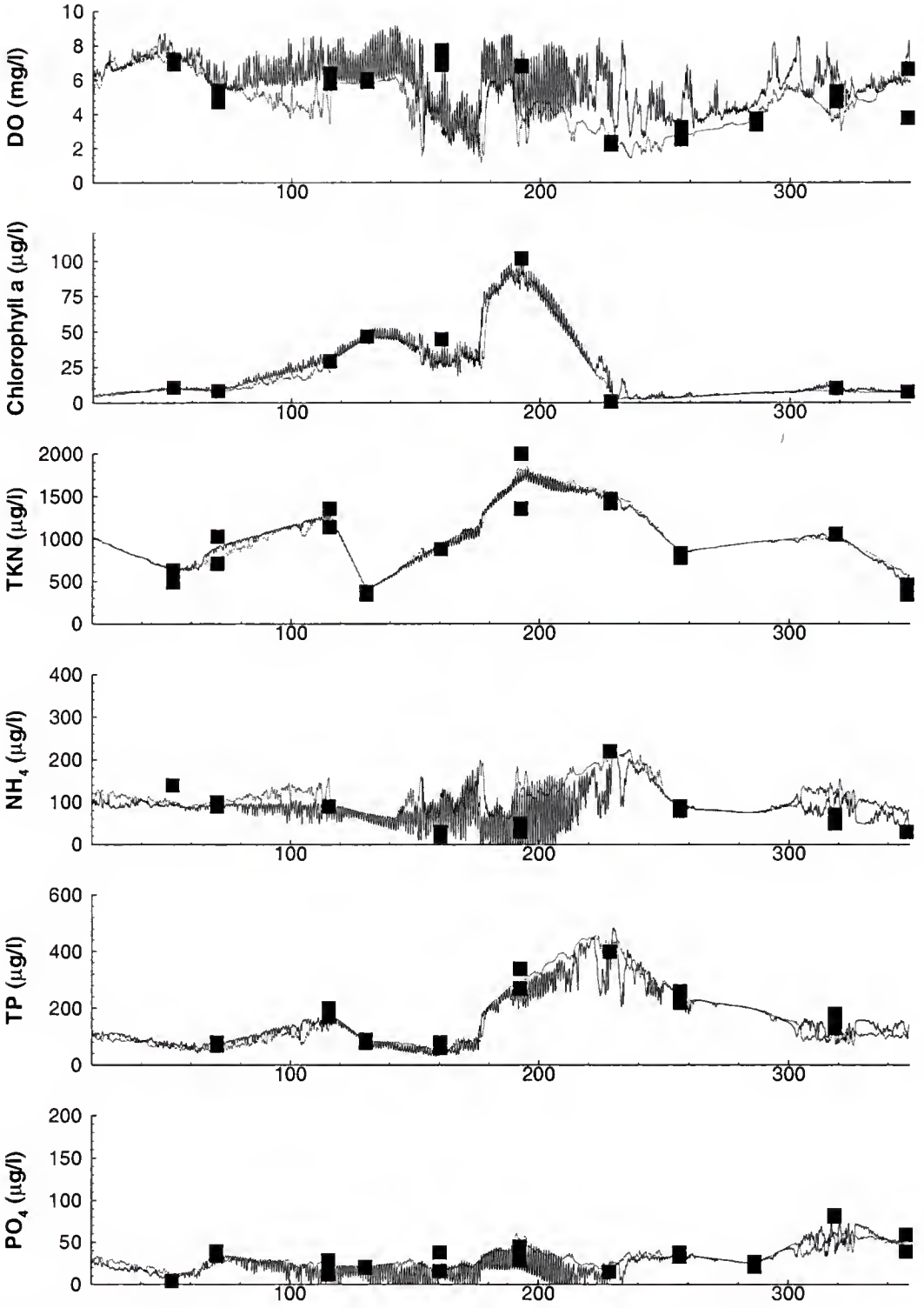

Figure 6.36 Temporal water quality variations at CES02 station in 2000.

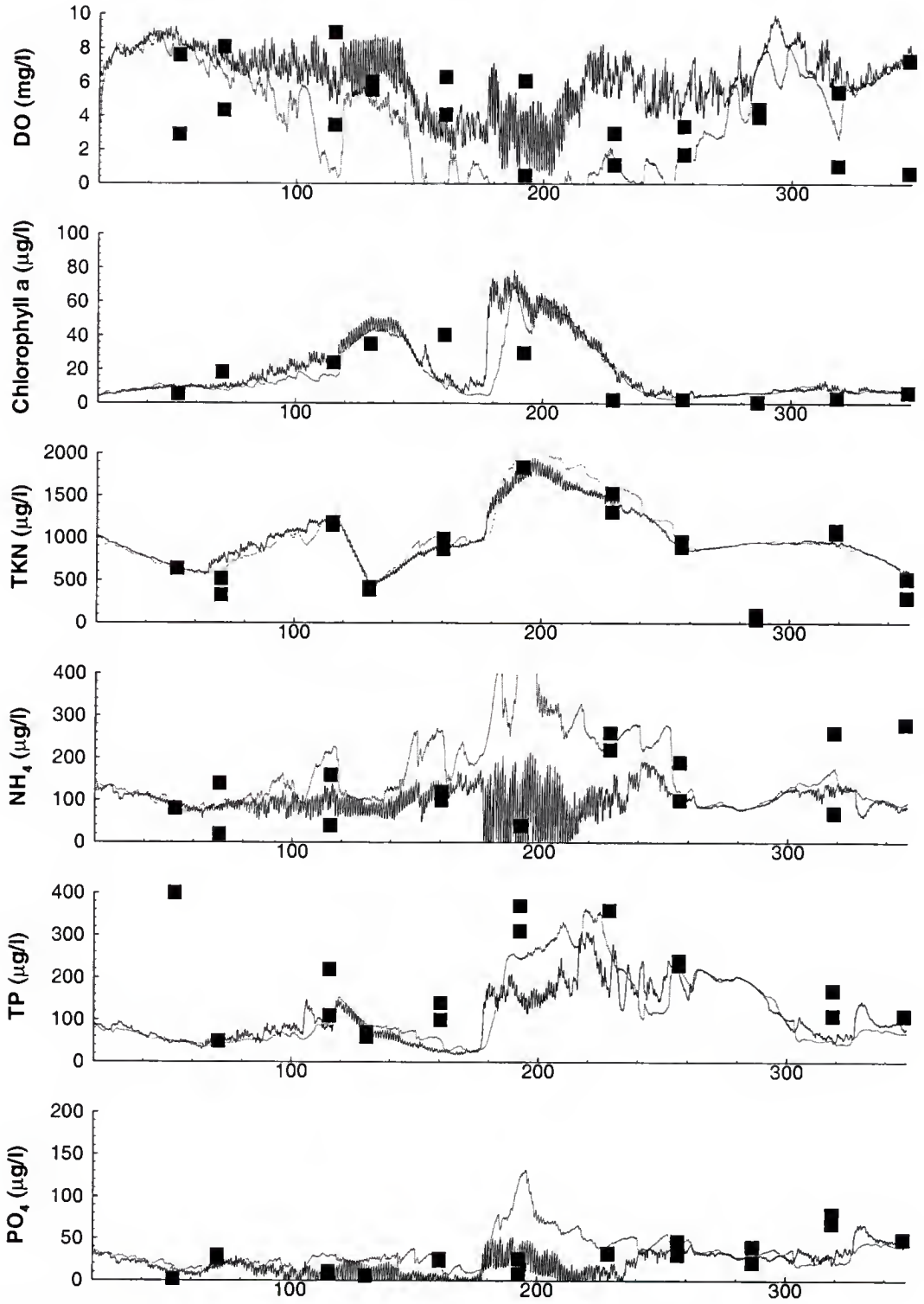

Figure 6.37 Temporal water quality variations at CES03 station in 2000.

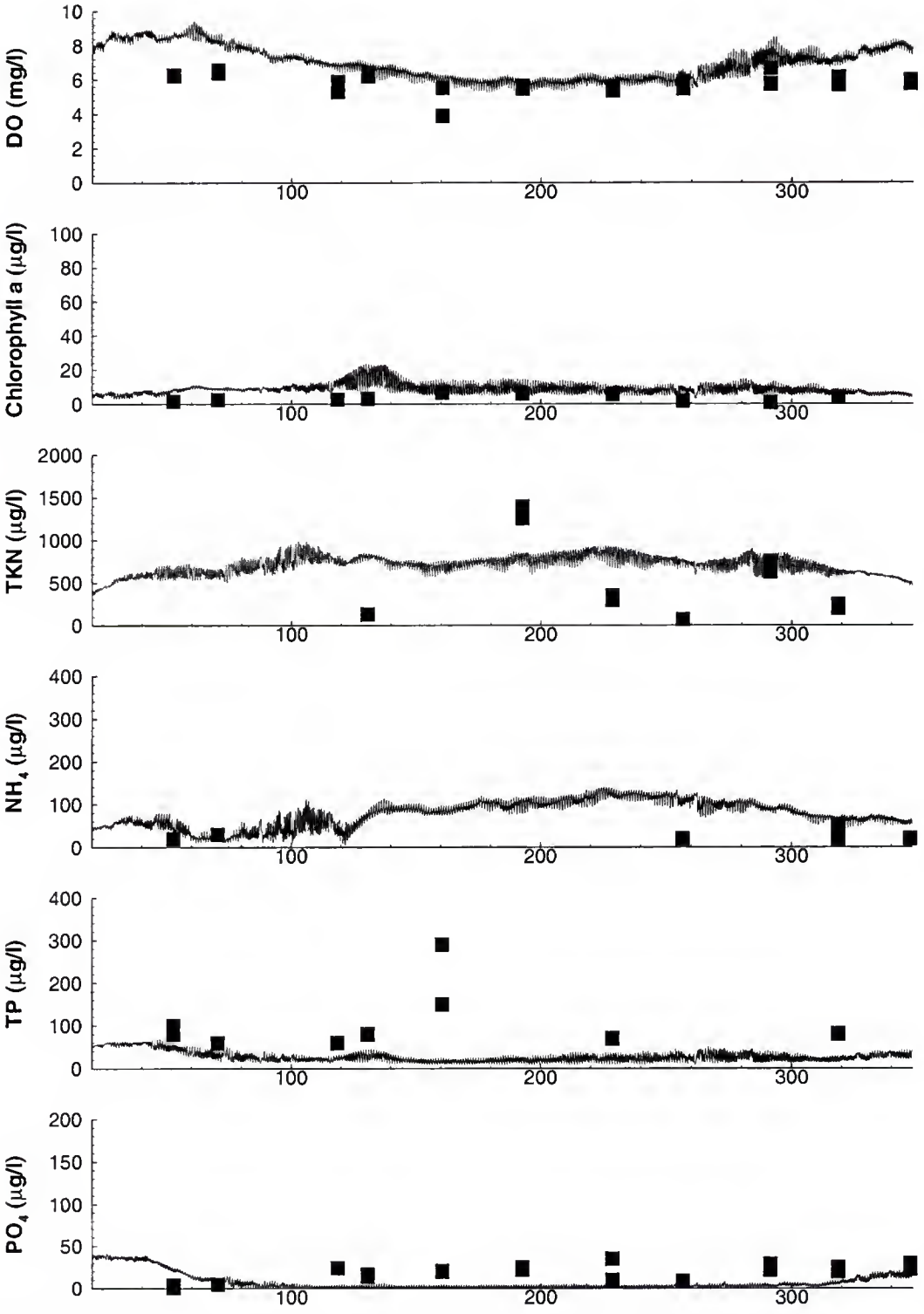

Figure 6.38 Temporal water quality variations at CES08 station in 2000.

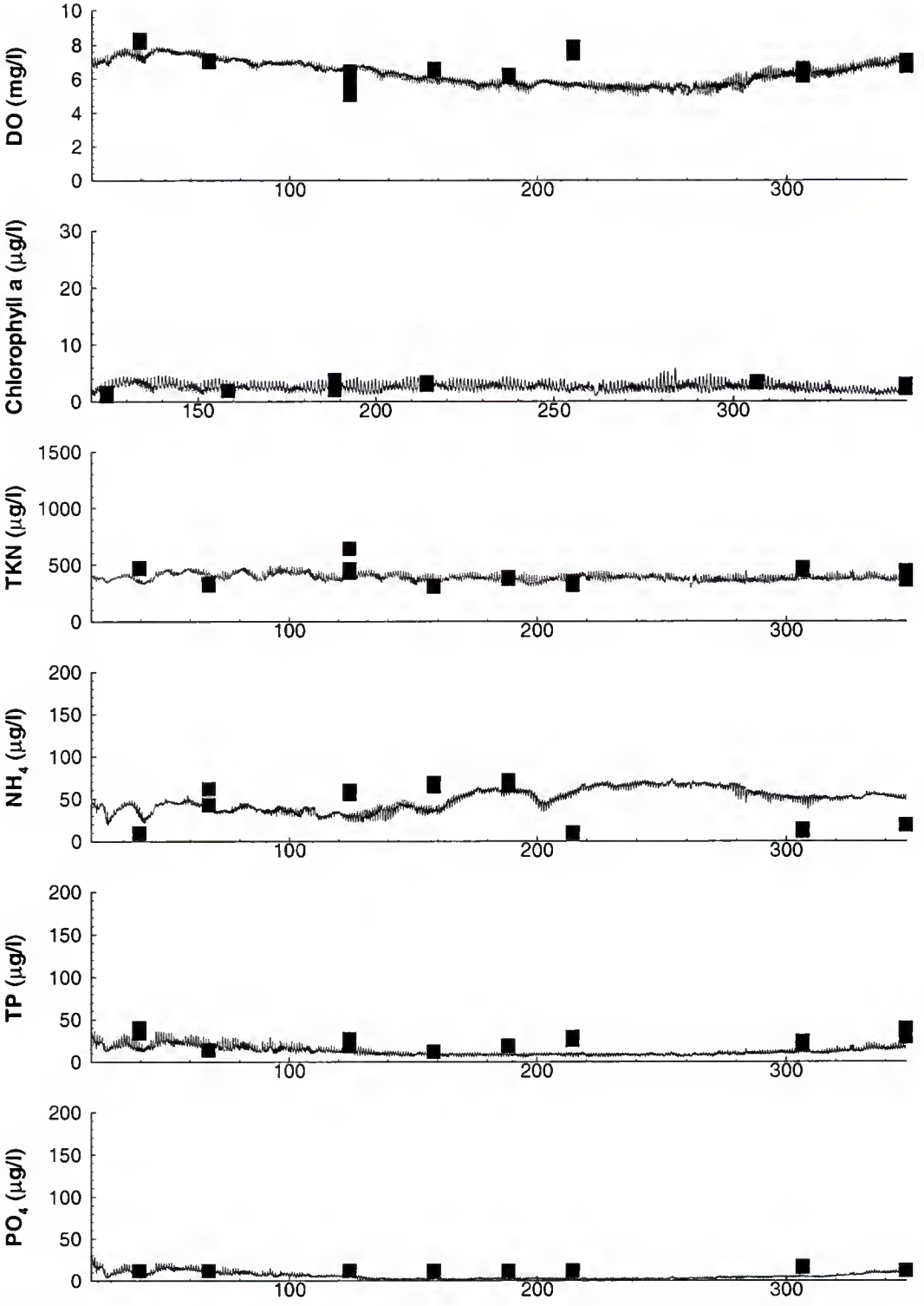

Figure 6.39 Temporal water quality variations at CH013 station in 2000.

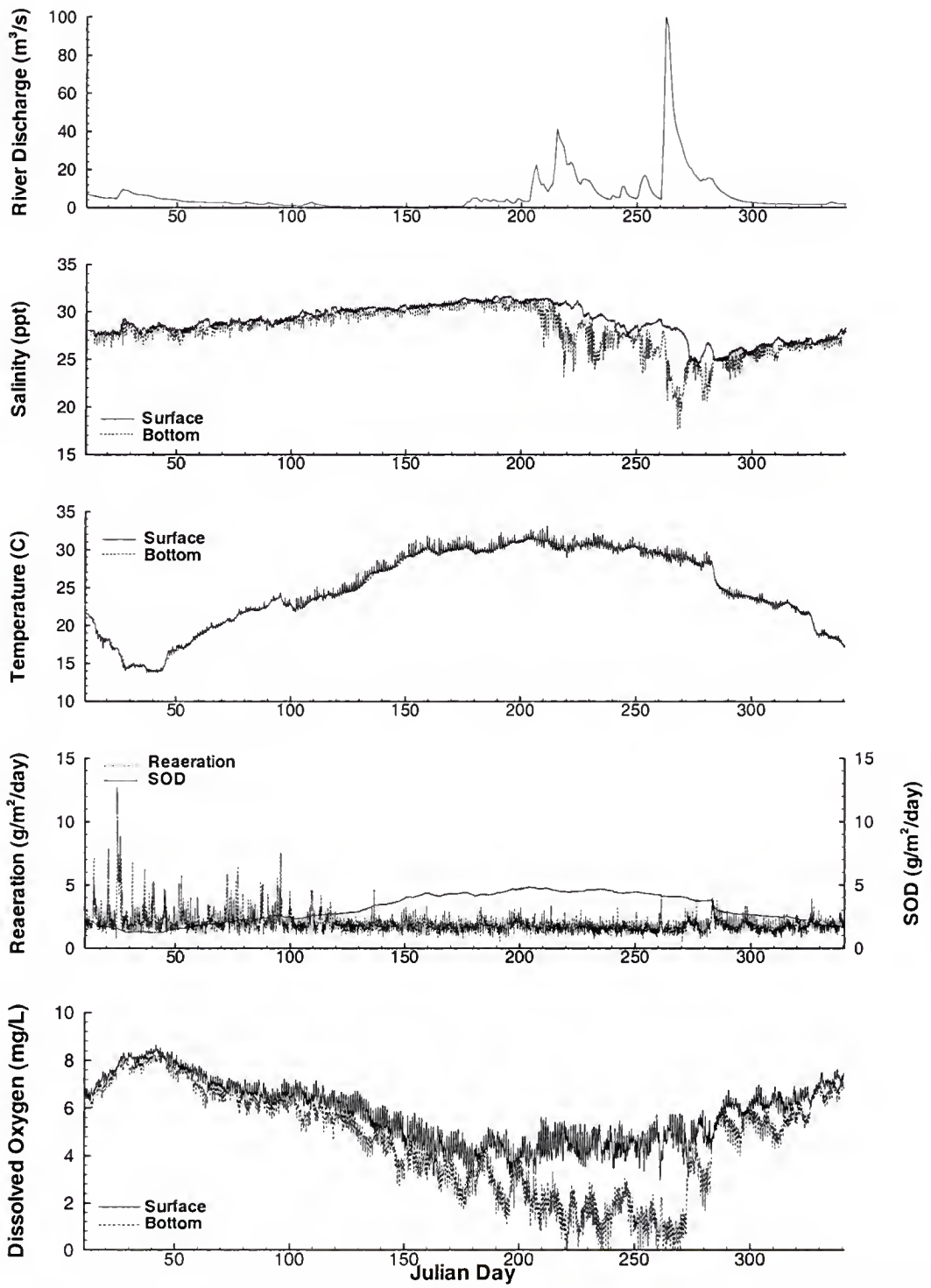

Figure 6.40 The comparison between simulated dissolved oxygen concentration and the possible causes of hypoxia: river discharge, salinity, temperature, and re-aeration and SOD fluxes at CH006 water quality measurement station.

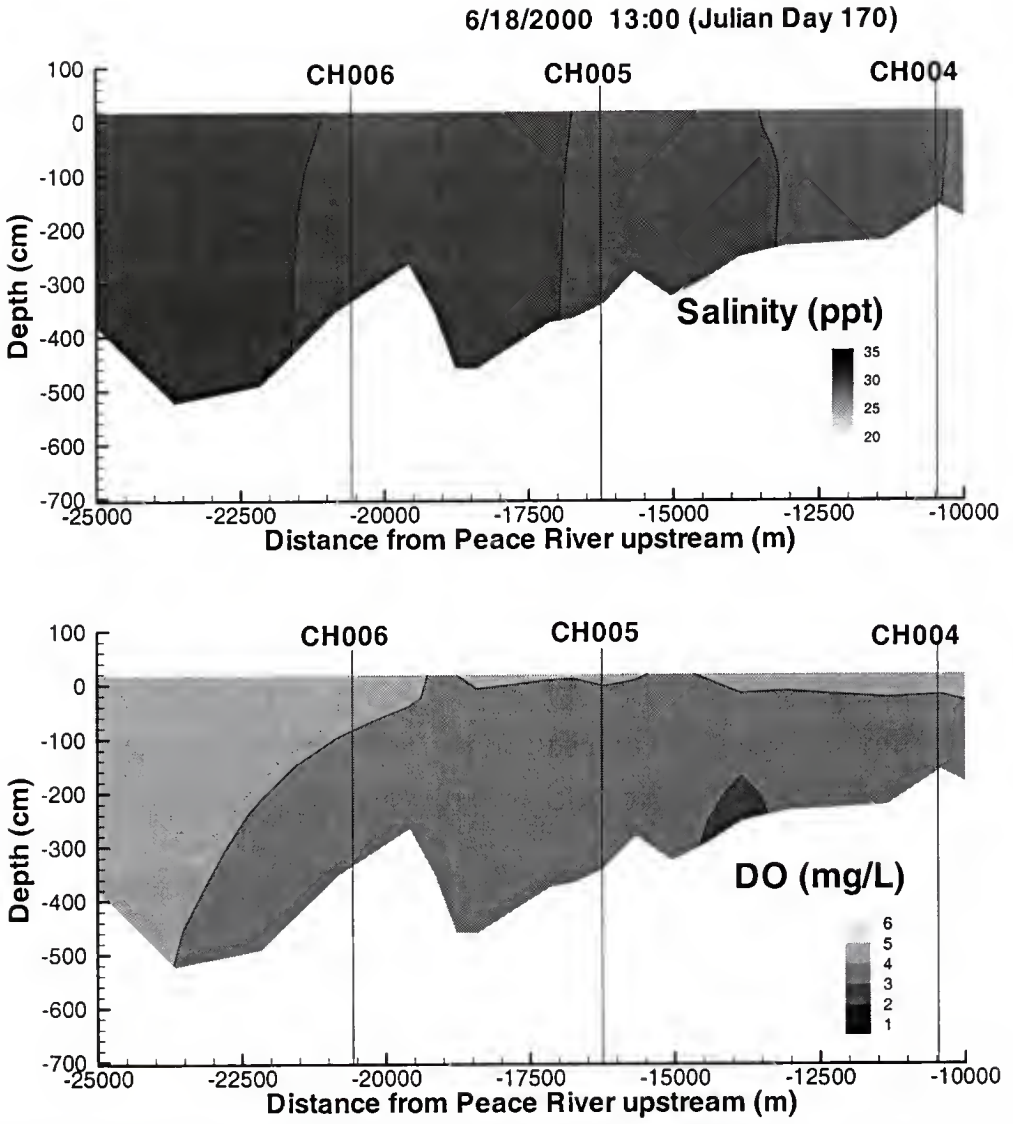

Figure 6.41 Simulated longitudinal-vertical salinity and dissolved oxygen concentration along the Peace River at 1 pm on June 18 (Julian Day 170), 2000.

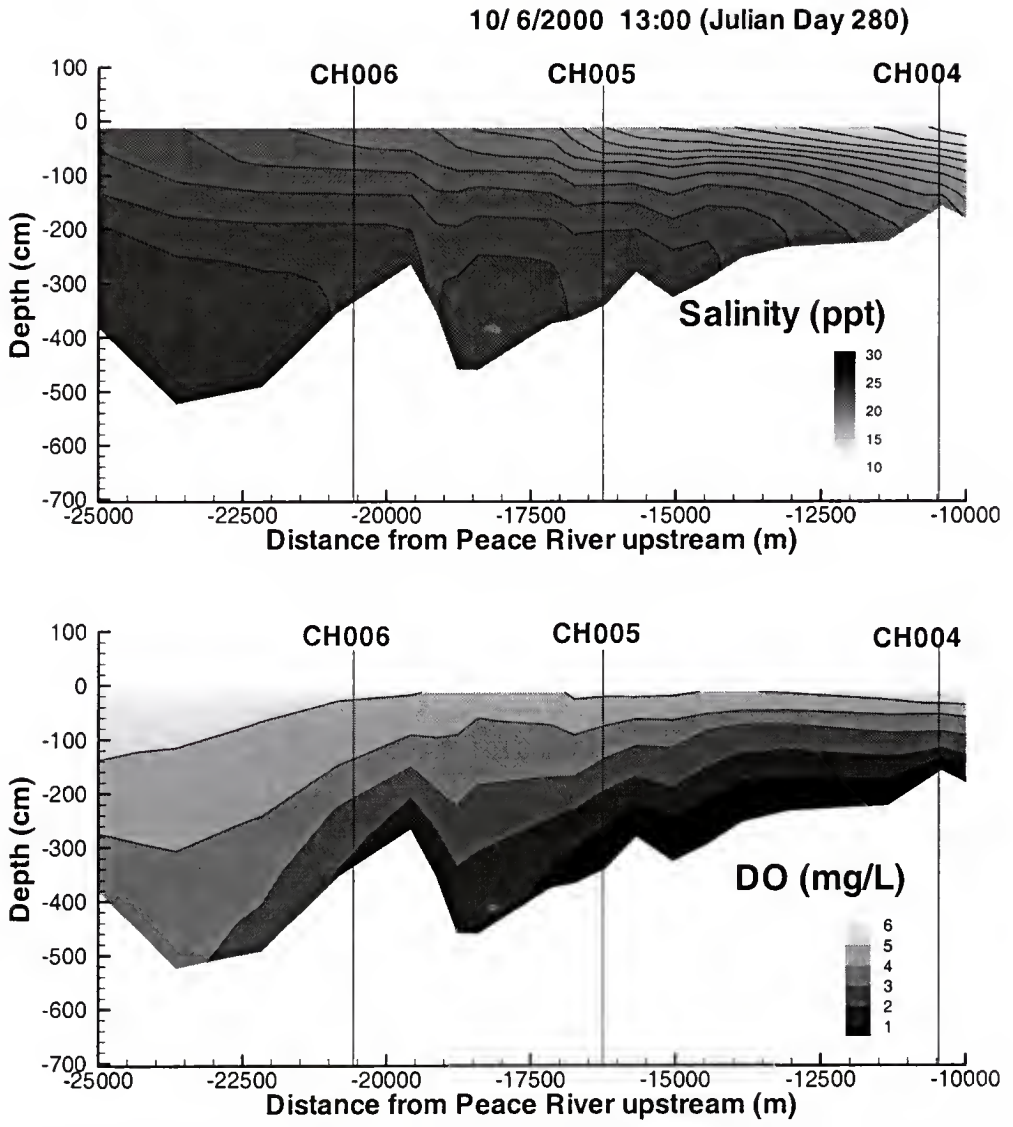

Figure 6.42 Simulated longitudinal-vertical salinity and dissolved oxygen concentration along the Peace River at 1 pm on October 6 (Julian Day 280), 2000.

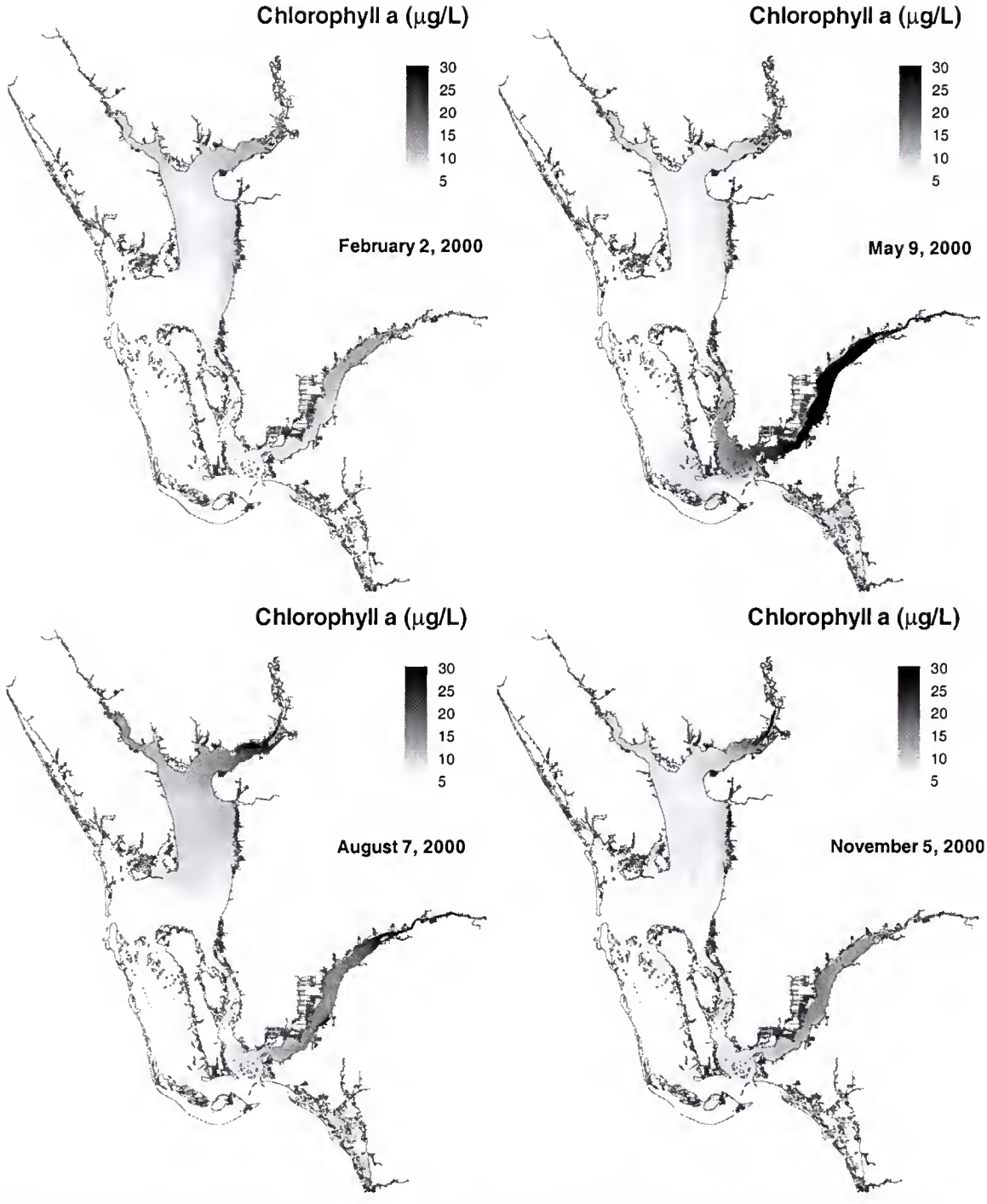

Figure 6.43 Simulated near-surface chlorophyll_a concentration in Charlotte Harbor estuarine system on February 9, May 9, August 7, and November 5, 2000.

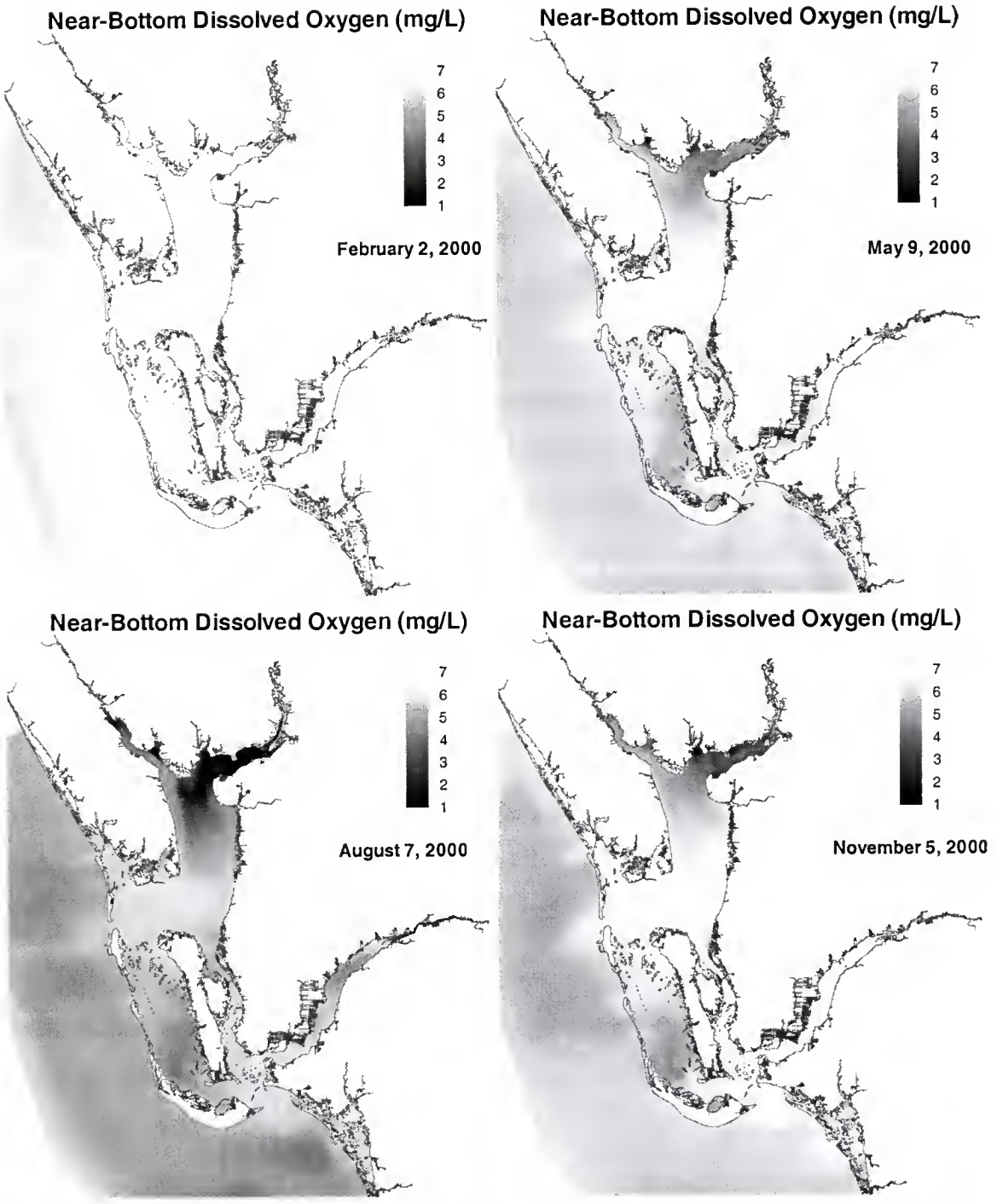

Figure 6.44 Simulated near-bottom dissolved oxygen concentration in Charlotte Harbor estuarine system on February 9, May 9, August 7, and November 5, 2000.

6.4.3 Application of 2000 Water Quality Simulations

Hydrologic alteration

The hydrodynamic and water quality models of the Charlotte Harbor estuarine system have been successfully developed and validated. The models can be used to address the effect of hydrologic alteration on the water quality as shown in Chapter 5. Using the validated water quality model, we performed several model simulations with the causeway islands removed and with the IntraCoastal Waterway removed during April 9 to June 10, 2000. The results are compared with those under existing conditions with both of them in place. The scenarios and stations for comparison are the same as those for comparison of flow and salinity in Chapter 5.

The chlorophyll_a concentrations for both cases were compared with those for the baseline simulation in Figure 6.45. The results at all three stations show that chlorophyll_a concentration is not noticeably affected by the absence of Intracoastal Waterway (NICW case) or the causeway (NSC case). Just like the chlorophyll_a concentration, the other water quality species do not show much effect by these hydrologic alterations.

To quantify the effect of these hydrologic alterations on the spatial distribution of water quality species, the snapshots of chlorophyll_a and dissolved ammonium nitrogen concentrations for these two cases were compared with those for the baseline simulation in Figures 6.46 and 6.47. There is not noticeable impact on the water quality species distribution in the San Carlos Bay area, consistent with the negligible effect of hydrologic alteration on flow and salinity in Chapter 5.

Table 6.6 shows the temporal average water quality species concentrations at the eleven comparison stations for the baseline run. Results of the hydrologic alteration cases

were compared to the baseline results and RMS differences calculated, then normalized with these averaged water quality species concentration in Table 6.6. Normalized RMS differences of water quality species concentrations for the no causeway case from April to June, 2000 are shown in Table 6.7. Table 6.8 shows the normalized RMS differences for the no ICW case, while Table 6.9 shows the normalized RMS differences when both the causeway islands and the ICW are removed. The RMS differences are less than 2% at all selected stations for hydrologic alteration. Therefore, it can be concluded that neither the causeway islands nor the Intracoastal Waterway had noticeable effect on the water quality in the San Carlos Bay and Pine Island Sound area.

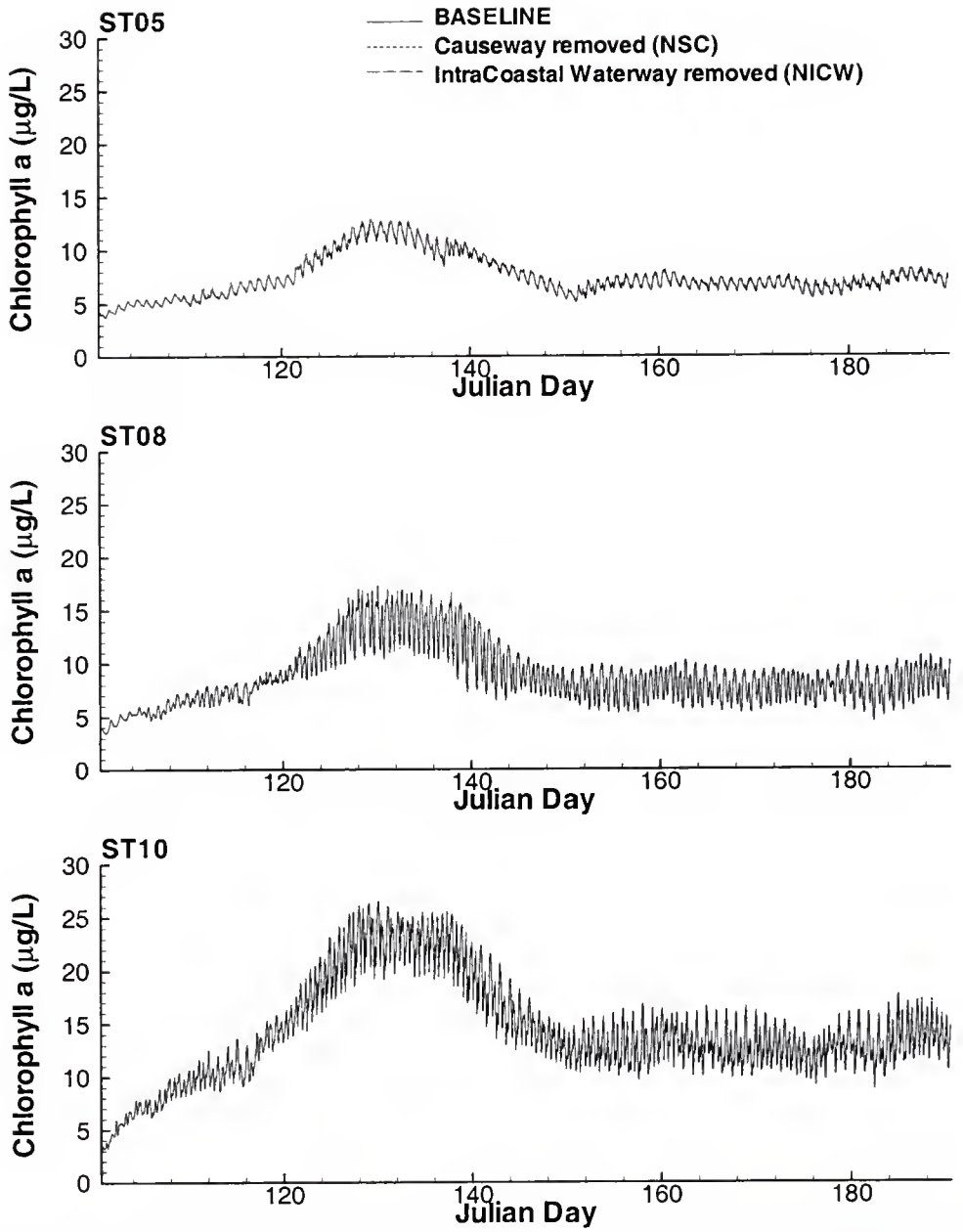

Figure 6.45 Comparisons of simulated surface chlorophyll_a concentration for three cases at three selected stations: ST05 (Pine Island Sound), ST08 (San Carlos Bay), and ST10 (Caloosahatchee River mouth)

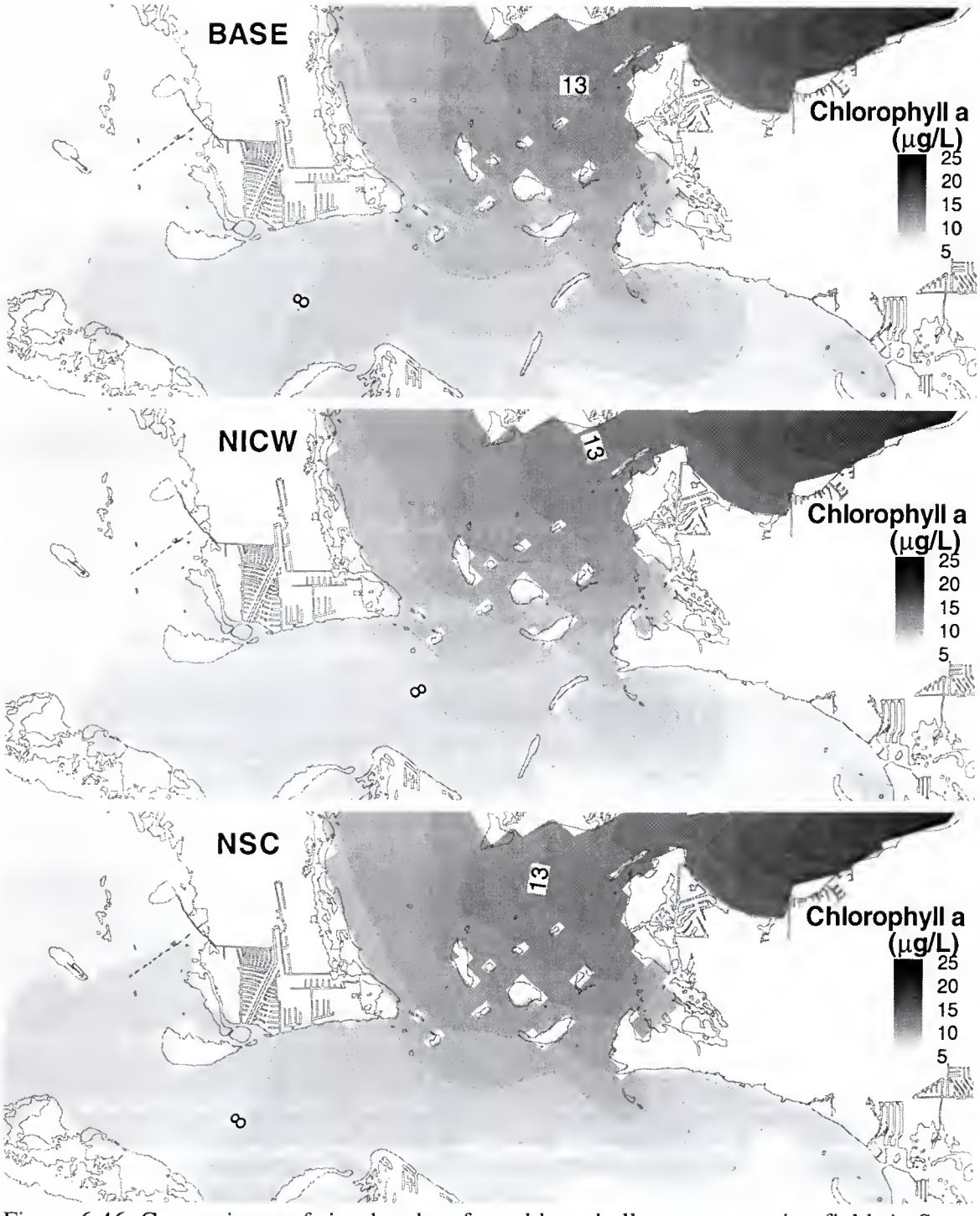

Figure 6.46 Comparisons of simulated surface chlorophyll_a concentration fields in San Carlos Bay after 90 days of simulation for three cases.

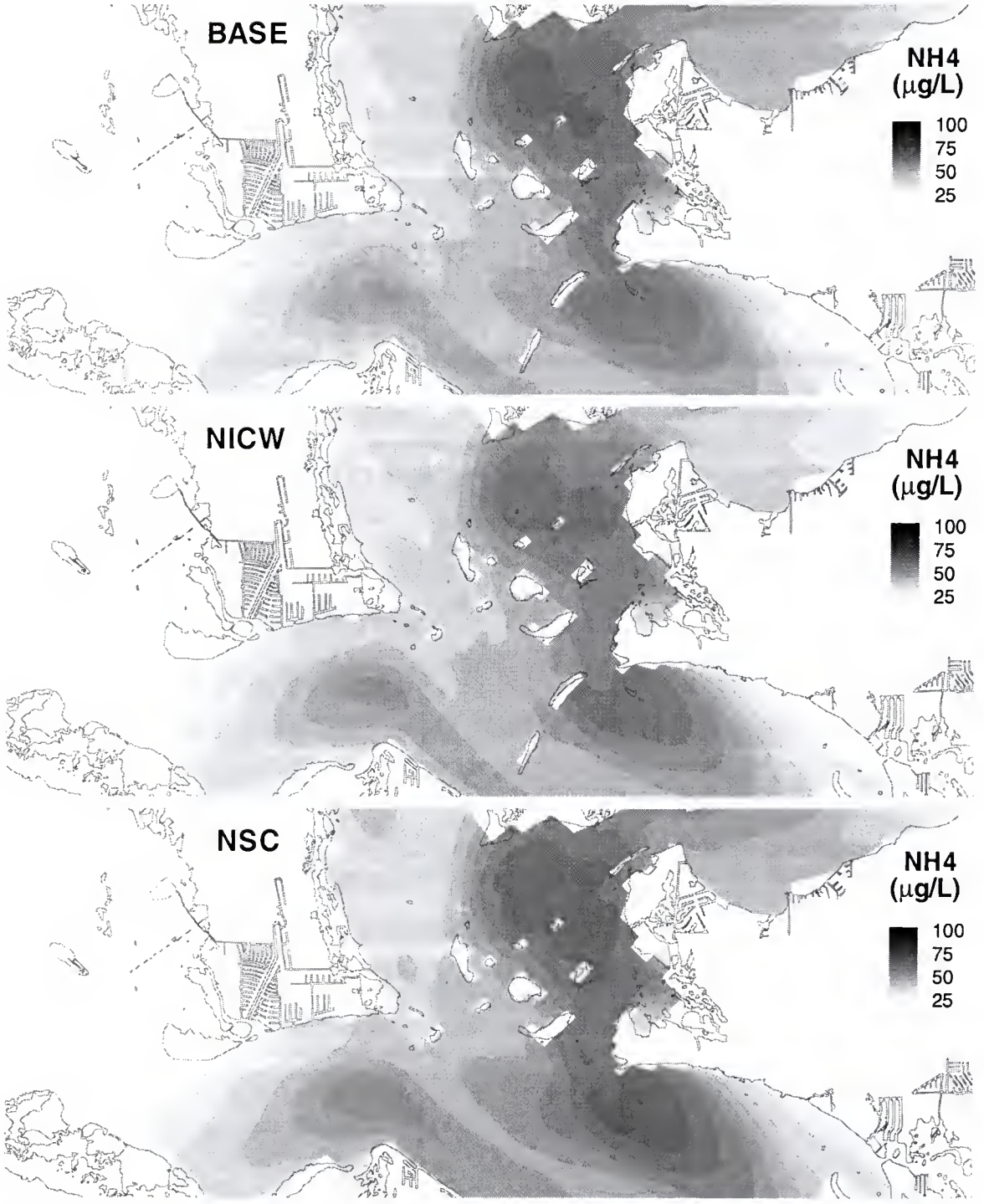

Figure 6.47 Comparisons of simulated surface dissolved ammonium nitrogen (NH4) concentration fields in San Carlos Bay after 90 days simulation for three cases.

Table 6.6 The temporally averaged water quality species concentrations for the baseline 2000 simulation.

Station number	ChlA (mg/L)	DO (mg/L)	NH4 (μg/L)	NOX (μg/L)	TKN (μg/L)	PO4 (μg/L)	PHOST (μg/L)	TOC (mg/L)
1	6.04	6.39	99.53	31.69	728.98	9.11	103.50	1.61
2	6.51	6.39	103.06	29.60	765.36	9.62	105.38	1.68
3	7.28	6.46	101.99	27.46	763.13	9.63	110.97	1.69
4	9.14	6.50	103.79	24.03	784.51	9.69	141.30	2.07
5	7.37	6.18	115.69	26.32	864.87	10.60	90.78	2.35
6	7.59	6.33	110.88	25.46	839.52	10.39	109.21	1.97
7	7.24	6.40	107.63	26.88	809.50	10.10	108.62	1.79
8	8.57	6.48	103.77	22.69	785.02	10.35	116.44	1.92
9	11.10	6.50	103.05	20.03	787.49	9.61	145.89	2.72
10	13.71	6.44	101.44	15.66	784.27	9.35	148.24	3.85
11	10.14	6.38	100.42	16.16	771.49	11.44	117.82	2.38
AVG	8.61	6.40	104.66	24.18	789.47	9.99	118.01	2.18

Table 6.7 Normalized RMS differences of water quality species concentrations at 11 stations during April to June 2000, showing the effect of no causeway islands.

Station number	ChlA (%)	DO (%)	NH4 (%)	NOX (%)	TKN (%)	PO4 (%)	PHOST (%)	TOC (%)
1	0.27	0.25	0.83	1.33	1.36	0.26	1.58	0.24
2	0.37	0.28	1.17	1.16	1.91	0.29	1.29	0.27
3	0.65	0.24	0.83	1.56	1.36	0.39	1.9	0.34
4	0.85	0.24	1.04	0.58	1.77	0.21	2.25	0.31
5	0.58	0.68	1.35	1.14	2.55	0.45	2.2	0.55
6	0.47	0.43	1.15	1.19	2.02	0.33	1.95	0.3
7	0.44	0.32	1.15	1.17	1.95	0.25	1.62	0.23
8	0.5	0.27	0.94	1.59	1.46	0.4	2.22	0.41
9	0.93	0.2	0.9	0.41	1.54	0.2	1.93	0.39
10	0.76	0.18	0.74	0.29	1.23	0.15	1.44	0.36
11	0.33	0.24	1.09	1.22	1.44	0.28	1.39	0.25
AVG	0.56	0.3	1.02	1.06	1.69	0.29	1.8	0.33

Table 6.8 Normalized RMS differences of water quality species concentrations at 11 stations during April to June 2000, showing the effect of no ICW.

Station number	ChlA (%)	DO (%)	NH4 (%)	NOX (%)	TKN (%)	PO4 (%)	PHOST (%)	TOC (%)
1	0.28	0.05	0.12	0.42	0.24	0.11	0.46	0.13
2	0.33	0.08	0.23	0.65	0.38	0.11	0.33	0.19
3	0.34	0.08	0.18	0.41	0.33	0.22	0.63	0.19
4	0.97	0.12	0.37	0.75	0.41	0.24	1.89	0.37
5	0.37	0.30	0.44	1.13	0.75	0.16	0.53	0.49
6	0.52	0.19	0.39	1.16	0.59	0.16	0.53	0.35
7	0.46	0.12	0.34	0.95	0.51	0.14	0.56	0.26
8	0.50	0.17	0.24	0.38	0.47	0.37	0.84	0.30
9	1.39	0.20	0.62	0.86	0.51	0.29	2.67	0.68
10	1.51	0.41	0.74	0.82	0.68	0.51	5.31	2.11
11	0.48	0.13	0.32	0.41	0.56	0.26	1.03	0.41
AVG	0.65	0.17	0.36	0.72	0.49	0.23	1.34	0.50

Table 6.9 Normalized RMS differences of water quality species concentrations at 11 stations during April to June 2000, showing the effect of no causeway island and ICW

Station number	ChlA (%)	DO (%)	NH4 (%)	NOX (%)	TKN (%)	PO4 (%)	PHOST (%)	TOC (%)
1	0.40	0.27	0.95	1.69	1.36	0.26	1.30	0.30
2	0.39	0.34	1.39	1.77	2.11	0.30	1.33	0.39
3	0.72	0.28	0.96	1.89	1.25	0.43	1.46	0.40
4	0.57	0.24	1.34	1.24	1.47	0.30	1.69	0.39
5	0.40	0.93	1.77	2.18	3.23	0.54	2.58	0.97
6	0.42	0.59	1.51	2.22	2.43	0.39	2.19	0.59
7	0.40	0.42	1.44	2.01	2.23	0.26	1.75	0.42
8	0.69	0.38	1.03	1.96	1.12	0.48	2.06	0.52
9	1.07	0.23	1.42	1.15	1.17	0.35	1.80	0.74
10	1.40	0.35	1.36	0.89	0.75	0.50	4.28	2.19
11	0.47	0.30	1.26	1.58	0.86	0.37	0.75	0.32
AVG	0.63	0.39	1.31	1.69	1.63	0.38	1.93	0.66

River load reduction

To provide a tool for studying management options and corresponding responses of the Charlotte Harbor estuarine system, which is one of the primary objectives of this study, the validated integrated model was used to evaluate the effectiveness of load reductions for improving estuarine water quality. To achieve this goal, it is necessary to use a common set of initial conditions for the water column and the sediments so that any differences observed between the results of different load reduction simulations would be attributable to the differences in load reduction. To analyze the potential impact of reduced nutrient loadings to the system, model simulations were carried out using 100% load reductions of nitrogen species concentrations, 100% load reductions of phosphorous species concentrations, and 100% load reduction of nitrogen and phosphorous species concentrations at Peace River and Caloosahatchee River.

One major assumption in the load reduction runs is that the SOD values are assumed to be the same as the baseline run. This is because the fact that SOD values for the baseline run were provided from field experiments and the model's inability to directly related the SOD values inside estuary to nutrient loading from the rivers. Hence the results presented in the following should be interpreted with caution, since large errors may be associated with the above assumption. In particular, since the SOD values are unchanged, load reduction is not expected to produce any improvement in hypoxia, hence the DO results are practically unchanged in the model results. In reality, load reduction is expected to lead to increased DO.

For the Peace River load reduction simulations, CH004 and CH006 stations are selected to compare the water quality species before and after load reduction. Figures 6.48

and 6.49 show the water quality species at CH004 and CH006 before and after 100% nitrogen load reduction. Due to reduction of nitrogen loading, the chlorophyll_a concentration decreased at both stations because the reduction of dissolved ammonium nitrogen as the limiting factor for phytoplankton. The amount of the decrease was 12 μg/L at the CH004 station and 4 μg/L at the CH006 station. The dissolved oxygen concentration is little decreased at the CH004 station because the amount of dissolved oxygen from photosynthesis is reduced due to decreasing of phytoplankton biomass, while those from re-aeration and SOD fluxes remained the same as the baseline simulation.

Figures 6.50 and 6.51 show the water quality species at CH004 and CH006 before and after 100% phosphorous load reduction from the Peace River. The chlorophyll_a concentrations decreased at both stations. The phytoplankton food limiting factor is changed to soluble reactive phosphorous after SRP concentration reached to less than phosphorous half saturation rate. The amounts of decrease 8 μg/L at CH004 station and 4 μg/L at CH006 station were smaller than those for 100% nitrogen load reductions. Dissolved ammonium nitrogen concentration was increased because phytoplankton consumed a smaller amount of NH4 concentration, as phytoplankton food limit was decreased by SRP concentration.

For the Caloosahatchee River load reduction, CES02 and CES08 stations are selected to compare the water quality species before and after load reduction. Figures 6.52 to 6.53 show the water quality species at CES02 and CES08 before and after 100% nitrogen load reduction, while Figures 6.54 to 6.55 show the corresponding results for 100% phosphorous load reduction. With reduction of nitrogen or phosphorous loading, the chlorophyll_a concentration decreased at CES02 while there is no significant difference at CES08. The Chlorophyll_a concentration at CES02 reached 94 μg/L due to large amount of chlorophyll_a

from the river loading. Most of the water quality species are strongly affected by the loading from Caloosahatchee River, as shown in the results at these two stations. The impacts resulting from load reductions were confined in Caloosahatchee River and became insignificant once outside the Caloosahatchee River.

As mentioned earlier, dissolved oxygen concentration was relatively unaffected by the loading reduction because the SOD kinetic process used in water quality model is an empirical formula which is a function of temperature, dissolved oxygen, and sediment type. Sediment oxygen demand (SOD) depends on the deposition and decomposition of organic matter on the seabed, and the exchange of nutrients and oxygen across the sediment-water interface. To provide detailed trends in hypoxia in response to organic loads, it is necessary to apply sediment flux model (DiToro and Fitzpatrick, 1993) with observed data for CH_4, H_2S, and organic matter in sediment column and river boundary as described in Figure 4.4. Although applying of sediment flux model provides rational predictions of sediment response to environmental alterations, it requires additional information as compared to the use of empirical SOD model.

Without any available data, the sediment flux model was tested for organic matter river load reduction in Peace River using DiToro's method described in Appendix F. Figure 6.56 shows the comparison of chlorophyll_a and dissolved oxygen concentrations at CH006 station between baseline and 100% organic matter loading reduction simulations. The result does not show much difference in dissolved oxygen concentrations between the baseline and 100% organic matter load reduction simulations, because SOD flux from methane and nitrogen calculated by the sediment flux model is not enough to create hypoxia in CH006. The measured total organic carbon concentration at CH006 is much lower than that at the

Peace River boundary (CH029). Therefore, the organic carbon concentration from Peace River does not reach to the hypoxia area (CH006). In the summer season, the dissolved oxygen concentration of the river load reduction scenario is even lower than that for the baseline simulation due to reduced chlorophyll_a concentration. Chlorophyll_a concentration from river loading in summer season is quickly reduced because of the nutrient load reduction from the river. The photosynthesis is decreased due to chlorophyll_a decrease, but CBOD is increased in the water column due to mortality of phytoplankton and settling to the sediment layer. This increase in CBOD will increase the SOD flux at the sediment-water interface.

The measured data show that total organic carbon concentration at CH006 was very low during the simulation period. Hence, the carbonaceous oxygen demand may not be a major factor of SOD flux in upper Charlotte Harbor. Sulfide flux could be a very important component of SOD in anoxic estuarine water (Chapra, 1997) such as the upper Charlotte Harbor. Hence, sulfide and iron fluxes should be included in the sediment flux model to better represent sediment oxygen demand for river load reduction simulations. In addition, more field data and modeling effort to determine sediment fluxes should be focused on the specific conditions of upper Charlotte Harbor, especially specifying the parameters for the sediment layer and the sediment-water interface.

To test the effect of reducing organic matter in river loading with current water quality model, the analysis of the potential impact of reduced organic matter loadings to the system was carried out by model simulations using 50% and 75% SOD load reductions at Peace River. Figure 6.57 shows the comparison of dissolved oxygen concentrations at CH004 and CH006 before and after 50% SOD reduction and 75% SOD reduction. The

dissolved oxygen concentration in the upper Charlotte Harbor is very sensitive with SOD reduction. With 50% SOD load reduction, the surface and bottom dissolved oxygen concentration are increased from maximum 2 mg/L to 0.2 mg/L. With 75% load reduction, no hypoxic event was found during this simulation and the dissolved oxygen distribution exhibit minimal vertical stratification. Although there is no hypoxia event, some localized low-levels of near-bottom dissolved oxygen and vertical stratification were maintained even during the 75% SOD load reduction scenario.

To quantify the relationship between SOD coefficient and hypoxia, the area which exposed in bottom water hypoxia condition (DO is less than 2 mg/L) was calculated with 0.5 (75% reduction), 1.0 (50% reduction), and 2.0 (baseline) rate constant of SOD at 20 °C during the simulation period (Figure 6.56). With 2.0 as the rate constant of SOD, over 60 km^2 of the upper Charlotte Harbor was hypoxic during the summer season, while hypoxia condition was not observed with 0.5 as the SOD rate constant. The maximum areal extent of hypoxia 67 km^2 was on August 21, 2000. This was also accompanied by a high degree of stratification as indicated in Figure 6.40.

With further scientific understanding, the integrated modeling approach would enable the development of a science-based management tool which is built on process-based understanding rather than simple regression. Subsequent refinement of this integrated model can be used to address ecosystem management issues such as controlling estuarine eutrophication and determining allowable external nutrient loading levels to restore water quality in estuarine system.

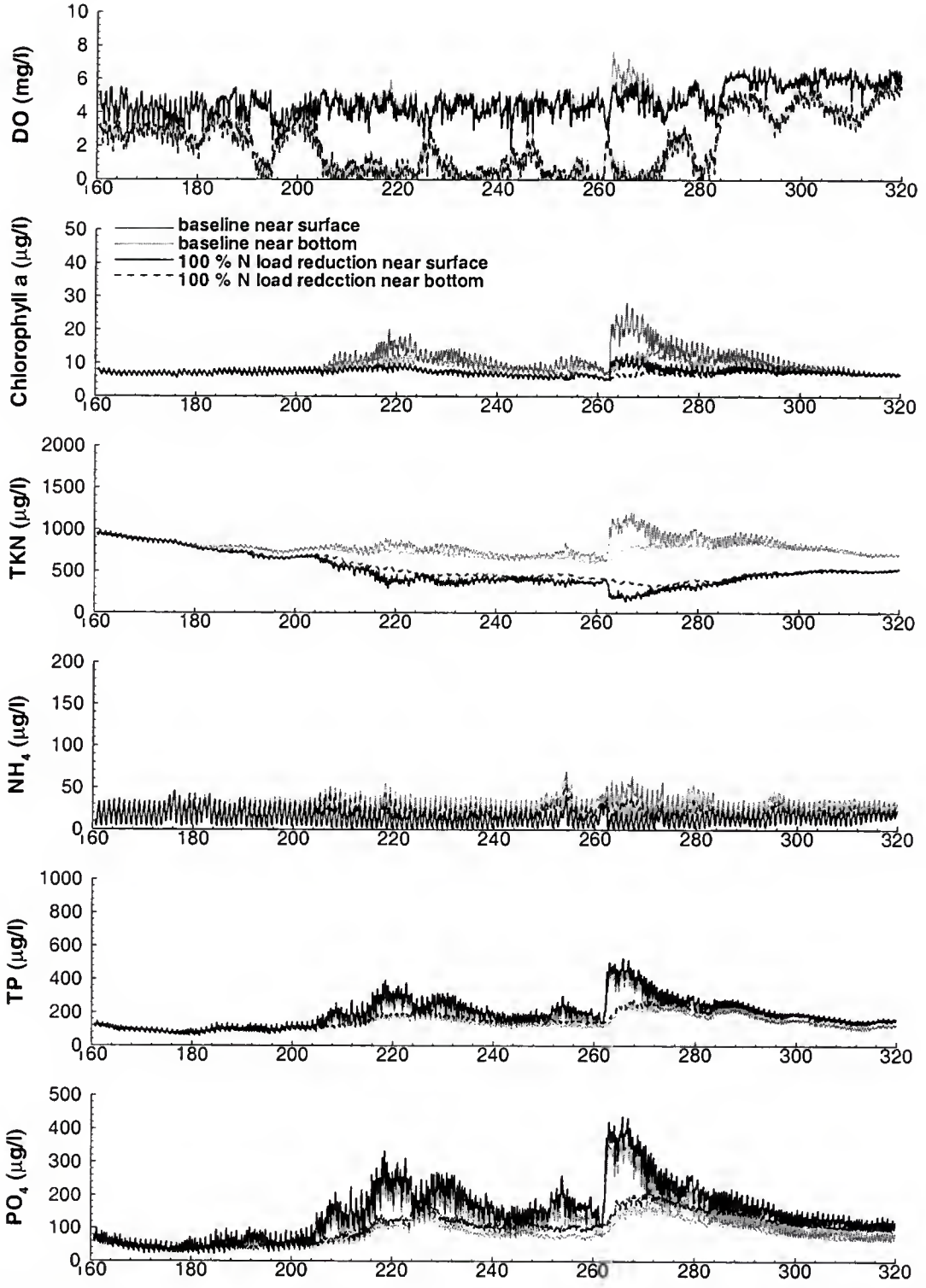

Figure 6.48 The water quality species concentrations at CH004 water quality measured station before and after 100 % nitrogen load reduction from the Peace River.

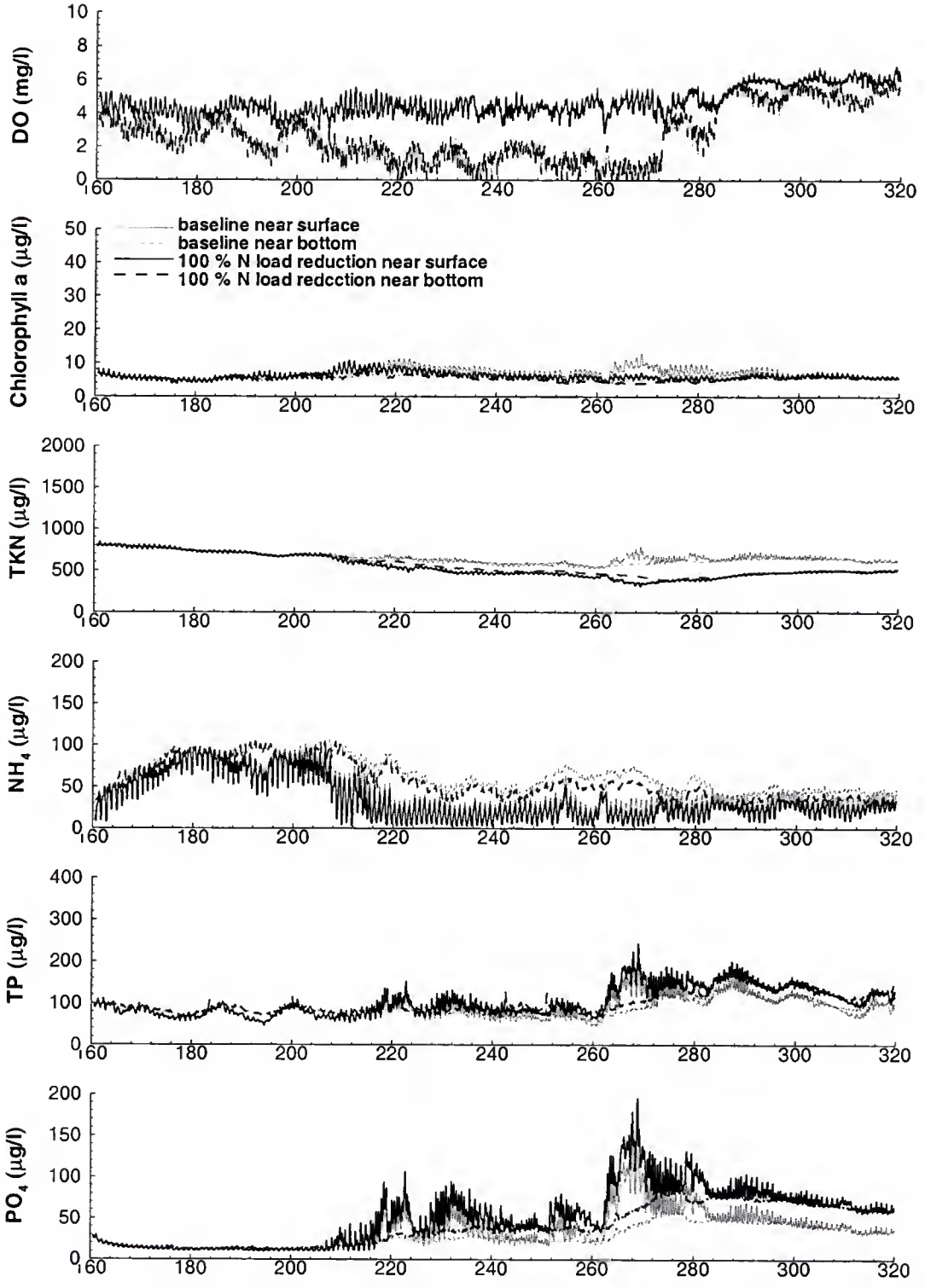

Figure 6.49 The water quality species concentrations at CH006 water quality measured station before and after 100 % nitrogen load reduction from the Peace River.

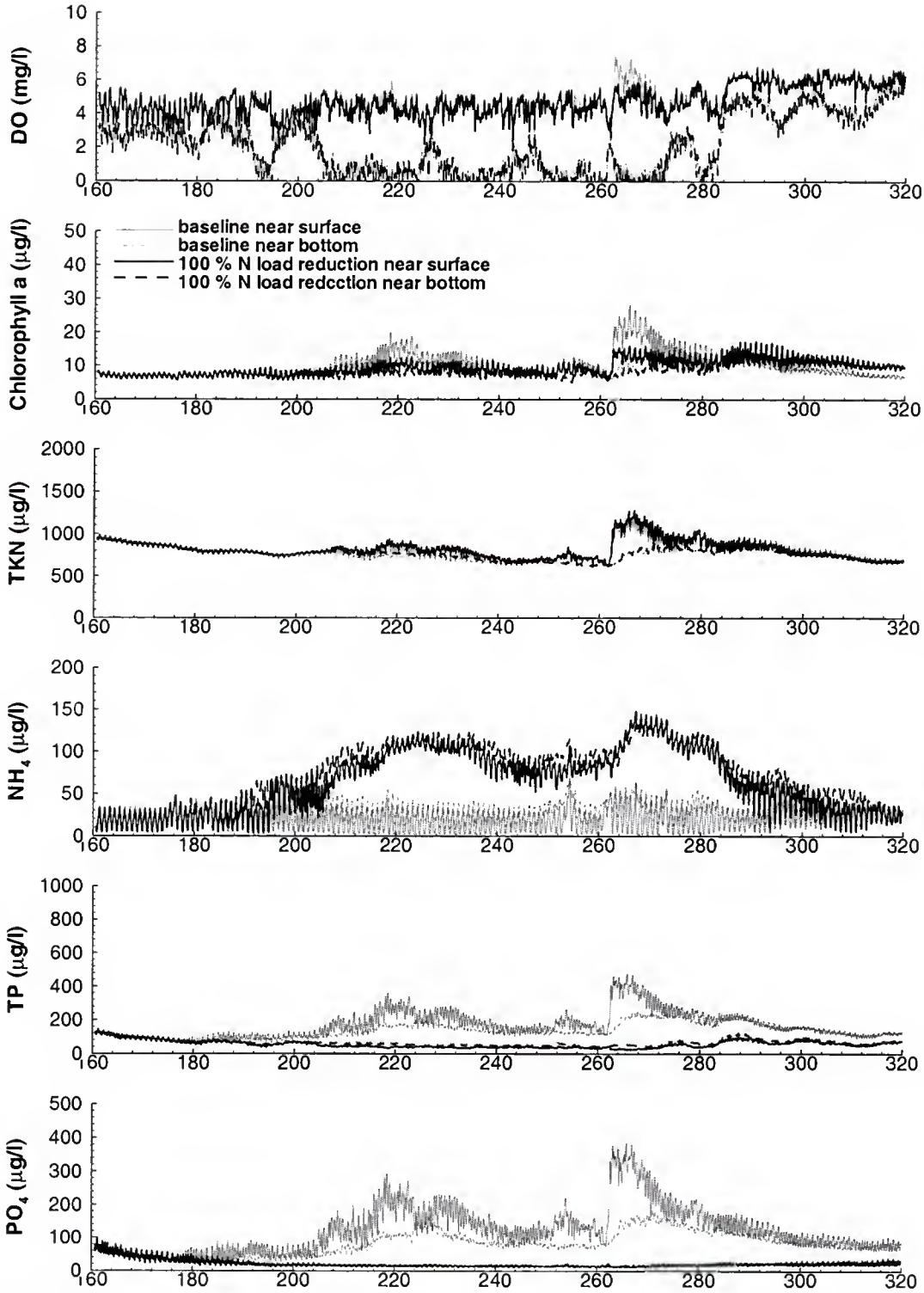

Figure 6.50 The water quality species concentrations at CH004 water quality measured station before and after 100 % phosphorous load reduction from the Peace River.

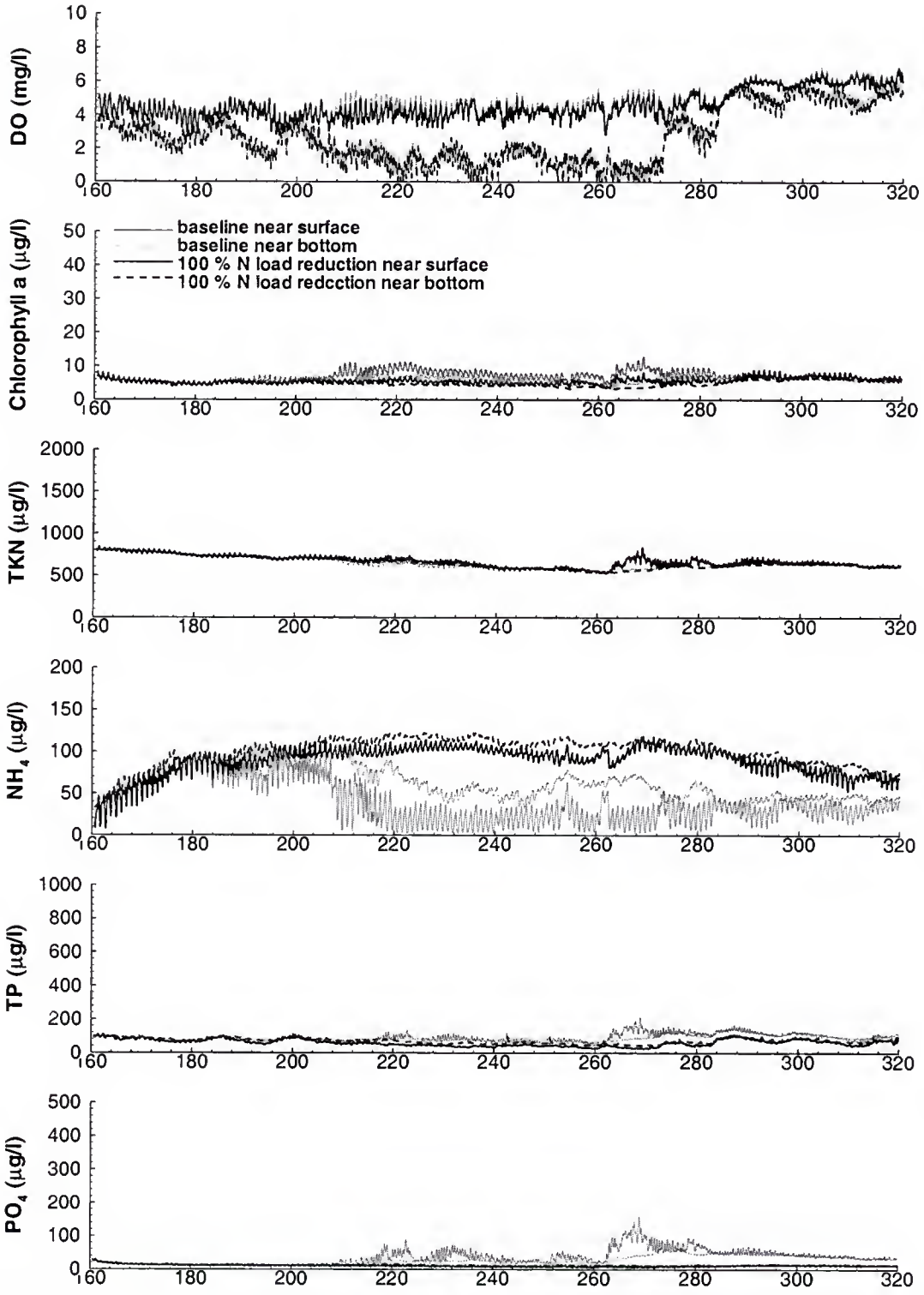

Figure 6.51 The water quality species concentrations at CH006 water quality measured station before and after 100 % phosphorous load reduction from the Peace River.

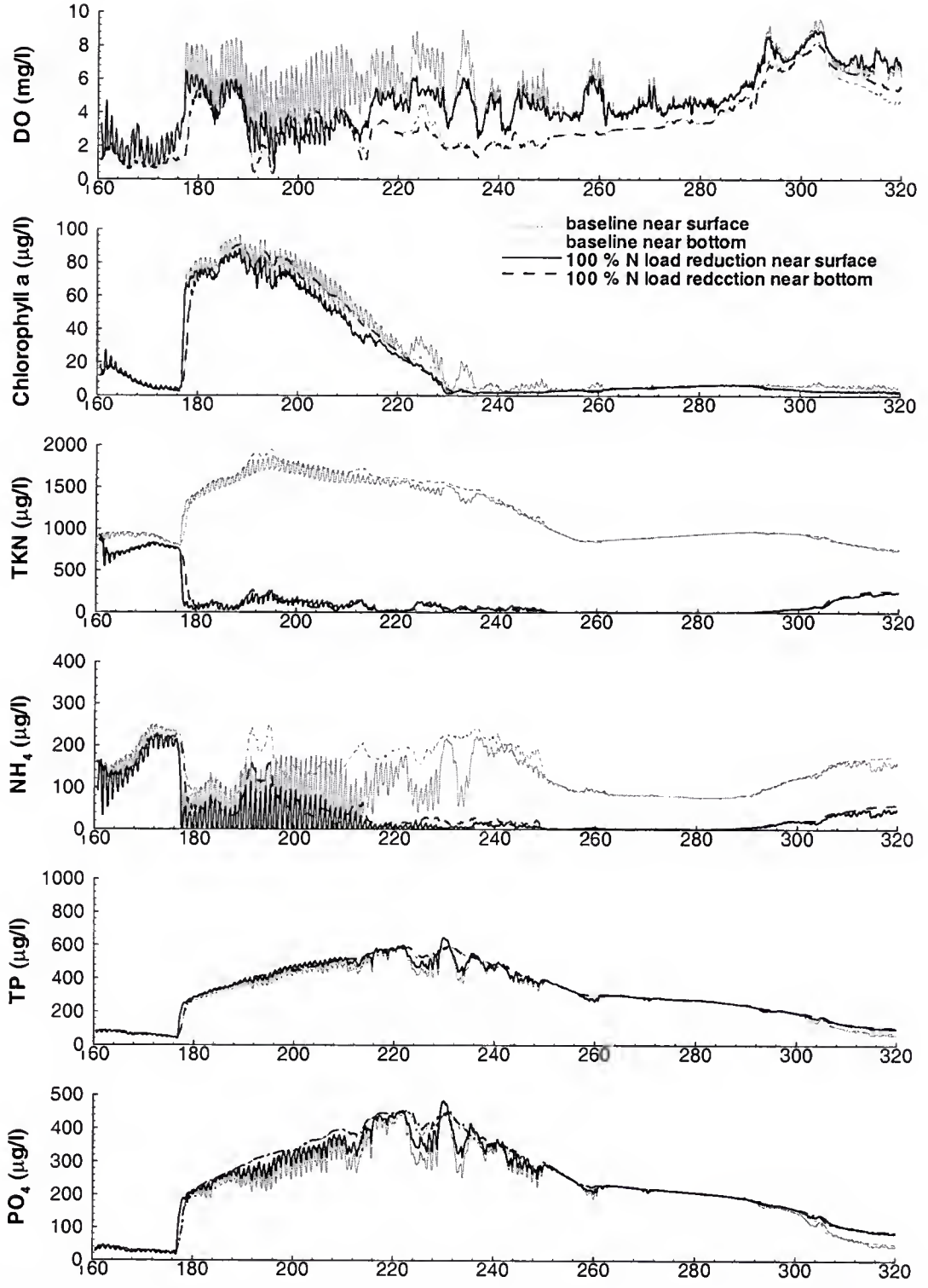

Figure 6.52 The water quality species concentrations at CES02 water quality measured station before and after 100 % nitrogen load reduction from Caloosahatchee River.

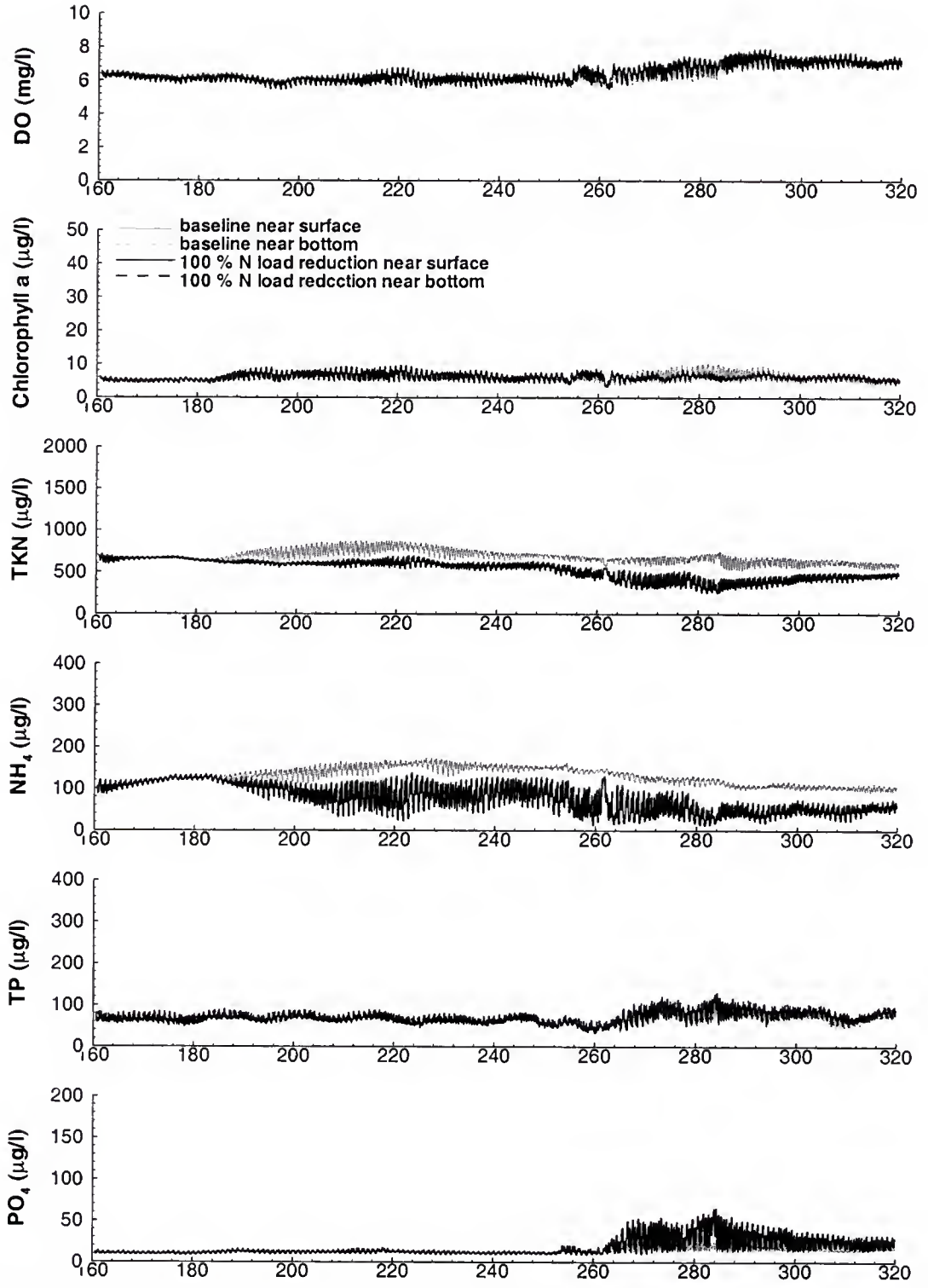

Figure 6.53 The water quality species concentrations at CES08 water quality measured station before and after 100 % nitrogen load reduction from Caloosahatchee River.

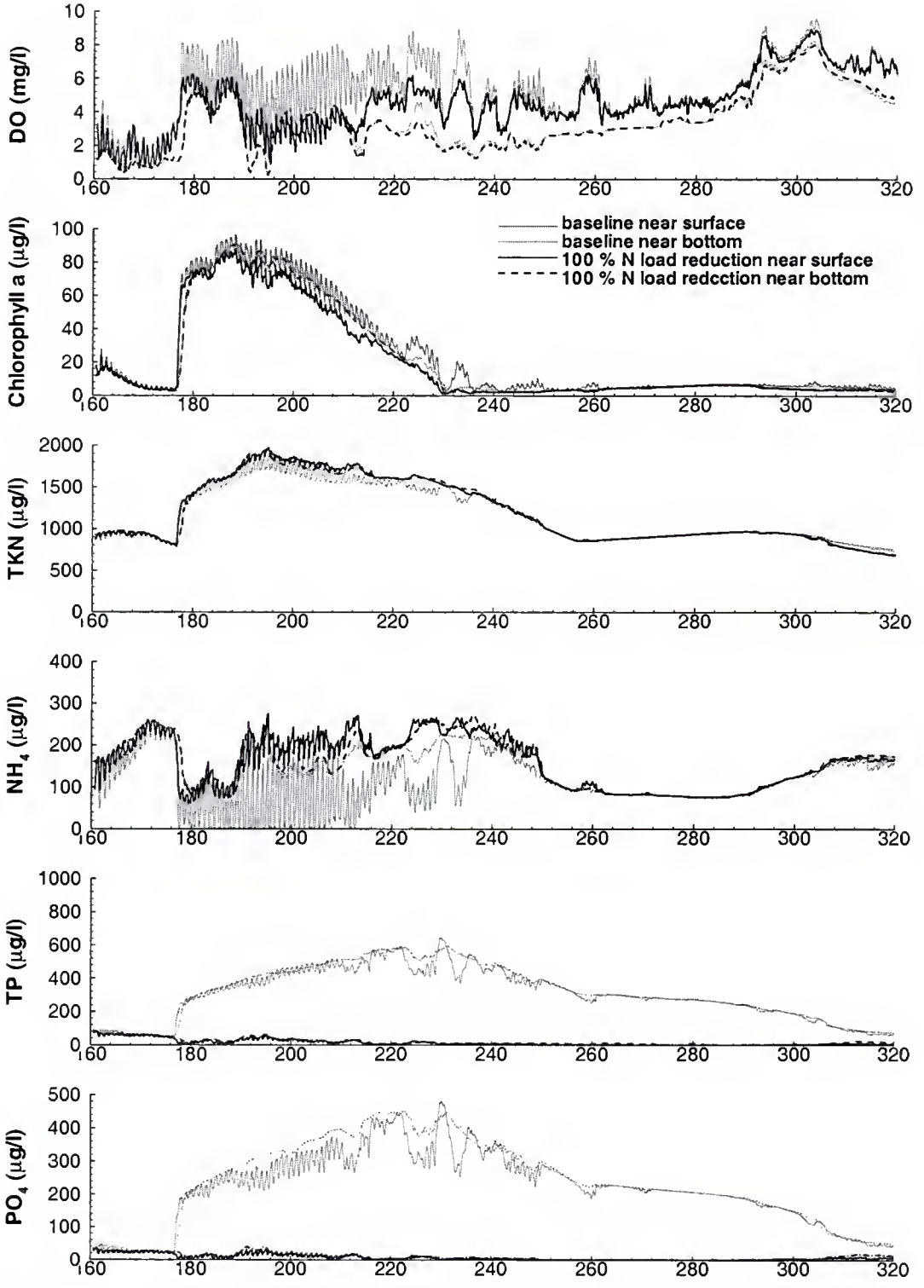

Figure 6.54 The water quality species concentrations at CES02 water quality measured station before and after 100 % phosphorous load reduction from Caloosahatchee River.

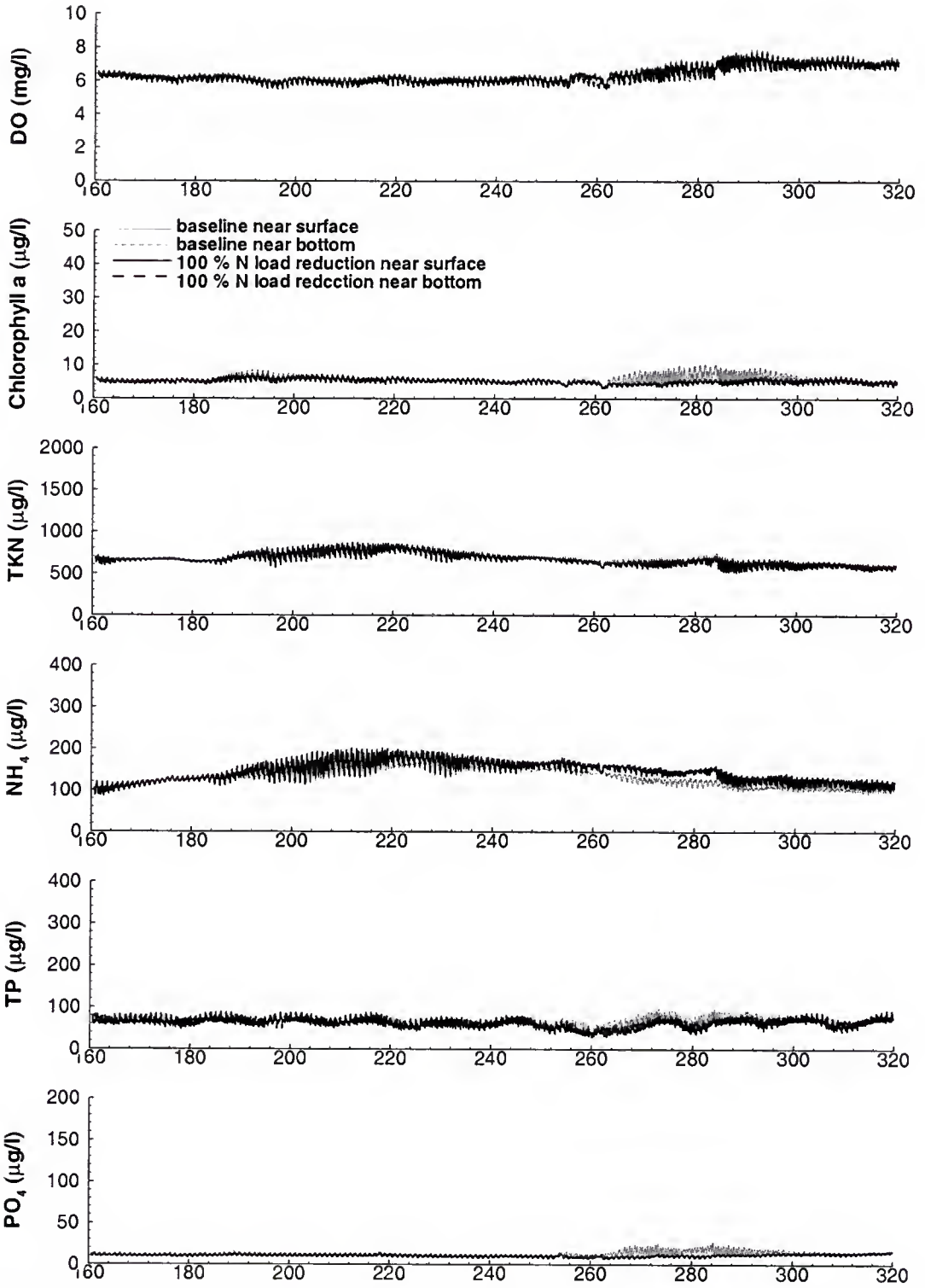

Figure 6.55 The water quality species concentrations at CES08 water quality measured station before and after 100 % phosphorous load reduction from Caloosahatchee River.

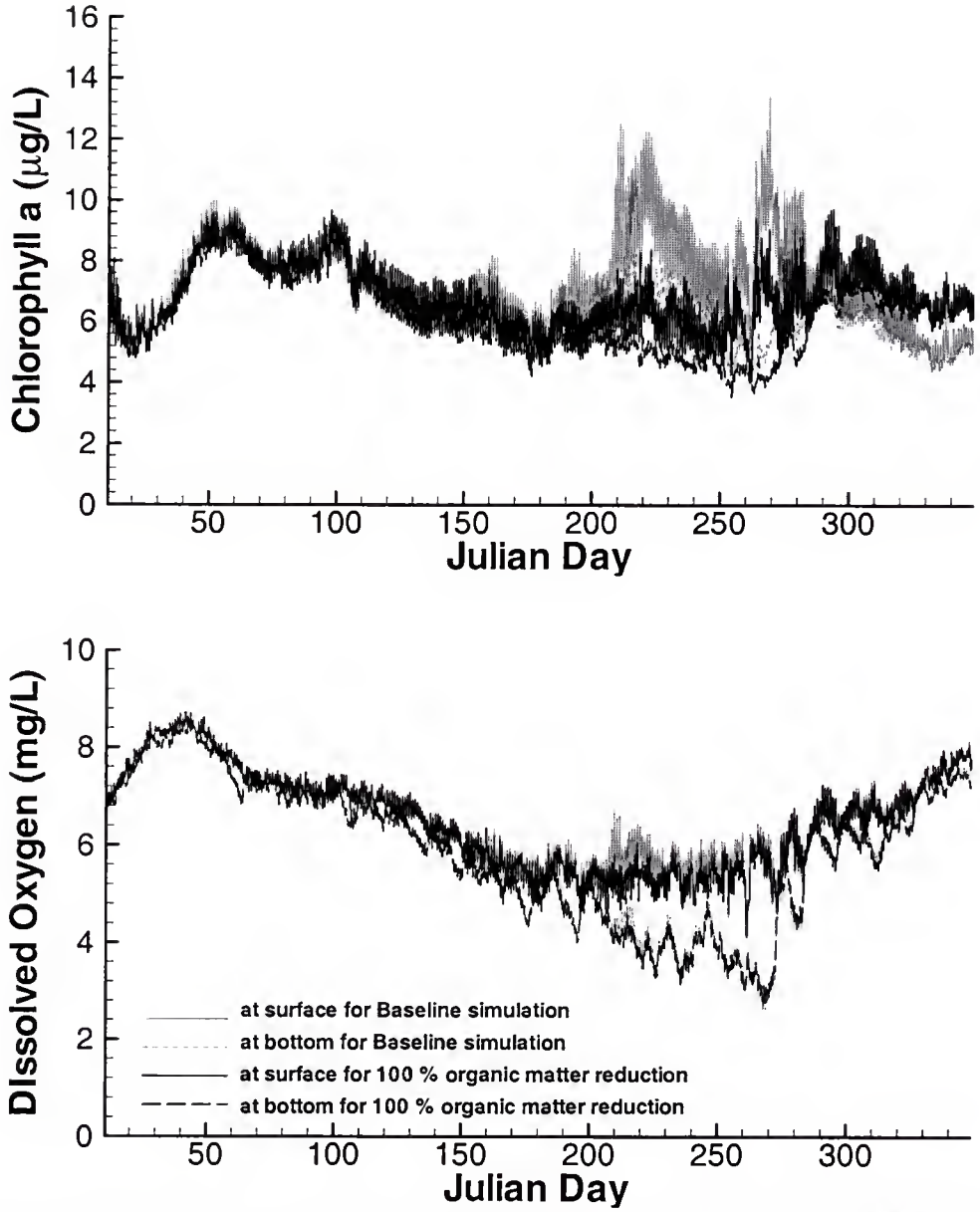

Figure 6.56 Dissolved oxygen and chlorophyll_a concentrations at CH006 water quality measured station before and after 100 % organic matter load reduction from Peace River using DiToro's sediment flux model.

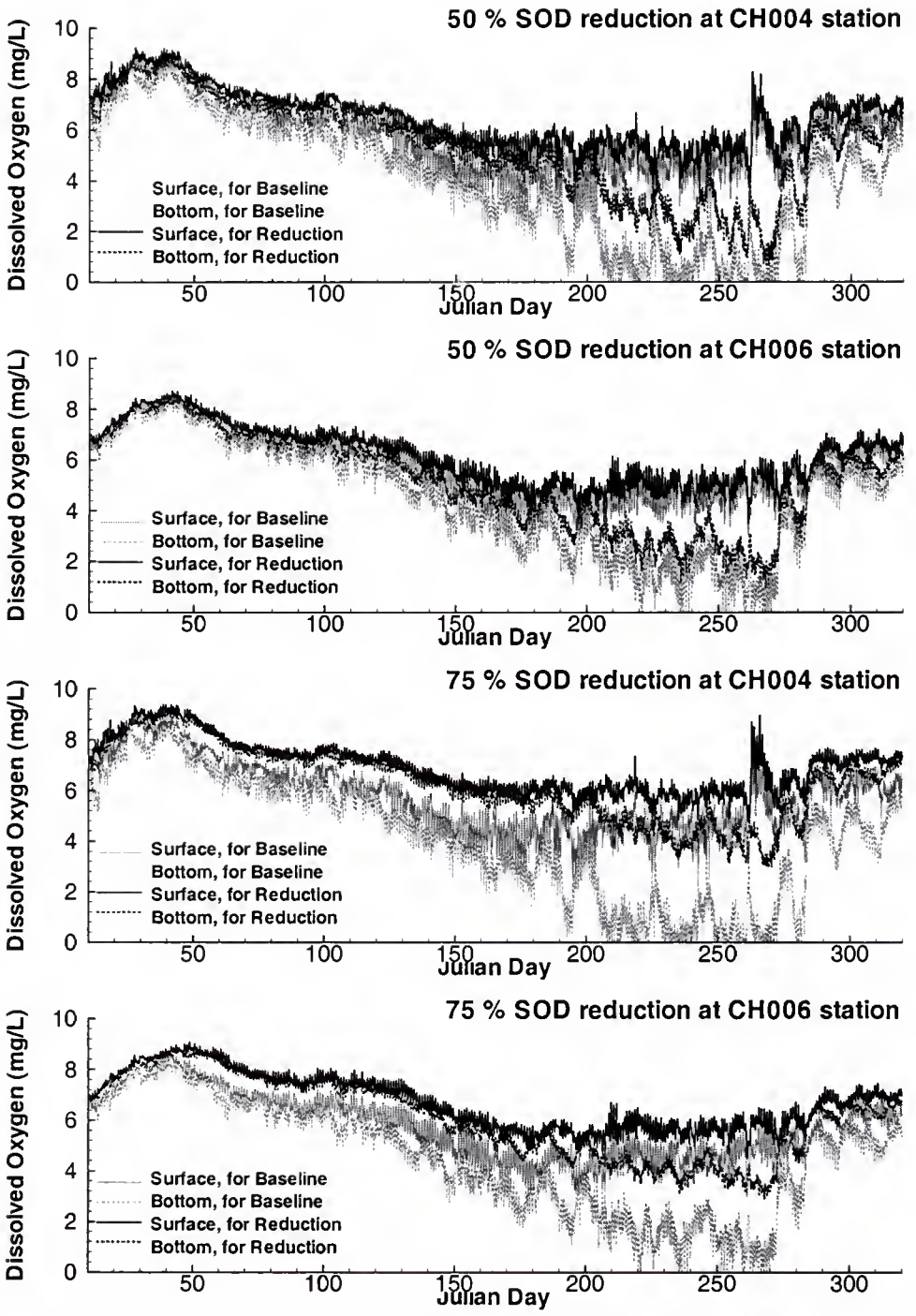
50 % SOD reduction at CH004 station
Dissolved Oxygen (mg/L)
Julian Day
Surface, for Baseline
Bottom, for Baseline
Surface, for Reduction
Bottom, for Reduction
50 % SOD reduction at CH006 station
75 % SOD reduction at CH004 station
75 % SOD reduction at CH006 station

Figure 6.57 Dissolved oxygen concentrations at CH004 and CH006 water quality measured stations before and after 50 % SOD reduction and 75% SOD reduction.

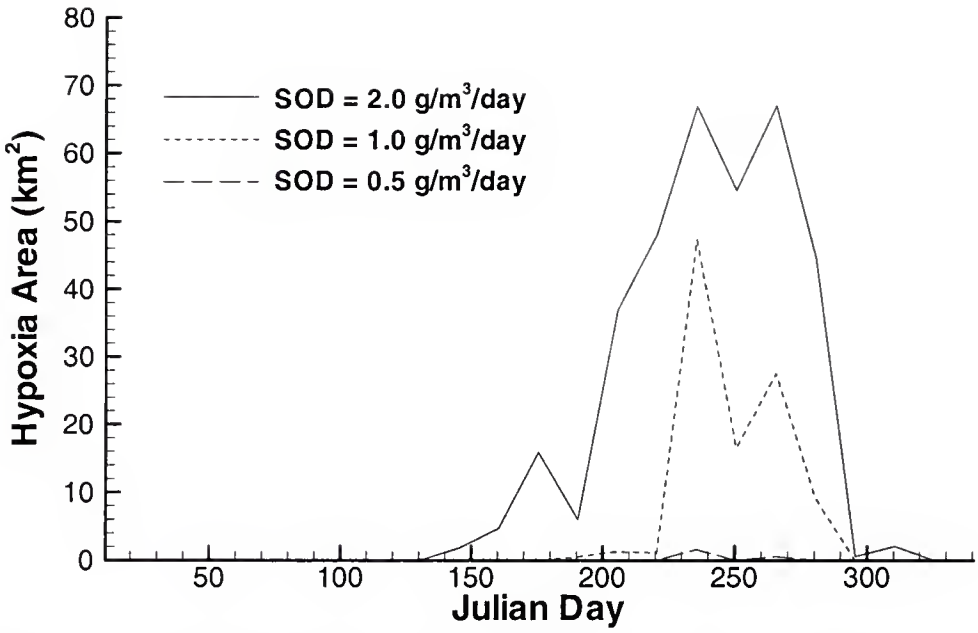

Figure 6.58 The comparison of hypoxia area at Upper Charlotte Harbor according to varying SOD constant rate at 20°C.

CHAPTER 7
CONCLUSION AND DISCUSSION

An integrated modeling system, CH3D-IMS (Sheng et al.,2002), which includes a 3-D hydrodynamics model, a 3-D sediment transport model, and a 3-D water quality model, has been enhanced and applied to the Charlotte Harbor estuarine system. Circulation and water quality in the entire estuarine system have been simulated and validated with field data from numerous sources in 1986, 1996, and 2000. To reproduce bottom water hypoxia in upper Charlotte Harbor, models of oxygen balance and oxygen fluxes at the air-sea and sediment-water interfaces are enhanced. To achieve a better understanding of the temporal and spatial variation of temperature and light, and their effect on water quality processes, the 3-D temperature model, with a heat flux model at the air-sea interface, and the physics-based light attenuation model (Christian and Sheng, 2003) were applied. Major conclusions of this study are summarized in the following:

1) A fine-resolution numerical grid which accurately represents the complex geometrical and bathymetric features in Charlotte Harbor estuarine system was generated and used to simulate the hydrodynamic, salinity and temperature characteristics in 1986 and 2000. A sensitivity study was conducted to examine the sensitivity of model results to such factors as boundary conditions, model coefficients, bathymetry, advection scheme, and grid resolution. Flow, salinity and temperature patterns produced by hydrodynamic model agree well with existing data. The normalized RMS error analysis demonstrated model's ability

to simulate water level, currents, salinity and temperature within 7.5 %, 20%, 6.5 % and 7% accuracy, respectively.

2) The calibrated circulation model was applied to assess the impact of the removal of the Sanibel Causeway and IntraCoastal Waterway on the flow and salinity pattern in the San Carlos Bay and Pine Island Sound and to develop minimum flow criteria for the Caloosahatchee River. The results show that these hydrologic alterations do not appear to show noticeable impact on the flow and salinity patterns in the San Carlos Bay and Pine Island Sound. The salinity at the Caloosahatchee River Mouth is reduced by about 1.36 ppt in the absence of the IntraCoastal Water way.

3) The relationship between salinity at Fort Myers and river discharge was established by comparing 1-day and 30-day averaged salinity values at Fort Myers and fresh water inflow at S79 (Figure 5.35). According to this relationship, a total river discharge of 18 m^3/s at S79 produces a 1-day averaged salinity of 20 ppt at Fort Myers.

4) The newly enhanced integrated model, CH3D-IMS, was used to perform 1996 and 2000 hydrodynamic, sediment transport, and water quality simulations of the Charlotte Harbor estuarine system. The normalized RMS errors of model simulation vary generally within 10 - 45% for all stations and all species. The agreement between simulated and measured DO is particularly good with less than 20% error everywhere. The daily and seasonal vertical distribution and fluctuation of DO are successfully simulated by applying measured SOD at the upper Charlotte Harbor.

5) The upper Charlotte Harbor system has been suffering summer hypoxia in bottom water in the past decade. In this study, CH3D-IMS was enhanced and calibrated to analyze this phenomenon. The calibrated model was used to examine the dynamics of various factors

that can affect hypoxia, including freshwater inflow, tides, SOD, and water column oxygen consumption. The model results suggest that hypoxia in the upper Charlotte Harbor is primarily caused by the combined effects of SOD and vertical salinity stratification, and also enhanced by water column oxygen consumption.

6) The integrated model was applied to assess the effects of hydrologic alterations and to provide a preliminary evaluation of pollutant load reduction goal (PLRG). The results show that these hydrologic alterations do not appear to show noticeable impact on the water quality patterns in the San Carlos Bay and Pine Island Sound. The dissolved oxygen concentration of the estuarine system does not response with different load reduction because of the use of the same SOD values for all load reduction simulation. In reality, SOD is expected to be reduced when nutrient loading is reduced. However, due to lack of detailed data of the sediment diagenesis and lack of understanding of the relationship between SOD and nutrient loading, the model cannot simulate the response of SOD to load reduction. Further research is needed to develop the ability to simulate the effect of nutrient load reduction.

7) A systematic calibration procedure has been developed for a more efficient and more objective calibration of the water quality model. A consistent framework for systematic calibration is formulated which include following step: model initialization, sensitivity analysis, parameterization, and formulation of calibration criteria.

8) Although the integrated model developed and applied in this study have performed well simulating hydrodynamic and water quality components in the Charlotte Harbor estuarine system, the model contains various uncertainties, assumptions and simplifications which need further investigation and improvement. Several possible improvements in the

developed integrated model and year-long simulation of hydrodynamic and water quality dynamics in the system are:

a) A finer grid system is needed to represent the navigation channel, causeway, small islands, and complex shoreline. With grid resolution used in this study, the model cannot solve the dynamics of the shallow regions less than 1.5 m in depth of the system, where wave interactions become important.

b) Sediment oxygen demand (SOD) depends on the deposition and decomposition of organic matter on the seabed, and the exchange of nutrients and oxygen across the sediment-water interface. In order to predict trends in hypoxia in response to organic loads, it is necessary to include oxidation-reduction processes with CH_4, H_2S, and organic matter (DiToro et al. 1990).

c) More accurate river discharge data are needed. The river discharge data at Peace and Myakka rivers are underestimated since not all freshwater inflows are accounted for by the data. To solve this problem, the integrated model need to be coupled with watershed model to supply missing freshwater discharge

d) Phytoplankton dynamics are different with different phytoplankton species. To better understand phytoplankton process and eutrophication characteristics, gathering more phytoplankton species data and applying models of multiple phytoplankton species are needed

e) Submarine groundwater is an important mechanism in delivering chemical elements to surface waters, and can be of the same order of magnitude as surface water sources (Oliveria et al, 2003). Rutkowski et al. (1999) suggest that the nutrient flux by submarine groundwater is on the same order of magnitude as a small river. To address this

issue, a nutrient advection by coupling with groundwater model with the integrated model.

f) Spatially more detailed and temporally more frequent hydrodynamic and water quality data inside the Charlotte Harbor and at the river mouths are needed. Data of nutrients and organic material in the sediment column should be gathered to enable simulation of hypoxia in the upper Charlotte Harbor.

APPENDIX A
FLOWCHARTS FOR CH3D-IMS

The following flow charts illustrate the order of operations performed in the integrated modeling for Charlotte Harbor estuarine system. Figures A.1 illustrate the flow chart of the main CH3D program (ch3d.f). Main program, ch3d.f, call the subroutine ch3dm2.f which is the driving subroutine for time stepping of the solution as well as defining the time varying forcing functions and generating output shown in Figure A.2. Water quality model and sediment transport model are coupled in this subroutine. Figure A.3 and A.4 show the initializing sediment parameters and main routine of sediment transport model, respectively. Water quality model was illustrated in Figure A.5 through A.7.

Chart 1: main program (ch3d.f)

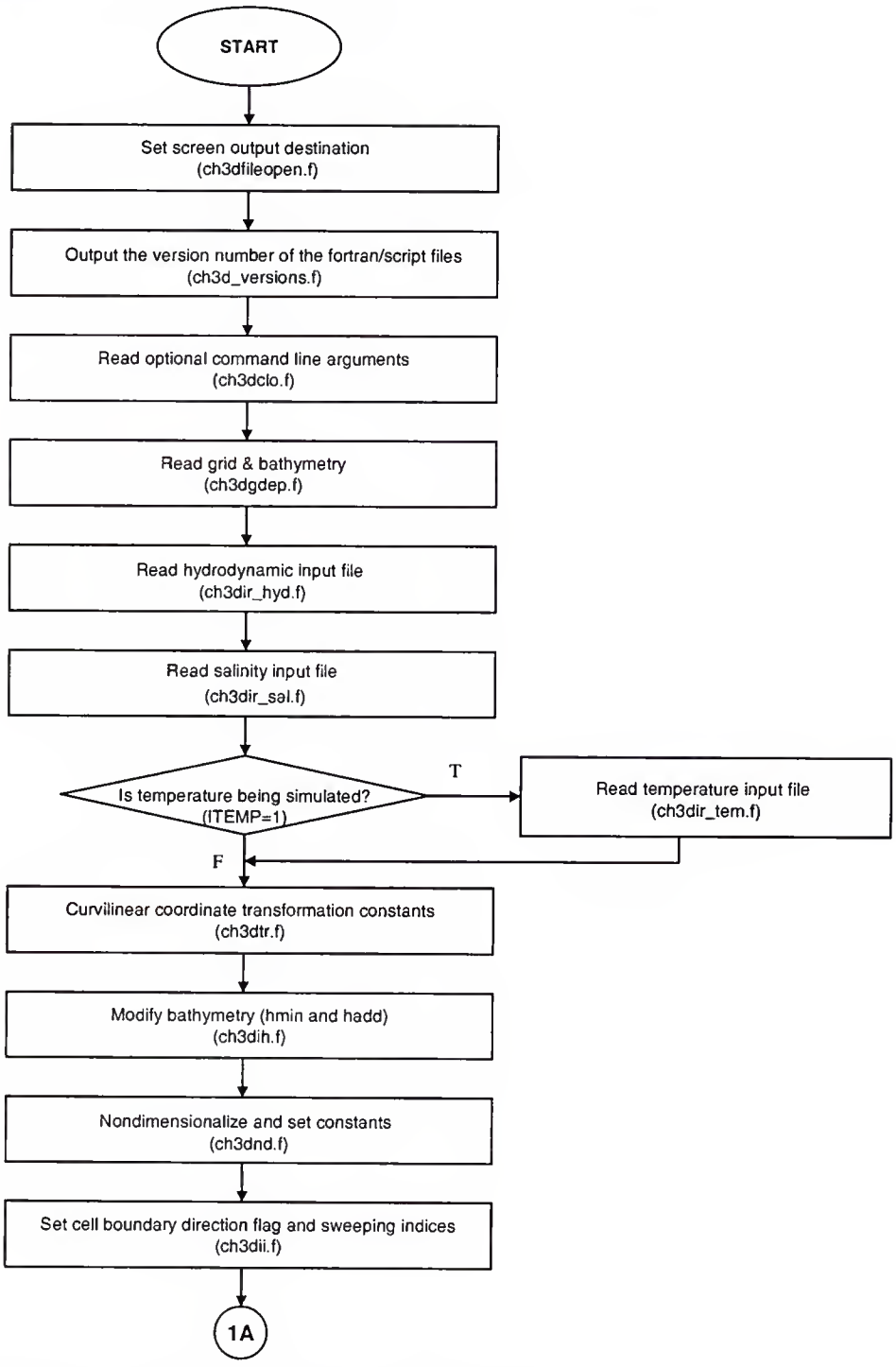

Figure A.1 Flow chart for the main CH3D program.

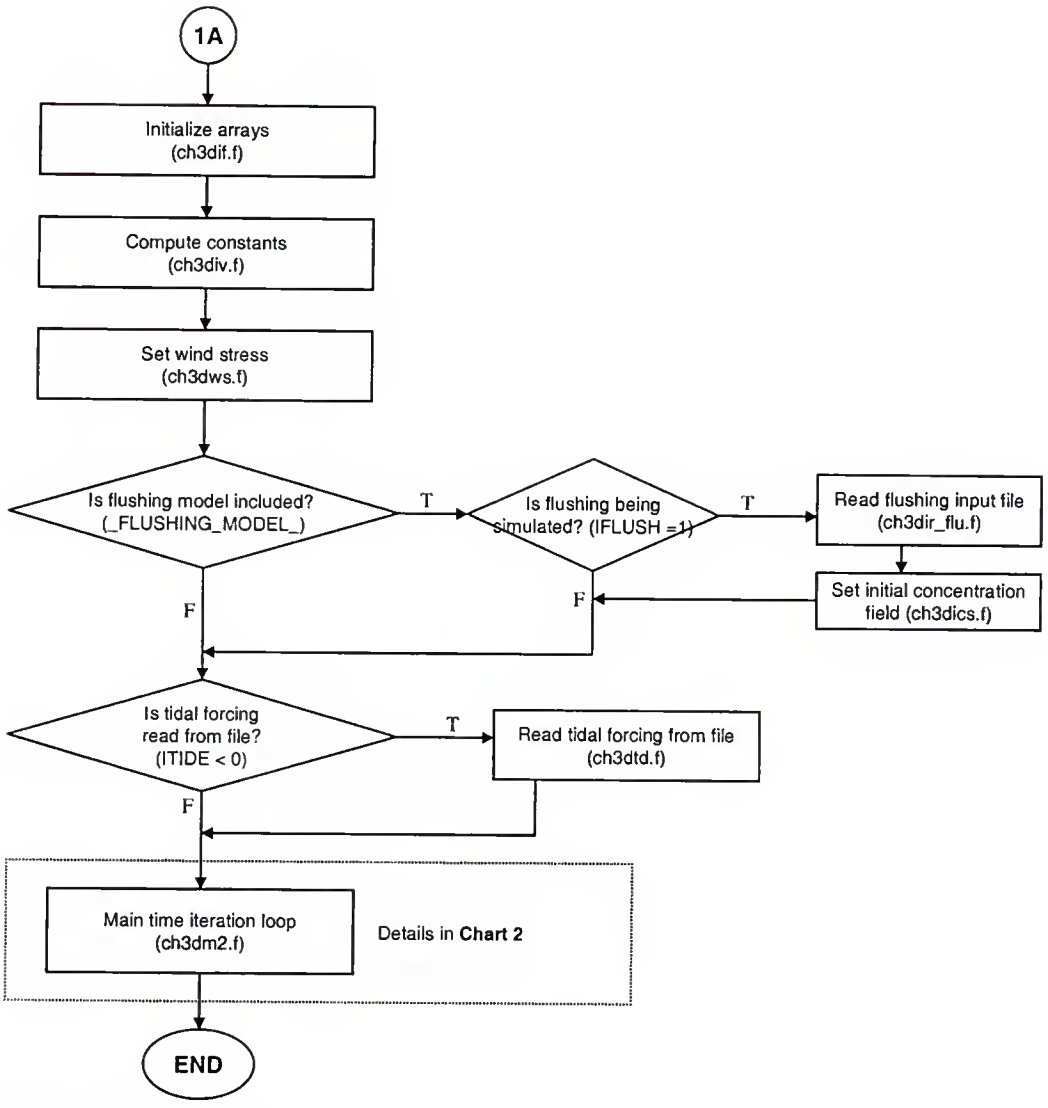

Figure A.1 continue.

Chart 2: main time-iteration loop (ch3dm2.f)

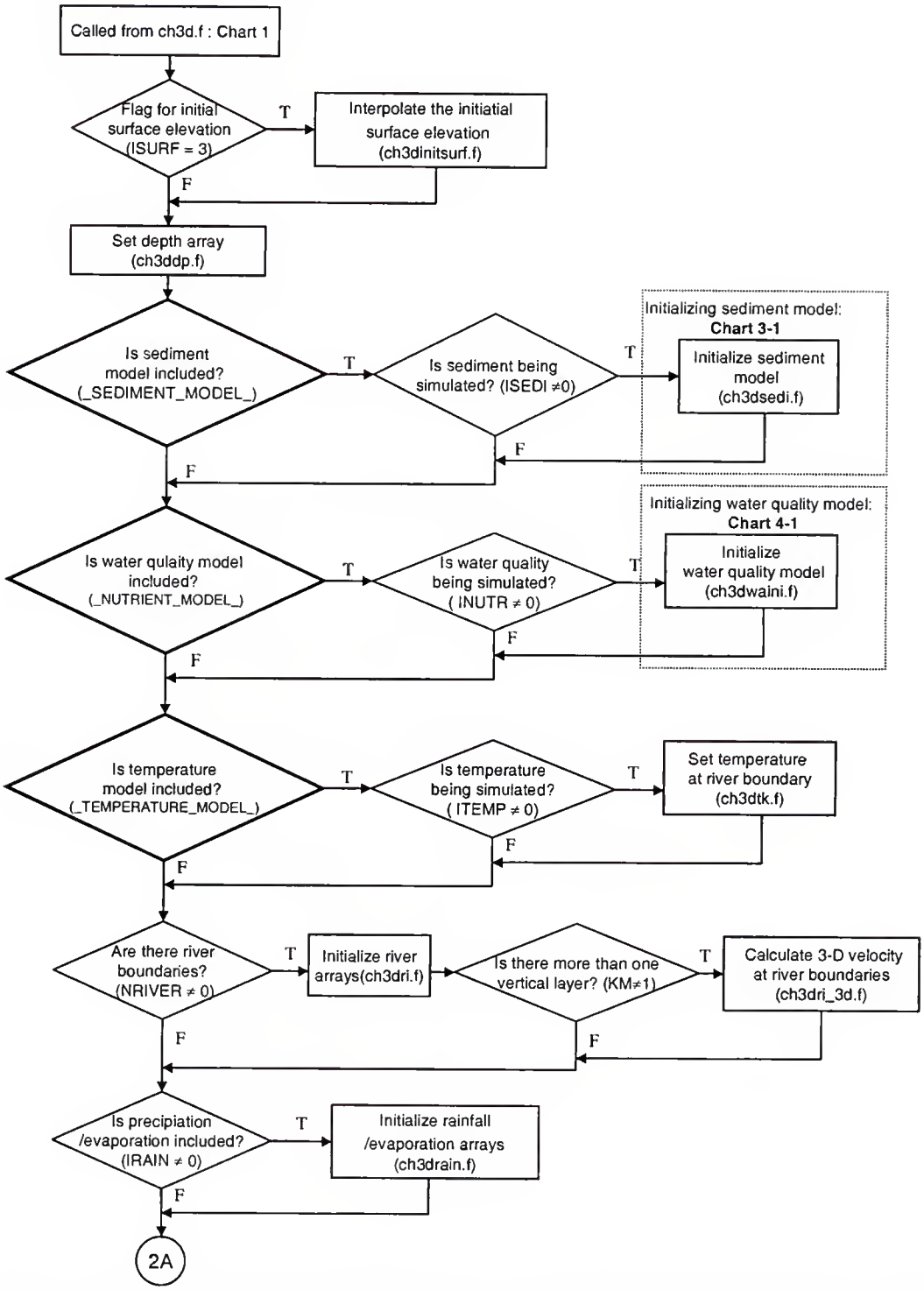

Figure A.2 Flow chart for the driving subroutine for the time stepping of the solution.

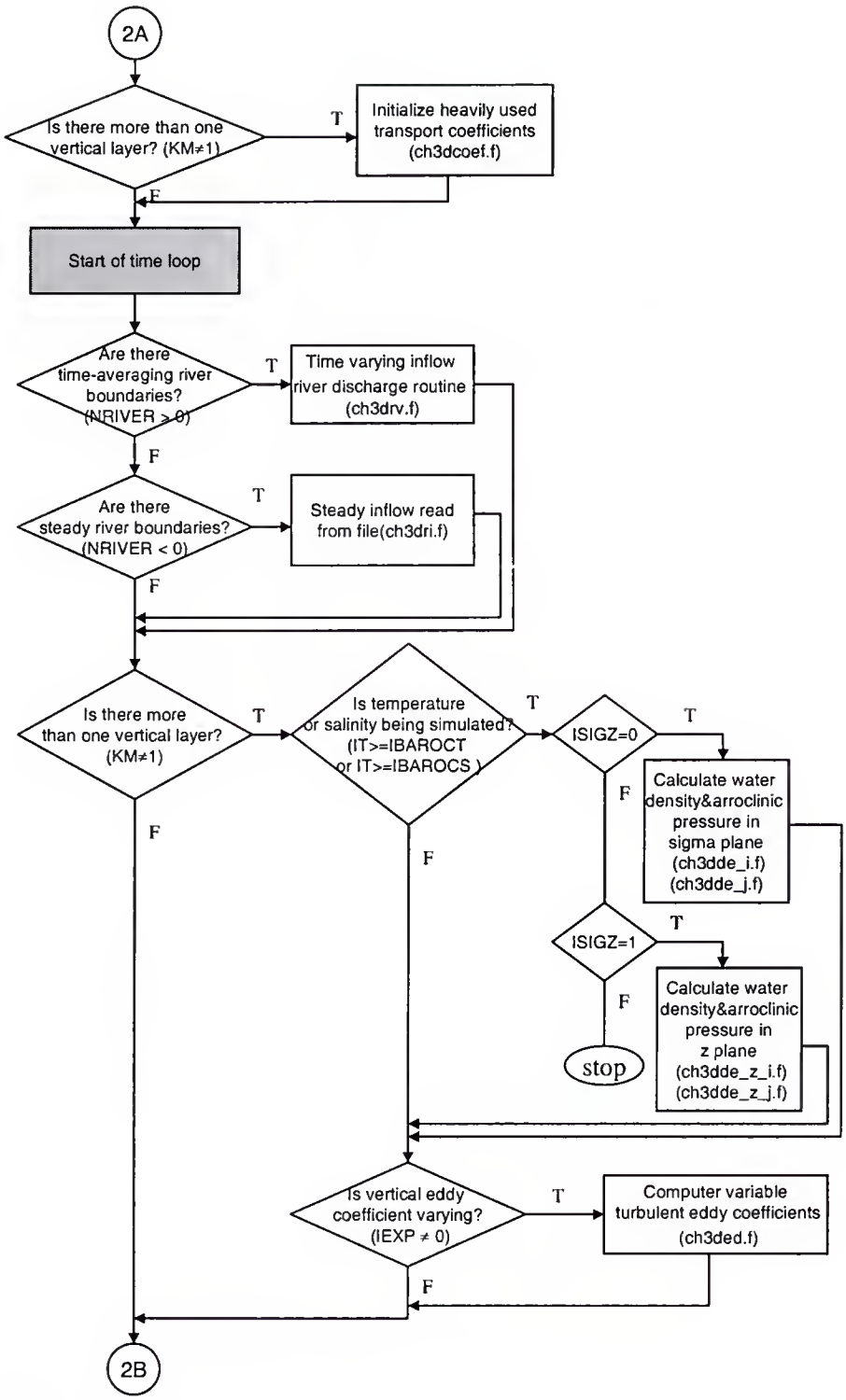

Figure A.2 continue.

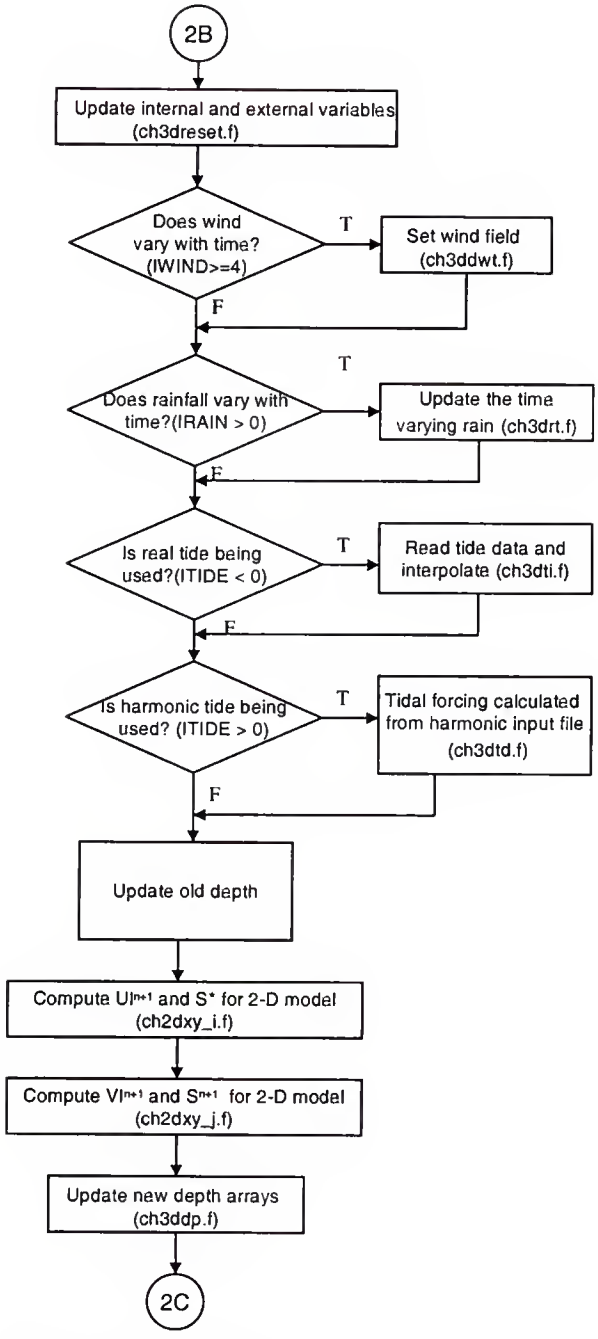

Figure A.2 continue.

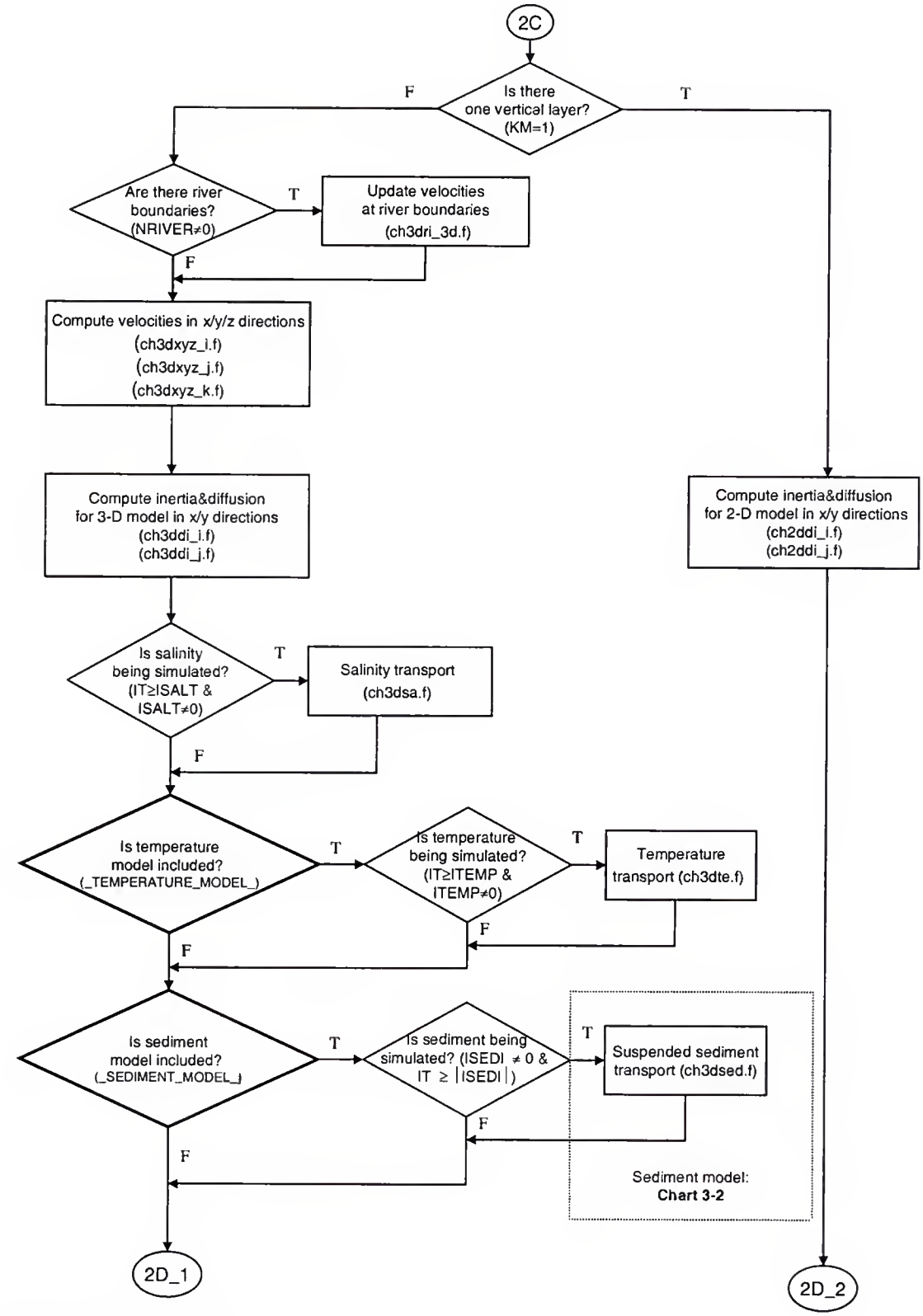

Figure A.2 continue.

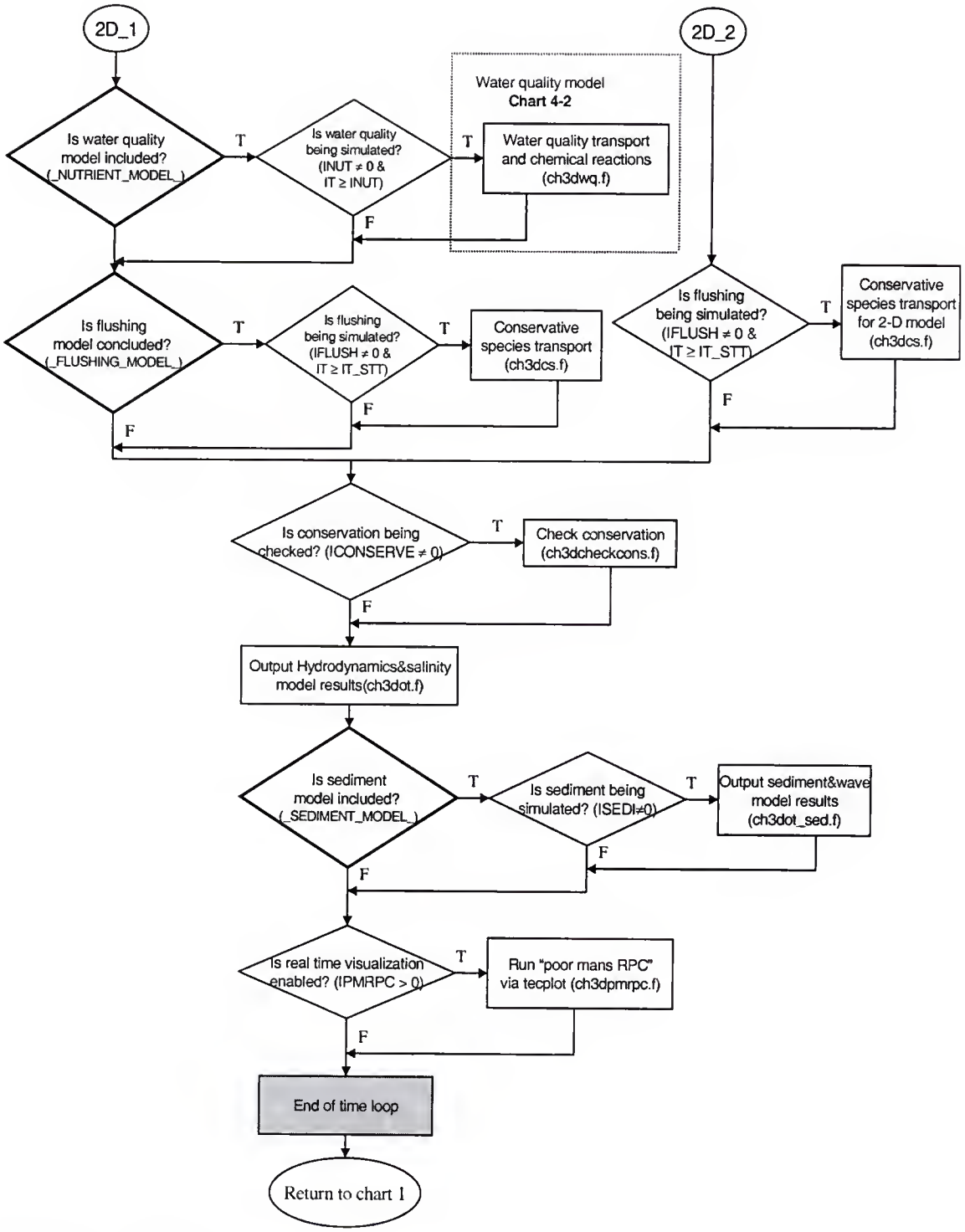

Figure A.2 continue.

Chart 3-1: Sediment initialization and fetch (ch3dsedi.f)

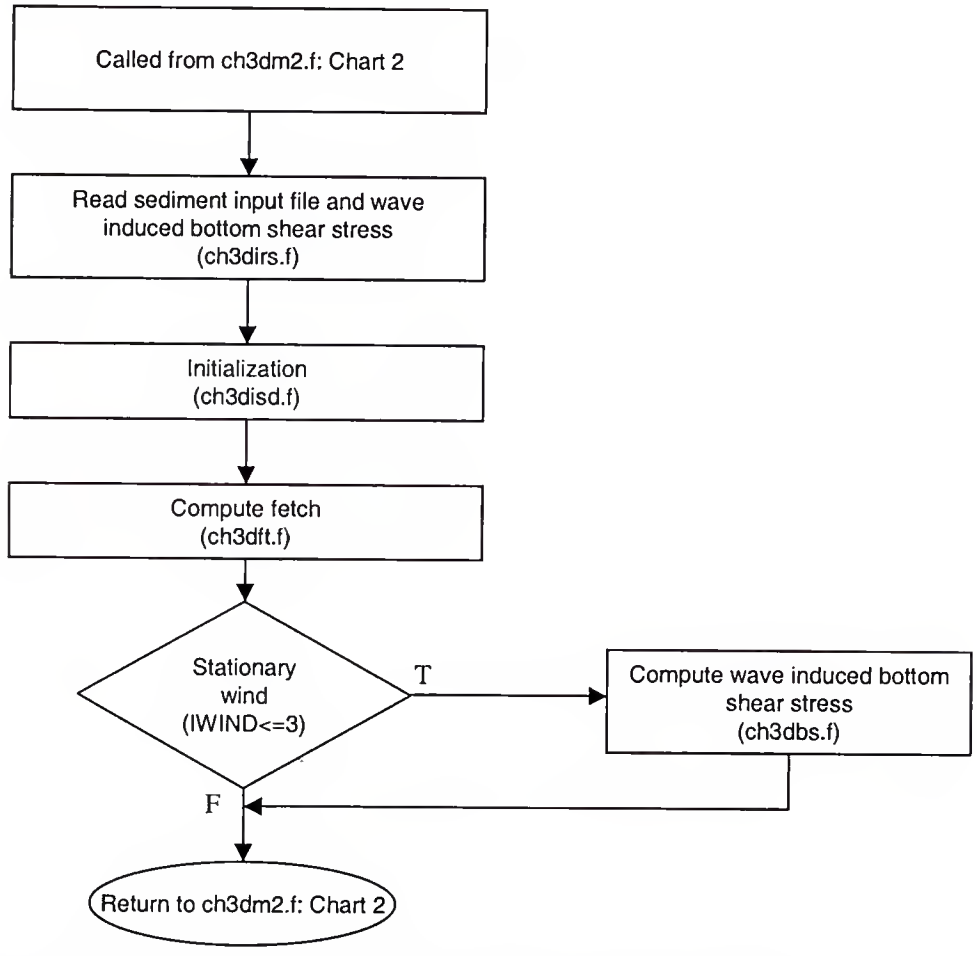
Called from ch3dm2.f: Chart 2
Read sediment input file and wave induced bottom shear stress (ch3dirs.f)
Initialization (ch3disd.f)
Compute fetch (ch3dft.f)
Stationary wind (IWIND<=3)
T
Compute wave induced bottom shear stress (ch3dbs.f)
F
Return to ch3dm2.f: Chart 2

Figure A.3 Flow chart for the initializing sediment transport model

Chart 3-2: Sediment model (ch3dsed.f)

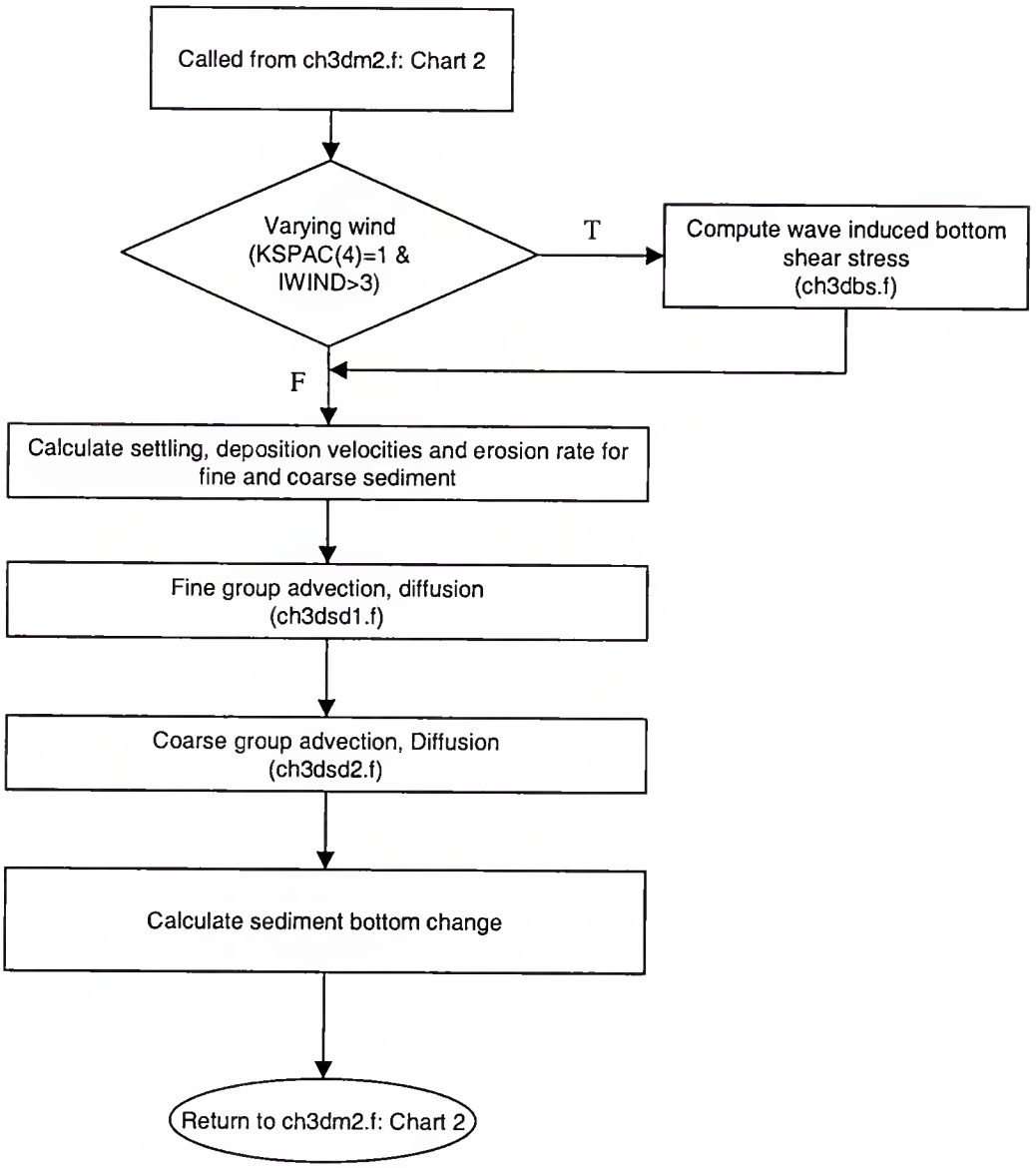
Called from ch3dm2.f: Chart 2
Varying wind (KSPAC(4)=1 & IWIND>3)
T
Compute wave induced bottom shear stress (ch3dbs.f)
F
Calculate settling, deposition velocities and erosion rate for fine and coarse sediment
Fine group advection, diffusion (ch3dsd1.f)
Coarse group advection, Diffusion (ch3dsd2.f)
Calculate sediment bottom change
Return to ch3dm2.f: Chart 2

Figure A.4 Flow chart for main sediment transport model

Chart 4-1 : Initializing Water Quality Model (ch3dwqini.f)

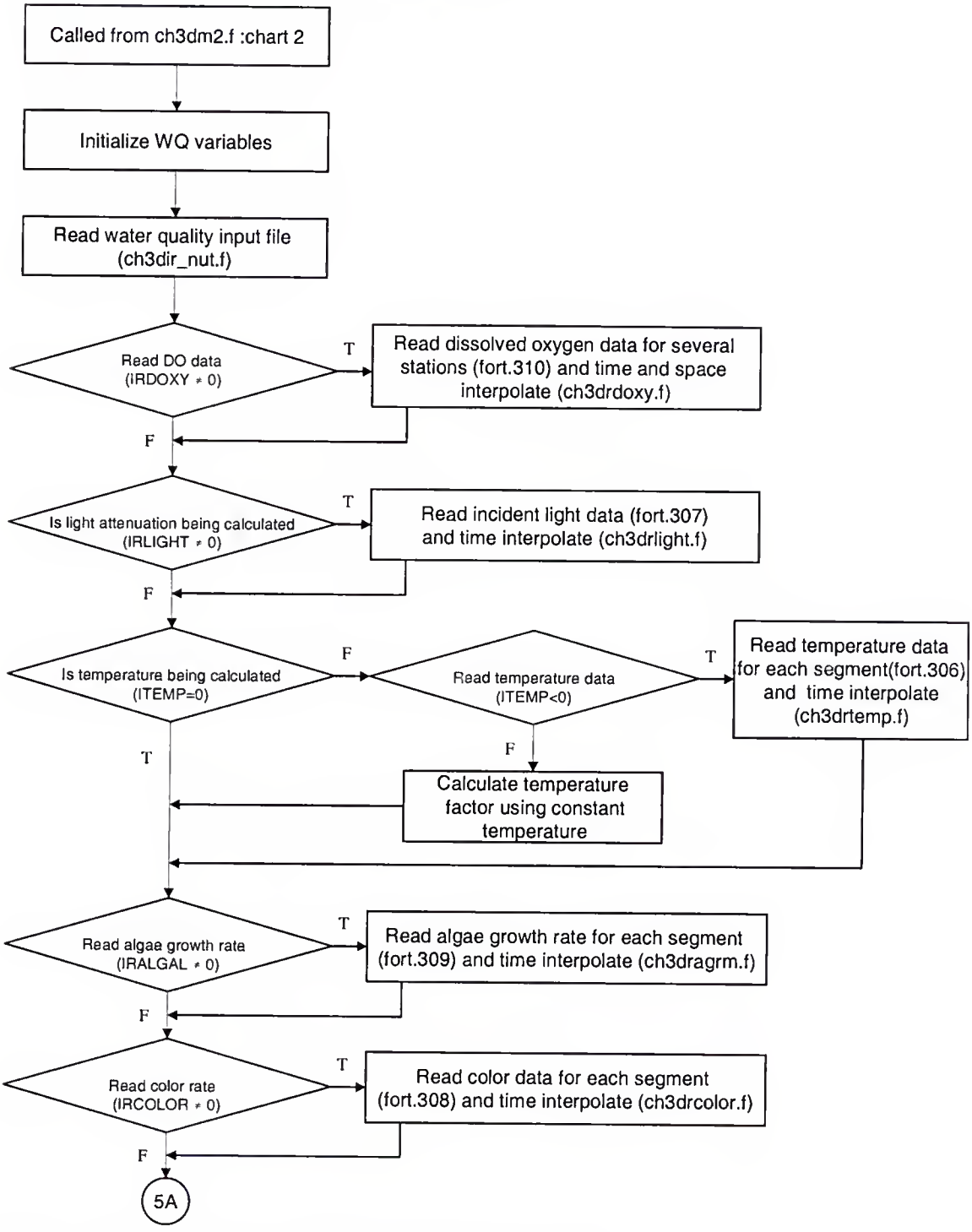
Called from ch3dm2.f :chart 2
Initialize WQ variables
Read water quality input file (ch3dir_nut.f)
Read DO data (IRDOXY ≠ 0)
T
Read dissolved oxygen data for several stations (fort.310) and time and space interpolate (ch3drdoxy.f)
F
Is light attenuation being calculated (IRLIGHT ≠ 0)
T
Read incident light data (fort.307) and time interpolate (ch3drlight.f)
F
Is temperature being calculated (ITEMP=0)
F
Read temperature data (ITEMP<0)
T
Read temperature data for each segment(fort.306) and time interpolate (ch3drtemp.f)
F
T
Calculate temperature factor using constant temperature
Read algae growth rate (IRALGAL ≠ 0)
T
Read algae growth rate for each segment (fort.309) and time interpolate (ch3dragrm.f)
F
Read color rate (IRCOLOR ≠ 0)
T
Read color data for each segment (fort.308) and time interpolate (ch3drcolor.f)
F
5A

Figure A.5 Flow chart for initializing water quality model

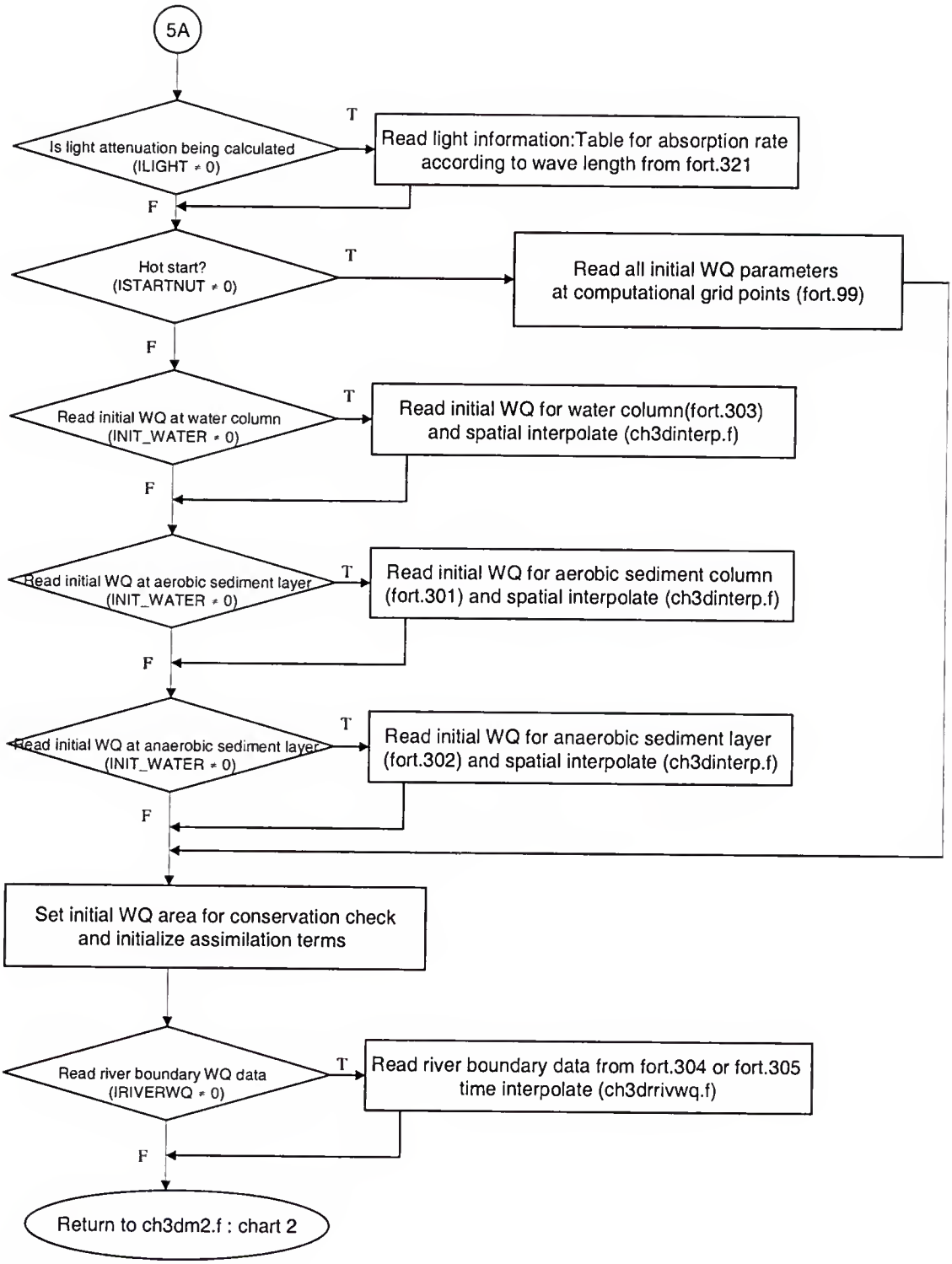
5A
Is light attenuation being calculated (ILIGHT ≠ 0)
T
Read light information:Table for absorption rate according to wave length from fort.321
F
Hot start? (ISTARTNUT ≠ 0)
T
Read all initial WQ parameters at computational grid points (fort.99)
F
Read initial WQ at water column (INIT_WATER ≠ 0)
T
Read initial WQ for water column(fort.303) and spatial interpolate (ch3dinterp.f)
F
Read initial WQ at aerobic sediment layer (INIT_WATER ≠ 0)
T
Read initial WQ for aerobic sediment column (fort.301) and spatial interpolate (ch3dinterp.f)
F
Read initial WQ at anaerobic sediment layer (INIT_WATER ≠ 0)
T
Read initial WQ for anaerobic sediment layer (fort.302) and spatial interpolate (ch3dinterp.f)
F
Set initial WQ area for conservation check and initialize assimilation terms
Read river boundary WQ data (IRIVERWQ ≠ 0)
T
Read river boundary data from fort.304 or fort.305 time interpolate (ch3drrivwq.f)
F
Return to ch3dm2.f : chart 2

Figure A.5 Continue.

Chart 4-2 : Water Quality Model (ch3dwq.f)

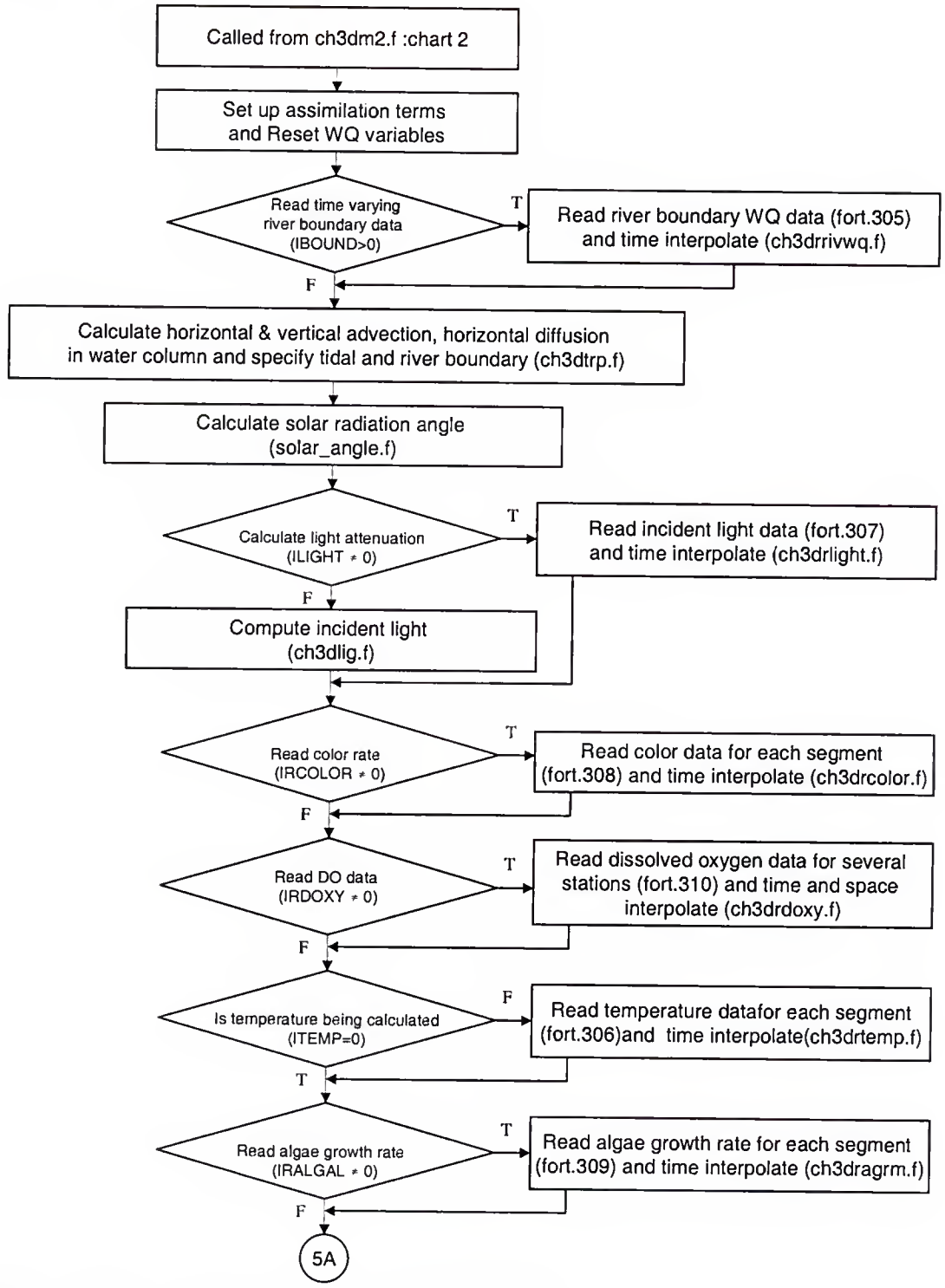
Called from ch3dm2.f :chart 2
Set up assimilation terms and Reset WQ variables
Read time varying river boundary data (IBOUND>0)
T
Read river boundary WQ data (fort.305) and time interpolate (ch3drrivwq.f)
F
Calculate horizontal & vertical advection, horizontal diffusion in water column and specify tidal and river boundary (ch3dtrp.f)
Calculate solar radiation angle (solar_angle.f)
Calculate light attenuation (ILIGHT ≠ 0)
T
Read incident light data (fort.307) and time interpolate (ch3drlight.f)
F
Compute incident light (ch3dlig.f)
Read color rate (IRCOLOR ≠ 0)
T
Read color data for each segment (fort.308) and time interpolate (ch3drcolor.f)
F
Read DO data (IRDOXY ≠ 0)
T
Read dissolved oxygen data for several stations (fort.310) and time and space interpolate (ch3drdoxy.f)
F
Is temperature being calculated (ITEMP=0)
F
Read temperature datafor each segment (fort.306)and time interpolate(ch3drtemp.f)
T
Read algae growth rate (IRALGAL ≠ 0)
T
Read algae growth rate for each segment (fort.309) and time interpolate (ch3dragrm.f)
F
5A

Figure A.6 Flow chart for main water quality model.

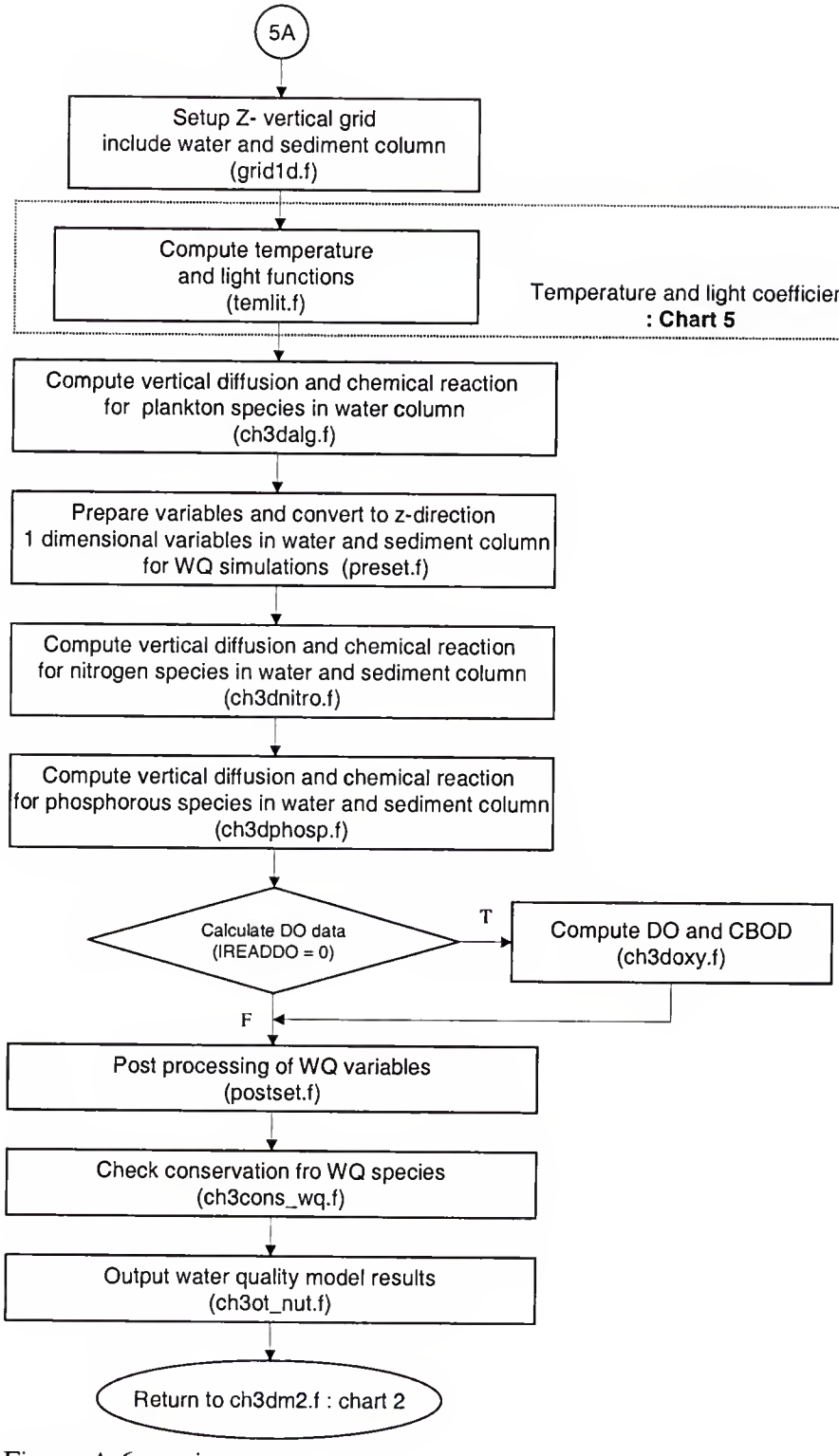

Figure A.6 continue.

Chart 5: Sets up temperature and light functions for water quality model and finds light intensity in a particular water column (temlit.f)

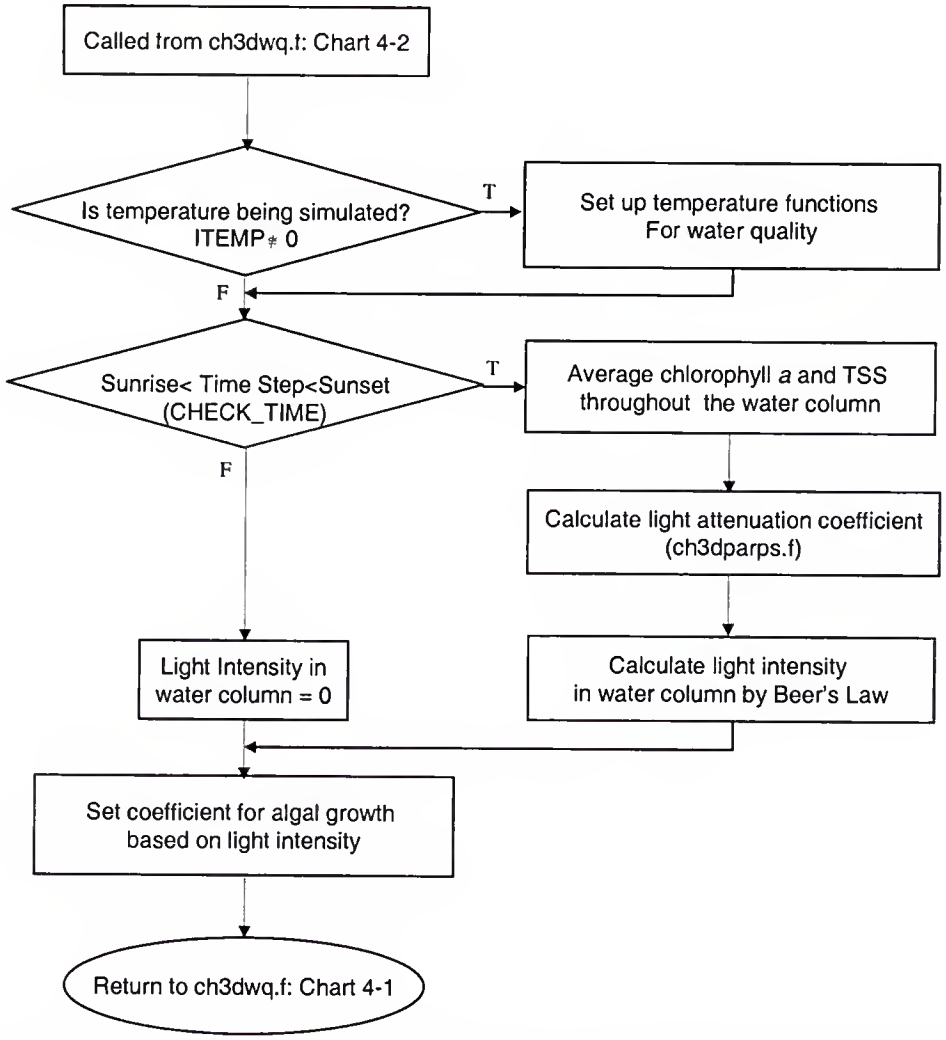

Figure A.7 Flow chart for computing the temperature and light attenuation functions for water quality model.

APPENDIX B
DIMENSIONLESS EQUATIONS IN CURVILINEAR BOUNDARY-FITTED AND SIGMA GRID

Non-dimensionalization of governing equations make it easy to compare the relative importance of various terms in the equations. The governing equations are non-dimensionalized using the following reference scales: X_r and Z_r are the reference lengths in the vertical and horizontal directions; U_r is the reference velocity; ρ, ρ_r and $\Delta\rho = \rho - \rho_0$ are the reference density, mean density and density gradient in a stratified flow; A_{Hr} and A_{Vr} are the reference eddy viscosities in the horizontal and vertical directions; D_{Hr} and D_{Vr} are the reference eddy diffusivities in the horizontal and vertical directions. The dimensionless variables can be written as (Sheng, 1983)

$$
\begin{aligned}
\left(x^*, y^*, z^*\right) &= \left(x, y, zX_r / Z_r\right) / X_r \\
\left(u^*, v^*, w^*\right) &= \left(u, v, wX_r / Z_r\right) / U_r \\
\omega^* &= \omega X_r / U_r \\
t^* &= tf \\
\left(\tau_x^*, \tau_y^*\right) &= \left(\tau_x^w, \tau_y^w\right) / \left(\rho_0 f Z_r U_r\right) = \left(\tau_x^w, \tau_y^w\right) / \tau_r \\
\zeta^* &= g\zeta / \left(fU_r X_r\right) = \zeta / S_r \\
A_H^* &= A_H / A_{Hr} \\
A_V^* &= A_V / A_{Vr} \\
D_H^* &= D_H / D_{Hr} \\
D_V^* &= D_V / D_{Vr}
\end{aligned}
\tag{B.1}
$$

These dimensionless variables can be combined to yield the following dimensionless parameters

Rossby number :
$$R_0 = \frac{U_r}{\sqrt{gZ_r}}$$

Froude Number :
$$F_r = \frac{U_r}{\sqrt{gZ_r}}$$

Densimetric Froude Number :
$$F_{rd} = \frac{F_r}{\sqrt{\varepsilon}} \qquad \text{(B.2)}$$

Vertical and Horizontal Ekman Number :
$$E_V = \frac{A_{Vr}}{fZ_r^2}, E_H = \frac{A_{Hr}}{fX_r^2}$$

Vertical and Horizontal Schmidt Number :
$$S_{CV} = \frac{A_{Vr}}{D_{Vr}}, S_{CH} = \frac{A_{Hr}}{D_{Hr}}$$

$$\varepsilon = \frac{\rho_r - \rho_0}{\rho_0}$$

$$\beta = \frac{gZ_r}{f^2 X_r^2} = \left(\frac{R_0}{F_r}\right)^2$$

In three-dimensional modeling, complex bottom topographies can be better represented with the application of σ-stretching (Sheng, 1983). This transformation allows the same vertical resolution in the shallow coastal areas and the deeper navigation channels. The vertical coordinate, z, is transformed into a new coordinate, σ, by (Phillips, 1957).

$$\sigma = \frac{z - \zeta(x, y, t)}{h(x, y) + \zeta(x, y, t)} \qquad \text{(B.3)}$$

where h is the water depth and ς is the surface elevation.

In this new vertical coordinate, the vertical velocity is calculated by the following equation.

$$w = H\omega + (1+\sigma)\frac{D\zeta}{Dt} + \sigma\left(u\frac{dh}{dx} + v\frac{dh}{dy}\right) \tag{B.4}$$

where $w = \frac{dz}{dt}$ in the z-plane, $\omega = \frac{d\sigma}{dt}$ in the σ-plane

Using non-orthogonal boundary-fitted horizontal grid, it is possible to better represent the circulation and transport processes in estuarine systems with complex shoreline geometries. Using the elliptic grid generation technique developed by Thompson (1982) and Thompson et al. (1985), a non-orthogonal boundary-fitted grid can be generated in the horizontal dimension. To solve for flow in a boundary-fitted grid, it is necessary to transform the governing equations from original coordinates (x, y) to the transformed coordinates (ξ, η). The spatial coordinate system in the computational plane (ξ, η) is dimensionless while the coordinates in the physical plane (x, y) have dimensions of length. During the transformations, the velocities are transformed into contra-variant velocities.

In the boundary-fitted, curvilinear, σ-stretched, non-dimensional coordinate system, the continuity and momentum equations are

$$\frac{\partial\zeta}{\partial t} + \frac{\beta}{\sqrt{g_0}}\left[\frac{\partial}{\partial\xi}\left(\sqrt{g_0}Hu\right) + \frac{\partial}{\partial\eta}\left(\sqrt{g_0}Hv\right)\right] + \beta\frac{\partial H\omega}{\partial\sigma} = 0 \tag{B.5}$$

$$\frac{1}{H}\frac{\partial Hu}{\partial t} = -\left(g^{11}\frac{\partial \zeta}{\partial \xi} + g^{12}\frac{\partial \zeta}{\partial \eta}\right) + \left(\frac{g^{12}}{\sqrt{g_0}}u + \frac{g^{22}}{\sqrt{g_0}}v\right)$$
$$+\frac{R_0}{g_0 H}\left\{x_\eta\left[\frac{\partial}{\partial \xi}\left(y_\xi\sqrt{g_0}Huu + y_\eta\sqrt{g_0}Huv\right) + \frac{\partial}{\partial \eta}\left(y_\xi\sqrt{g_0}Huv + y_\eta\sqrt{g_0}Hvv\right)\right]\right.$$
$$-y_\eta\left[\frac{\partial}{\partial \xi}\left(x_\xi\sqrt{g_0}Huu + x_\eta\sqrt{g_0}Huv\right) + \frac{\partial}{\partial \eta}\left(x_\xi\sqrt{g_0}Huv + x_\eta\sqrt{g_0}Hvv\right)\right] \quad \text{(B.6)}$$
$$\left.-g_0\frac{\partial Huw}{\partial \sigma}\right\}$$
$$-\frac{R_0}{F_r^2}\left[H\int_\sigma^0\left(g^{11}\frac{\partial \rho}{\partial \xi} + g^{12}\frac{\partial \rho}{\partial \eta}\right)d\sigma + \left(g^{11}\frac{\partial H}{\partial \xi} + g^{12}\frac{\partial H}{\partial \eta}\right)\left(\int_\sigma^0 \rho d\sigma + \sigma\rho\right)\right]$$
$$+\frac{E_V}{H^2}\frac{\partial}{\partial \sigma}\left(A_V\frac{\partial u}{\partial \sigma}\right) \quad + E_H A_H(\textit{Horizontal Diffusion of } u)$$

$$\frac{1}{H}\frac{\partial Hv}{\partial t} = -\left(g^{21}\frac{\partial \zeta}{\partial \xi} + g^{22}\frac{\partial \zeta}{\partial \eta}\right) + \left(\frac{g^{11}}{\sqrt{g_0}}u + \frac{g^{21}}{\sqrt{g_0}}v\right)$$
$$+\frac{R_0}{g_0 H}\left\{x_\xi\left[\frac{\partial}{\partial \xi}\left(y_\xi\sqrt{g_0}Huv + y_\eta\sqrt{g_0}Hvv\right) + \frac{\partial}{\partial \eta}\left(y_\xi\sqrt{g_0}Huv + y_\eta\sqrt{g_0}Hvv\right)\right]\right.$$
$$-y_\xi\left[\frac{\partial}{\partial \xi}\left(x_\xi\sqrt{g_0}Huu + x_\eta\sqrt{g_0}Huv\right) + \frac{\partial}{\partial \eta}\left(x_\xi\sqrt{g_0}Huv + x_\eta\sqrt{g_0}Hvv\right)\right] \quad \text{(B.7)}$$
$$\left.-g_0\frac{\partial Hvw}{\partial \sigma}\right\}$$
$$-\frac{R_0}{F_r^2}\left[H\int_\sigma^0\left(g^{21}\frac{\partial \rho}{\partial \xi} + g^{22}\frac{\partial \rho}{\partial \eta}\right)d\sigma + \left(g^{21}\frac{\partial H}{\partial \xi} + g^{22}\frac{\partial H}{\partial \eta}\right)\left(\int_\sigma^0 \rho d\sigma + \sigma\rho\right)\right]$$
$$+\frac{E_V}{H^2}\frac{\partial}{\partial \sigma}\left(A_V\frac{\partial v}{\partial \sigma}\right) \quad + E_H A_H(\textit{Horizontal Diffusion of } v)$$

$$\sqrt{g_0} = J = x_\xi y_\eta - x_\eta y_\xi \quad \text{(B.8)}$$

is the determinant of the matric tensor, g_{ij}, which is defined as

$$g^{ij} = \begin{bmatrix} x_\xi^2 + y_\xi^2 & x_\xi x_\eta + y_\xi y_\eta \\ x_\eta x_\xi + y_\eta y_\xi & x_\eta^2 + y_\eta^2 \end{bmatrix} = \begin{bmatrix} g_{11} & g_{12} \\ g_{21} & g_{22} \end{bmatrix} \quad \text{(B.9)}$$

whose inverse is

$$g^{ij} = \begin{bmatrix} x_\eta^2 + y_\eta^2 & -(x_\xi x_\eta + y_\xi y_\eta) \\ -(x_\eta x_\xi + y_\eta y_\xi) & x_\xi^2 + y_\xi^2 \end{bmatrix} = \begin{bmatrix} g^{11} & g^{12} \\ g^{21} & g^{22} \end{bmatrix} \tag{B.10}$$

As shown in Sheng (1986), the contravarient components (u^i) and physical components ($u(I)$) of the velocity vector in the non-Cartesian system are locally parallel or orthogonal to the grid lines, while the covarient components (u_i) are generally not parallel or orthogonal to the local grid lines. The relationship between the physical velocity and contravarient velocity is given by (Sheng, 1986)

$$u^i = \frac{u(i)}{\sqrt{g_{ii}}} \tag{B.11}$$

with summation on i.

The salinity and temperature transport equations can be written as

$$\begin{aligned} \frac{\partial HS}{\partial t} = {} & \frac{E_V}{H \cdot S_{CV}} \frac{\partial}{\partial \sigma}\left(D_V \frac{\partial S}{\partial \sigma} \right) - R_0 \frac{\partial HwS}{\partial \sigma} \\ & - \frac{R_0}{\sqrt{g_0}} \left[\frac{\partial}{\partial \xi}\left(\sqrt{g_0} HuS \right) + \frac{\partial}{\partial \eta}\left(\sqrt{g_0} HvS \right) \right] \\ & + \frac{E_V}{S_{CH}\sqrt{g_0}} \left[\frac{\partial}{\partial \xi}\left(\sqrt{g_0} H g^{11} \frac{\partial S}{\partial \xi} + \sqrt{g_0} H g^{12} \frac{\partial S}{\partial \eta} \right) \right] \\ & + \frac{E_V}{S_{CH}\sqrt{g_0}} \left[\frac{\partial}{\partial \eta}\left(\sqrt{g_0} H g^{21} \frac{\partial S}{\partial \xi} + \sqrt{g_0} H g^{22} \frac{\partial S}{\partial \eta} \right) \right] \end{aligned} \tag{B.12}$$

and

$$\frac{\partial HT}{\partial t} = \frac{E_V}{H \cdot S_{CV}} \frac{\partial}{\partial \sigma}\left(D_V \frac{\partial T}{\partial \sigma} \right) \quad - R_0 \frac{\partial HwT}{\partial \sigma}$$
$$- \frac{R_0}{\sqrt{g_0}}\left[\frac{\partial}{\partial \xi}\left(\sqrt{g_0} HuT \right) + \frac{\partial}{\partial \eta}\left(\sqrt{g_0} HvT \right) \right]$$
$$+ \frac{E_V}{S_{CH}\sqrt{g_0}}\left[\frac{\partial}{\partial \xi}\left(\sqrt{g_0} Hg^{11} \frac{\partial T}{\partial \xi} + \sqrt{g_0} Hg^{12} \frac{\partial T}{\partial \eta} \right) \right] \qquad \text{(B.13)}$$
$$+ \frac{E_V}{S_{CH}\sqrt{g_0}}\left[\frac{\partial}{\partial \eta}\left(\sqrt{g_0} Hg^{21} \frac{\partial T}{\partial \xi} + \sqrt{g_0} Hg^{22} \frac{\partial T}{\partial \eta} \right) \right]$$

The sediment transport equation can be written as

$$\frac{\partial Hc_i}{\partial t} = \frac{E_V}{H \cdot S_{CV}} \frac{\partial}{\partial \sigma}\left(D_V \frac{\partial c_i}{\partial \sigma} \right) \quad - R_0 \frac{\partial (H\omega - w_{si}) c_i}{\partial \sigma}$$
$$- \frac{R_0}{\sqrt{g_0}}\left[\frac{\partial}{\partial \xi}\left(\sqrt{g_0} Huc_i \right) + \frac{\partial}{\partial \eta}\left(\sqrt{g_0} Hvc_i \right) \right]$$
$$+ \frac{E_V}{S_{CH}\sqrt{g_0}}\left[\frac{\partial}{\partial \xi}\left(\sqrt{g_0} Hg^{11} \frac{\partial c_i}{\partial \xi} + \sqrt{g_0} Hg^{12} \frac{\partial c_i}{\partial \eta} \right) \right] \qquad \text{(B.14)}$$
$$+ \frac{E_V}{S_{CH}\sqrt{g_0}}\left[\frac{\partial}{\partial \eta}\left(\sqrt{g_0} Hg^{21} \frac{\partial c_i}{\partial \xi} + \sqrt{g_0} Hg^{22} \frac{\partial c_i}{\partial \eta} \right) \right]$$

where c_i represents cohesive (i=1) and non-cohesive (i=2) sediment concentrations and w_{si} is settling velocity for sediment group i.

APPENDIX C
COMPARISON OF WATER QUALITY MODELS-WASP, CE-QUAL-ICM, and CH3D-WQ3D

The CH3D water quality model (CH3D-WQ3D) was compared with existing water quality models, specially Water Quality Analysis ans Simulation Program (WASP), the integrated Compartment water quality model developed by the US Army Corps (CE-QUAL-ICM). The methods of coupling with hydrodynamic and sediment transport models, the simulated parameters, the assumptions, the chemical/biological processes, and the limitations of each model are discussed and compared in Table C.1. The first criterion in model comparison is its ability to simulated hydrodynamic, sediment transport, and water quality with the efficient coupling.

The WASP box modeling framework has proven to be an excellent water quality model for riverine systems, where the steady state assumption is applicable. In addition, this simple box model can be successfully used to perform numerical experiments like sensitivity test. However, in marine environments, it should not be used without proper linkage with 3-D hydrodynamics and sediment models, because tide wind and baroclinic forcing underact in an unsteady balance.

As pointed out by Chen and Sheng (1994), the loosely coupled models such as CE-QUAL-ICM, cannot account for nutrient release by sediments in episodic events. Because these models were not coupled with a dynamic model for sediment transport, they could not

accurately consider sediment-process effects such as resuspension, deposition, flocculation, and settling on nutrient dynamics in estuaries. Furthermore, this model use equilibrium partition with function of biomass for hydrolysis process. This may be a reasonable assumption when the time step of the water quality simulation is large compared to the time it takes to reach equilibrium. However, sometimes a water quality model may use a small time step during which the absorbed and the dissolved nutrient may not achieve equilibrium. In this case, a kinetics model, such as sorption/desorption kinetic process in CH3D-WQ3D, is needed. Analytical chemists repeatedly found that complete recovery of contaminants from soil/sediments frequently requires lengthy extraction periods, abrasive mixing, and strong solvents (Witkowski and Jaffe, 1978). These observations are in contradiction with the equilibrium models which assume that sorption-desorption reactions are accomplished instantaneously.

The light attenuation model need chlorophyll a and suspended sediment concentrations to calculate light attenuation in water column. The water quality model use light intensity for limitation of algae growth rate and photosynthesis processes. Therefore, without fully coupling these models, it could not be accomplished to communicate each others with both direction.

The chemical/biological processes in all three models are basically similar and compatible with each others. Most of them are the adjustable coefficients. Thus, the ability to simulate water quality depends on modeler experience, and necessity of model complexity. Also the data availability is the key to ensure reliability and accuracy of the results. The CE-QUAL-ICM include much more simulating species than those for the other model. Without measured data for those species, these complex nutrient cycles could create more uncertainty

than simple nutrient species model. CE-QUAL-ICM use sediment flux model developed by Ditoro and Fitzpatric (1990) for sediment oxygen demand. Although, applying of sediment flux model provides rational predictions of sediment response to environmental alterations, it increases information requirements and computation time compare to employment of user-specified fluxes (Cerco and Cole, 1995). They point out that employment of user-specified fluxes show the better calibration of the water quality model than employment of the sediment flux model.

Overall, with the similarity and compatibility of chemical/biological processes which is depend on data availability, coupling with hydrodynamic model, sediment transport model, temperature model, and light attenuation model is the key to ensure reliability and accuracy of model. Specially, the Charlotte Harbor estuarine system which has a strong linkage between hydrodynamics and water quality dynamics suggests the importance of coupling with hydrodynamics and sediment transport. Therefore, CH3D-WQ3D is better to simulate water quality in Charlotte Harbor estuarine system than the other water quality models.

Table C.1 Comparison of water quality models

model	WASP5.x	CE_QUAL_ICMv1.0	CH3D-WQ3D
Hydrodynamic model	Read into the model as input parameters	read into the model as input parameters	fully coupled with circulation, salinity and temperature transport model
Sediment transport model	Read into the model as input parameters	loosely coupled with simple model	fully coupled with sediment dynamic model
Light attenuation model	loosely coupled with empirical formula	loosely coupled with empirical formula	fully coupled with physics-based light attenuation model
Nitrogen cycle	NH3, NO3, ON	NH4, NO3, SON, LPON, RPON	NH4, NO3, SON, PON, PIN, NH3
phosphorous cycle	SRP, OP	SRP, SOP, LPOP, RPOP	SRP, SOP, POP, PIP
carbon cycle	Using CBOD	SOC, LPOC, RPOC	Using CBOD
silica cycle	No	Available Silica, Particulate Biogenic silica	No
metal cycle	No	Iron & Manganese	No
phytoplankton	One species	Three species	One species
zooplankton	Using zooplankton grazing rate	Using phytoplankton predation rate	Yes
Metabolism	Respiration and non-predator mortality	One parameter	Respiration and non-predator mortality
re-aeration	Function of current velocity and depth	Constant	Function of current velocity, depth, and wind speed
sediment oxygen demand	Empirical formula	Sediment flux model	Empirical formula
Variation of Ammonification	Function of temperature	Function of algae biomass	Function of temperature
Variation of mineralization	Function of temperature	Function of algae biomass	Function of temperature

Hydrolysis	No particulate species	Equlibrium partition with function of algae biomass	Sorption/desorption kinetic
phosphorous /carbon ratio	Constant	Variable ratio described by empirical approximation	Constant

APPENDIX D
NUMERICAL SOLUTION TECHNIQUE FOR WATER QUALITY PROCESSES

In the finite difference solution of the water quality model, the advection and horizontal diffusion terms are treated explicitly, whereas the vertical diffusion and biogeochemical transformations are treated implicitly. Fractional step methods, which guarantee numerical stability and prevent negative concentrations, are applied in the numerical solution (Chen and Sheng, 1994). The horizontal diffusion and horizontal and vertical advection terms are solved first. The numerical solutions proceeds with the calculation of vertical diffusion, and then biogeochemical transformation reactions. Finally, the sorption/desorption reaction terms are solved. Equation (D.1) shows a schematic of the numerical solution algorithm method used in this study.

$$\begin{aligned}
\frac{N^{n1}-N^{n}}{\Delta t} &= \left[Horiz.\ Advection + Vertical\ Advection + Horiz.\ Diffusion\right]^{n} \\
\frac{N^{n2}-N^{n1}}{\Delta t} &= \left[Vertical\ Diffusion\right]^{n2} + \left[Q\right]^{n2} \\
\frac{N^{n+1}-N^{n2}}{\Delta t} &= \left[Sorption\right]^{n+1} + \left[desorption\right]^{n+1}
\end{aligned} \tag{D.1}$$

By solving the sorption/desorption terms separately from other terms, it is possible to treat these terms implicitly. To illustrate this, the difference equations for the sorption/desorption reactions are examined:

$$\frac{N_d^{n+1} - N_d^{n2}}{\Delta t} = +(d_x N_p^{n+1} - d_x \cdot p_x \cdot c \cdot N_d^{n+1})$$
$$\frac{N_p^{n+1} - N_p^{n2}}{\Delta t} = -(d_x N_p^{n+1} - d_x \cdot p_x \cdot c \cdot N_d^{n+1}) \quad \text{(D.2)}$$

where N_d and N_p are concentrations of dissolved and particulate nutrients such as,NH4 and PIN, SON and PON, SRP and PIP, and SOP and POP; dx is desorption rate for a specific nutrient species; and p_x is partition coefficient for a specific nutrient species.

In solving the second step of the fractional step method for organic/inorganic phosphorous and nitrogen species, the difference equations for the entire water column and sediment column are solved simultaneously. The kinetic processes for particulate nutrient and plankton species need to include a settling process, which accounts for the limited vertical motion of these species.

For dissolved species
$$\frac{\partial N_d}{\partial t} = \frac{\partial}{\partial z}\left(D_v \frac{\partial N_d}{\partial z} \right) + Q \quad \text{(D.3)}$$

For particulate species
$$\frac{\partial N_P}{\partial t} = \frac{\partial}{\partial z}\left(w_s N_p + D_v \frac{\partial N_p}{\partial z} \right) + Q \quad \text{(D.4)}$$

The exchanges of particulate nutrients at the water-sediment interface are determined by the sediment resuspension and deposition fluxes while the exchange of dissolved nutrient species between the water and sediment column are automatically included in the numerical solutions, with diffusion term. In order to ensure that the water quality model is consistent with the sediment model, in terms of bottom exchanges, the erosion and deposition rates calculated in the sediment model can be imported into the governing equations for particulate nutrients. Therefore, the particulate nutrient concentrations are solved with the unit of percentage (μg/μg). Let p be any particulate species (N_p) mass per unit mass of sediments, then,

$$N_p = p \cdot c \tag{D.5}$$

where c is the suspended sediment concentration. Substitute N_p with pc into second step of fractional step method:

$$\frac{\partial pc}{\partial t} = \frac{\partial}{\partial z}\left(w_s pc + D_v \frac{\partial pc}{\partial z} \right) + Q \tag{D.6}$$

$$p\frac{\partial c}{\partial t} + c\frac{\partial p}{\partial t} = \frac{\partial}{\partial z}\left[p\left(w_s c + D_v \frac{\partial c}{\partial z} \right) \right] + \frac{\partial}{\partial z}\left[D_v c \frac{\partial p}{\partial z} \right] + Q \tag{D.7}$$

Since the vertical one-dimensional sediment equations are:

$$\frac{\partial c}{\partial t} = \frac{\partial}{\partial z}\left(w_s c + D_v \frac{\partial c}{\partial z} \right) \tag{D.8}$$

Equation (D.7) becomes:

$$c\frac{\partial p}{\partial t} = \left(w_s c + D_v \frac{\partial c}{\partial z} \right)\frac{\partial}{\partial z} + \frac{\partial}{\partial z}\left[D_v c \frac{\partial p}{\partial z} \right] + Q \tag{D.9}$$

This equation allows us to import the erosion and deposition rates calculated in the sediment model into the particulate nutrient species. Since the boundary condition for the sediment model at the water-sediment interface is:

$$w_s c + D_v \frac{\partial c}{\partial z} = D - E \tag{D.10}$$

Equation (D.9) at the water-sediment interface becomes:

$$c\frac{\partial p}{\partial t} = (D - E)\frac{\partial}{\partial z} + \frac{\partial}{\partial z}\left[D_v c \frac{\partial p}{\partial z} \right] + Q \tag{D.11}$$

where D and E are deposition and erosion rate, which are calculated at sediment model.

Due to the difference in the partial pressures of oxygen and carbon and because of other physical and biochemical factors, the transformation processes in the water column and in the sediment column are different. There are no phytoplankton and zooplankton species

in the sediment column. When these plankton species die, they are treated as particulate organic species. In the sediment column, there exist two distinctive layers: an aerobic layer and an anaerobic layer, within which the transformation processes are not the same. For example, in the anaerobic layer, there is no nitrification process due to a lack of oxygen, while in the aerobic layer, there is no denitrification process due to the availability of oxygen. The vertically, one dimensional z-grid is shown in Figure D.1.

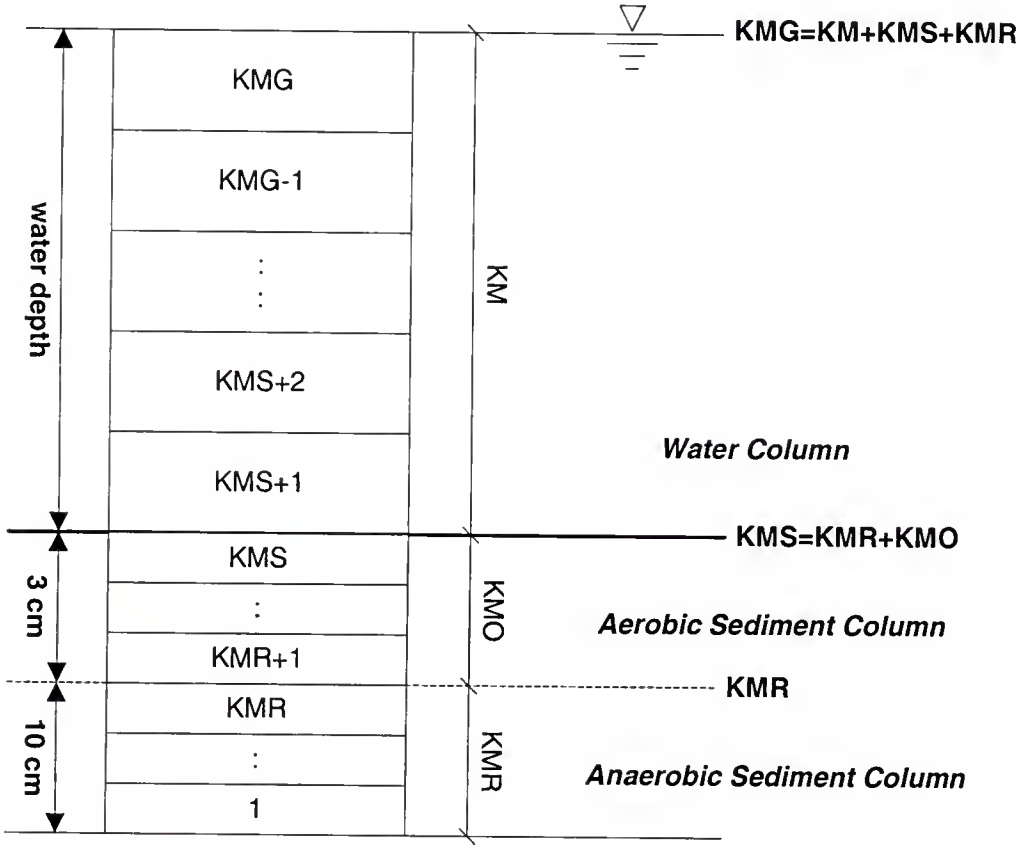

Figure D.1 The vertical one-dimensional z-grid

Since the horizontal transport is generally very weak in the sediment column, the mass flows of nutrient species are mainly vertical, and the governing equations are:

For dissolved species in a sediment layer $$\frac{\partial N_d}{\partial t} = \frac{\partial}{\partial z}\left(\phi M \frac{\partial N_d}{\partial z}\right) + Q \qquad \text{(D.12)}$$

For particulate species in a sediment layer $$\frac{\partial N_P}{\partial t} = \frac{\partial}{\partial z}\left(w_c N_p + M \frac{\partial N_p}{\partial z} \right) + Q \quad \text{(D.13)}$$

where N_d is dissolved nutrient species such as NH4, SON, SRP, SOP concentrations (per unit volume of porewater), w_c is the consolidation velocity of sediments, M is the molecular diffusivity, and ϕ is the porosity.

APPENDIX E
NUTRIENT DYNAMICS

Nutrients are essential elements for life processes of aquatic organisms. Nutrients of concern include carbon, nitrogen, phosphorous, silica and sulfur. Among these nutrients, the first three elements are utilized most heavily by zooplankton and phytoplankton. Since carbon is usually available in excess, nitrogen and phosphorous are the major nutrients regulating the ecological balance in an estuarine system. Nutrients are important in water quality modeling for several reasons. For example, nutrient dynamics are critical components of eutrophication models since nutrient availability is usually the main factor controlling algae bloom. Algae growth is typically limited by either phosphorous or nitrogen. (Bowie et al., 1980)

Nutrient inputs to estuarine systems are related to point and non-point sources from land, atmospheric deposition, and fixation. Additionally, internal loadings such as from resuspended sediments containing inorganic and organic forms are also important. The specification and quantification of each of these contributions are the first steps towards the determination of nitrogen and phosphorous budgets in an estuarine system.

Nutrient cycles are highly dependent on the hydrodynamics and sediment dynamics of the estuarine system. Resuspension events, combined with desorption processes, can significantly change the input and budget of nitrogen and phosphorous in the system. On the other hand, deposition and sorption may contribute to major losses of nitrogen and

phosphorous from the water column. The hydrodynamics not only derive the sediment processes, but also affect the sorption/desorption reactions, through turbulent mixing.

E.1 Nitrogen Cycle

Nitrogen can be classified into two groups: dissolved nitrogen and particular nitrogen. The criterion of this division is established in the laboratory using filtering technique. The dissolved nitrogen include ammonia nitrogen (NH3), dissolved ammonia nitrogen (NH4), nitrite and nitrate nitrogen (NO3), and dissolved organic nitrogen (SON). Particulate nitrogen includes particulate inorganic nitrogen (PIN), and particulate organic nitrogen (PON). Phytoplankton nitrogen (PhyN) and zooplankton nitrogen (ZooN) related biomass to nitrogen concentration through a fixed stoichiometric ratio: nitrogen-to-carbon ratio (A_{NC}).

The model nitrogen cycle (Figure E.1) includes the following processes.

1) Ammonification of organic nitrogen

2) Nitrification of ammonium

3) Volatilization of ammonia

4) Denitrification of nitrate

5) Uptake of ammonia and nitrate by phytoplankton

6) Conversion of phytoplankton nitrogen to zooplankton nitrogen by grazing

7) Excretion and mortality by phytoplankton and zooplankton

8) Settling for particulate nitrogen

9) Sorption/desorption reactions

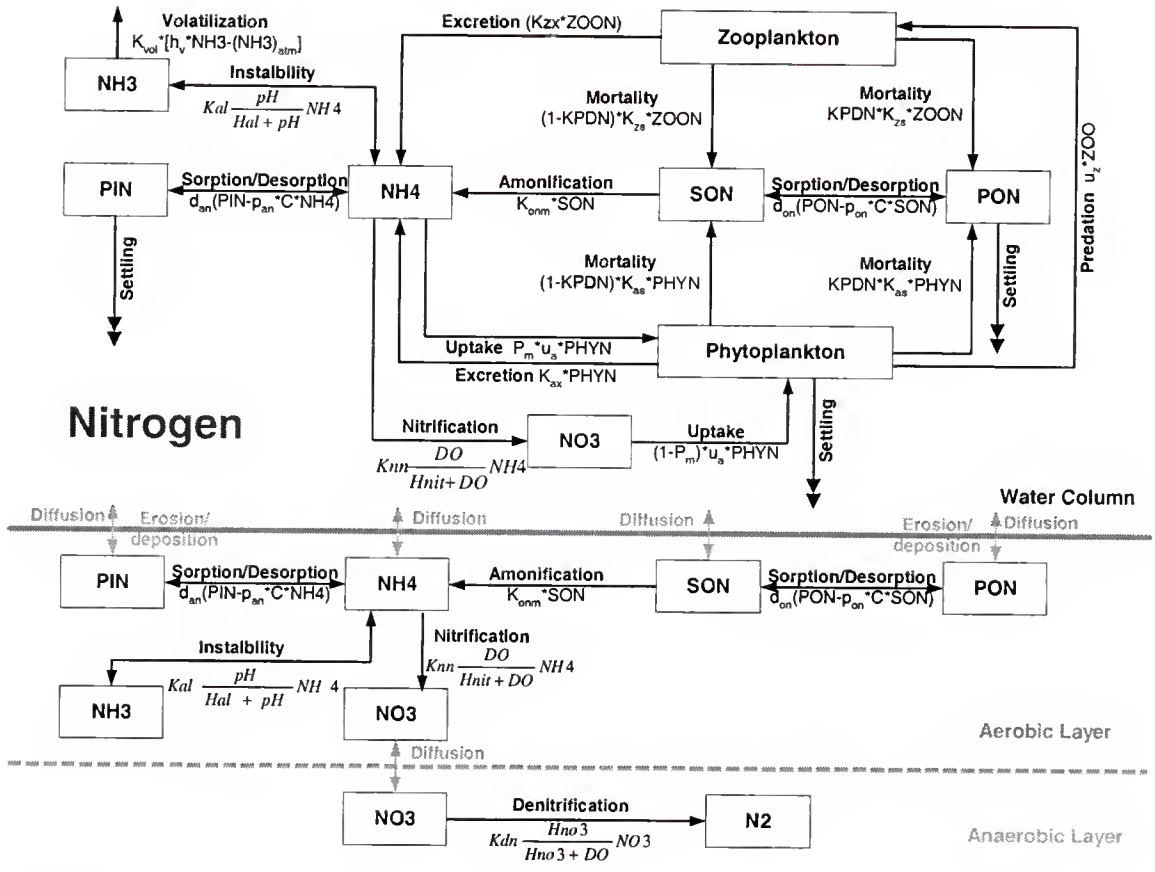

Figure E.1 Nitrogen Cycle

Ammonification is the biological process of formation of ammonium from soluble organic nitrogen. It is the first step of nitrogen mineralization, in which organic nitrogen is converted to the more mobile, inorganic state. The rate of ammonification is expressed as a first order reaction (Rao et al, 1984) :

$$Q_{ammonification} = -K_{ONM} \cdot SON \tag{E.1}$$

where K_{ONM} is the rate constant of ammonification which is a function of water temperature, pH, and the C/N ratio of the residue (Reddy and Patrick, 1984).

The second step of mineralization of organic nitrogen is nitrification, which is an oxidation of ammonia to nitrate(NO_3^-) directly or to nitrite (NO_2^-) and then to nitrate:

$$NH_4^+ + 1.5O_2 \rightarrow NO_2^- + 2H^+ + H_2O$$
$$NO_2^- + 0.5O_2 \rightarrow NO_3^- \quad \text{(E.2)}$$

Nitrification requires oxygen as the electron acceptor. Therefore, nitrification is a strictly aerobic process, occurring only in the water column and in the aerobic layer of the sediment column. This process is related to a sink of dissolved oxygen in the system as shown in eq 4.11. The kinetics of nitrification are modeled as function of available ammonia, dissolved oxygen, and temperature.

$$Q_{nitrification} = -K_{NN} \frac{DO}{H_{nit} + DO} NH_4 \quad \text{(E.3)}$$

where K_{NN} is nitrification rate which is a function of temperature; and H_{nit} is the half-saturation constant for the bacteria growth.

The dissolved form of ammonium in water is generally not stable and can exist in its gaseous form, or ammonia nitrogen. Because the ammonia concentration in the atmosphere is very low, ammonia in the water column can escape to the air. This is a volatilization process of ammonia. The volatilization of ammonia is a sink for nitrogen in an aquatic system. A first order rate equation can be used to describe the kinetics of the ammonia volatilization process (Chen and Sheng, 1994):

$$Q_{volatilization} = K_{VOL}\left[h_v NH_3 - NH_3^{atm}\right] \quad \text{(E.4)}$$

where K_{VOL} is rate constant of volatilization which is a function of temperature. It can be derived from the so-called two-film model (Jorgensen, 1983); h_v is henry's constant; and NH_3^{atm} is the ammonia concentration in the air.

Denitrification is defined as the biogeochemical transformation of nitrate nitrogen to gaseous end products such as molecular nitrogen or nitrous oxide (Reddy and Patrick, 1984).

While nitrification occurs in the water column and aerobic layer of the sediment column, denitrification occurs only in the anaerobic layer of the sediment column. The denitrification process can be described by the standard Michaelis-Menten equation (Bowman and Focht, 1974).

$$Q_{denitrification} = -K_{dn} \frac{H_{no3}}{H_{no3} + DO} NO_3 \tag{E.5}$$

where K_{dn} is the denitrification rate, which is a temperature function; and H_{no3} is the half-saturation constant for denitrification.

In the nitrogen species, sorption processes refer to conversion from a soluble to a solid phase of inorganic (NH4 to PIP) and organic (SON to PON) species, while desorption reactions describe the inverse process. Sorption/desorption processes, combined with resuspension events can significantly alter the nitrogen cycle in the system. The kinetics of sorption/desorption reactions are dependent on nitrogen species characteristics, sediment properties, pH, temperature, and dissolved oxygen concentration (Simon, 1989) The most commonly used mathematical representation of sorption/desorption processes is the linear, reversible, isotherm (Berkheiser et al., 1980; Reddy et al., 1988):

$$\frac{\partial}{\partial t} N_{ad} = -D_r \cdot N_{ad} + S_r \cdot N_s \tag{E.6}$$

where D_r is the desorption rate constant which is a temperature function; S_r is the sorption rate constant; N_{ad} is the adsorbed nitrogen concentration such as particulate inorganic and organic nitrogen; N_s is the dissolved nitrogen concentration such as dissolved ammonium nitrogen and dissolved organic nitrogen.

The ratio between the desorption and sorption rates gives the partition coefficient dissolved and particulate forms, because $\partial N_{ad} / \partial t = 0$ at equilibrium.

$$\frac{S_r}{D_r} = \frac{N_{ad}^0}{N_s^0} = p_c \tag{E.7}$$

where N_{ad}^0 and N_s^0 are the adsorbed and dissolved nitrogen, respectively, at the equilibrium condition; and p_c is the partition coefficient. Therefore, the kinetic equation for sorption/desorption reaction is:

$$\frac{\partial}{\partial t} N_{ad} = -D_r \cdot \left(N_{ad} - p_c \cdot N_s \right) \tag{E.8}$$

Inorganic nitrogen is incorporated by phytoplankton during growth and release as ammonium and organic nitrogen through respiration and non-predatory mortality. The phytoplankton nitrogen can be converted to zooplankton nitrogen by grazing process. The kinetic processes for particulate nitrogen species need to include settling process, which accounts for the limited vertical motion of particulate nitrogen. For this species, it is reasonable to assume the same settling velocity of the suspended sediment particles.

The mass balance equations for nitrogen state variables are written by combining nitrogen transformation processes.

Ammonia nitrogen (NH3)

include ammonia conversion and volatilization processes

For water column:

$$\frac{\partial}{\partial t} NH_3 = K_{al} \cdot \frac{pH}{H_{al} + pH} NH_4 - K_{VOL} \cdot \left[h_v \cdot NH_3 - NH_3^{atm} \right] \tag{E.9}$$

For sediment column:

$$\frac{\partial}{\partial t} NH_3 = K_{al} \cdot \frac{pH}{H_{al} + pH} NH_4 \tag{E.10}$$

where K_{al} is the ammonia conversion rate constant which is a temperature function; H_{al} is half-saturation constant for ammonia conversion.

Dissolved ammonium nitrogen (NH4)

include phytoplankton uptake and respiration, zooplankton respiration, ammonification, nitrification, ammonia conversion, and sorption/desorption reaction.

For water column:

$$\frac{\partial}{\partial t}NH_4 = -\left[\left(P_n \cdot \mu_a - K_{ax}\right) \cdot PhyC - K_{zx} \cdot ZooC\right] \cdot A_{NC} + K_{ONM} \cdot SON - K_{NN} \cdot \frac{DO}{H_{nit} + DO} \cdot NH_4 - K_{al} \cdot \frac{pH}{H_{al} + pH} \cdot NH_4 + d_{an}\left(PIN - p_{an} \cdot c \cdot NH_4\right) \quad \text{(E.11)}$$

For sediment column:

$$\frac{\partial}{\partial t}NH_4 = +K_{ONM} \cdot SON - K_{NN} \cdot \frac{DO}{H_{nit} + DO} \cdot NH_4 - K_{al} \cdot \frac{pH}{H_{al} + pH} \cdot NH_4 + d_{an}\left(PIN - p_{an} \cdot c \cdot NH_4\right) \quad \text{(E.12)}$$

where d_{an} is sorption/desorption rate of NH4 from sediment particles; p_{an} is the partition coefficient between NH4 and PIN; and c is the suspended sediment concentration.

Nitrate and nitrite nitrogen (NO3)

include nitrification, denitrification and phytoplankton uptake processes.

For water column:

$$\frac{\partial}{\partial t}NO_3 = +K_{NN} \cdot \frac{DO}{H_{nit} + DO} \cdot NH_4 - K_{DN} \cdot \frac{H_{no3}}{H_{no3} + DO} \cdot NO_3 - A_{NC} \cdot \left[(1 - P_n) \cdot \mu_a \cdot PhyC\right] \quad \text{(E.13)}$$

For sediment column:

$$\frac{\partial}{\partial t}NO_3 = +K_{NN} \cdot \frac{DO}{H_{nit} + DO} \cdot NH_4 - K_{DN} \cdot \frac{H_{no3}}{H_{no3} + DO} \cdot NO_3 \quad \text{(E.14)}$$

Soluble organic nitrogen (SON)

include ammonification and sorption/desorption reaction.

For water column:

$$\frac{\partial}{\partial t}SON = -K_{ONM} \cdot SON + d_{on} \cdot \left(PON - p_{on} \cdot c \cdot SON\right) \quad \text{(E.15)}$$

For sediment column:

$$\frac{\partial}{\partial t} SON = -K_{ONM} \cdot SON + d_{on} \cdot \left(PON - p_{on} \cdot c \cdot SON \right) \tag{E.16}$$

where d_{on} is sorption/desorption rate of SON from sediment particles; and p_{on} is the partition coefficient between SON and PON

Particulate organic nitrogen (PON)

include mortality of phytoplankton and zooplankton, settling, and a sorption-desorption reaction.

For water column:

$$\frac{\partial}{\partial t} PON = A_{NC} \cdot \left[K_{as} \cdot PhyC + K_{zs} \cdot ZooC \right] - \frac{\partial}{\partial z} ws_p \cdot PON - d_{on} \left(PON - p_{on} \cdot c \cdot SON \right) \tag{E.17}$$

For sediment column:

$$\frac{\partial}{\partial t} PON = -\frac{\partial}{\partial z} ws_p \cdot PON - d_{on} \left(PON - p_{on} \cdot c \cdot SON \right) \tag{E.18}$$

where ws_p is settling velocity for particulate species, which is same with that of suspended sediment particles.

Particulate inorganic nitrogen (PIN)

include settling and a sorption/desorption reaction.

For both water and sediment columns:

$$\frac{\partial}{\partial t} PIN = -\frac{\partial}{\partial z} ws_p \cdot PIN - d_{an} \left(PIN - p_{an} \cdot c \cdot NH_4 \right) \tag{E.19}$$

E.2 Phosphorous Cycle

Phosphorous can be classified into two groups: dissolved phosphorous and particulate phosphorous. The criterion for this division is established in the laboratory, using a filtering technique. The dissolved phosphorous include soluble reactive phosphorous (SRP) and dissolved organic phosphorous (SOP). Particulate phosphorous includes particulate inorganic phosphorous (PIP), and particulate organic phosphorous (POP). Phytoplankton

phosphorous (PhyP) and zooplankton phosphorous (ZooP) related biomass to phosphorous concentration, through a fixed stoichiometric ratio: phosphorous-to-carbon ration (A_{PC}).

The model phosphorous cycle (Figure E.2) includes the following processes:

1) Mineralization of organic phosphorous

2) Uptake of soluble reactive phosphorous by phytoplankton

3) Conversion of phytoplankton phosphorous to zooplankton phosphorous by grazing

4) Excretion and mortality by phytoplankton and zooplankton

5) Settling for particulate phosphorous

6) Sorption/desorption reactions

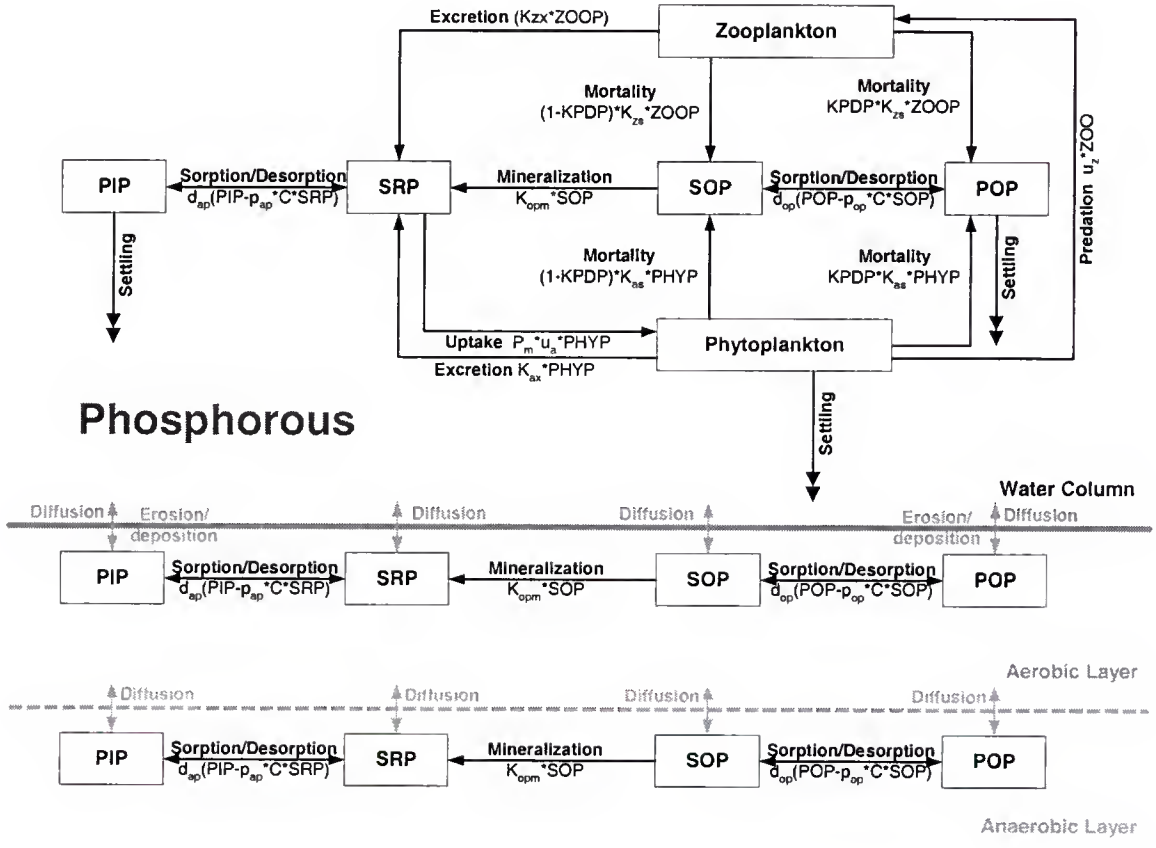

Figure E.2 Phosphorous Cycle

The mineralization process is mediated by bacteria, which transfers dissolved organic phosphorous to soluble reactive phosphorous, through the uptake of SOP and excretion of

SRP. Since bacteria abundance is related to algae biomass, the rate of organic phosphorous mineralization is related to algae biomass. The mineralization of SOP is a relatively fast process, it can take a few hours, compared to the mineralization of carbon and nitrogen, which takes place in a few days (Golterman, 1973). Mineralization is highest when algae are strongly phosphorous limited and is lowest when no limitation occurs. Thompson et al. (1954) found that the mineralization of dissolved organic phosphorous is influenced by pH value. An increase in pH causes a temporary increase in the rate of mineralization of dissolved organic phosphorous. Temperature can also affect the speed of the mineralization by stimulating the mineralization process with high temperatures.

The mineralization rate of SOP is usually modeled by a first order equation, as follows (Jorgensen, 1983)

$$Q_{\text{min}eralization} = -K_{opm} \cdot SOP \qquad \text{(E.20)}$$

where *Kopm* is a rate constant for mineralization of SOP, which is a function of pH and temperature.

Soluble reactive phosphorous is incorporated by phytoplankton, during growth and release, as soluble reactive phosphorous; and organic phosphorous through respiration and mortality. The phytoplankton phosphorous is converted to zooplankton phosphorous by grazing processes. The settling and sorption/desorption processes are similar to the nitrogen species.

The mass balance equations for phosphorous state variables are written by combining these phosphorous transformation processes.

Soluble reactive phosphorous (SRP)

include mineralization, uptake by phytoplankton, mortality of zoo and phytoplankton,

and sorption/desorption reaction.

For water column:

$$\frac{\partial}{\partial t}SRP = K_{opm} \cdot SOP + A_{PC}\left[-\mu_a \cdot PhyC + K_{ax} \cdot PhyC + K_{zx} \cdot ZooC\right] + d_{ip}\left(PIP - p_{ip} \cdot c \cdot SRP\right) \quad \text{(E.21)}$$

For sediment column:

$$\frac{\partial}{\partial t}SRP = K_{opm} \cdot SOP + d_{ip}\left(PIP - p_{ip} \cdot c \cdot SRP\right) \quad \text{(E.22)}$$

where d_{ip} is sorption/desorption rate of SRP from sediment particles; and p_{ip} is the partition coefficient between SRP and PIP.

Soluble organic phosphorous (SOP)

include mineralization and sorption/desorption reaction.

For both water and sediment columns:

$$\frac{\partial}{\partial t}SOP = -K_{opm} \cdot SOP - d_{op} \cdot \left(POP - p_{op} \cdot c \cdot SOP\right) \quad \text{(E.23)}$$

where d_{op} is sorption/desorption rate of SOP from sediment particles; and p_{op} is the partition coefficient between SOP and POP.

Particulate organic phosphorous (POP)

include respiration of zooplankton and phytoplankton, settling, and a sorption/desorption reaction.

For water column:

$$\frac{\partial}{\partial t}POP = A_{PC}\left(K_{as} \cdot PhyC + K_{zs} \cdot ZooC\right) - \frac{\partial}{\partial z}ws_p \cdot POP - d_{op} \cdot \left(POP - p_{op} \cdot c \cdot SOP\right) \quad \text{(E.24)}$$

For sediment column:

$$\frac{\partial}{\partial t}POP = -\frac{\partial}{\partial z}ws_p \cdot POP - d_{op} \cdot \left(POP - p_{op} \cdot c \cdot SOP\right) \quad \text{(E.25)}$$

Particulate inorganic phosphorous (PIP)

include settling and a sorption/desorption reaction

For both water and sediment columns:

$$\frac{\partial}{\partial t} PIP = -\frac{\partial}{\partial z} ws_p \cdot PIP - d_{ip} \cdot \left(PIP - p_{ip} \cdot c \cdot SRP \right) \qquad \text{(E.26)}$$

APPENDIX F
SEDIMENT FLUX MODEL

DiToro et al. (1990) developed a model of the SOD process in a mechanistic fashion using the square-root relationship of SOD to sediment oxygen carbon content. Using similar analysis as applied to carbon, they also evaluate the effect of nitrification on SOD. In this model, carbon and nitrogen diagenesis are assumed to occur at uniform rates in a homogeneous layer of the sediment of constant depth (active layer). The sediment oxygen demand and sediment fluxes are calculated by simple first-order decay processes of the concentrations of particulate organic carbonaceous material and of particulate organic nitrogenous material in this active layer as follow:

$$\frac{dC_{poc}}{dt} = -k_{poc}C_{poc} + M_C \tag{F.1}$$

$$\frac{dC_{pon}}{dt} = -k_{pon}C_{pon} + M_N \tag{F.2}$$

where C_{POC} is a concentration of POC in sediment (g O_2/m^3)

C_{PON} is a concentration of PON in sediment (g O_2/m^3)

K_{POC} is a decay rate of POC in sediment (g O_2/m^3)

K_{PON} is a decay rate of POC in sediment (g O_2/m^3)

M_N is a source term for C_{POC} (g/m^3-day)

M_C is a source term for C_{PON} (g/m^3-day)

Sediment carbon and nitrogen diagenesis fluxes, J_C and J_N, are the most important

parameters in the equations for sediment oxygen demand and sediment fluxes as defined by

$$J_C = -k_{poc} C_{poc} H$$
$$J_N = -k_{pon} C_{pon} H \quad \text{(F.3)}$$

where H is the depth of the active layer (m)

Using these diagensis fluxes, DiToro and Pitzpatrick developed sediment flux model which include NSOD, CSOD, ammonia and nitrate flux, methane flux, and sulfide flux.

F.1 Sediment Flux Equations inCH3D-WQ3D

The reactive portion of particulate organic carbon and particulate organic nitrogen in the sediment are presented by CBOD and NH4 in CH3D-WQ3D model system. The equation (F.3) can be rewritten as

$$J_C = -k_{oxy} \cdot \Theta_{oxy}^{T-20} \cdot CBOD_{sed} \cdot H$$
$$J_N = -k_{nit} \cdot \Theta_{nit}^{T-20} \cdot NH4_{sed} \cdot H \quad \text{(F.4)}$$

where k_{oxy} is a oxidation rate in sediment (g O_2/m^3)

k_{nit} is a nitrification rate in sediment (g O_2/m^3)

Θ_{oxy}^{T-20} is a temperature effect of oxidation

Θ_{nit}^{T-20} is a temperature effect of nitrification

In this study, sediment fluxes include sediment oxygen demand, benthic dissolved methane flux, and benthic methane gas flux. Sediment oxygen demand (SOD) can be determined for the set of equations developed by DiToro and Fitzpatrick (1993).

Carbonaceous sediment oxygen demand (g/m^2/d):

$$CSOD = \sqrt{2K_D C_S J_C}\left(1 - \sec h\left[\frac{K_C O_2}{SOD}\right]\right) \quad \text{(F.5)}$$

Note: The square root term is replaced by J_C if $J_C < 2K_D C_s$

Nitrogenous sediment oxygen demand (g/m^2/d):

$$NSOD = 1.714 \cdot J_N \left(1 - \sec h \left[\frac{K_N O_2}{SOD} \right] \right) \tag{F.6}$$

Total sediment oxygen demand (g/m^2/d):

$$SOD = CSOD + NSOD \tag{F.7}$$

where O2 is a concentration of dissolved oxygen in overlying water column (g O2/m3).

k_D is a dissolved methane diffusion mass transfer coefficient (g O_2/m^3)

k_C is a reaction velocity for methane oxidation (g O_2/m^3)

k_N is a reaction velocity for ammonia oxidation (g O_2/m^3)

C_s is a methane solubility (g O_2/m^3)

The magnitude of the fluxes at the sediment water interface of aqueous methane and gaseous methane are predicted to be

$$J_{CH4(aq)} = \sqrt{2K_D C_S J_C} \left(\sec h \left[\frac{K_C O_2}{SOD} \right] \right) \tag{F.8}$$

$$J_{CH4(g)} = J_C - \sqrt{2K_D C_S J_C} \tag{F.9}$$

The original DO kinetic equation in CH3D-WQ3D is modified to incorporate the sediment exchange predictions of the DiToro model, given by equation (F.10).

$$\frac{\partial DO}{\partial t} = -Oxydation - Nitrification + reaeration + photosynthesis - respiration - \frac{SOD}{H} - \frac{J_{CH4(aq)}}{H} - G_{frac} \frac{J_{CH4(g)}}{H} \tag{F.10}$$

where G_{frac} is a fraction of gaseous methane produced in the sediment.

H is a water depth.

The first five source and sink terms in the equation (F.10) are the same with the original DO kinetic equation, while the last three terms represent oxygen demand due to sediment exchange processes, where SOD and aqueous and gaseous methane flux rates.

APPENDIX G
MODEL PERFORMANCE TEST WITH PARALLEL CH3D-IMS

To reduce the computational time necessary to simulate multiple-year seasonal response of the Charlotte Harbor estuarine system with a serial CH3D model, a parallel CH3D model was developed and validated. The parallel approach is applied to the parallel CH3D model via parallel constructs added to the serial CH3D model (Davis and Sheng, 2000; Sheng et al., 2003). These parallel constructs are implemented by adding additional macros to the original serial source code. By defaults, the parallel CH3D model uses OpenMP constructs although due to the flexible nature of the implementation process, either Sun Microsystems-style or Clay-style constructs can be used. The parallel source code closely resembles the serial source code and maintains perfect compatibility with the serial code. In other words, the parallel CH3D model can be executed using the same input files as the serial CH3D model and parallel CH3D output format is identical to the output format of the serial CH3D model. To determine how well the parallel CH3D model performs in Charlotte Harbor estuarine system, the serial and parallel CH3D simulations performed for the parallel model validation.

G.1 Validation of Parallel Model

To validate the parallel CH3D model, simulations are performed using both the serial and parallel CH3D model. CH3D model output from all of the parallel simulations are then compared to their respective serial simulations to fully validate the parallel CH3D model.

The computational grid for Charlotte Harbor estuarine system contains 92 x 129 horizontal cells (Figure 5.1) and 8 vertical layers, with a total 11648 grid cells which include 5367 water cells and 6281 land cells. Grid spacing varies from 40 to 2876 meters (average 598 meters). Using this grid, the 3-D hydrodynamic and water quality simulation simulate the circulation, sediment transport, and water quality dynamics of the Charlotte Harbor estuarine system from May 23 to June 22, 1996. The initial condition for simulation is provided by a 30-day spin up simulation (April 23 to May 23) previously performed during the dry season with all forcing mechanisms (tides, river discharges, wind) to allow water level, velocity and salinity field to reach dynamic steady-state throughout the computational domain. A more detailed description of the simulation can be found in Chapter 6.

Simulated time series and field parameters at the end of 30-day simulation of each parallel simulation are compared to the all corresponding simulated parameters from the serial CH3D simulation which include water level, current velocity, temperature, salinity, sediment concentration, and all water quality species. For all comparisons, the simulated time series and field parameters obtained from the serial CH3d model are identical to the simulated parameters obtained from the parallel CH3D model. Thus the parallel CH3D model is completely validated.

G.2 CPU Times of Parallel Routines

The 1-month simulation is simulated using both serial and parallel CH3D models on the SGI orgin system witch is Silicon Graphyics Origin 3400, 400 MHz MIPS R12000 (IP 35). This platform has 16 processors and 8 GB main memory size. The parallel model is executed using from 1 to 4 processors on this system. Table F.1 report the CPU times per iteration for the parallel CH3D model executed on this platform. This timing results show

that the time necessary for CH3D simulation can be significantly reduced using multi-processor computers coupled with parallel techniques.

Table G.1 CPU time for the parallel, shared memory, CH3D procedures on SGI origin platform. Time shown are per time step iteration of the model using computational grid (92x129) and are given in seconds, n is the number of processors used and speed up is shown in parenthesis.

	Serial	n=1	n=2	n=3	n=4
Main WQ	1.221(1.00)	1.287(0.95)	0.680(1.80)	0.469(2.60)	0.370(3.30)
Main Sediment	0.126(1.00)	0.125(1.01)	0.078(1.62)	0.060(2.10)	0.052(2.41)
Turbulence	0.100(1.00)	0.107(0.93)	0.059(1.70)	0.045(2.21)	0.038(2.61)
Sediment transport	0.090(1.00)	0.089(1.01)	0.047(1.94)	0.032(2.85)	0.025(3.62)
Dimensionalize	0.075(1.00)	0.083(0.90)	0.047(1.62)	0.033(2.28)	0.026(2.89)
Baroclinic (J)	0.071(1.00)	0.075(0.95)	0.042(1.70)	0.038(1.87)	0.036(1.97)
Baroclinic (I)	0.070(1.00)	0.067(1.05)	0.038(1.86)	0.025(2.75)	0.020(3.49)
Salinity	0.055(1.00)	0.059(0.95)	0.030(1.85)	0.020(2.51)	0.016(3.43)
N.L./Diffusion (J)	0.055(1.00)	0.055(1.00)	0.033(1.65)	0.030(1.84)	0.029(1.87)
N.L./Diffusion (I)	0.042(1.00)	0.043(0.98)	0.025(1.65)	0.018(2.34)	0.015(2.82)
Layer Vel. (v)	0.040(1.00)	0.041(0.97)	0.027(1.48)	0.021(1.86)	0.019(2.12)
Layer Vel. (u)	0.028(1.00)	0.029(0.97)	0.016(1.73)	0.011(2.60)	0.009(3.28)
Layer Vel. (w)	0.011(1.00)	0.011(0.99)	0.006(1.70)	0.004(2.37)	0.003(2.85)
Interpolation	0.011(1.00)	0.011(1.00)	0.006(1.79)	0.005(2.62)	0.004(3.52)
integrate Vel. (U)	0.008(1.00)	0.008(1.00)	0.006(1.34)	0.004(1.69)	0.004(1.87)
integrate Vel. (V)	0.006(1.00)	0.006(0.97)	0.004(1.35)	0.005(1.32)	0.005(1.26)
Bottom sheer stress	0.001(1.00)	0.001(1.01)	0.001(1.89)	0.000(2.76)	0.000(3.60)
Wave H/T	0.001(1.00)	0.001(1.03)	0.000(1.95)	0.000(2.93)	0.000(3.87)
All Parallel Routine	1.973(1.00)	2.060(1.00)	1.152(1.71)	0.843(2.34)	0.701(2.82)
Total Routine	2.022(1.00)	2.107(1.00)	1.204(1.68)	0.895(2.26)	0.753(2.69)

G.3 Parallel Speedup

The parallel speed up for the Charlotte Harbor 1-month simulation described earlier on the SGI Origin platform is shown in Figure G.1. As the lines get close to the theoretical maximum, the parallel model is performing better. The speedups of the individual parallel procedures are shown as values inside parenthesis in the previous table G.1 and also illustrate

how computationally intense routines have higher speedups. Applying parallel method for CH3D model achieved a 1.71x and 2.82x speedups using 2 processors and 4 processors, respectively.

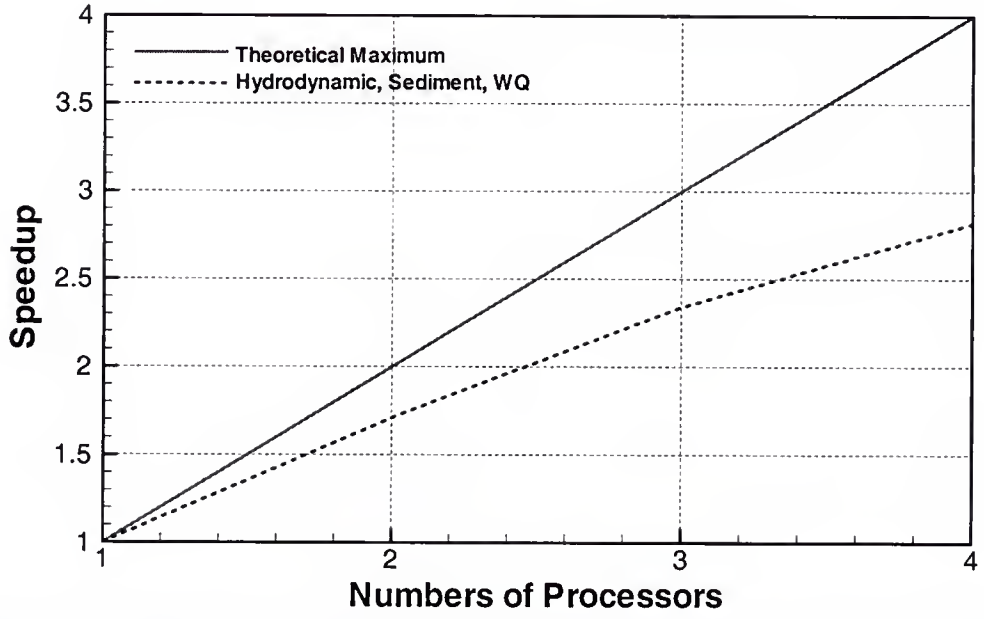

Figure G.1 Parallel speedup gained in performing the simulation on the SGI Origin platform

APPENDIX H
TIDAL BENCH MARKS FOR CHARLOTTE HARBOR

Table H.1 Tidal datum referred to Mean Low Low Water (MLLW), in meter.

Station Number	Station Name	Latitude	Longitude	MHHW	MHW	MLW	NAVD
8725853	Venice	27 04.3	82 27.3	0.671	0.589	0.113	0.496
8725791	Peace River	26 59.3	81 59.6	0.615	0.537	0.119	0.501
8725781	Shell Creek	26 58.8	81 57.6	0.668	0.570	0.135	0.472
8725541	Bokeelia	26 42.4	82 09.8	0.526	0.481	0.072	0.495
8725520	Fort Myers	26 38.8	81 52.3	0.401	0.335	0.191	0.318
8725391	Sanibel	26 29.3	82 00.8	0.689	0.614	0.145	0.570
8725110	Naples	26 07.8	81 48.7	0.874	0.797	0.184	0.696

REFERENCES

Ambrose, R. B. Jr., Wool, T.A., Martin, J.L., Connolly, J.P., Schanz, R.W. (1994) WASP5, A hydrodynamic and water quality model-model theory, user's manual, and programmer's guide. U.S.EPA Environmental Research Laboratory. Athens, Georgia.

American Public Health Association(APHA) (1985). Standard methods for the examination of water and wastewater. APHA. Washington, D.C.

Banks, R.B. (1975). Some features of wind action on shallow lakes, ASCE, Journal of Environmental Engineering Division, Vol. 101, No. EE5, p813-827

Banks, R.B. and Herrera, F.F. (1977). Effect of wind and rain on surface reaeration, ASCE, Journal of Environmental Engineering Division, Vol. 103, No. EE3, p489-504

Baker, B. (1990). Draft Caloosahatchee water quality based effluent limitations documentation (Lee County). Florida Department of Environment Regulation. Water Quality Tech. Ser. 2. No. 121: 18.

Berkheiser, V.E., Street, J.J., Rao, P.S.C., and Yuan, T.L. (1980) Partitioning of inorganic orthophosphate in soil-water systems. CRC Critical Review in Environmental Control.

Berliand, M.E., and Berliand, T.G. (1952). Determining the net longwave radiation of the Earth with the consideration of the effect of cloudiness, Isv. Acad. Nauk., SSSR Ser. Geofis, No. 1.

Boler, R.N., Malloy, R.C., and Lesnett, E.M. (1991) Surface water quality monitoring by the Environmental Protection Commission of Hillsborough County. In (S.F. Treat and Clark P.A., eds.) Proceedings of Tampa Bay Area Scientific Information Symposium 2, 1991. Tampa, FL.

Bowie, G.L., Mills, W.B., Porcella, D.B., Campbell, C.L., Pagenkopf, J.R., Rupp, G.L., Johnson, K.M., Chan, P.W.H., Gherini, S.A. and Chamberlin, C.E. (1985). Rates, constants, and kinetics formulations in surface water quality modeling. In: (Editors), U.S. Environmental Protection Agency, Office of Research and Development, Athens, GA

Bowie, G.L., Chen, C.W. and Dykstra, D.H. (1980) Lake Ontario ecological modeling, phase III. Tectra-Tech, Inc., Lafayete, CA.

Bowman, R.A. and Focht, D.D. (1974). The influence of glucose and nitrate concentrations upon denitrification rates in sandy soils. Soil Biol. Biochem. 6: 297-301.

Bricaud, A., Morel, A., and Prieur, L. (1981). Absorption by dissolved organic matter of the sea (yellow substance) in the uv and visible domains. Limnology and Oceanography, 28(5):43-53.

Budyko, M. I. (1974). Climate and Life. Academic Press Inc., New York, 508pp.

Camp, Dresser, & Mckee (1998). The Study of Seasonal and Spatial Patterns of Hypoxia in the Upper Charlotte Harbor. Prepared for SWFWMD, Prepared by Camp, Dresser, & Mckee

Canale, R.P., DePalma, L.M., and Vogal, A.H. (1976). A plankton-based food web model for Lake Michigan, in (R.P. Canale, ed.) Modeling Biochemical Processes in Aquatic Ecosystem, Ann Arbor Science Publishers Inc., P.O. Box 1452, Ann Arbor, Michigan 48160.

Cerco, D.F., and Cole, T.M. (1994). Three-dimensional eutrophication model of Chesapeake Bay. Technical Report El-94-4, U.S. Army Engineer Waterways Experiment Station, Vicksburg, MS.

Cerco, D.F., and Cole, T.M. (1995). User Guide to the CE-QUAL-ICM three-dimensional eutrophication model, Technical Report EL-95-15, U.S. Army Corps of Engineers, Washington, DC.

Chamberlain, R.H. and Doering, P.H. (1998). Freshwater inflow to the Caloosahatchee Estuary and the resource-based method for evaluation. Proceedings of the Charlotte Harbor public conference and technical symposium, Technical Report No. 98-02: 81-90.

Chapra, S.C. (1997). Surface water-quality modeling. The McGRAW-HILL companies, INC., New York.

Chen, C.W., and Orlob, G.T. (1975). Ecologic simulation of aquatic environments. Systems Analysis and Simulation in Ecology, Vol. 3, B.C. Pattern (ed.). Academic Press, New York: 475-588.

Chen, X. and Sheng, Y.P.(1994). Effects of hydrodynamics and sediment transport processes on nutrient dynamics in shallow lakes and estuaries. Ph.D. dissertation. University of Florida, Gainesville, Florida

Christian, D.J. and Sheng, Y.P.(2003). Modeling the Effects of Hydrodynamics, Suspended Sediments, and Water Quality on Light Attenuation in Indian River Lagoon, Florida. PhD dissertation, University of Florida., Gainesville, Florida.

Clark, N. E., Eber R. M. Renner J. A., and Saur J. F. T. (1974) Heat exchange between ocean and atmosphere in the eastern North Pacific for 196-71. NOAA Tech. Rep. NMFS SSRF-682, U.S.Dept. Commerce, Washington.,D.C.

Davis, J.R. and Sheng, Y.P. (2000). High performance estuarine and coastal environmental modeling: The CH3D example. In Estuarine and Coastal Modeling, Vol. 6, p470-486. American Society of Civil Engineers.

Davis, J.R. and Sheng, Y.P. (2001). High Performance Modeling of Circulation and Transport in the Indian River Lagoon, Florida. PhD dissertation, University of Florida., Gainesville, Florida.

Day, J.W. Jr., Hall, C.A.S, Kemp, K.M., and Arancibia, A.J. (1989). Estuarine Ecology. John Wiley & Sons. New York.

DeCosmo, J., Katsaros, K.B., Smith, S.D., Anderson, R.J., Oost, W.A., Bumke, K., and Chadwick, H.M. (1996). Air-sea exchange of water vapor and sensible heat: The Humidity Exchange Over the Sea (HEXOS) results. J. Geophys. Res.-Oceans, 101: 12,001-12,016.

Degrove, B. (1981). Caloosahatchee River wasterload allocation documentation. Florida Dept. Of Env. Reg., Water Quality Tech ser. 2. No. 52: 17.

Degrove, B. and Nearhoof, F. (1987). Water quality assessment for Caloosahatchee River. Florida Dept. Of Env. Reg. Water Quality Tech. Ser. 3. No. 19.

DiToro, D.M., Paquin, P.R., Subburamu,K., and Gruber, D.A. (1990). Sediment oxygen demand model:Methan and ammonia oxidation. Journal of Evironmental Engineering, 116(5), p945-986.

DiToro, D.M. and Fitzpatrick, J.J. (1993). Chesapeaka bay sediment flux model. U.S. Army Corps of Engineers, Waterways Experiment Station, Tech. Report EL-93-2.

Dixon, L.K., and Gary, J.K. (1999). Cause of light attenuation with respect to seagrasses in upper and Lower Charlotte Harbor. Marine Laboratory Technical Report No. 650. Prepared for Southwest Florida Water Management District.

Doering, P.H. (1996). Temporal variability of water quality in the St. Lucie Estuary, South Florida. Water Resource Bulletin 32:1293-1306.

Echternacht, K.L. (1975). A study of the precipitation regimes of the Kissimmee River-Lake Okeechobee watershed. Florida Department of Environmental Regulation Technical Service (3)1. Tallahassee, Florida.

Eckart, C. (1958). Properties of water. Part II. The equation of state of water and sea water at low temperatures and pressures. American Journal of Science, 256(4): 224-240.

Edwards, R.E., Lung, W., Montagna, P.A., and Windom, H.L. (2000). Final review report. Caloosahatchee Minimim Flow Peer Review Panel, September 27-29, 2000. Report to the south Florida Water Management District, West Palm Beach, Florida.

Environmental Quality Laboratory, Inc. (1979). Hydrobiological monitoring report to the Southwest Florida Water Management District, Port Charlotte, Florida.

Environmental Quality Laboratory, Inc. (1987). Hydrobiological monitoring program, data report for the period from March 1986 through Feburaury 1987 covering the lower Peace River abd Charlotte Harbor. Port Charlotte, Florida, Environmental Quality Laboratory, Inc.: 92.

Eppley, R.W. (1972). Temperature and phytoplankton growth in the sea. Fish. Bull., 70:1063-1085.

Estevez, E. D. (1986). Infaunal macro invertebrates of the Charlotte Harbor estuarine system and surrounding inshore waters, Florida.. U.S. Geological Survey Water-Resources Investigations Report 85-4260: 116.

Estevez, E.D. (1998). The story of the greater Charlotte Harbor Watershed, Charlotte Harbor Estuarine Program, North Fort Myers, Florida.

Fraser, T.H. (1986). Long-term water-quality characteristics of Charlotte Harbor, Florida. U.S. Geological Survey Water-Resources Investigations Report 86-4180: 43.

Fraser, T.H. and Wilcox, W.H. (1981). Enrichment of a subtropical estuary with nitrogen, phosphorous, and silica, in Neilson, B.J., and Cronin, L.E., eds., Estuarine and Nutrients, Humana Press, New Jersey: 481-498.

Friehe, C. A. and Schmitt, K. B. (1976). Parameterization of air-sea interface fluxes of sensible heat and moisture by the bulk aerodynamic formulas. Journal of Physical Oceanography, 6, 801-809.

Gallegos, C.L. (1993). Determination of optical water quality requirements in the Indian River near Ft. Pierce, FL, with emphasis on the impact of colored water discharges. Technical report, South Florida Water Management District.

Gallegos, C.L. and Correl, D.L. (1990). Modeling spectral diffuse attenuation, absorption, and scattering coefficients in a turbid estuary. Limnology and Oceanography, 35(7):1484-1502.

Gallegos, C.L. and Kenworthy, W.J. (1996). Seagrass depth limits in the Indian River Lagoon (Florida, USA). Estuarine, Coastal, and Shelf Science, 42:267-288.

Garret, J.R. (1977). Review of drag coefficients over oceans and continents. Monthly Weather Review 105:915-929.

Golterman, H.L. (1973). Vertical Movement of Phosphorous in Freshwater, in (E.J. Griffith, A. Beeton, J.M Spencer, and D.T. Mitchell, eds.) Environmental Phosphorous Handbook, John Wiley & Sons., New York.

Goodwin, C.R. (1996). Simulation of tidal-flow, circulation, and flushing of the Charlotte Harbor estuarine system, Florida. U.S. Geological Survey Water-Resources Investigations Report 93-4153.

Goodwin, C. R. and Michaelis, D.M. (1976). Tides in Tampa Bay, Florida: June 1971 to December 1973. U.S. Geological Survey Open-File Report FL-75004: 338.

Hammet, K. M. (1990). Land use, water use, streamflow characteristics, and water-quality characteristics of the Charlotte Harbor inflow area, Florida. U.S. Geological Survey Water-Supply Paper 2350-A: 64.

Hammet, K. M. (1992). Physical processes, salinity characteristics, and potential salinity changes due to freshwater withdrawals in the tidal Myakka River, Florida. U.S. Geological Survey Water-Resources Investigations Report 90-4054:20

Heyl, M.G. (1997). Hypoxia in upper Charlotte Harbor. Proceedings of the Charlotte Harbor public conference and technical symposium, Technical Report No. 98-02: 219-228.

Hwang, T.C. (1966). A Sedimentologic Study of Charlotte Harbor, Southwestern Florida. Master's thesis, Florida State University, Tallahassee, Florida.

Jaworski, N.A. (1981). Source of Nutrients and the scale of eutrophication problems in estuaries, in Neilson, N.J., Jersey, Humana Press: p83-110.

Jerlov, N.G. (1976). Marine Optics. Elsevier Scientific Publishing Company, New York.

Jorgensen, S.E. (1976). A eutrophication model for a lake. Ecological Modeling 2:147-165.

Jorgensen, S.E. (1983). Modeling the ecological processes. In: (G.T. Orlob, ed.) Mathematical Modeling of Water Quality: Streams, Lakes, and Reservoirs. John Wiley and Sons. New York. Pp 116-149.

Jorgensen, S.E., Sorensen, B.H., and Nielsen, S.N. (editors) (1996). Handbook of Environmental and Ecological Modeling. CRC Press, Inc.

Jorgensen, S.E., and Gromiec, M.E. (editors) (1989). Mathematical sub-models in water quality systems. Development in Environmental Modeling, 14. Elsevier Science Publishers.

Ketchem, B.H. (1967). Phytoplankton nutrients in estuaries, in Lauff, G. H., ed., Estuaries. National Oceanic and Atmospheric Administration

Kirk, J.T.O. (1984). Dependence of relationship between inherent and apparent optical properties of water on solar altitude. Limnology and Oceanography, 29(2):350-356.

Lam, D.D.L., Schertzer, W.M., and Fraser, A.S. (1983). Simulation of Lake Erie water quality responses to loading and weather variations, I.W.D. Scientific Series, 134, Environment Canada, Ottawa:299.

McEwan, J., Gabric, A.J. & Bell, P.R.F. (1998). Water quality and phytoplankton dynamics in Moreton Bay, Southeastern Queensland. II. Mathematical modeling. Marine and Freshwater Research, Vol. 40, No. 3, p215-225.

McPherson, B. F. and Miller, R.L. (1990). Nutrient distribution and variability in the Charlotte Harbor estuarine system, Florida. Water Resource Bulletin 26: 67-80.

McPherson, B. F., Miller, R. L. and Stoker, Y. E. (1996). Physical, Chemical, and Biological Characteristics of the Charlotte Harbor Basin and Estuarine System in Southwestern Florida-A Summary of the 1982-89 U.S. Geological Survey Charlotte Harbor Assessment and Other Studies. U.S. Geological Survey Water-Supply Paper 2486.

Metha, A.J. (1986). Characterization of cohesive sediment properties and transport processes in estuaries. In:A.J. Metha (ed.), Estuarine Cohesive Sediment Dynamics. Springer, New York:290-325.

Mehta, A.J. (1989). On estuarine cohesive sediment suspension behavior. Journal of Geophysical Research 94(C10):14303-14314.

Mellor, G. L., (1996), Introduction to Physical Oceanography, Springer, Verlag New York.

Miller R. L. and McPherson B. J., (1995). Modeling Photosynthetically Active Radiation in Water of Tampa Bay, Florida, with Emphasis on the Geometry of Incident Irradiance. Estuarine, Coastal and Shelf Science, 40, 359-377 .

Morel, F. (1983). Principles of aquatic chemistry. John Wiley and Sons, New York, NY:150.

Morel, A., and Gentili, B. (1991). Diffuse reflectance of oceanic waters: Its dependence on sun angle as influenced by the molecular scattering contribution. Applied Optics 30:4427-2238.

Morrison, G. (1997). Proposed trophic state goals and nitrogen management objectives for the tidal reaches of the Peace and Myakka rivers. Draft. Prepared by Southwest Florida Water Management District, Surface Water Improvement and Management (SWIM) Section.

O'Connor, D.J. and Thomann, R.V. (1972). Water quality models: chemical, physical and biological constituents. In: Estuarine Modeling: an Assessment. EPA Water Pollution Control Research Series 16070 DZV, Section 702/71.

Oliveria, J., Burnett, W.C., Mazzilli, B.P., Brags, E.S., Farias, L.A., Christoff, J., and Furtado, V.V. (2003). Reconnaissance of submarine groundwater discharge at ubatuba coast, Brazil, using rn-222 as a natural tracer, Journal of Radioact., 69:37-52.

Orth, R.J. and Moore, K.A. (1983). Chesapeake Bay: An unprecedented decline in submerged aquatic vegetation. Science, v. 222, No. 4619: 51-53.

Phillips, N.A. (1957). A coordinate system having some special advantage for numerical forecasting. Journal of Meteor. 14:184-185.

Pickard , G. L . and Emery, W. J. (1990). Descriptive physical Oceanography. Pergamon Press, New York. Fifth (SI) Enlarged Edition: 320.

Pribble, J.R., Wade, D.L., Squires, A.D., and Janicki, A.J. (1998). A mechanic water quality model for the tidal Peace and Myakka rivers. Proceedings of the Charlotte Harbor public conference and technical symposium, Technical Report No. 98-02: 242-258.

Prieur, L. and Sathyendranath, S. (1981). An optical classification of coastal and oceanographic waters based on the specific spectral absorption curves of phytoplankton pigments, dissolved organic matter, and other particulate materials. Limnology and Oceanography, 26(4):671-689.

Rao P.S.C., Jessup, R.E., Reddy, K.R. (1984). Simulation of nitrogen dynamics in flooded soils. Soil Science 138:54-62.

Reddy, K.R., Jessup, R.E., Rao, P.S.C. (1988). Nitrogen dynamics in a eutrophic lake sediment. Hydrobiologia 159:177-188.

Reddy, K.R., and Patrick, W.H. (1984). Nitrogen transformations and loss in flooded soil and sediments. CRC Critical Reviews in Environmental Control 13(4):273-309.

Redfield, A., Ketchman, B., and Richar, F. (1966). The influence of organisms on the composition of sea-water. The Sea VolII. Interscience Publishers, New York, 26-48.

Reed, R. K. (1977). On estimating insolation over the ocean. Journal of Physical Oceanography, 7, 482-485. Research 49(3): 227-239.

Rutkowski, C.W., Burnett, W.C., Iverson, R.L., and Chanton, J.P. (1999). The effect of groundwater seepage on nutrient delivery and seagrasss distribution in the northern Gulf of Mexico. Estuaries, 22:2033-1040.

Schropp, S.J. (1998). Charlotte Harbor Sediment Quality Data Review and Evaluation. Proceedings of the Charlotte Harbor public conference and technical symposium, Technical Report No. 98-02: 35-47.

Sheng, Y.P. (1983). Mathematical modeling of three-dimensional coastal currents and sediment dispersion: model development and application. Coastal Engineering Research Center Tech. Rep. CERC-TR-83-2. U.S. Army Corps of Engineers.

Sheng, Y.P. (1986). Modeling bottom boundary layers and cohesive sediment dynamics. In:(A.J. Mehta, ed.) Estuarine Cohesive Sediment Dynamics. Pp.360-400. Springer-Verlag. Berlin.

Sheng, Y.P. (1987). On modeling three-dimensional estuarine and marine hydrodynamics. In Nihoul and Jamart, editors, Three-dimensional models of marine and estuarine dynamics, pages 35-54. Elswvier, Amsterdam.

Sheng, Y.P. (1989). Evolution of a 3-D curvilinear grid hydrodynamic model: CH3D. In:(M.L. Spaulding, ed.) Proceedings of the Estuarine and Coastal Modeling Conference. ASCE, Newport, R.I., pp.40-49.

Sheng, Y.P. (1994). Modeling hydrodynamics and water quality dynamics in shallow waters. In Proceedings of the first International Symposium on Ecology and Engineering, Taman Negara, Malaysia. University of Western Australia and Malaysian Technical University.

Sheng, Y.P. (1995). On Modeling circulation in Florida Bay. In American Geophysical Union Conference on Circulation in Intra-American Seas, Pueto Rico. American Geophysical Union.

Sheng, Y.P. (1998). Circulation in the Charlotte Harbor estuarine system. Proceedings of the Charlotte Harbor public conference and technical symposium, Technical Report No. 98-02: 91-110.

Sheng, Y.P. (2000). A framework for integrated modeling of coupled hydrodynamic-sedimentary-ecological processes. In Estuarine and Coastal Modeling, Volume 6, pages 350-362. American Society of Civil Engineers.

Sheng, Y.P., Ahn, K.M., and Choi, J.K. (1990). Wind-wave hindcasting and estimation of bottom sheer stress in Lake Okeechobee. Technical Report UFL/COEL-93/021, Coastal and Oceanographic Engineering Department, University of Florida, Gainesville, Florida.

Sheng, Y.P., Chen, X.J., Schofield, S., and Yassuda, E. (1993). Hydrodynamics, sediment and phosphorous dynamics in Lake Okeechobee during an episodic event. Technical Report, Coastal and Oceanographic Engineering Department, University of Florida, Gainesville, Florida.

Sheng, Y.P., and Chiu, S.S. (1986). Tropical cyclone generated currents. In Proceedings of the 20th International Conference on Coastal Engineering, pages 737-751. American Society of Civil Engineers.

Sheng, Y.P., Christian, D., and Kim, T.Y. (2002c). A IRL light attenuation model. Indian River Lagoon Pollutant Load Reduction (IRLPLR) Model Development Project. Final Report Volume II (A 3-D Water Quality Model) to St. Johns River Water Management District. Coastal and Oceanographic Engineering Department, University of Florida, Gainesville, Florida.

Sheng, Y.P., Davis, J.R., and Park, K. (2003) Development of parallel computing version of CH3D: Parallel CH3D User's Manual. Amendment to the three dimensional water quality model of the Charlotte Harbor estuarine system for the South Florida Water Management District.

Sheng, Y.P., Davis, J.R., Sun, D.,Qiu, C., Park, K., Kim, T.Y., and Zhang, Y. (2001). Application of an integrated modeling system of estuarine and coastal ecosystem to Indian River Lagoon, Florida. In Estuarine and Coastal Modeling, Session 4B. American Society of Civil Engineers. pp.329-343

Sheng, Y.P., and Lick, W. (1979). Resuspension and transport of sediments in a shallow lake. Journal of Geophysical Research, V. 84, pp. 1809-1826.

Sheng, Y.P. and Park, K. (2000). A 3-D Circulation and Salinity Model of Charlotte Harbor Estuarine System. Phase I Final Report to Southwest Florida Water Management Department (SFWMD), University of Florida, Gainesville, Florida.

Sheng, Y.P. and Park, K. (2001). Modeling the Effects of Caloosahatchee Discharges on Circulation and Salinity in Charlotte Harbor. Interim Report Southwest Florida Water Management Department (SFWMD), University of Florida, Gainesville, Florida.

Sheng, Y.P. and Park, K. (2002). 3-dimensional Water Quality model for Charlotte Harbor estuarine system. Phase III Final Report Southwest Florida Water Management Department (SFWMD), University of Florida, Gainesville, Florida.

Sheng, Y.P., Qiu, Q., Park, K., and Kim, T.Y. (2002b). A 3-D water quality model. Indian River Lagoon Pollutant Load Reduction (IRLPLR) Model Development Project. Final Report Volume II (A 3-D Water Quality Model) to St. Johns River Water Management District. Coastal and Oceanographic Engineering Department, University of Florida, Gainesville, Florida.

Sheng, Y.P., Sun, D., and Zhang, Y. (2002a). A 3-D IRL suspended sediment transport model. Indian River Lagoon Pollutant Load Reduction (IRLPLR) Model Development Project. Final Report to St. Johns River Water Management District. Coastal and Oceanographic Engineering Department, University of Florida, Gainesville, Florida.

Sheng, Y.P., and Villaret, C. (1989). Modeling the effect of suspended sediment stratification on bottom exchange processes. Journal of Geophysical Research - Oceans, 94(C10):14229-14444.

Simon, N.S. (1989). Nitrogen cycling between sediment and the shallow-water column in the transition zone of the Potomac River and Estuary. II. The role of wind-driven resuspension an adsorbed ammonium. Estuarine, Coastal and Shelf Science 28:531-547.

Smith, R.C. and Baker, K. (1981). Optical properties of the clearest waters. Applied Optics, 20(2):177-184.

Smith, S. D. (1980). Wind stress and heat flux over the ocean in gale force winds. Journal of Physical Oceanography, 10, 709-726

Smith, S. D. (1989). Coefficients for sea surface wind stress, heat flux, and wind profiles as a function of wind speed and temperature. Journal of Geophysics Research, 93, 15467-15472

Steele, J.A. (1974). The structure of marine ecosystem. Oxford, Blackwell: p74-91.

Steele, J.M. (1965) Notes on some theoretical problems in production ecology. In:(C.R. Goldman ed.) Primary Production in Aquatic Environments. University of California Press. Berkeley

Steinberger, N., and Hondzo, M. (1999). Experimental study of the hydrodynamic control of diffusional mass transfer at the sediment-water interface. Journal of Environmental Engineering, 125(2): 192-200

Stoker, Y.E. (1986). Water quality of the Charlotte Harbor estuarine system, Florida, November 1982 through October 1984. U.S. Geological Survey Open-File Report 85-563: 213.

Stoker, Y.E. (1992). Salinity distribution and variation with fresh-water inflow and tide, and potential changes in salinity due to altered freshwater inflow in the Charlotte Harbor estuarine system, Florida. U.S. Geological Survey Water-Resources Investigations Report 92-4062: 30.

Stull, R. B. (1988). An Introduction to Boundary Layer Meteorology. Kluwer Academic Publishers, Netherlands, 660pp.

Sun, D. and Sheng, Y.P. (2001). Modeling suspended sediment transport under combined wave current interactions in Indian River Lagoon. PhD dissertation, University of Florida, Gainesville, Florida.

Taylor, P., Gulev, S., Barnier, B.,Bradley, F.,Charlock, T.,Gleckler, P.,Kubota, M., Kutsuwada, M.,Legler, D., Lindau, R., Rothrock, D., Schulz, J.da-Silva, A., Sterl, A., and White, G. (2000). Intercomparison and validation of ocean-atmosphere energy flux fields. Final Report of the joint WCRP/SCOR working group on air-sea fluxes, WCRP-112, WMO/ TD-No. 1036, 303 S

Thomann, R.V. (1992). Section 14.1. in Technical guidance manual for performing waste load allocations. Book III: Estuaries-Part 4, Critical review of coastal embayment and estuarine waste load allocation modeling. U.S. EPA Technical Report EPA-823-R-92-005. Washington, D.C.

Thomann, R.V., and Fitzpatrick, J.F. (1982). Calculation and verification of a amthematical model of the eutrophication of the Potomac Estuary. Prepared for the Department of Environmental Services, Government of the Distric of Columbia.

Thompson, J.F. (1982). Numerical Grid Generation, chapter General Curvilinear Coordinate Systems, pages 1-30. Elsevier, Amsterdam.

Thompson, J.F., Warsi, Z.U.A. and Mastin, C.W. (1985). Numerical Grid Generation: Foundations and Applications. North-Holland. New York

Weast (1977). Handbook of chemistry and physics, 58th ed., Table F-200

Witkowski, J. and Jaffe, P.R. (1987). Kinetic and equlibrium formulations in modeling of hydrophobic organic chemicals in surface and ground waters. System Analysis in Water Quality Management (M.B. Beck, ed.), Advences in Water Pollution Control- Aseries of Conferences Sponsored by IAWPRC.

Wolfe, S.H., and Drew R. D., eds. (1990). An ecological characterization of the Tampa Bay watershed. U.S. Fish Wildl. Serv. Biol. Rep. 90: 20.

Yassuda, E.A. and Sheng, Y.P. (1996). Integrated modeling of Tampa Bay Estuarine System. PhD dissertation, University of Florida, Gainesville, Florida.

Zison, S., Mills, W.B., Deimer, D., and Chen, C.W. (1978). Rates, constants and kinetic formulations in surface water quality modeling. Prepared by Tetra Tech, Inc., Lafayette, CA for Environmental Research Laboratory, U.S. Environmental Protection Agency, Athen, GA. EPA-600/3-78-105:335.

BIOGRAPHICAL SKETCH

Kijin Park was born in Pusan, the largest harbor of Korea, on the 25th of October. He received the Bachelor of Science degree and M.S. degree in department of Marine Science at the Pusan National University in February, 1991 and 1994, respectively. After finished M.S. degree, he had worked as research scientist at Korea Oceanography Research & Development Institute (KORDI) and Korea Meteorological Administration (KMA) until June, 1997. The following summer he left for Gainesville, Florida , and began his graduate studies in coastal and oceanographic engineering at the University of Florida.

I certify that I have read this study and that in my opinion it conforms to acceptable standards of scholarly presentation and is fully adequate, in scope and quality, as a dissertation for the degree of Doctor of Philosophy.

Y. Peter Sheng, Chair
Professor of Civil and Coastal Engineering

I certify that I have read this study and that in my opinion it conforms to acceptable standards of scholarly presentation and is fully adequate, in scope and quality, as a dissertation for the degree of Doctor of Philosophy.

Robert G. Dean
Graduate Research Professor of Civil and Coastal Engineering

I certify that I have read this study and that in my opinion it conforms to acceptable standards of scholarly presentation and is fully adequate, in scope and quality, as a dissertation for the degree of Doctor of Philosophy.

Robert J. Thieke
Assistance Professor of Civil and Coastal Engineering

I certify that I have read this study and that in my opinion it conforms to acceptable standards of scholarly presentation and is fully adequate, in scope and quality, as a dissertation for the degree of Doctor of Philosophy.

Louis H. Motz
Associate Professor of Civil and Coastal Engineering

I certify that I have read this study and that in my opinion it conforms to acceptable standards of scholarly presentation and is fully adequate, in scope and quality, as a dissertation for the degree of Doctor of Philosophy.

K. Ramesh Reddy
Graduate Research Professor of Soil and Water Science

This dissertation was submitted to the Graduate Faculty of the College of Engineering and to the Graduate School and was accepted as partial fulfillment of the requirements for the degree of Doctor of Philosophy.

August, 2004

Pramod P. Khargonekar
Dean, College of Engineering

Kenneth J. Gerhardt
Interim Dean, Graduate School

LD
1780
2004
.P236

UNIVERSITY OF FLORIDA
3 1262 08554 5670